2017-01-01

Advancing high spatial and spectral resolution remote sensing for observing plant community response to environmental variability and change in the Alaskan Arctic

Sergio Armando Vargas
University of Texas at El Paso, savargas@miners.utep.edu

ADVANCING HIGH SPATIAL AND SPECTRAL RESOLUTION REMOTE SENSING FOR OBSERVING PLANT COMMUNITY RESPONSE TO ENVIRONMENTAL VARIBILITY AND CHANGE IN THE ALASKAN ARCTIC

SERGIO A. VARGAS ZESATI

Environmental Science and Engineering Doctoral Program

APPROVED:

Craig E. Tweedie, Ph.D., Chair

Vanessa Lougheed, Ph.D.

Steven Oberbauer, Ph.D.

Jose M. Hurtado, Ph.D.

Charles Ambler, Ph.D.

Dean of the Graduate School

Dedication

I dedicate this dissertation to my parents and sister whom undeniably have guided me through life and have shown me the true meaning of love through their humbleness, actions and strength despite all of life's hardships. I owe my discipline and success thus far to them and will forever be grateful for such valuable teachings and wisdom. They have always been my true inspiration to pursue my goals and will continue to be my motivation to continue this journey towards knowledge and enlightenment of self.

ADVANCING HIGH SPATIAL AND SPECTRAL RESOLUTION REMOTE SENSING FOR OBSERVING PLANT COMMUNITY RESPONSE TO ENVIRONMENTAL VARIBILITY AND CHANGE IN THE ALASKAN ARCTIC

by

SERGIO A. VARGAS ZESATI, B.Sc.

DISSERTATION

Presented to the Faculty of the Graduate School of

The University of Texas at El Paso

in Partial Fulfillment

of the Requirements

for the Degree of

DOCTOR OF PHILOSOPHY

Environmental Science and Engineering Doctoral Program

THE UNIVERSITY OF TEXAS AT EL PASO

May 2017

Acknowledgements

I would first like to thank my advisor and friend Dr. Craig E. Tweedie for all of the amazing opportunities and wisdom he has shared with me throughout this journey, without them this research and my overall personal awakening would not have been possible. Additionally, I'd like to thank my dissertation committee members, namely Dr. Lougheed, Dr. Oberbauer and Dr. Hurtado, for their crucial support, insight and research guidance which helped me get through this chapter in my life. I will forever be grateful to Dr. Santonu Goswami for introducing me to the beautifully interesting topic of Arctic research and for showing me the basics of remote sensing. I could not have completed this undertaking without the endless hours and hard work provided by my colleagues and field mates I worked with and I'd like to take this opportunity to thank them all including Dr. Christian Andresen, Dr. Mark Lara, Dr. Sandra Villarreal, Dr. Dave Lin, Dr. Christine Laney, Dr. David Johnson, Dr. Nathan Healey, Adrian Aguirre, Walker Johnson, Gesuri Ramirez, Geovany Ramirez, Mayra Melendez, Abdiel Lopez, Ryan Cody, Ari Kassin, Robin Luna, Raul Armendariz, Stephen Escarzaga and Lina Hamdan. In addition, I'd like to recognize the International Tundra Experiment (ITEX) community, Grand Valley State University (GVSU) as well as the Florida International University (FIU) research teams lead by Dr. Robert Hollister and Dr. Steve Oberbauer for providing a wonderful and life-changing collaborating experience throughout the course of this project. I thank the Utqiaġvik and Atqasuk, Alaska communities for their interest in Arctic research and their understanding and acceptance of such activities to occur on their beautiful sacred land as well as the UMIAQ, BASC and CH2MHills Polar Field services crews for providing endless hours of logistical support and invaluable wisdom. I am indebted to the crew at the Polar Geospatial Center (PGC) at the University of Minneapolis, Dr. Cathy Wilson at Los Alamos National Laboratory, and to the field engineers Marianne Okal and Brendan Hodge

at UNAVCO in Boulder, Colorado for providing data, knowledge, instrument training and professional guidance throughout the course of this project.

Lastly, I could not have personally accomplished this project without the support of my family and friends. I have the most amazing parents and sister anyone could have asked for and their guidance and life-lessons have shaped me into the person I am today. Without them I wouldn't be where I am today as they have always been able to accept me for who I am and have never judged or doubted my abilities which has played a large part in my success thus far and will continue to drive my future endeavors. Additionally, the love, support and advice I received from my wonderful friends including my beautiful girlfriend Marcela Aragon have always served as encouragement throughout this process and have played a key role in my ability to withstand rough times.

Funding for this research was provided by the Office of Polar Programs (OPP) of the National Science Foundation (NSF) and the Arctic Observing Network (AON) ITEX (grant no. 0856710). Also many thanks to Dr. Diana Natalicio, a person I highly admire for her economic support at the final stages of this dissertation through the Dr. Natalicio Doctoral Fellowship.

Abstract

The Arctic is being impacted by climate change more than any other region on Earth. Impacts to terrestrial ecosystems have the potential to manifest through feedbacks with other components of the Earth System. Of particular concern is the potential for the massive store of soil organic carbon to be released from arctic permafrost to the atmosphere where it could exacerbate greenhouse warming and impact global climate and biogeochemical cycles. Even though substantial gains to our understanding of the changing Arctic have been made, especially over the past decade, linking research results from plot to regional scales remains a challenge due to the lack of adequate low/mid-altitude sampling platforms, logistic constraints, and the lack of cross-scale validation of research methodologies. The prime motivation of this study is to advance observational capacities suitable for documenting multi-scale environmental change in arctic terrestrial landscapes through the development and testing of novel ground-based and low altitude remote sensing methods. Specifically this study addressed the following questions:

- How well can low-cost kite aerial photography and advanced computer vision techniques model the microtopographic heterogeneity of changing tundra surfaces?
- How does imagery from kite aerial photography and fixed time-lapse digital cameras (Pheno-cams) compare in their capacity to monitor plot-level phenological dynamics of arctic vegetation communities?
- Can the use of multi-scale digital imaging systems be scaled to improve measurements of ecosystem properties and processes at the landscape level?
- How do results from ground-based and low altitude digital remote sensing of the spatiotemporal variability in ecosystem processes compare with those from satellite remote sensing platforms?

Key findings from this study suggest that cost-effective alternative digital imaging and remote sensing methods are suitable for monitoring and quantifying plot to landscape level ecosystem structure and phenological dynamics at multiple temporal scales. Overall, this study has furthered our knowledge of how tundra ecosystems in the Arctic change seasonally and how such change could impact remote sensing studies conducted from multiple platforms and across multiple spatial scales. Additionally, this study also highlights the urgent need for research into the validation of satellite products in order to better understand the causes and consequences of the changing Arctic and its potential effects on global processes. This study focused on sites located in northern Alaska and was formed in collaboration with Florida International University (FIU) and Grand Valley State University (GVSU) as a contribution to the US Arctic Observing Network (AON). All efforts were supported through the National Science Foundation (NSF), the Cyber-ShARE Center of Excellence, and the International Tundra Experiment (ITEX).

Table of Contents

List of Tables

List of Figures

Chapter 1: General Introduction

1.1 Motivations for this Dissertation

The Arctic is experiencing among the most dramatic climate change impacts on Earth (*ACIA* 2004). Some changes can be related to the direct effects of warmer temperatures such as the loss of sea ice and glaciers, a reduction in snow cover, as well as broad-scale increases in near surface air temperature (*IPCC*, 2014). Other changes are related to indirect feedbacks such as rapid gains/losses in lake area associated with permafrost degradation, increased green biomass and geographic shifts in vegetation, longer growing seasons, and thawing permafrost (*ACIA* 2004, *Callaghan et al*. 2011, *Groisman et al*. 1994, *Hinzman et al*. 2005, *Post et al*. 2009). Of particular concern, is how the combined alteration of air and soil temperature, as well as altered surface hydrology will affect the structure and function of arctic terrestrial ecosystems, particularly terrestrial ecosystem carbon balance (*Post et al*. 2009, *Schuur et al*. 2008). If the increases in biomass and carbon uptake potential forecast for most arctic terrestrial ecosystems (*Euskirchen et al*. 2009, *Mcguire et al*. 2006) do not offset predicted losses of greenhouse gases to the atmosphere due to permafrost thaw and microbial decomposition of the substantial arctic soil carbon store (*Schuur et al*. 2008), regional to global greenhouse warming will be enhanced (*Kimball et al*. 2006).

Improved ground to satellite observation of plant and landscape phenology and scaling of ecosystem properties and processes are key to further understanding the impact of climate and other environmental change in arctic terrestrial ecosystems (*Vorosmarty et al*. 2010). Some of the main advantages of satellite remote sensing include the large spatial coverage of Earth's surface, the automation of imaging and the standardization of derived land surface products that facilitate resampling in a timely fashion (*Tucker and Sellers*, 2007). Remote sensing of ecosystem properties and processes is challenging in any terrestrial ecosystem, especially in the Arctic, where satellite remote sensing is severely challenged by logistical capabilities, environmental factors (e.g. cloud cover), and cost (*Stow et al*. 2004). As such, improving ground and low-altitude remote sensing capabilities arguably offer the greatest potential for low-cost technological innovation and subsequent gains in capacities to spatiotemporally extrapolate ecosystem structural and functional

properties and processes, and thereby advance knowledge and scientific understanding of how arctic landscapes are changing.

1.2 Challenges to Remote Sensing the Changing Arctic

To date, few coordinated efforts have focused on ground to satellite multi-scale observations of ecosystem properties and processes in the Arctic. While satellite platforms have expanded coverage of large areas by providing both imagery and data (e.g. *Bhatt et al*. 2010), these have generally been focused on low spatial and temporal resolution products relative to that collected from ground (e.g. *Goswami et al*., 2011) and low altitude sampling platforms, such as those from unmanned aerial vehicles (*Fraser et al.,* 2016). Although high spatial resolution satellite and air-borne multispectral imagery has been used for deriving improved land cover classifications (*Lin et al*., 2012, *Lara et al*., 2016, *Johansson et al*., 2006), this imagery remains expensive for multi-temporal acquisitions that are difficult to acquire in the Arctic where cloud cover persists for much of the snow free growing period (*Stow et al*., 2004). Plot level measurements have provided detailed insight into a range of ecosystem properties such as surface water cover (*Goswami et al*., 2011), phenology (*Hollister et al*., 2005) and relatedness to other ecosystem properties (*Lara et al*., 2012, *Boelman et al*., 2003), but are limited in spatial extent and important landscape features and processes remain poorly documented at the regional and landscape levels using high spatial resolution remote sensing approaches.

1.3 The Coupled Bio-Physical Environment of the Arctic

In arctic terrestrial ecosystems, there is a close coupling of biological and physical factors, where a change in one manifests a change in another (*Lara et al*., 2012). Trajectories of climate change trends and impacts in the Arctic suggest that numerous ecosystem properties and processes will continue to change in the foreseeable future including surface temperature (*IPCC,* 2014), surface hydrology (*Sommerkorn,* 2008), active layer thaw depth (*Schuur et al.*, 2008; *Park et al.*, 2016), vegetation cover (*Lin et al.*, 2012), plant community composition (*Villarreal et al.*, 2012) and microtopography (*Oberbauer et al.*, 2007; *Gamon et al.*, 2012). Many of these changes have the capacity to alter surface structure and variability through enhanced thermokarst terrain (*Osterkamp et al.*, 2009; *Jorgenson et al.*, 2015; *Liljedahl et al.*, 2016) ultimately leading to a positive feedback effect which enhances permafrost degradation. Microtopography is an important

control of tundra ecosystem structure and function including trace gas exchange (*Sullivan et al.*, 2008; *Sommerkorn*, 2008; *Lara et al.*, 2014; *Von Fischer et al.*, 2010) energy fluxes (*Liljedahl, A.K., et al.*, 2012), vegetation distribution (*Webber et al.*, 1978*)*, eco-hydrology (*Engstrom et al.*, 2005), and nutrient cycling (*Stewart et al.*, 2014). To date, however, quantifying microtopographic variability at landscape scales at a resolution suitable for scaling fundamental ecological properties and processes has been challenging (*Zona et al.*, 2011). As a result, the importance of microtopographic variability and change has been arguably poorly represented in ecosystem models and landscape to regional scale syntheses of ecosystem or landscape change. Justifiably, improving techniques for mapping high resolution microtopographic variability, change, and uncertainty has been recognized as an urgent research priority (*Sullivan et al.*, 2008; *Stewart et al.*, 2014; *Engstrom et al.*, 2005).

1.4 Phenology of Arctic Tundra Vegetation and Landscapes

Plant phenology is the observation of the timing of shifts in a plants life cycle and how these particular events are influenced by seasonal and inter-annual climate-induced variations. In the Arctic, shifts in the timing and magnitude of vegetation phenology and green-up has become recognized as among the most poignant and high-profile responses documented for arctic terrestrial ecosystems (*Myneni et al.*, 1997; *Goetz et al.*, 2005; *Bhatt et al.*, 2010; *Epstein et al.*, 2012). The majority of these arctic phenological studies have been conducted at either regional to circum-arctic scales through the analysis of satellite remote sensing products or plant to plot scales through human observation.

Contrasting evidence has surfaced for enhanced (*Sweet et al.*, 2014) or decreased (*Humphreys and Lafleur*, 2011; *Gamon et al.*, 2013) productivity of ecosystem vegetation communities as a response to earlier snowmelt. Mixed "browning" and "greening" signals of different arctic areas (*Myneni et al.*, 1997; *Goetz et al.*, 2005; *Bunn et al.*, 2007), and some studies attribute these seemingly conflicting signals to surface hydrology (*Huemmrich et al.*, 2010; *Goswami et al.*, 2011; *Ma et al.*, 2012; *Yi et al.*, 2014). Moreover, the Normalized Difference Vegetation Index (NDVI) has been identified and used as a proxy of primary productivity for some vegetation types (e.g. deciduous vegetation) but doesn't capture variability well for growth forms such as evergreens (*Gamon et al.*, 1995, *Gamon et al.*, 2015). Because of contrasting evidence, and the uncertainty related to differences in trends of NDVI at different spatiotemporal scales and

for various vegetation types, reliance on this vegetation index alone can lead to interpretation difficulties of actual drivers of productivity (*Gamon et al.,* 2015).

Plot level plant phenological studies have shown the sensitivity of arctic plant species and communities to climatic variability (*Hollister et al.*, 2014), and have highlighted the utility of using phenological change as an ecological indicator of climatic change impacts (*Oberbauer et al.*, 2013). Such studies have provided great insight into species and functional plant type seasonal trends such as start of season (SOS), end of season (EOS), peak of season (POS), timing of snowmelt, and timing of senescence but have been generally limited in spatial coverage (*Hollister et al.*, 2005; *Oberbauer et al.*, 2013). Phenological trends vary between ecosystems (*Walker et al.*, 2006) and land cover classes as seen across multiple plot-level experimental warming studies such as those associated with the International Tundra Experiment (ITEX) (*Elmendorf et al.*, 2012b). Phenological trends also vary across spatial scales (*Elmendorf et al.*, 2012a) and respond differently to changing landscape characteristics such as those observed in surface hydrology studies (*Goswami et al.,* 2011), and in association with permafrost degradation (*Jorgenson et al.*, 2013) and subsidence (*Streletskiy et al.*, 2007). Generally, however, plot level monitoring of vegetation phenology remains time consuming, expensive and logistically challenging in the Arctic. Scaling plot-level research to regional and landscape scales has been challenging due to the lack of adequate low/mid-altitude sampling platforms, logistical constraints and the lack of cross-scale validation of research methodologies.

Clearly, the development and innovation of mid-scale remote sensing methods have the greatest potential to link understanding of phenological trends at plot and regional to circum-arctic scales and improve validation of satellite-based sensing (*Gamon et al.,* 2013; *Westergaard-Nielsen et al.,* 2013). Networks of low-cost sensors and other remote sensing platforms have the capacity to complement satellite derived measurements if deployed in an extensible manner (*Goswami et al.*, 2011; *Gamon et al.*, 2013; *Healey et al.*, 2014; *Andresen et al.*, 2014; *Vargas et al. in prep*). Additionally, repeat photography from inexpensive consumer grade digital camera traps can be used to calculate a range of spectral indices from the red, green and blue (RGB) color space (e.g. green excess (GI) and green chromatic coordinate (% G)), and have a proven capacity to capture phenological dynamics in numerous ecosystems (*Richardson et al.*, 2009; *Saitoh et al.*, 2012; *Ide and Oguma*, 2013; *Westergaard-Nielsen et al.*, 2013; *Peichl et al.*, 2014; *Toomey et al.*, 2015; *Beamish et al.*, 2016). However, among the few studies focused on capturing phenology using

vegetation indices derived from RGB cameras, none have explored their performance in high-arctic tundra ecosystems from either small format aerial photography systems (SFAP) or repeat photography (Pheno-cams). Moreover, few studies appear to have explored how indices of vegetation properties differ between those derived from digital photography platforms and those derived from hyperspectral spectrometers. These systems vary markedly in both cost and suitability for mid-scale sampling and have the potential to bridge the gap between traditional plot-level and landscape scale studies.

1.5 GOALS AND OBJECTIVES

This study aims to improve capacities for scaling observations of arctic terrestrial ecosystem properties and processes from plot to regional scales by developing and testing a cost effective low altitude remote sensing platform that can be used to derive i) high spatial resolution digital elevation models, ii) landscape-scale time series plant community and landscape phenology observations, and iii) plot to landscape scale land cover classifications. The specific objectives and underlying questions that will be posed throughout the dissertation are outlined immediately below.

Objective 1 (Chapter 2):

Establish the capacity to derive landscape scale Digital Elevation Models (DEMs) of low relief tundra landscapes from multiple remote sensing platforms, and test the accuracy and uncertainty associated with each method.

- How do DEMs compare between Terrestrial Light Detection and Ranging (T-LiDAR), Kite Aerial Photography (KAP), Airborne Light Detection and Ranging (A-LIDAR), and stereo satellite imagery (SSI)?
- Based on the resulting DEMs and associated accuracy assessments, and relative to the high precision DEMs produced by T-LiDAR and from ground control point (GCP) data, what are the advantages, disadvantages, and limitations of each respective method for DEM derivation?
- What are the differences of each approach in modeling surface hydrology?

Objective 2 (Chapter 3):

Assess the outputs from a range of optical sampling platforms (e.g. ground based spectrometers, Pheno-cams, and KAP) to determine which platforms can adequately be used to monitor plant and landscape phenological dynamics and other ecosystem properties and processes.

- How do different remote sensing platforms and their spectral properties vary in their capacity to document plant and landscape phenological dynamics?
- What differences in accuracy and uncertainty, related to phenological patterns of arctic tundra, are seen between the various remote sensing platforms?
- How can KAP and digital red, green, and blue (RGB) images and derived indices be used to document seasonal phenology of arctic plant communities and how do these compare to spectrometer-derived indices?

Objective 3 (Chapter 4):

Use results from chapter 3 to assess whether or not phenological trends and cross-platform and cross-sensor results from Chapter 3 (Objective 2) scale to the landscape-scale footprint of global orbiting satellite platforms.

- Which indices and spatial resolutions are most effective at capturing phenological dynamics among predominant vegetation types?
- Can digital cameras and digital photogrammetry be used to capture tundra land surface structure (DEM) across larger (1 km^2) study areas?
- What uncertainty is related to the scaling of observations to the landscape level?

Objective 4 (Chapter 5):

Utilize objectives 1-3 above to further explore the use of time-series satellite-derived land surface products for observing seasonal and inter-annual plant phenological trends.

- How do results from ground-based and low-altitude digital remote sensing of the spatiotemporal variability in ecosystem processes compare with those from satellite remote sensing platforms?
- How could results of plot to landscape scaling of vegetation phenology impact global ecosystem models that utilize these land surface products as inputs?

1.6 STUDY AREA

This study was conducted at two locations on the Coastal Plain of the North Slope of Alaska near the towns of Utqiaġvik (Utqiaġvik) (71°18'N, 156°40'W) and 100 km south of Utqiaġvik near Atqasuk (70°29'N, 157°25'W). The landscape in the Utqiaġvik area is vast and diverse and is composed of oriented lakes, drained thaw lake basins and small ponds, in addition to being underlain by continuous permafrost (*Sellmann and Brown*, 1973). The landscape includes a range of thermokarst features such as high/low-centered polygons, low lying wet troughs or pits, ridges and small hummocks (*Webber et al*. 1980; *Brown et al.*, 1980; *Lara et al.*, 2014). The Atqasuk landscape is predominantly characterized by dry heath and wet meadow plant communities that are more diverse than those found in Utqiaġvik. Characteristic of both areas, low-lying, wet troughs are mostly dominated by standing water and graminoid species (e.g. *Carex* sp.), while areas of higher elevation are mainly covered by non-vascular plants (e.g. *Alectoria* sp. and *Polytrichum* sp.), and forbs (e.g. *Saxifraga* sp.) (*Hollister et al.*, 2005). Atqasuk tends to be warmer than Utqiaġvik, where fog and clouds typically dissipate by early noon and weather patterns are more dynamic (*Haugen, R.K., and Brown*, 1980). Additionally, mean July temperature is 3.7°C in Utqiaġvik and 9 °C in Atqasuk and summer precipitation is approximately 57 mm and 55 mm respectively. Seasonal landscape freeze-thaw dynamics yield a maximum thaw depth between 30 and 90 cm in Utqiaġvik and between 40- 100+ cm in Atqasuk (*Hole*, 1998). Mean July air temperature and annual precipitation is 3.7°C, and ~200mm for Utqiaġvik and Atqasuk respectively (*Haugen and Brown*, 1980).

Two main sites were established at each location, namely the Circum-arctic Active Layer Monitoring (CALM) grid and the Mobile Instrumented Sensor Platform (MISP) transect, as a contribution to the Arctic Observing Network's International Tundra Experiment (AON-ITEX). The CALM grids, formerly known as the Arctic System Science (ARCSS) grids, were established in the mid-1990s in an effort to monitor changes in the active layer of tundra landscapes. Both grids measure 1000 meters by 1000 meters (1 km^2 or 100 hectares), with nodes spaced on a 100 meter grid (*Brown et al.*, 2000). During the summers of 2011 and 2012, 1 x 1 meter plots were established approximately 3 x 3 meters to the south and west of each CALM node. The central aim of this study was to build a capacity to monitor plot level plant community composition and structure across a spatial domain typically sampled by a global orbiting satellite platform (e.g. MODIS). Using a geographical information system (GIS), a subset of 30 plots was chosen from

each CALM grid in Utqiaġvik and Atqasuk and are referred to as the CALM grids for the rest of this dissertation. These plots spanned a large area within the CALM grid, were logistically feasible to sample periodically, and represented a wide range of plant community types and landscape geography encountered within the greater study areas. This study also utilized the Mobile Instrumented Sensor Platform (MISP) transects (2 x 50 meters) established at both sampling locations in 2011, which consisted of contiguous 2 x 1 meter plots and a range of vegetation types found throughout the CALM grid (figures 1.1 and 1.2). Table 1.1 summarizes vegetation classes utilized throughout this dissertation.

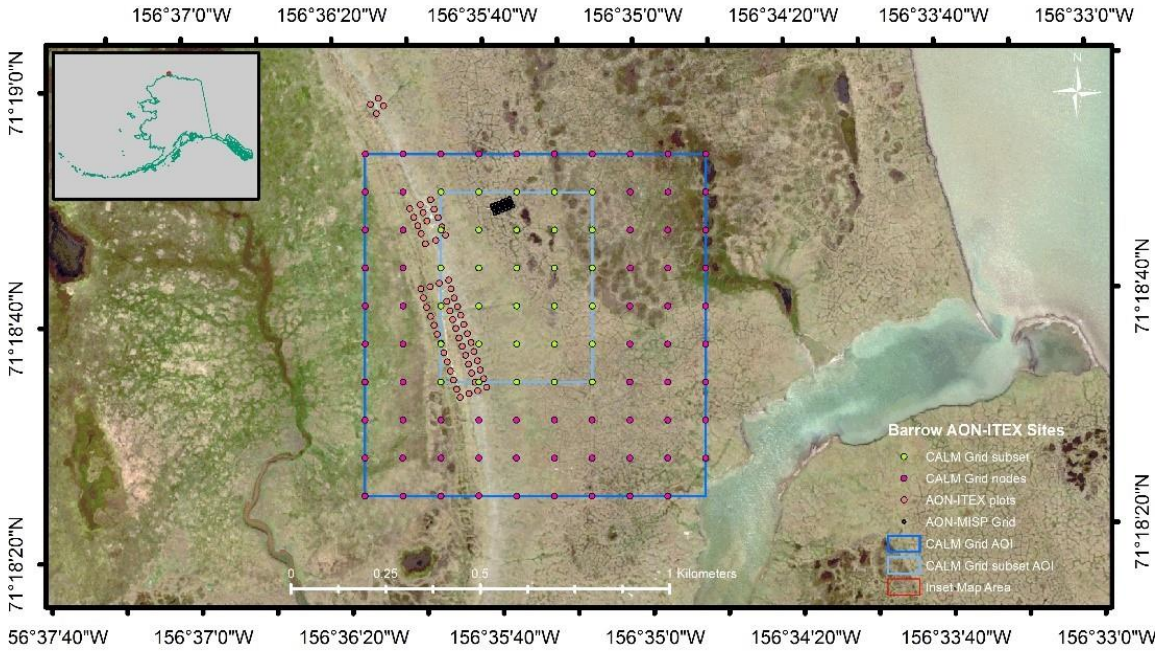

Figure 1.1: True color World View 2 image captured during the summer of 2013 displaying location of the Utqiaġvik AON-ITEX sites including ITEX warming plots, MISP transect, CALM grid with corresponding nodes and areas of interest.

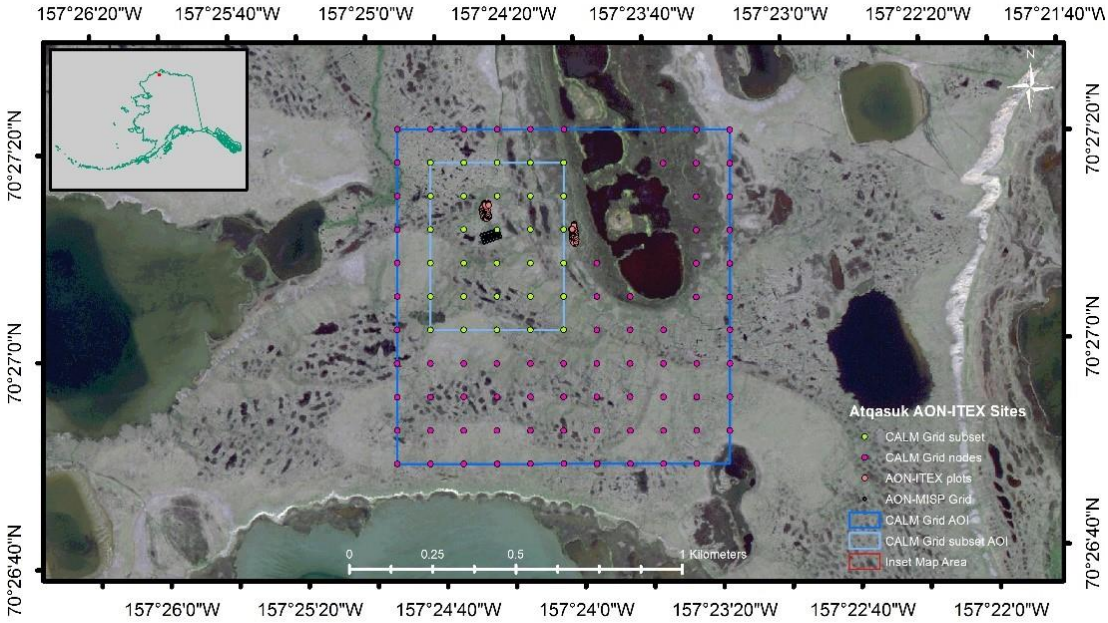

Figure 1.2: True color World View 2 image captured during the summer of 2013 displaying location of the Atqasuk AON-ITEX sites including ITEX warming plots, MISP transect, CALM grid with corresponding nodes and areas of interest.

Table 1.1: Summary of the vegetation types, classified classes, dominant plant species and landform types present at both MISP and CALM plots in Utqiaġvik and Atqasuk. Based on *Lin et al.* (2011), *Webber*, (1978), *Healey et al.*, (2014), and *Andresen et al.* in prep.

Parameters	Barrow					Atqasuk				
Vegetation Type	Dry Heath/ Mesic Heath		Moist Meadow	Wet Meadow		Dry Heath/ Mesic Heath	Moist Meadow		Wet Meadow	
Wetland Name	Dry dwarf shrub graminoid tundra	Dry-moist dwarf shrub graminoid tundra	Moist graminoid tundra	Seasonally flooded gramonoid tundra	Wet graminoid tundra	Dry shrub graminoid tundra	Moist graminoid tundra	Moist shrub graminoid tundra	Wet graminoid tundra	Aquatic graminoid tundra
Vegetation Class	Dry shrub	Dry-moist shrub-gram	Moist gram	Seasonally flooded	Wet gram	Dry	Moist	Moist shrub	Wet	Aquatic
Dominant Species	*Salix pulchra, Lazula arctica*	*Eriophorum spp.*	*Carex aquatilis/stans*	*pleaurocarpous mosses/ Arctophila fulva*	*Arctophila fulva*	*Cassiope tetragona*	*Vaccinium Vitis-idaea*	*Salix pulchra*	*Carex aquatilis*	*Arctophila fulva*
Landform Type	High center polygon/ Stabilized sand dune	High center polygon	Low center polygon/ low land	Marsh	Pond/lake	Stabilized sand dune/ snow patch	High center polygon	Low center polygon/low land	Marsh	Pond/lake
Mean Peak Season VWC (%)	42	35.4	55.8	70.5	63.5	30.6	31.03	40.1	59.3	49.8
Elevation (MASL)	3					30				
Mean Annual Temperature (°C)	-12.6					-11.9				
Mean July Temperature (°C)	3					7.2				
Average Maximum Thaw Depth (cm)	35-39					36-75+				

1.7 STRUCTURE OF THIS DISSERTATION

This dissertation is composed of six chapters that include a general introduction (this chapter) and discussion (Chapter 6) and four research intensive chapters that have been formatted for publication. The author of this dissertation is the primary author (writing and data analysis) on all chapters/draft publications presented below (Table 1.2) and oversaw field data collection conducted by multiple mostly undergraduate research assistants. The study was designed in a manner where each chapter builds upon the knowledgebase gained in previous chapters and includes the use and re-use of data collected from sites and sampling platforms associated with the International Tundra Experiment (ITEX) that is supported in the US through the National Science Foundation (NSF) funded Arctic Observing Network (AON). In addition to the work presented in this dissertation, the author has contributed to several peer review manuscripts as a co-author including one technical remote sensing paper (*Healey., et al.,* 2014) and one remote sensing methodological note (*Andresen et al.*, 2014).

Table 1.2: Publication status of the chapters presented in this dissertation.

Chapter	Title and planned publications
1	**Introduction** Vargas Z., S.A. No submission intended
2	**Inter-comparison of Digital Elevation Models (DEMs) derived from multiple sensing platforms: capturing microtopographic variability in an arctic tundra landscape** Authorship: Vargas Z., S.A.; Melendez, M.; Cody, R.P.; Oberbauer, S.F.; Wilson, C.; Hollister, R. D.; Tweedie, C. E. Target Journal: Photogrammetry and Remote Sensing Estimated date of submission: July 2017
3	**Plot-level Seasonal and Inter-annual Phenological Variability is Greatest in Low-Arctic and Wet Sites Across the North Slope of Alaska** Authorship: Vargas Z., S.A.; Ramirez, G.E.; Ramirez, G.; Cody, R.P.; Melendez, M.; Oberbauer, S.F.[2]; Hollister, B.; Laney C.M., Andresen, C.G.; Healey, N.C.; Tweedie, C.E Target Journal: Remote Sensing of the Environment Estimated date of submission: December 2017
4	**Spatial and Temporal Scaling of Surface Characteristics: A Case Study in a High Arctic Tundra Ecosystem** Authorship: Vargas Z., S.A.; Ramirez, G.E.; Ramirez, G.; Cody, R.P.; Oberbauer, S.F.; Hollister, R.D.; Laney C.M.; Tweedie, C.E. Target Journal: Geophysical Research Letters Estimated date of submission: December 2017
5	**Multi-temporal Comparison of Primary Productivity (NDVI) Across High Arctic Tundra Landscapes as Observed From Multi-scale Optical Sensing Platforms** Authorship: Vargas Z., S.A.; Ramirez, G.E.; Ramirez, G.; Cody, R.P.; Oberbauer, S.F.; Hollister, R.D.; Laney C.M.; Andresen, C.G., Healey, N.C., Tweedie, C.E. Target Journal: Arctic, Antarctic and Alpine Research Estimated date of submission: September 2017
6	Conclusion Authorship: Vargas Z., S.A No submission intended

Chapter 2: Inter-comparison of Digital Elevation Models (DEMs) Derived From Multiple Sensing Platforms: Capturing Microtopographic Variability in an Arctic Tundra Landscape

2.1 INTRODUCTION

Trajectories of climate change trends and impacts in the Arctic suggest that numerous ecosystem properties and processes will continue to change in the foreseeable future including surface temperature (IPCC, 2014), surface hydrology (*Sommerkorn*, 2008), active layer thaw depth (*Schuur et al*., 2008; *Park et al*., 2016), vegetation cover (*Lin et al*., 2012), plant community composition (*Villarreal et al*., 2012) and microtopography (*Oberbauer et al*., 2007; *Gamon et al*., 2012). Many of these changes have the capacity to alter surface structure and variability through enhanced thermokarst terrain and permafrost degradation (*Osterkamp et al*., 2009; *Jorgenson et al*., 2015; *Liljedahl et al*., 2016). Microtopography is an important control of tundra ecosystem structure and function including trace gas exchange (*Sullivan et al*., 2008; *Sommerkorn*, 2008; *Lara et al*., 2014; *Von Fischer et al*., 2010), energy fluxes (*Liljedahl, A.K., et al*., 2012), vegetation distribution (*Webber et al*., 1978), eco-hydrology (*Engstrom et al*., 2005), and nutrient cycling (*Stewart et al*., 2014). To date, however, quantifying microtopographic variability at landscape scales at a resolution suitable for scaling fundamental ecological properties and processes has been challenging (*Zona et al*., 2011). As a result, the importance of microtopographic variability and change has been arguably poorly represented in ecosystem models and landscape to regional scale syntheses of ecosystem or landscape change. Justifiably, improving techniques for mapping high resolution microtopographic variability, change, and uncertainty has been recognized as a research priority (*Sullivan et al*., 2008; *Stewart et al.*, 2014; *Engstrom et al*., 2005).

Elevation data across landscapes can be acquired using various remote sensing methods and, over the past couple of decades, several improved methods for deriving these data, and resulting surface models have been developed (*Liu et al.*, 2008; *Dowling et al.*, 2009; *Dandois and Ellis*, 2010; *Wilson*, 2012). The majority of these techniques have benefited from innovations in computational power and typically differ in both how spatially explicit point clouds (PCs) are acquired from platforms and how such point clouds are processed to derive DEMs (*Leberl et al.*, 2010). Light detection and ranging (LiDAR) is a similar technique to radar but emits laser pulses of light instead of radio waves and detects and records (as millions of points that make up PCs)

the reflected light from surrounding surfaces. Each one of these points contains an X, Y, and Z value projected in a three-dimensional space to a local Cartesian coordinate system defined by the laser system. The most widely used platforms for collecting LiDAR data are from airborne systems (A-LiDAR) such as airplanes or helicopters that are typically used to collect data over tens to thousands of square miles; whereas fixed-point terrestrial (T-LiDAR) or mobile platforms are normally executed over smaller areas or when higher density data is required. This approach has become a popular method for collecting dense and accurate elevation and surface data across various ecosystems (*Antonarakis et al.*, 2008; *Carter et al.*, 2012; *Ward et al.*, 2013; *Lefsky et al.*, 2014), even across the cryosphere (*Bhardwaj et al.*, 2016). Direct measurements using LiDAR systems have several advantages over other methods, which include rapid sampling, high resolutions, sub-centimeter accuracies, limited post-processing, and ground detection through dense vegetation canopy (i.e. forests) (*Sumerling*, 2011; *Carter et al.*, 2012). The majority of systems incorporate a survey-grade Global Positioning System (GPS), and an inertial measurement unit (IMU), which ultimately eliminates the need for triangulation, reducing acquisition and post-processing times as well as field labor. Another added advantage of laser scanners is the direct measurement of "raw" PCs, which require minimal post-processing steps and geo-rectification is semi-automated. However, these approaches require the dependency on relatively bulky and expensive equipment that can be limiting when repeat-sampling is required for studies targeting change detection or long-term ecological monitoring efforts (*Wehr and Lohr*, 1999). The large amounts of data produced by LiDAR systems has also been identified as a persistent challenge, especially for groups lacking the adequate computing power required to store, process and analyze large datasets. Another limitation of LiDAR acquired from different platforms (T-LiDAR vs. A-LiDAR) is compromising between spatial resolutions and sampling area as both offer different parameters with varying results.

Alternative approaches to PC production motivated by limitations of LiDAR systems have been developed over the last decade and a half and have been shown to offer potential for 3D modeling of surfaces across a range of applications (*Heimsath and Farid*, 2002; *Harwin and Lucieer*, 2012; *Fonstad et al.*, 2013; *Bangen et al.*, 2014; *Javernick et al.*, 2014; *Fraser et al.*, 2016). These remote sensing methods include measurements from different platforms such as from the ground using booms, from the air using unmanned aerial vehicles (UAVs), and satellites that utilize different sensors and processing approaches (e.g. digital photogrammetry and stereoscopy).

These systems offer a more robust, flexible and cost-effective alternative to traditional remote sensing methods (*Marzolff et al.*, 2002; *Rango et al.*, 2008; *Aber et al.*, 2002; *Rosnell and Honkavaara*, 2012; *Dandois and Ellis*, 2013). Furthermore, innovative advances in computer vision technologies such as improved 3D scene reconstruction from sets of overlapping multi-angle images (multi-view stereopsis (MVS)) by means of computer vision algorithms such as Structure from Motion (SfM) techniques (*Snavely et al.*, 2008; *Dandois and Ellis*, 2010; *Harwin and Lucieer*, 2012; *Westoby et al.*, 2012), have facilitated the use of such alternative applications. Another innovative development within the computer vision field includes the Scale Invariant Feature Transform (SIFT) algorithm, which helps match feature points from overlapping images and is closely coupled with the bundle block technique used to automatically solve for the orientation of the internal and external camera parameters needed for image triangulation (*Triggs et al.*, 2000*; Harwin and Lucieer*, 2012). These modern digital techniques expand upon traditional photogrammetric methods by allowing automatic calculations of scene geometry and camera orientations and positions without the need to manually specify these types of parameters (*Snavely et al.*, 2008), which greatly reduces processing times and ultimately reduces potential user error. These advanced photogrammetric approaches, however, require additional field and post-processing steps such as manual installation of GCPs for image alignment, manual inspection of resulting images, and PC coordinate system transformations where close attention is needed in order to avoid introduction of errors that compromise accuracy. Similar to the LiDAR approach, advanced digital photogrammetry produces large quantities of data, although not nearly as much as the laser systems, but can also limit those groups with minimal computing power.

Considerable differences exist between workflows for PC generation acquired from laser scanners and SfM photogrammetry and/or 3D vision (*Leberl et al.*, 2010; *Westoby et al.*, 2012; *Dandois and Ellis*, 2013). Similarly, many approaches and methods exist for the interpolation of DEM surfaces using these point data acquired from various sensors. Studies by the photogrammetric research community have attempted to address the accuracy of interpolation techniques and DEM estimates of error (*Fisher*, 1998; *Gong et al.*, 2000; *Raaflaub and Collins*, 2006; *Chaplot et al.*, 2006; *Darnell et al.*, 2008; *Wu et al.*, 2008; *Erdoğan*, 2010; *Chen and Yue*, 2010; *Vaze et al.*, 2010). Sources of error are largely dependent on the interpolation method used to convert point clouds to TIN or rasterized surfaces, which affect the accuracy associated with the final DEM and products that can be derived from such interpolations such as hydrological models

(*Jarihani et al.*, 2015) and surface energy balance models. *Gong et al.*, (2000) showed that sources of error can be grouped into three classes: a) accuracy, b) density and distribution of source data, c) terrain surface characteristics, and d) interpolation method used. *Carlisle*, (2005) and Erdoğan (2010), define error and accuracy as the difference between the in-situ measurement and the modeled or interpolated DEM calculation. DEM error estimates have traditionally been reported using global measures of model accuracy (e.g. RMSE) ultimately leading to assumptions of error rates being uniform throughout the area of interest (*Carlisle*, 2005). This introduces error by representing a global estimation of error rates rather than a more detailed accuracy error estimation, which typically assess the spatial pattern of elevation error throughout the entire study site. Due to the heterogeneous surface structure of thermokarst tundra landscapes, this global approach may result in false assumptions and therefore erroneous results, hence more detailed and local approaches are needed for assessing DEMs and related error estimations.

Climate variability and change has greatly impacted permafrost degradation in arctic regions and will significantly alter landscape hydro-geomorphological processes resulting in changes in properties and processes related to soil moisture and active layer depth (*Throckmorton et al.*, 2016). The current understanding of hydrological processes in high-latitude regions in response to climate change is poorly understood and directly affects future predictions and models of hydrology, water cycling and balance across various soil moistures and types (*Zhang et al.*, 2000; *Painter et al.*, 2012; *Helbig et al.*, 2013). The ability to accurately measure fine-scale (i.e. cm) microtopography and related error estimates of tundra landscapes at high resolutions is needed to facilitate geomorphological modeling with response to climate variability and change. Calculating parameters such as drainage and flow lines, flow accumulation area, and catchment boundaries can provide a detailed view of how each DEM interpolation method varies in its ability to model surface hydrology (*Wu et al.*, 2008) (Figure 2.4).

2.2 OBJECTIVES

The purpose of this study was to derive and compare landscape scale DEMs with an attempt to capture microtopographic characteristics of dominant high-arctic low relief tundra landscapes using different approaches. Remote sensing platforms included a) terrestrial LiDAR (T-LiDAR), b) airborne LiDAR (A-LiDAR), c) kite aerial photography (KAP), and d) satellite stereo imagery

(SSI), which were used with an aim to assess data collection methods – direct (laser) versus indirect (photogrammetry), spatial resolutions (sub-meter) of data, DEM interpolation methods, and final surface models and respective accuracies. Specifically, elevations, error variability, capacity to capture elevation in different landscape units (i.e. vegetation cover and landform types), and the ability of a given method to model surface water accumulation and flow dynamics were all explored. Modeling land surface structure in high-arctic ecosystems has been a persistent challenge and evaluating existing models and data products used to derive these models for spatial autocorrelation, clustering, accuracy and capacity is important to better understand these complex landscapes and how they might respond to future global climate change.

2.3 METHODS

2.3.1 Study Area

This study was executed on the Coastal Plain of the Alaskan North Slope near the city of Utqiaġvik (71°18'N, 156°40'W) (Figure 2.1). The primary study site measured 2500 m^2 (0.25 ha) and is situated at an elevation of approximately 3 meters (Figure 2.2) within the Utqiaġvik Environmental Observatory (BEO) over a highly irregular thermokarst tundra landscape dominated by continuous permafrost (about 400 m thick) (Sellmann and Brown, 1973). Seasonal landscape freeze-thaw dynamics yield a maximum thaw depth between 30 and 90 cm (*Hole*, 1998). Mean July air temperature and annual precipitation is 3.7°C, and ~200mm, respectively (Haugen and Brown, 1980). The study site was chosen among a well-studied area of polygonised tundra that represents a range of common thermokarst features (Webber et al. 1980; *Lara et al.*, 2014), including high-centered polygons, low lying wet troughs or pits, small hummocks, and ponds. Low-lying, wet troughs were mostly dominated by standing water and graminoids (e.g. *Carex* sp.), while areas of higher elevation were mainly covered by non-vascular plants (e.g. *Alectoria* sp. and *Polytrichum* sp.), and forbs (e.g. *Saxifraga* sp.) (*Hollister et al.*, 2005) (Figure 2.2).

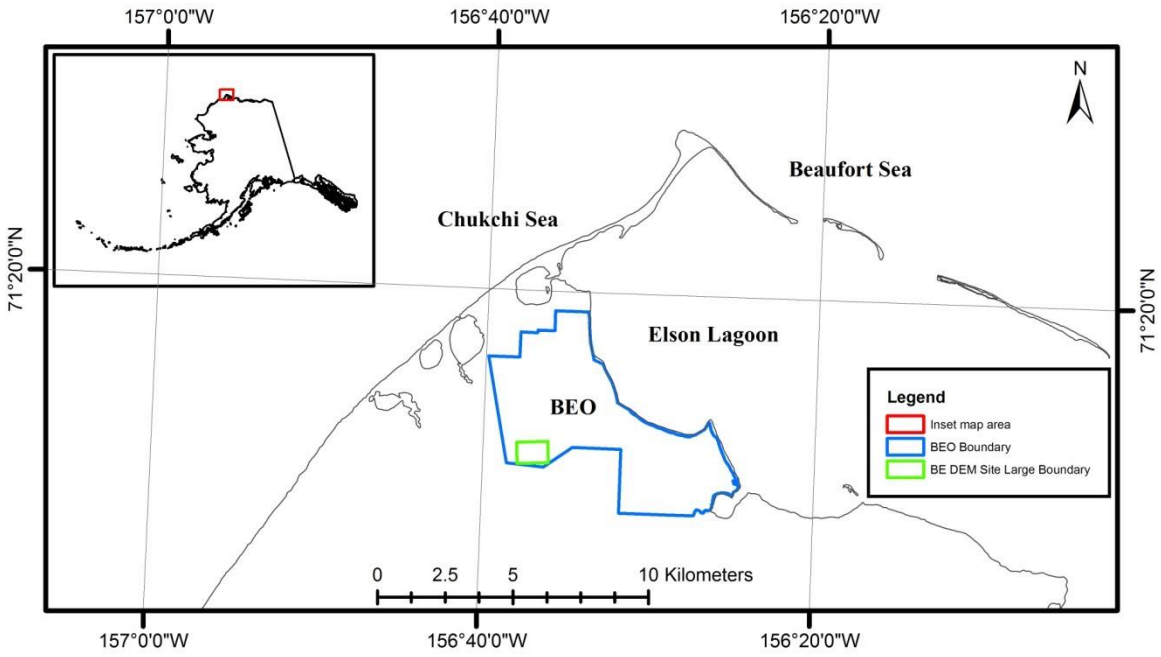

Figure 2.1: The BE DEM study site located in the Utqiaġvik Experimental Observatory (BEO) on the north slope of Alaska near the town of Barrow (Utqiaġvik).

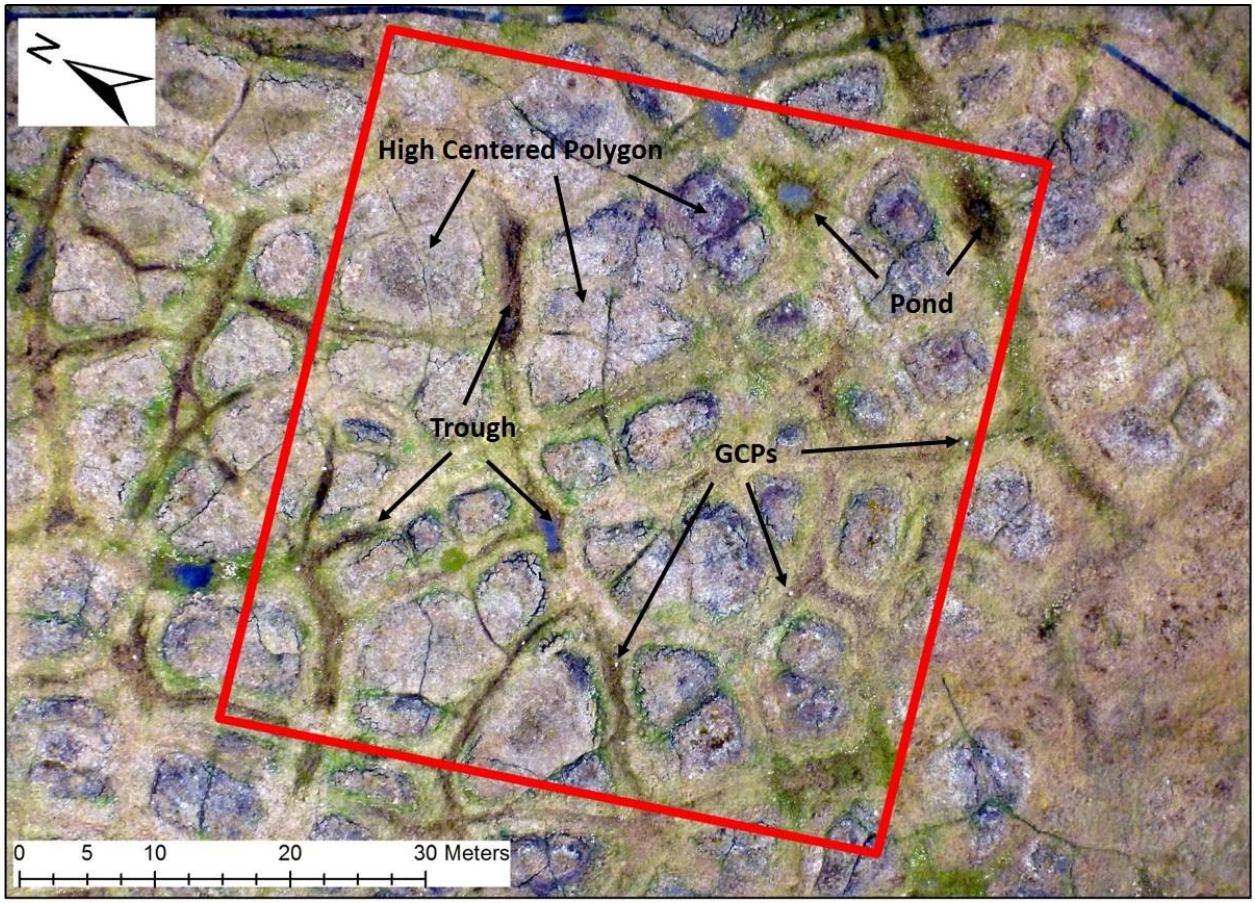

Figure 2.2: Kite aerial photograph showing the BE DEM study site (outlined in red, 0.25 ha) that is situated in polygonised tundra with thermokarst features including high-centered polygons, (dominated by non-vascular plants and forbs), troughs (dominated by graminoids), pits, and ponds (standing water). Ground control points used for alignment of aerial images are also highlighted.

2.3.2 Data collection

2.3.2.1 Laser scanners (T-LiDAR and A-LiDAR)

Four remote sensing approaches were used to acquire data for the purpose of modeling land surface structure and elevation. These included terrestrial and airborne LiDAR (T-LiDAR and A-LiDAR), digital Kite Aerial Photography (KAP), and stereo satellite imagery (SSI). Table 2.1 showcases key characteristics of each method used.

Table 2.1: Key characteristics of each remote sensing platform used for this study. The price range refers to the cost of each system overall and the acquisition cost corresponds to the approximate cost per field execution. The altitude range highlights altitudinal capacity of each and the study altitude refers to the average height above the surface for each field acquisition used in this study. All values are approximate.

Method	Price Range ($US)	Acquisition Cost ($US)	Spatial Resolution (cm)	Altitude Range (m)	Study Altitude (m)	DEM Processing Time (days)	Raw file size (GB)
T-LiDAR	200K	10K	20	1-3	2	3	10
KAP	1K	0	40	1-500	17.5	1	2
A-LiDAR	200K	15K	100	500-1500	700	2	5
SSI	NA	NA	500	800K-900K	800,000	7	5

Terrestrial LiDAR surveys were conducted from a height of approximately 1.75 meters using a *Riegl VZ-400* T-LiDAR system coupled to a *Nikon D700 DSL camera* during late August 2012. This system is a Class 1 laser product operating in the narrow near infrared spectral range, has a distance range of up to 600 meters, a scan rate of approximately 42 kHz, and an accuracy of up to 5 mm (Riegl USA). The DSLR camera was utilized to capture panoramic images of each scan position; however, the resulting scenes and RGB data values were not used for this study. Five UNAVCO-machined reflective disc targets (12 cm diameter) were mounted on fiberglass tripods (used for stability) and strategically placed and leveled throughout the site. These targets facilitated the sensors ability to measure the travel time of all laser pulses and also served as GCPs as the precise positions of all targets were acquired between 30-45 minutes logging at 5 second intervals and acquired using a static differential global positioning system (DGPS, *Trimble 5700 receiver paired with a R7* controller and a Zephyr Geodetic Antenna). One of the targets was used as a local base station and acquired data continuously over the approximate five-hour survey period to ensure a high-precision post-correction fix. A total of five scanning positions were occupied for the T-LiDAR survey. Each scan resulted in dense PCs (i.e. ~10 million points) acquired in LAS and ASCII formats and consisting of a Cartesian coordinate system.

The A-LiDAR field acquisition was made by the Next-Generation Ecosystem Experiments (NGEE) research group and executed by *AeroMetric, Inc*., under contract to the Earth and Natural Sciences Division of the Los Alamos National Laboratory (LANL) in mid July 2013. The acquisition spanned 32.7 km^2 and was collected using a Leica A-LiDAR-70 HP (Leica Geosystems) system mounted to an aircraft flown at approximately 700 m above the ground

surface. The A-LiDAR system executes at a view angle of 40°, with a rate of 350 kHz, a 58 Hz mirror scan frequency, and a side lap of 50%. The on-board GPS and IMU data were processed using Leica IPAS TC software to determine the airborne Global Navigation Satellite System (GNSS) trajectory and the blending of inertial data. This survey operated a DGPS base station during the collection of the airborne data that was used for post-processing of aircraft data. Surveyors from UMIAQ, a local logistics organization, acquired 285 Ground Control Points (GCPs) throughout the entire project area, which were used to determine the vertical accuracy of the raw laser scanner data.

2.3.2.2 Photogrammetry (Structure from Motion and stereoscopy)

A total of 987 digital true-color red, green and blue (RGB) kite aerial photographs with >60% overlap were acquired at a flying altitude of 17-20 meters above the ground surface in late August 2015. Imagery was acquired every five seconds with a picavet-mounted remote controlled (pan, tilt and shutter) single-camera rig system (SCRS) equipped with a *Panasonic Lumix (DMC-TS3)* point-and-shoot digital camera (12MP) as described by Andresen *et al.*, (2014). To enhance alignment of images for 3D scene reconstruction and dense PC production, 31 GCPs were distributed within the study area in a grid spacing of approximate 10 meters. An additional 13 GCPs were installed along the perimeter of the study area to reduce error around the site boundary (Figure 2.2). Precise locations for each GCP were measured using post-processed kinematic surveys with the same DGPS equipment described above (*Trimble R7 receiver, a Zephyr Geodetic antenna, and a TSC2 survey controller*) and data was used during post-processing for alignment of aerial images.

The SSI-derived DEM used in this study was clipped from version 1 of the ArcticDEM released on September 1, 2016. The ArcticDEM is a public-private effort coordinated by The Polar Geospatial Center (PGC) in collaboration with the National Geospatial-Intelligence Agency (NGA), National Science Foundation (NSF) and several other institutions. The main focus of this effort was to automatically produce a high-resolution, high quality, digital surface model (DSM) of the Arctic using open-source photogrammetric software and high-performance computing powers. These stereo auto-correlation techniques are applied to overlapping stereo-pairs of high-resolution satellite scenes. The ArcticDEM was developed from several years of high-resolution (0.5 meter) panchromatic imagery acquired throughout the year (including the snow-covered and

snow-free period) by the Worldview 1, Worldview 2, and Worldview 3 optical satellites maintained by DigitalGlobe (*Noh and Howat*, 2015).

2.3.3 Point cloud processing

2.3.3.1 Laser scanner point clouds (PCs) (T-LiDAR and A-LiDAR)

UNAVCO field engineers utilized *RiSCAN Pro software* (version 1.8.0) to post-process each T-LiDAR scan file collected in the field by applying a 100 m range gate filter for removing outlier points, registered GCP target data to the local base station data, and applied coordinate system transformations from a Cartesian to a geographical system for further analysis. The A-LiDAR data were georeferenced by Aerometric field engineers using *Leica A-LiDARPP v 2.79* and parsed into, tiled grids using the software *GeoCue* (version 2012.1.27.7). A total of 146 PC tiles were created for the entire Utqiaġvik peninsula, of which only one tile covered the BE DEM site and was used for the A-LiDAR DEM analysis.

2.3.3.2 Structure from Motion (SfM) PCs

Post-field survey processing consisted of manually reviewing the collection of KAP-derived images and removing those that were out of focus, contained condensation, and/or considered poor quality. Of the 987 images acquired, 513 were used for the alignment and sparse PC production process. Image alignment using the GCPs was executed using the software *Agisoft Photoscan Pro* (version 1.1.6.2038). After alignment of images a raw dense PC was created resulting in 4,952,653 points. The analysis report from the software approximated a mean flying altitude of 17.5 meters and a PC resolution of 0.005 meters, derived from 28,887 tie points.

2.3.3.3 Stereo Satellite Imagery (SSI) and DEMs

The ArcticDEM version 1 (stereo satellite DSM developed by The Polar Geospatial Center (PGC) at the University of Minnesota (www.agic.umn.edu)) was utilized for this study. The goal of this initiative was to produce an initial high-resolution, surface model of Alaska using satellite stereo imagery, high performance computing, and the Surface Extraction from TIN-Based Search Minimization (SETSM) open source photogrammetry software (ArcticDEM; *Noh and Howat*, 2015). Using this approach, no PC's were generated therefore inter-comparison was only possibly for the DEM analysis portion of this study.

2.3.4 Data analysis

ArcMap (version 10.2.2) was utilized to perform the majority of post-processing steps such as clipping data to the study area boundary, merging all scans, projecting data, and performing geostatistical analysis on and surface interpolation of the data. Each method collected data referenced to different horizontal and vertical datums, therefore all datasets were transformed to the same horizontal and vertical (NAD 83, UTM zone 4) datum prior to geospatial analysis. The vertical datum for the A-LiDAR dataset was converted from NAVD88 to NAD83 using the *National Oceanic and Atmospheric Administration's (NOAA) Vertical Datum Transformation* program (version 3.4, http://vdatum.noaa.gov), in order to establish a similar baseline for all datasets. *Trimble Business Center* (version 2.6) was used to process all DGPS ground survey data (i.e. GCPs).

2.3.4.1 PC analysis

Along with basic statistical analysis (Table 2.2) of all PCs and DEMs, the *Geostatistical Analyst* toolkit in *ArcMap (Version 10.2.2)* was used for a range of additional spatial analytics. The workflow utilized throughout this chapter follows that outlined by the *Geostatistical* Analyst toolbox within *ArcMap* (*Esri*, 2001) as well as following steps used by (*Erdoğan*, 2010) . Spatial data exhibit two main properties a) geographic features tend to contain similar values (spatial autocorrelation) b) processes involved locally behave differently than those located in different portions of any given area (non- stationary) (*Esri*, 2001). These properties were investigated using exploratory spatial data analysis tools in order to gain insights into the data and which ultimately assisted with selecting proper parameters for each interpolation method. Prior to interpolation, each PC dataset was assessed for normal distribution, spatial variability using Voronoi maps, spatial trends, and for spatial dependence which are all very important characteristics of spatial data. Through this initial step we were also able to locate outliers and remove them from the datasets to help maintain clean PCs. Next, cross-validation was implemented on all 3 PCs using the kriging approach prior to interpolation in order to depict which parameters provided the most accurate predictions. This validation procedure omits one data point at a time from the PC, performs the interpolation and predicts the value for that geospatial location based on surrounding data points, calculates the residuals between the predicted and measured values and finally exports them as a separate PC dataset that represents errors and from which the standard error surface maps

(SESMs) are created. Normally, the best predictor should have a mean error (ME) close to 0, root mean squared error (RMSE) and average standard error (ASE) as small as possible, and the root mean squared standardized error should be close to 1 (*Esri*, 2001). Final selected cross-validation results for each platform analyzed with the EBK algorithm are shown in Table 2.3. The global extent of error clustering, which measures the degree of clustering for either high or low values, were examined using the *high and low clustering* (Getis-Ord general G) and the *spatial autocorrelation* (global Morans I) spatial statistics tools. These methods however, assume uniform error throughout the entire DEM surface and are, therefore, problematic when modeling heterogeneous terrain such as tundra landscapes which are characterized by spatial variability which could lead to errors in modeling (*Chaplot et al.*, 2006; *Erdoğan*, 2010). Therefore, local spatial distributions and data density patterns of each PC were also investigated by employing the *cluster and outlier analysis* (Anselin local Morans I), and *hot spot analysis* (Getis-Ord's Gi*) tools.

In order to explore the accuracy of elevation values from each PC prior to interpolation, two buffers of 10 cm and 20 cm radius were created around each GCP. Points that geographically fell within these two buffers were extracted from each PC, and values were compared to the GCP elevation values using correlations. Since the accuracies and ground resolution of the DGPS systems utilized to capture the coordinates for each GCP are survey grade (mm-cm) these data was used as a reference for comparing accuracies of PC elevation values from all platforms. These accuracies were determined using Pearson's correlations and linear regression models between the reference GCP points and all measured datasets.

2.3.4.2 DEM analysis

The *Topo to Raster* and *Geostatistical Analyst* tools within the *ArcGIS* package were employed to interpolate DEMs from post-processed ASCII PCs (*i.e.* T-LiDAR, KAP, and A-LiDAR; Figure 2.3). The aforementioned tool offers an interpolation procedure specifically designed to produce hydrologically correct digital elevation models using the ANUDEM algorithm (*Hutchinson et al.*, 2011), which is well suited to the relatively low-gradient and heterogeneous topography of the study area and the primary objectives of this study. We also explored another method, namely the Empirical Bayesian Kriging (EBK) method within the *Geostatistical Analyst* toolkit, which offers a number of analytical tools, such as cross validation and standard error surface maps (SESM) that visually highlight predicted versus field-measured values and regions

of high error (Figure 2.3) (*Krivoruchko*, 2004). This method facilitated the calculation of uncertainty associated with the predicted or modeled elevation values and results were used to further explore relationships with surface parameters. All final DEMs were resampled to have a 25 cm pixel size prior to DEM statistical analysis to improve inter-comparison efforts.

It seemed intuitive that terrain characteristics have a great influence on accuracy of modeled DEMs. Studies such as those from (*Gao*, 1997) suggest that DEM errors are lower in terrain that is less complex. Similarly, results from (*Hunter and Goodchild*, 1997) point to error being related to the steepness of the terrain slope. To determine if terrain characteristics such as slope, curvature and aspect have any influence on DEM surface interpolated errors and to determine whether or not these parameters can help explain elevation value variations, Ordinary Least Squares (OLS) and Geographically Weighted Regression (GWR) analysis were applied to all DEMs using a method similar to that employed by *Carlisle*, (2005) and *Erdoğan*, (2010). For both regressions used, the DEM error was used as the dependent variable while elevation, slope, curvature and aspect were used as the independent variables. Slope is normally used to determine steepness of a surface and calculates rate of change from one pixel to its neighboring pixels, while curvature is said to be the slope of the slope (i.e. convex or concave). Aspect identifies the down slope direction of the slope from one pixel to its neighboring pixels therefore exploring these characteristics further was crucial in order to depict DEM capabilities. Additionally to OLS and GWR, 2 datasets of 1000 and 5000 random points were created and placed over each DEM surface and elevation values from each were extracted at those point locations. Pearson's correlations and linear regression were calculated between terrain characteristics and standard error values acquired from these locations and are summarized in Table 2.6.

To assess the resulting DEM elevation values and how they compare to one another, these same random point datasets were used to compare values at the exact same geographical locations. The datasets were created within the BE DEM site and positioned over each interpolated DEM, then coordinates including elevation values from the DEMs were extracted at each random point location and plotted against one another to visualize correlations between elevation values derived from each remote sensing platform at all random point sampling locations (Table 2.9). Pearson's correlations and linear regression models were used for quantifying relationships between these datasets.

Resulting DEMs from the A-LiDAR, KAP and SSI platforms were also subtracted from the T-LiDAR DEM to quantify DEM difference (DoD) maps in efforts to improve understanding of error distributions by visually depicting areas of corresponding and differing areas of elevation values between models (Figure 2.3). Additionally, each DEM was also analyzed for the capacity to model tundra surface hydrology by exploring surface water flow direction and drainage systems using the *ArcHydro toolkit* and following workflows of *ESRI*, (2013) and *Li*, (2014).

2.4 RESULTS

The field survey for the T-LiDAR system yielded high alignments between each of the five scan positions and reflector targets (standard deviations: <0.002 m, 0.002 m, 0.001 m, 0.001 m, and 0.002 m) and registration with target GPS points had standard deviations of 0.006 m (n = 5), indicating a highly accurate survey was achieved. Similarly, Aerometric reported a RMSE of 0.143 meters, p= 0.05 for the A-LiDAR survey and combined separation results showed an approximate 0.02 m and 0.04 m horizontal and vertical error respectively for the aircraft GPS and IMU data. After alignment of all kite-based images a ground resolution of 0.5 cm/pixel was reported from the *Agisoft Photoscan* software.

The cost of each system was also considered in order to assist future studies with decision making of what system is appropriate for the desired analysis at hand. Overall the cost of the KAP system is by far the most cost-effective approach that can yield highly accurate and high resolution models with an average cost of about $500 US dollars depending on camera and rig casing utilized. The cost of the particular system used for this study was slightly over the average cost since the camera used was equipped with characteristics to facilitate sensing in the Arctic. Additionally, the ease of execution of this system allows for multi-temporal sampling at high frequencies with little to no cost per acquisition, which is an advantage over the T-LiDAR and A-LiDAR systems where costs per acquisition are expensive especially for studies in the Arctic. Another advantage of the KAP system over the LiDAR and SSI approaches is the shorter PC and DEM processing times, however this does depend on the ability of computational power available.

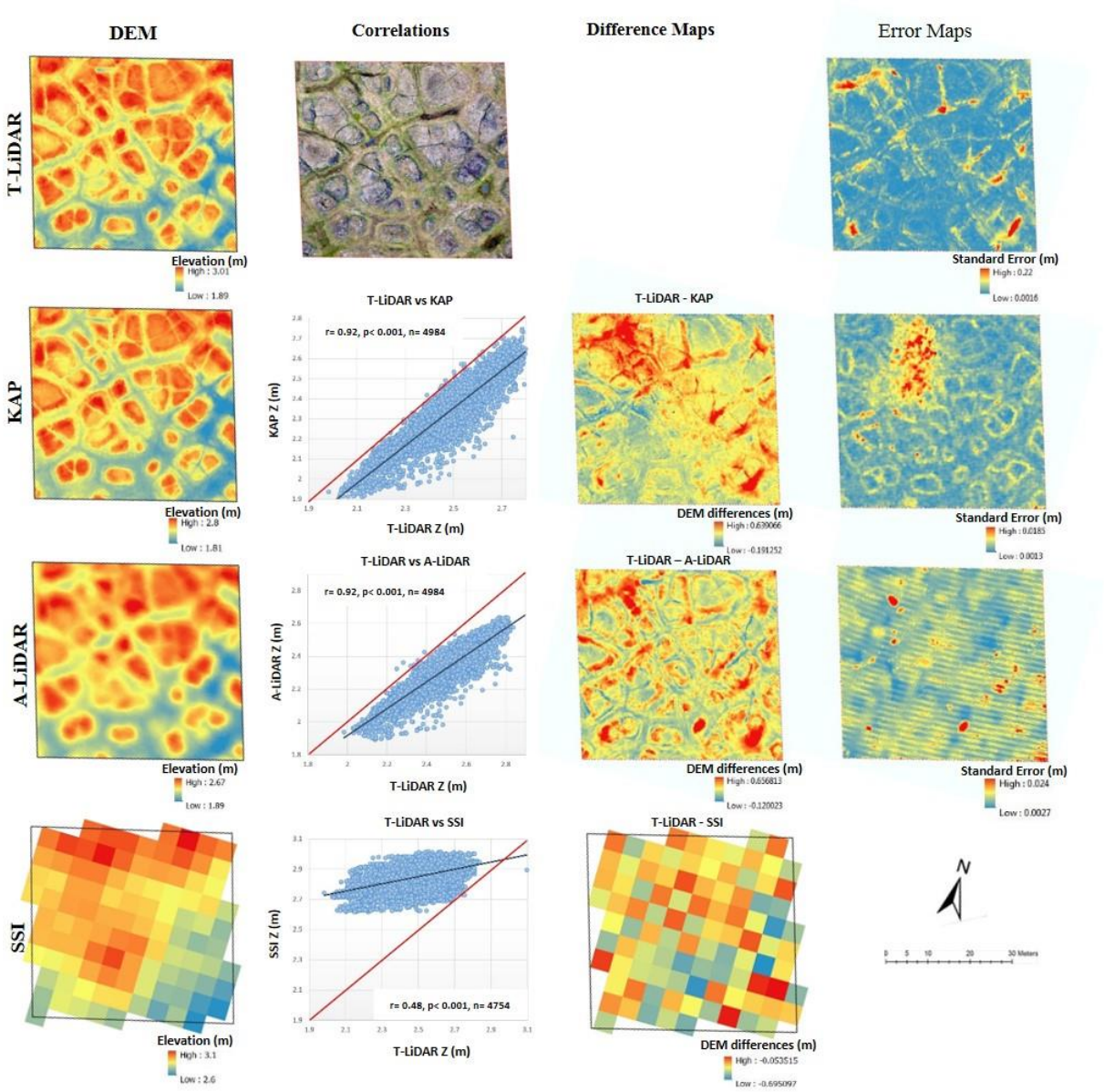

Figure 2.3: Shown from left to right: final EBK interpolated DEMs, kite-based aerial image of BE DEM site and inter-platform Pearson's elevation correlations (red line depicts 1:1; elevation (Z) values are in meters), differences between final DEMs (all DEM surfaces were subtracted from the T-LiDAR DEM which was used as the reference surface) and standard error maps highlighting areas of uncertainty for each approach.

2.4.1 Point Clouds

The majority of ecosystem studies focus on processes occurring at spatial scales ranging from plot to landscape levels and this study has assessed the capacity of the KAP system to provide an inexpensive solution to assist in monitoring at these scales. Initially, basic statistics of each PC were calculated and are summarized in Table 2.2 along with calculated statistics for final DEM surfaces. Cross validation was then applied to each PC to assist in calculating proper parameters needed for accurate interpolation of surfaces. Table 2.3 displays cross-validation results for each method used.

Table 2.2: Summarized are basic statistics of each calculated PC and corresponding final interpolated DEM surface for all approaches. Values pertain to those that fell within the BE DEM study site only (0.25 ha).

	Point Cloud							DEM		
Method	Total Pts (0.25 ha)	Point Density (pts/m2)	Mean PC Z (m)	Median PC Z (m)	St. Dev.	Kutosis	Skewness	Max DEM Z (m)	Min DEM Z (m)	Mean DEM Z (m)
T-LiDAR	2,646,804	1059	2.47	2.4	0.16	2.73	-0.11	3.01	1.89	2.45
KAP	2,122,596	850	2.33	2.33	0.164	2.23	-0.141	2.8	1.81	2.31
A-LiDAR	36,284	15	2.3	2.3	0.154	2.4	-0.31	2.67	1.89	2.28
SSI	NA	NA	NA	NA	NA	NA	NA	3.1	2.6	2.85

Table 2.3: EBK cross-validation results for each platform.

Method	Mean Error (m)	Mean Stand. Error (m)	RMS Error (m)	RMS Stand. Error (m)	Avg. Stand Error (m)
T-LiDAR	0.00019	0.00346	0.02373	1.0709	0.02608
KAP	-7.11E-08	-6.51E-07	0.00482	0.13776	0.03503
A-LiDAR	-0.00002	-0.0003	0.0114	0.35148	0.03447

Once these parameters were calculated each PC dataset was processed using both the EBK and ANUDEM interpolation methods described in section 2.4.2 below. The interpolation results yielded two surfaces for each dataset analyzed, namely a final interpolated surface representing elevation models and the other was a corresponding SESM which was calculated from the cross-validation process (see Figure 2.3). We explored the error PCs produced by the cross-validation process further, in order to examine the density of errors, by applying global spatial autocorrelation and clustering metrics to all error datasets. Global Moran's I (spatial autocorrelation) indices

displayed positive values for all datasets suggesting all PCs displayed clustering of error values. The Getis-Ord General G (high/low clustering) method was also used to measure the degree of clustering for either high or low values. This tool yielded positive z scores suggesting high error values were clustered for all PCs. Both of these methods highlighted a clustering of error values for all datasets, however since they represent global measures across the entire study area, they lack the capacity to pinpoint where exactly these clusters are located. Consequently, similar local measures were then applied to the datasets to aid in visualizing the magnitude and locations of error clusters across all datasets. The Anselin Local Moran's I (cluster and outlier analysis) and the Getis-Ord Gi* (hot spot analysis) tools helped to identify local spatial clusters of features containing high or low error values. Both local spatial tools yielded similar results for all error PCs. The T-LiDAR dataset had the greatest error clustering in troughs and low-lying wet areas while lowest error clustering occurred on high centered polygon regions. Outliers were mostly located along transition areas between slopes and ridges. The KAP dataset displayed random high error clustering mostly around ridges and sloping terrain, while low error values were mainly located in troughs with very few outliers scattered randomly throughout the BE DEM site. The A-LiDAR system captured data that seemed to display clusters of high errors in both low-lying troughs and high centered polygon locations and low error clustering were observed to be mostly randomly dispersed. Outliers were also randomly distributed throughout the study area for the A-LiDAR system. Based on the results from the cluster and outlier analysis, error vales seemed to depend mostly on land surface structure as expected for datasets acquired from all remote sensing platforms. All spatial statistics values reported above were statistically significant with a $p \leq 0.01$.

Due to the high accuracy of the DGPS system used to acquire the GCP coordinates and following methodologies of other studies, it seemed reasonable to compare PC elevation values to GCP elevation values that were spatially proximal (i.e. cm apart) for all datasets. According to the correlation coefficients summarized in Table 2.4 and linear regressions displayed in Figure 2.4, PC elevation values from the T-LiDAR and KAP system correlated strongly with GCP elevation values ($r= 0.99$, $n= 23$; $r= 0.99$, $n= 25$, $p<0.001$) and ($r= 0.97$, $n= 29$; $r= 0.97$, $n= 29$, $p< 0.001$) for both buffers (10 and 20 cm) respectively. While values for the A-LiDAR system were slightly less correlated resulting with values of $r= 0.88$, $n= 11$, $p<0.001$ for the 10 cm buffers and $r= 0.93$, $n= 21$, $p<0.001$ for the 20 cm buffers. The RMSE values are also reported for each method and suggest that the KAP dataset is generally more approximate to the GCP dataset given the lower RMSE

(0.056 meters) and mean residuals (0.0037 meters) between the measured (GCP) and predicted (PC) values. Moreover, Figure 2.4 helps visualize that the T-LiDAR system seems to be over-estimating elevations based on the regression line shift from the 1 to 1 line, where higher over-estimation seems to occur in areas of lower elevations and lower over-estimation in higher elevation areas (high-centered polygon). The KAP regression line follows the 1 to 1 line more closely throughout all high and low elevation values, while the A-LiDAR regression line seemed to over-estimate in lower elevations while under-estimate in higher elevations. Out of the 31 total GCP buffers created (excluding the GCPs located on the perimeter of the study site), points from the A-LiDAR system fell within 11 GCP buffers for the 10 cm and 21 buffers for the 20 cm sized buffer, while points from the T-LiDAR system fell within 23 and 25 buffers for both sizes respectively. Alternately, KAP PC points fell within 29 buffers for both sizes used for the analysis. The results from this analysis also suggests that the statistical variation experienced in the GCP elevation data can be greatly explained by elevation values acquired by all three explored datasets (T-LiDAR, A-LiDAR and KAP).

Table 2.4: Correlation coefficient results between point cloud elevation and GCP elevation values acquired within 2 buffers surrounding each GCP (10 and 20 cm) and calculated for each dataset.

Method	10 cm buffer					20 cm buffer				
	r	p	n	RMSE	Mean Residuals	r	p	n	RMSE	Mean Residuals
T-LiDAR	0.99	<0.001	23	0.1290165	-0.118314	0.99	<0.001	25	0.131101	-0.12086
KAP	0.97	<0.001	29	0.0585397	0.003711	0.98	<0.001	29	0.058369	0.004824
A-LiDAR	0.88	<0.001	11	0.1250843	0.030261	0.93	<0.001	21	0.106564	0.035465

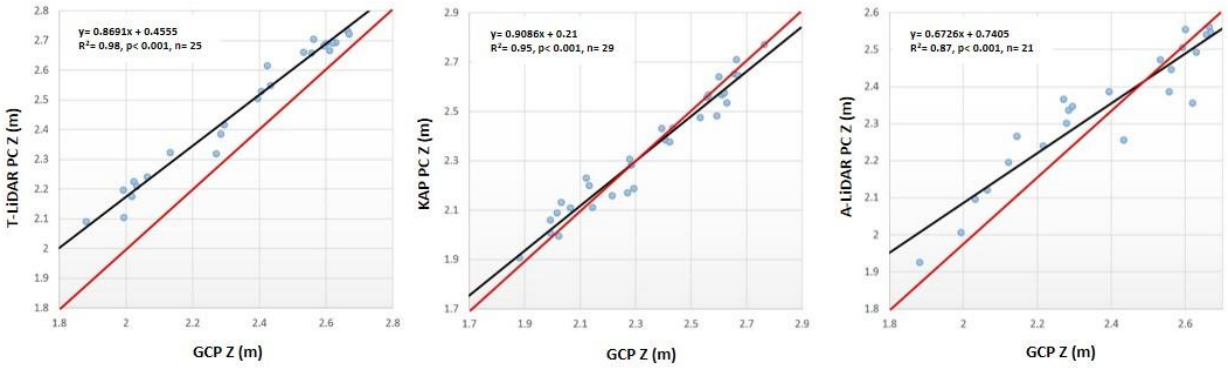

Figure 2.4: Simple linear regressions between GCP elevation and each PC dataset elevation (meters) acquired from T-LiDAR, KAP and A-LiDAR for 20 cm buffers. The red line depicts 1:1 relationship between the variables. Additionally, the 10 cm buffer data displayed similar results (not displayed).

2.4.2 DEMs

As described in section 2.3.4.2, in order to visualize the distribution of error within the study site, SESM were generated and examined further (Figure 2.3). All platforms displayed uncertainty related to predicted values differently. The EBK algorithm calculated that the T-LiDAR and A-LiDAR datasets both showed high error values clustered mostly in or near low-lying troughs and ponds, while KAP displayed one main cluster of error values located in the north western section of the study area. Flight path lines and spotting are clearly seen throughout the A-LiDAR SESM. Additionally, utilizing the SESMs and final DEMs, values were extracted from each final surface using the locations of the random sampling datasets and correlations were calculated in order to test the measure of strength and relationship between elevation and error. Based on this analysis, there seems to be no correlation between DEM elevation values (e.g. Z) and DEM error for any of the datasets (Table 2.5).

Table 2.5: Correlation coefficients between elevation and standard elevation errors from the 5000 random points sampling dataset for all platforms utilized in this study. The results from the smaller 1000 random sampling dataset were similar and are not displayed.

Method	r	p	n
T-LiDAR	0.01	0.3811	4983
KAP	0.08	2.33E-08	4987
A-LiDAR	-0.088	4.50E-10	4986

Results from the PC spatial pattern analysis suggest that elevation errors might be greatly influenced by terrain microtopography. Therefore, the relationship of the DEM standard errors and the characteristics of the landscape were observed by calculating terrain characteristic surfaces such as slope, curvature, and aspect from each final interpolated DEM. Again, using the random sampling datasets, values from each of the terrain surfaces were extracted and correlation coefficients were analyzed between each and the standard error surface data and are summarized in Table 2.6. These results suggest that slope derived from all datasets could explain elevation error slightly better than curvature and aspect, however these results displayed very weak associations, some of which are not statistically significant and alone could not explain the variation seen in elevation error. Due to the nature of these terrain parameters and what they describe these results were expected and lack the potential to explain uncertainties of accuracy and error at high spatial resolutions.

Table 2.6: Correlation coefficients between individual terrain parameters and standard error values acquired using the 1000 random point sampling dataset. The results from the larger 5000 random sampling dataset were similar and are not displayed.

Method	Slope r	Slope p	Curve r	Curve p	Aspect r	Aspect p
T-LiDAR Z Error	0.19	<0.001	0.07	0.04017	-0.02	0.52
KAP Z Error	0.43	<0.001	-0.011	0.7106	-0.07	0.01985
A-LiDAR Z Error	0.33	<0.001	0.06	0.07274	-0.05	0.1015

Combining all parameters (i.e. slope, curvature, and aspect) was assumed to help explain terrain standard error values slightly better than when DEM error values are being compared to

terrain parameters individually, hence, a multivariate OLS regression model was applied to explore this further (Table 2.8). Even though these models demonstrate that error can be explained slightly better using the combination of terrain parameters, these relationships seem to be more complex than expected. Results from the OLS models concluded that all explanatory variables (i.e. terrain parameters) calculated were statistically significant based on the T-test, robust T, probability, and robust probability model analysis, which suggest these results are compromised by multicollinearity. Specifying a multiple regression model using highly correlated predictor variables can only indicate how well all as a whole they can predict the dependent variable but fail to give any valid information about individual exploratory variables. Furthermore, the Koenker statistic determines whether the independent variables (e.g. elevation, slope, curvature, aspect) have a consistent relationship with the dependent (e.g. standard error) variable. All platforms rejected the null hypothesis of stationarity (values 84-757, $p< 0.05$) in favor of non-stationarity, meaning that surface processes behave differently in different parts of the study area, which is expected to occur over highly irregular thermokarst terrain. The Jarque-Bera statistic is an indicator of whether or not the residuals are normally distributed and was used to measure model bias. Based on these statistical results, (values 19,056- 431,223, $p<0.05$) and on global spatial autocorrelation analyses (Table 2.7), all residuals were not normally distributed, ultimately rejecting the null hypothesis due to a biased OLS model for all datasets indicating that the models are incapable of demonstrating spatial variability and ultimately suggests that local (i.e. GWR) rather than global methods are used for such complex landscapes. The numerous spatial statistics and applied regression models mentioned previously provide insight to the relationship between tundra surface characteristics and the final elevation error values resulting from the DEM interpolation algorithms. However, the calculations for the majority of these methods are based on the assumption that the processes being explored are constant over the study area and that the OLS model is representative of each point within the study site and therefore the relationships are uniform throughout. Other studies suggest that with respect to spatial data, these types of assumptions are not valid and DEM errors are more closely related to terrain surface and are more spatially complex than simple uniform error distributions as those suggested by OLS regression and global spatial statistics (*Desmet*, (1997); *Fisher*, (1998); *Chaplot et al.*, (2006); *Erdoğan*, (2010)). Considering these processes and the surface complexity of arctic landscapes results

provided by the OLS regression model suggests a lack of ability to explain elevation error and related uncertainty.

Table 2.7: Global Moran's Index of residuals for the OLS and GWR models of each method used for this study.

Method	OLS			GWR		
	Moran's Index	Expected Index	Z-score	Moran's Index	Expected Index	Z-score
T-LiDAR	0.902978	-0.000024	259.587708	0.600227	-0.000024	172.550979
KAP	0.894649	-0.000024	257.211863	0.592073	-0.000024	170.23107
A-LiDAR	0.807177	-0.000024	232.061248	0.680068	-0.000024	195.507736

Hence, GWR was utilized to explore these relationships in more depth considering its ability to analyze whether relationships among variables vary from point to point (local variability), making this an especially useful tool for analyzing each models terrain parameters and their relationship to local errors. Figure 2.5 shows the spatial distributions of the GWR parameters (e.g. elevation, slope, curvature and aspect) in modeling standard error values throughout the study site. Over and under-predictions, for the most part, seem to be randomly distributed except for limited locations throughout some parts of the study area where clustering of GWR values is apparent. The majority of the clustering of standard residual values (uncertainty) was mostly observed within low lying troughs and slopes for both LiDAR systems and random clustering was seen for the KAP system. GWR yielded better correlations than the OLS models between the predictor variables and the outcome variable. The GWR analysis summarizes that the elevation, slope, curvature and aspect terrain characteristics can explain about 78% of the variability in elevation standard error values for the T-LiDAR DEM, between 82% for the KAP modeled surface, and between 49% for the A-LiDAR surface. Final OLS and GWR correlations are summarized in Table 2.8 below.

Table 2.8: OLS and GW regression and corresponding AICc values between combined terrain parameters and standard error values for each platform utilized. Standard error was the dependent variable, while elevation, slope, curvature and aspect were utilized as exploratory variables for both regression approaches.

Method	OLS R^2	AICc	GWR R^2	AICc
T-LiDAR z Error	0.03	-208167.21	0.78	-265721.41
KAP Z Error	0.18	-454138.71	0.82	-512524.97
A-LiDAR Z Error	0.12	-432846.17	0.49	-454510.54

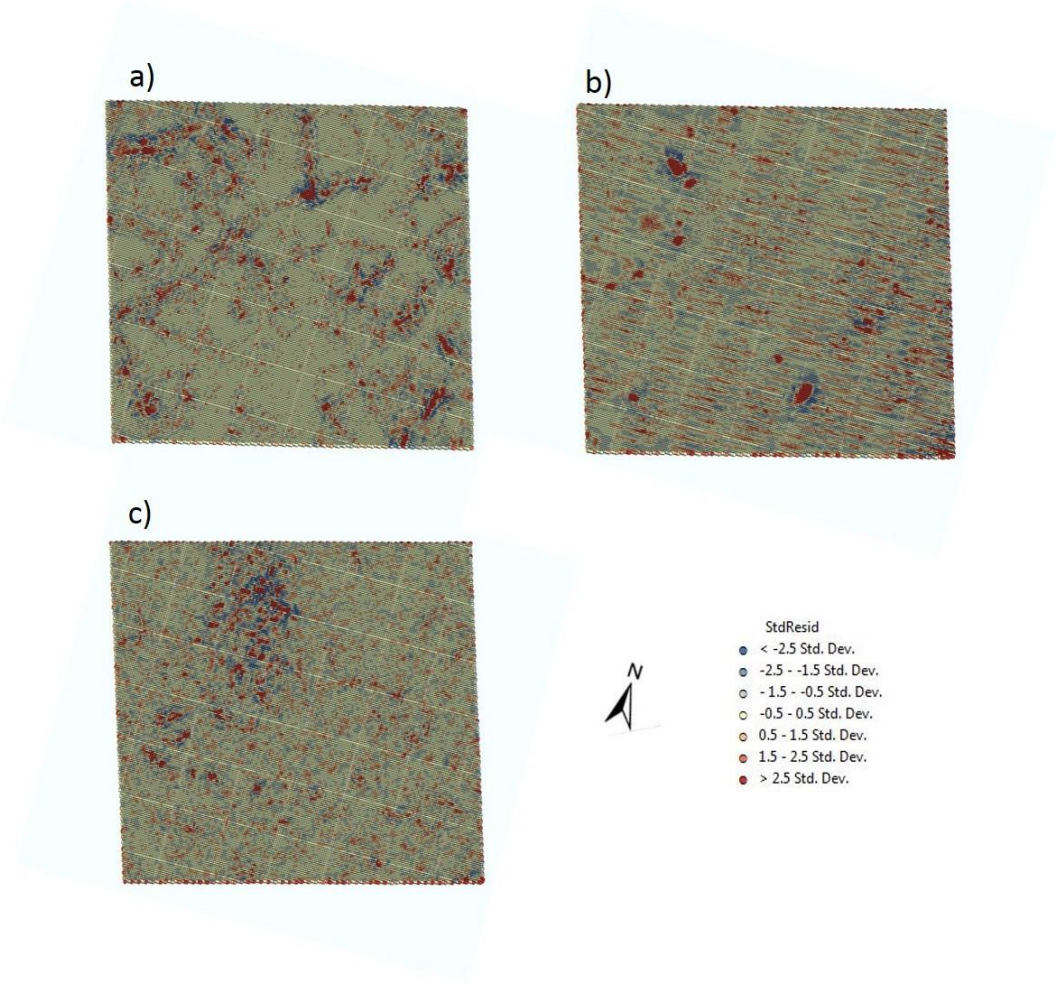

Figure 2.5: Spatial distributions of GWR parameters (elevation, slope, curvature, and aspect) in modeling standard error for each approach a) T-LiDAR, b) A-LiDAR, and c) KAP datasets.

In addition to local parameter values the GWR tool calculated diagnostic statistics such as local R^2 values for each relationship throughout the BE DEM site. Traditionally, this statistic is used as a measure of model performance, ultimately explaining the proportion of variance of the dependent variable accounted for by the model *Esri*, (2001). Using these data, local R^2 maps were produced in order to visualize the areas and variables (terrain parameters) that might be responsible for the variation in the dependent variable (standard error), or suggest the possibility of missing explanatory variables (i.e. surface roughness) within the model. Figure 2.6 depicts local R^2 maps for both LiDAR datasets and the KAP system. The map produced from the T-LiDAR platform displays values ranging from low (0.000675) in low lying areas and troughs, to moderately high (0.77) within high centered polygon areas. The A-LiDAR system map also contained very low values (0.000109) in the low-lying areas, to moderate values (0.43) where high centered polygons are present. Similarly, the R^2 map generated from the KAP dataset provided the largest range of values consisting of very low values (0.000173) in low lying areas where ponds and troughs are present, to high values (0.82) along ridges and on high-centered polygons. Using this regression approach, all three remote sensing platforms displayed the capacity to explain elevation error variability using elevation, slope, curvature and aspect as explanatory variables in the same way, however with slightly different resolutions as expected (Table 2.8; Figures 2.5 and 2.6).

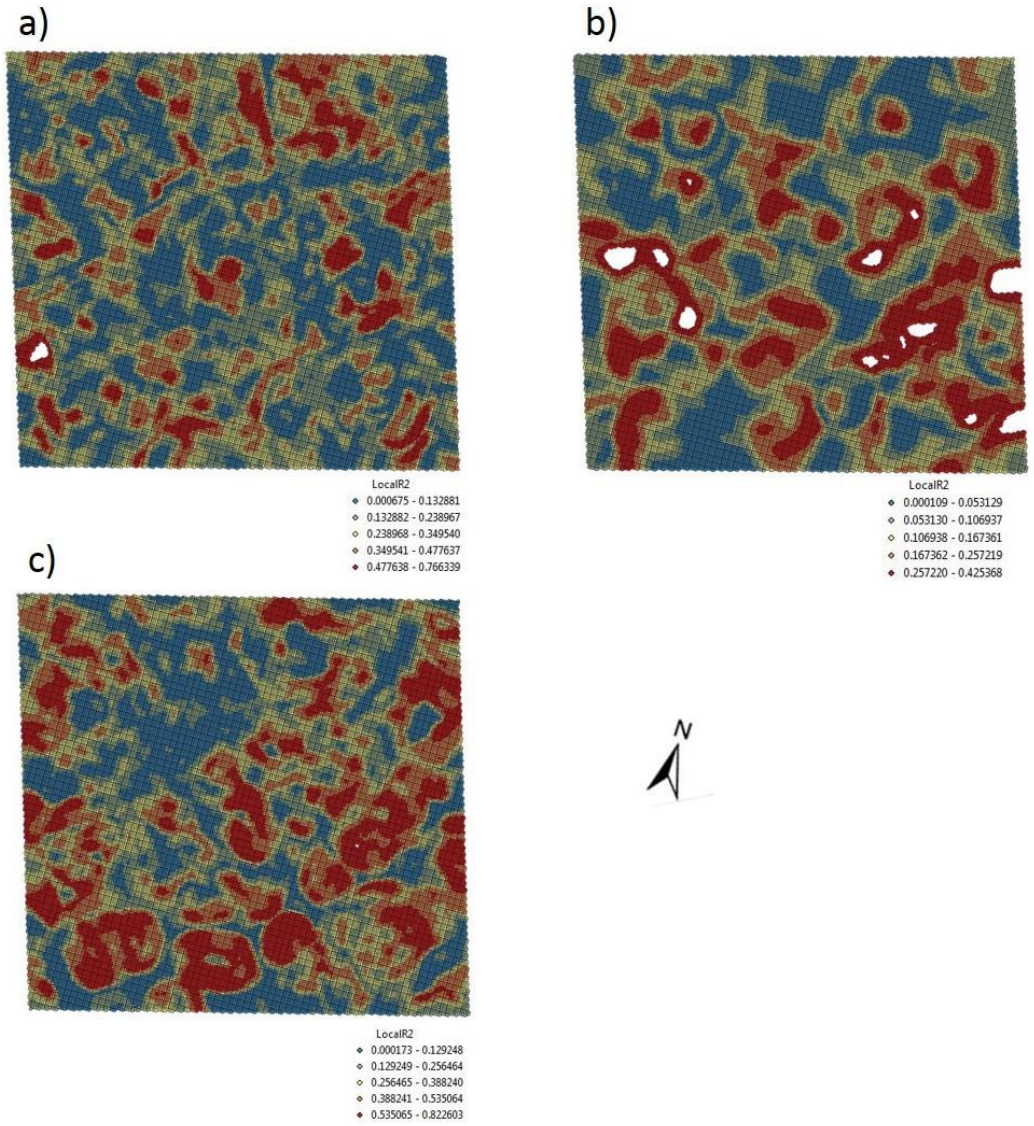

Figure 2.6: Spatial distributions of local correlation coefficients (R^2 values) between independent variables (e.g. elevation, slope, aspect, and curvature) and dependent variable (e.g. standard error) for the a) T-LiDAR, b) A-LiDAR, and c) KAP datasets.

The next step was to analyze how well the final modeled DEM elevations compared to the T-LiDAR DEM elevations as this platform was used as the reference considering the close proximity of sampling and high accuracy of the system. As seen in Table 2.9 below, correlations were highest between KAP and A-LiDAR elevation values (r= 0.8642, p<0.001, n= 993 and r=

0.8507, p< 0.001, n= 4985) using the EBK interpolation method, while KAP and T-LiDAR had the strongest correlations (r= 0.8642, p< 0.001, n= 994 and r= 0.8624, p<0.001, n= 4983) for the ANUDEM interpolation approach, although the EBK method also displayed strong correlations results. The SSI platform had the strongest correlation with the A-LiDAR platform resulting with r values of 0.3711 and 0.3757 (p< 0.001, n= 936, n= 4752) for the ANUDEM method and 0.2991 and 0.3139 (p<0.001, n= 937, n= 4755) for the EBK method. DEM elevation value correlations between the SSI system and T-LiDAR were the lowest (ANUDEM: r= 0.2321, p< 0.001, n= 938 and r= 0.2477, p< 0.001, n=4757); EBK: r= 0.2083, p< 0.001, n= 937 and r= 0.2276, p< 0.001, n= 4754) when compared to the other two platforms. Overall, the SSI DEM resulted with low correlations between all other DEMs, while the T-LiDAR and KAP DEMs seemed to model elevation very similarly.

Table 2.9: Matrix tables depicting cross-platform correlation coefficients between final DEM elevation values extracted from the 5000 random point sampling dataset. Similar results were observed for the smaller 1000 point dataset but are not summarized here.

EBK 5K	KAP	A-LiDAR	T-LiDAR	SSI
KAP		0.85	0.84	0.22
A-LiDAR			0.84	0.31
T-LiDAR				0.23
SSI				

ANUDEM 5K	KAP	A-LiDAR	T-LiDAR	SSI
KAP		0.85	0.86	0.25
A-LiDAR			0.85	0.38
T-LiDAR				0.25
SSI				

In order to visualize the locations of elevation differences between the DEM surfaces, a simple raster subtraction was applied between the T-LiDAR DEM and the other three DEMs (Figure 2.3), once again with the intent of using this DEM as the reference and standard for comparison. The strongest contrast between elevation values for the T-LiDAR and KAP surfaces were seen within the highly clustered error values displayed from the KAP platform in the northwestern region of the grid, as well as along ridges and within troughs in some areas. Differences between T-LiDAR and A-LiDAR DEMs were seen in both high and low-lying areas, with the majority of low error values being located within troughs, and the higher differences were located on-top of high-centered polygons. Given the low spatial resolution of the SSI dataset, differences between the T-LiDAR dataset were not clear.

Two main components define the behavior of a certain terrain and related surface water dynamics, namely the flow direction that defines the movement of surface water throughout the terrain and the drainage system made up of drainage areas and how they are connected. These processes are poorly understood in arctic ecosystems and methods for modeling complex surface water dynamics as a result of climate variability is needed. We explored the ability of each final EBK and ANUDEM interpolated surface model to predict surface water drainage lines and flow accumulation, and catchment boundary locations (Figures 2.7 and 2.8). The ANUDEM produced DEMs showed that the T-LiDAR and KAP platforms seemed to model drainage and flow very similarly with slight differences mostly between high centered polygons. The resulting catchment boundaries differed mostly around the edges of the DEM site boundary. The A-LiDAR and SSI DEM were not able to model all the drainage and flow lines, or delineate the catchment boundaries identified by the T-LiDAR and KAP systems. The EBK derived DEMs not only produced more detailed surfaces than the ANUDEM but as a result drainage flow, direction and catchment boundaries from the surface hydrology analysis followed those modeled by the T-LiDAR derived DEM. Specifically, these drainage lines extended further into the low lying troughs and catchments boundaries and followed more precise lines between high centered polygons and ridges.

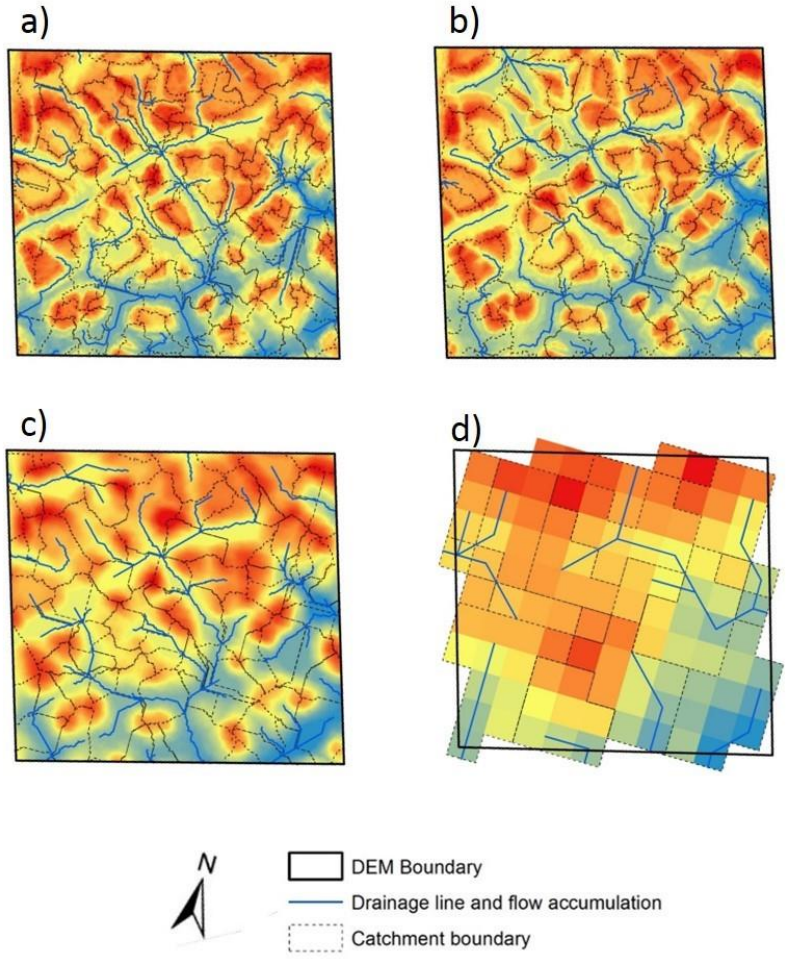

Figure 2.7: Hydrology maps showing final EBK DEMs with corresponding drainage lines and flow accumulation locations and catchment boundaries for the a) T-LiDAR, b) KAP, c) A-LiDAR, and d) SSI datasets.

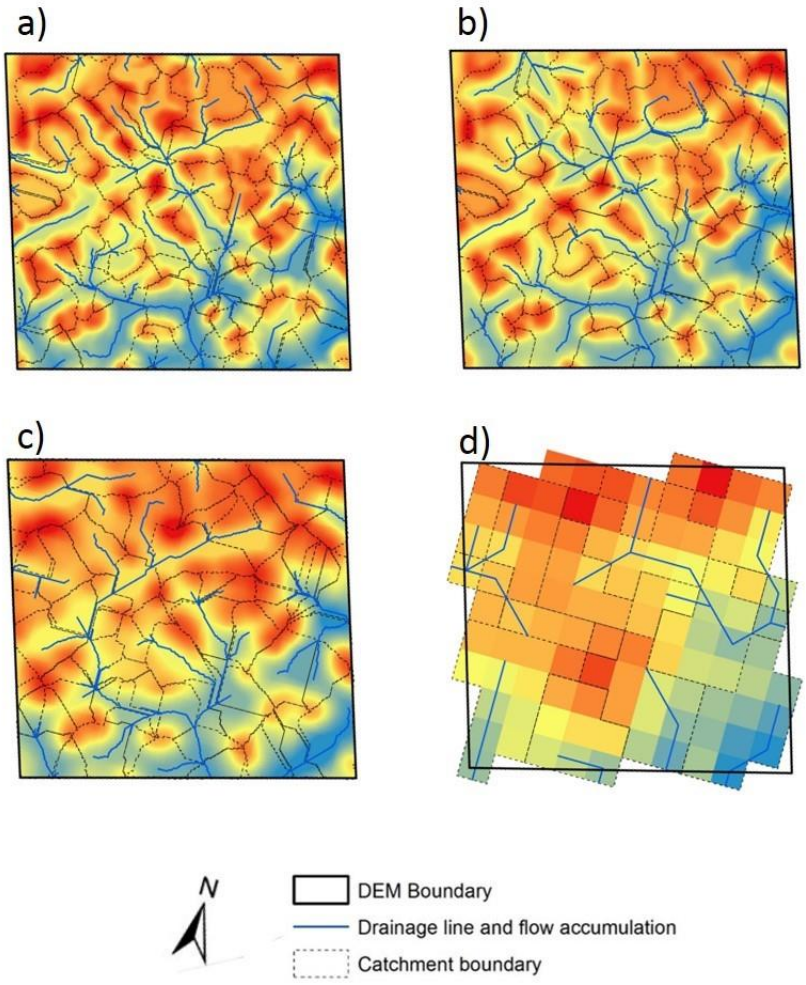

Figure 2.8: Hydrology maps showing final ANUDEM DEMs with corresponding drainage lines and flow accumulation locations and catchment boundaries for the a) T-LiDAR, b) KAP, c) A-LiDAR, and d) SSI datasets.

2.5 DISCUSSION

Advanced ice-wedge degradation has been predicted to alter surface water balance, reducing inundation and increasing run-off across most of the Pan-Arctic (*Liljedahl et al.*, 2016). Not only is it important to understand how these process will respond to projected climate variability but methods for monitoring and modeling such processes are also needed. Key findings from this study highlight the potential of using low-cost small-format aerial platforms (i.e. KAP) to model small-scale arctic tundra landscapes (1 ha) with high precision and resolution and how resulting data products are comparable to those derived from traditional remote sensing platforms.

A main object of this study was to model a highly thermokarsted high-arctic tundra landscape using various remote sensing methods and assess each on the following criteria which are important factors for ecosystem studies and key findings are summarized in more detail below 1) overall cost of the system including cost per survey 2) accuracy of each approach relative to reference data (GCPs) 3) capacity to depict true ground terrain and related errors 4) capacity to model surface hydrology and surface energy balance parameters 5) skill sets needed to execute each approach.

2.5.1 T-LiDAR

The T-LiDAR system is able to capture three dimensional measurements quickly and with high precision across small to mid-scale study areas. The capacity of this system to model the tundra terrain across a 0.25 ha study area was fairly accurate according to the PC vs. GCP elevation analysis which resulted with strong correlations between the reference GCP data. Additionally, the resulting surface model produced from the T-LiDAR system was used to model surface hydrology and terrain parameters of the BE DEM site, which facilitated the understanding of microtopographic processes that contribute to surface energy balance. This approach also offers the ability to include RGB intensity values coupled with each point acquired from an optional DSLR digital camera which offers additional data across the study site.

The learning curve on how to operate this system is rather large and requires understanding of geographical information systems (GIS) and geodesy, understanding of laser scanners and software packages used to execute equipment, and field-setup (these systems tend to employ bulky and heavy equipment which normally require extra man-power during field surveys), data collection and data handling. The most important of which is the latter, since large volumes of data are produced from these systems and knowing how to handle and ultimately having the proper computing power to process the data is critical. The cost of a LiDAR system (including hardware for data processing) is relatively expensive in addition to the added cost of multi-temporal studies which are crucial for monitoring ecosystem responses to climate variability in the Arctic. Even though the accuracy of the T-LiDAR PC was quite high based on the GCP elevation analysis, the regression line seemed to be off the 1 to 1 line, suggesting that this laser system is over-estimating true elevation values throughout the thermokarst landscape. Additionally, results from the spatial clustering analysis suggests that this approach showed high error clustering throughout low-lying

areas and troughs which are mainly dominated by graminoids and inundated with surface water forming ponds in some cases. The cause of these errors might be due to the view angle (~ 2 meters above the surface) of the scanner limiting the coverage of the low-lying troughs and drastic sloping polygon sides. The high resolution and accuracy of this system might be counter-productive in the case of representing topography for these types of ecosystems where grasses are characteristic of the landscape. Given the view angle of the system and the canopy structure and leaf area of the plant species present across the troughs and wet cover this approach might be capturing the leaves of these species which could be another cause of error when all laser returns are used for analysis such as in this study. The light being emitted by the scanner can possibly be affected by water vapor in areas of high humidity or those that experience evaporation fog which is caused when cold air passes over warmer areas consisting of high moisture and could also be a possible source of error when using this system over these particular ecosystems. A possible solution to the lack of spatial coverage with this system is to position the scanner slightly higher during future acquisition as well as scan the study area from more positions to ensure coverage of all areas. These issues pose the question of whether or not this system is ideal for capturing microtopography of highly thermokarsted arctic tundra terrain and whether or not they are better suited for application across other ecosystems. This approach is limited in its capacity to cover large areas frequently (>300 meters) and might perform better for inter-annual studies spanning small to mid-scale areas.

2.5.2 KAP

The kite photography system produced a high resolution and accurate PC and DEM, that contained very low error values and that correlated well with the T-LiDAR produced model as well as with the GCP elevations values. The linear regression model followed the 1 to 1 line closely and suggests accurate measurement of elevation values when compared to the GCP data. This system can easily be executed multi-temporally with minimal knowledge of remote sensing and photogrammetry at a fraction of the cost of executing other traditionally applied approaches (T-LiDAR and A-LiDAR). This photogrammetric approach was able to acquire high density data points that captured all areas of the study site including those low-lying troughs and ridges which resulted to be problematic locations for the other approaches explored. Moreover, terrain parameters and hydrological modeling was possible using the resulting high-resolution DEM

acquired from this system, which can ultimately assist with understanding small-scale energy balance across arctic landscapes. An advantage of using this approach is clearly attributed to the NADIR view angle of the sensor as well as to the highly advanced computer vision and photogrammetry algorithms currently available for such approaches. However, it is important to note that these algorithms might be picking up features that are below the surface of shallow water such as in the case of low-lying troughs and inundated sections of the tundra, whereas the T-LiDAR and A-LiDAR systems simply reflect the light pulses being emitted once they hit the surface of the water. Future studies might need to address the sensitivity of each sensor to account for the misalignment between approaches, especially for water-rich landscapes like the arctic coastal plain, which are characterized by abundant wetland, ponds, and lakes. The ability to capture the study area from a NADIR view angle is a clear advantage over the T-LiDAR system, where scanning normally occurs between 1-3 meters above the surface.

The KAP standard error map displayed error values localized to one section of the study area, which may have been caused by four sources of error: a) user error related to GCP distribution or lack there-of, b) complex surface characteristics, c) photogrammetric image processing algorithm, and/or d) interpolation algorithm. It is also highly unlikely that complex surface characteristics seem to be the source of error for the KAP system since the errors resulted mostly within one location of the study area and all others were covered precisely. Errors resulted to be more random and less predictable using this approach which might introduce uncertainty when studying larger areas. The main limitations of this system are the need for winds between 5-20 mph as well as the need for GCPs, which is a critical aspect of this approach. Without GCPs the precise alignment of each image is compromised and resulting PCs and ultimately DEMs are greatly affected. Additionally, similar to the T-LiDAR system, data processing times greatly depend on data volumes and computing power although normally vary in the degree of dependence according to the nature of the study at hand.

The overall potential spatial coverage attainable by this particular kite system is approximately 400 m^2 per scene acquired from an altitude of roughly 400 m, making this method a good candidate for low to mid-scale remote sensing efforts. Numerous advantages of using SFAP (e.g. kites), computer vision methods (e.g. SfM), and digital photogrammetric approaches exist, including but not limited to relatively less expensive acquisitions than traditional methods, user friendly, higher frequency of multi-temporal acquisitions, can be applied to different ecosystems

and landscapes (*Andresen et al.*, 2014), and offer comparable results using consumer-grade products (*Aber et al.*, 1999; *Aber et al.*, 2005; *Lassueur et al.*, 2006; *Leberl et al.*, 2010; *Fonstad et al.*, 2013).

2.5.3 A-LiDAR

The final surface model produced from the A-LiDAR system depicted elevation relatively well for high centered polygons but not that well for low-lying areas. Similar to the T-LiDAR system, the airborne LiDAR generated high error in low-lying areas, especially those inundated by water. As previously mentioned, these areas might be getting misrepresented using the LiDAR approaches and should be looked into further. The overall spatial resolution is low and polygon ridges are not clear when compared to the T-LiDAR and KAP systems, which was expected based on the acquisition height and point density of the data acquired. Overall this system resulted in low-accuracy when exploring the relationship between the PC data elevation values and the GCP data values. The linear regression line seems to wean off the 1 to 1 line suggesting that this system is over-estimating across low-lying vegetation types and under-estimating for those types located in higher elevations. A possible source of error might be due to corn-rowing or striping (Figure 2.3), which was clearly observed in the resulting standard error map suggesting that the flight path lines from the aerial survey have a direct effect on the overlap, quality and accuracy of the resulting DEM surface as also highlighted in other studies (*Liu*, 2008; *Leberl et al.*, 2010; *Carter et al.*, 2012). Interpolation can help fill these gaps but the overall DEM accuracy will depend entirely on the accuracy of the onboard sensor and the resulting raw data post-rectification. Like T-LiDAR, these types of laser systems also tend to have bulky and heavy equipment making multi-temporal surveys more difficult and costly and require a large learning gap for filed data collection and processing. Also, A-LiDAR requires an additional expensive per survey towards fuel for the aircraft alone and depending on the length of flight and area to be covered, the total cost can add up quickly. However, these systems have been shown to be useful for identifying areas of subsidence and can cover large areas with one acquisition (*Leberl et al.*, 2010) which is clearly an advantage to some SFAP systems. The A-LiDAR approach seemed to be limited in modeling small-scale microtopographic features and processes (i.e. terrain parameters and hydrology), which suggests that this system is better suited for studies ranging from middle to large-scale ecosystem processes.

2.5.3 SSI

The SSI DEM utilized for this study resulted with limited accuracy as the inter-comparison analysis suggested where a large misalignment was seen between the other surface models. The data processing for this approach did not require a PC to interpolate a surface model unlike the other approaches and therefore limited the exploration of elevation and quantification of error accuracy from PC data. The satellite approach had the highest correlation with the A-LiDAR system for the DEM random point sampling assessment. The GWR tool failed to model correlations between the error values and the slope, curvature and aspect surface parameters which suggest that the input data or model is not properly specified or that the input data resolution is very low. As the DEM accuracy analysis suggests, the SSI DEM seems to be over-estimating elevation values across all landform types as the range of values are between 2.6 and 3.1 meters, when compared to the T-LiDAR DEM (1.89 - 3.01 m) and KAP DEM (1.81 – 2.8 m). The SSI DEM was developed using a range of WV2 and WV3 satellite imagery spanning scenes acquired during difference seasons and spanning several years which can be a large source of error since the majority of the Arctic is snow-covered during most of the year and suggests this approach might be calculating elevation at the top of the snow yielding higher elevations and ultimately fails at representing the true surface elevation. Other possible sources or error might include lack of proper atmospheric correction for scenes prior to stereoscopic processing.

Overall, the performance of the SSI in its ability to model surface structure, elevation, terrain parameters and hydrology for surface energy balance efforts at a fine spatial scale was poor when compared to the other approaches. The fact that this method can cover large areas in one scene is an advantage over the other approaches (i.e. large spatial coverage), however it compromises the accuracy and spatial resolution of the resulting surface model, which might not be sufficient for detecting small scale surface processes occurring at high temporal frequencies for permafrost dominated landscapes. Other advantages of using these data over other datasets is the low-cost of acquiring imagery since the majority is freely available online however the skill sets needed to learn proper workflows and processing techniques demands a big learning curve.

2.6 CONCLUSION

This study reports on the applicability of SfM methods and related digital photogrammetric approaches to analyze digital representations of terrain characteristics over a highly heterogeneous landscape on the north-slope coastal plain of Alaska. Additionally, our interest was to quantify errors from this system and compare it to those models acquired from tradition remote sensing approaches as well as to assess the cost, capacity to detect landform types and terrain, capacity to model hydrology and terrain parameters, and skill sets required for each approach. Our results suggest that DEM errors are closely related to terrain structure and data density and can be calculated from a number of different methods. Overall each method displayed advantages and disadvantages as no one approach seems appropriate for all types of studies, therefore we suggest that all methods be utilized and data fused in order to assist in validation of global modeling efforts. For example, the T-LiDAR and KAP methods offer accurate measurements to model dynamics at small to mid-scale spatial scales while the A-LiDAR and SSI approaches offer a better solution for middle to large-scale landscape studies that do not require high accuracy of high resolution products. Given the low-cost and ease of execution of the KAP system, it seems like the best option for modeling small-scale arctic landscape dynamics and shows potential for unmanned aerial vehicles (UAVs) that utilized photogrammetric approaches for modeling. This study highlights the many new and mostly underutilized methods for improving knowledge of surface dynamics in tundra landscapes that traditionally have been difficult places to work and execute inter-comparison studies at multiple spatial scales.

2.7 REFERENCES

Aber, J. S., R. J. Sobieski, D. a Distler, and M. C. Nowak (1999), Kite Aerial Photography for Environmental Site Investigations, , *102*(1), 57–67, doi:10.2307/3628217.

Aber, J. S., S. W. Aber, and F. Pavri (2002), Unmanned Small-Format Aerial Photography From Kites for Acquiring Large-Scale , High-Resolution , Multiview-Angle Imagery, *Int. Arch. Photogramm. Remote Sens. Spat. Inf. Sci.*, *34*(1), 1–6.

Aber, J. S., D. Eberts, and S. W. Aber (2005), Applications of kite aerial photography: Biocontrol of salt cedar (Tamarix) in the western United States, *Trans. Kansas Acad. Sci.*, *108*(1 & 2), 63–66, doi:10.1660/0022-8443(2005)108[0063:AOKAPB]2.0.CO;2.

ACIA (2004a), Impacts of a Warming Arctic: Arctic Climate Impact Assessment, *Cambridge Univ. Press*, 1046, doi:10.2277/0521617782.

ACIA (2004b), Impacts of a Warming Arctic: Arctic Climate Impact Assessment, *Cambridge Univ. Press*, 1046, doi:10.2277/0521617782.

Andresen, C. G. (2014), Monitoring and understanding decadal scale changes in hydrology, productivity and carbon balance in Arctic tundra ponds, , 108.

Andresen, C. G., and V. L. Lougheed (2015), Disappearing Arctic tundra ponds: Fine-scale analysis of surface hydrology in drained thaw lake basins over a 65 year period (1948–2013), , 1–14, doi:10.1002/2014JG002778.Received.

Andresen, C. G., S. A. Vargas, V. L. Lougheed, and C. E. Tweedie (2014), Kite-based Aerial Photography (KAP): A Low Cost, Effective Tool for Wetland Research, *Wetl. Sci. Pract.*, *Dec*(December), 28–31.

Arft, a. M. et al. (1999), Responses of Tundra plants to experimental warming: Meta-analysis of the International Tundra Experiment, *Ecol. Monogr.*, *69*(4), 491–511, doi:10.1890/0012-9615(1999)069[0491:ROTPTE]2.0.CO;2.

Bangen, S. G., J. M. Wheaton, N. Bouwes, B. Bouwes, and C. Jordan (2014), A methodological intercomparison of topographic survey techniques for characterizing wadeable streams and rivers, *Geomorphology*, *206*, 343–361, doi:10.1016/j.geomorph.2013.10.010.

Battersby, S. E., D. "daan" Strebe, and M. P. Finn (2016), Shapes on a plane: evaluating the impact of projection distortion on spatial binning, *Cartogr. Geogr. Inf. Sci.*, *406*(May), 1–12, doi:10.1080/15230406.2016.1180263.

Beamish, A. L., W. Nijland, M. Edwards, N. C. Coops, and G. H. R. Henry (2016), Phenology and vegetation change measurements from true colour digital photography in high Arctic tundra, *NRC Res. Press*, *49*(May), 33–49.

Bhardwaj, A., L. Sam, A. Bhardwaj, and F. J. Martín-Torres (2016), LiDAR remote sensing of the cryosphere: Present applications and future prospects, *Remote Sens. Environ.*, *177*, 125–143, doi:10.1016/j.rse.2016.02.031.

Bhatt, U. S. et al. (2010), Circumpolar Arctic tundra vegetation change is linked to sea ice decline, *Earth Interact.*, *14*(8), doi:10.1175/2010EI315.1.

Bhatt, U. S., D. a. Walker, M. K. Raynolds, P. a. Bieniek, H. E. Epstein, J. C. Comiso, J. E. Pinzon, C. J. Tucker, and I. V. Polyakov (2013), Recent declines in warming and vegetation greening trends over pan-arctic tundra, *Remote Sens.*, *5*(9), 4229–4254, doi:10.3390/rs5094229.

Biasi, C., W. Wanek, O. Rusalimova, C. Kaiser, C. Biasi, W. Wanek, C. Kaiser, H. Meyer, and A. Richter (2017), Microtopography and Plant-Cover Controls on Nitrogen Dynamics in Hummock Tundra Ecosystems in Siberia Meyer , Pavel Barsukov and Andreas Richter Published by : INSTAAR , University of Colorado Stable URL : http://www.jstor.org/stable/4095862 REFERENCES Li, , *37*(4), 435–443.

Boelman, N. T., M. Stieglitz, H. M. Rueth, M. Sommerkorn, K. L. Griffin, G. R. Shaver, and J. a Gamon (2003), Response of NDVI, biomass, and ecosystem gas exchange to long-term warming and fertilization in wet sedge tundra., *Oecologia*, *135*(3), 414–421, doi:10.1007/s00442-003-1198-3.

Boelman, N. T., L. Gough, J. R. McLaren, and H. Greaves (2011a), Does NDVI reflect variation in the structural attributes associated with increasing shrub dominance in arctic tundra?, *Environ. Res. Lett.*, *6*(3), 35501, doi:10.1088/1748-9326/6/3/035501.

Boelman, N. T., L. Gough, J. R. McLaren, and H. Greaves (2011b), Does NDVI reflect variation in the structural attributes associated with increasing shrub dominance in arctic tundra?, *Environ. Res. Lett.*, *6*, 35501, doi:10.1088/1748-9326/6/3/035501.

Bradley, N. L., C. A. Leopold, J. Ross, and W. Huffaker (1999), Phenological changes reflect climate change in Wisconsin., *Proc. Natl. Acad. Sci. U. S. A.*, *96*(August), 9701–9704, doi:10.1073/pnas.96.17.9701.

Brown, J., P. C. Miller, L. L. Tieszen, and F. L. Bunnell (1980), *An Arctic Ecosystem: The Coastal Tundra at Barrow, Alaska*.

Brown, J., F. E. Nelson, and K. M. Hinkel (2000), The circumpolar active layer monitorign (CALM) program research designs and initial results, *Polar Geogr.*, *3*(May 2012), 162–165.

Cabin, R. J., R. J. Mitchell, E. Siemann, D. Wedin, and K. S. N. Bio (2000), To Bonferroni or Not to Bonferroni : When and How Are the Questions Published by : Wiley on behalf of the Ecological Society of America Stable URL : http://www.jstor.org/stable/20168454 How Are the Questions To Bonferroni or Not to Bonferroni : When and, , *81*(3), 246–248.

Carlisle, B. H. (2005), Modelling the spatial distribution of DEM error, *Trans. GIS*, *9*(4), 521–540, doi:10.1111/j.1467-9671.2005.00233.x.

Carter, J., Schmid, K., Waters, K., Betzhold, L., Hadley, B., Mataosky, R., Halleran, J. (2012), Lidar 101 : An Introduction to Lidar Technology , Data , and Applications, *NOAA Coast. Serv. Cent.*, (November), 76.

Chapin, F. S. et al. (2005), Role of Land-Surface Changes in Arctic Summer Warming, *Science (80-.).*, *657*(2005), 9–13, doi:10.1126/science.1117368.

Chaplot, V., F. Darboux, H. Bourennane, S. Leguédois, N. Silvera, and K. Phachomphon (2006), Accuracy of interpolation techniques for the derivation of digital elevation models in relation to landform types and data density, *Geomorphology*, *77*(1–2), 126–141, doi:10.1016/j.geomorph.2005.12.010.

Chen, C., and T. Yue (2010), A method of DEM construction and related error analysis, *Comput. Geosci.*, *36*(6), 717–725, doi:10.1016/j.cageo.2009.12.001.

Claudio, H. C., Y. Cheng, D. a. Fuentes, J. a. Gamon, H. Luo, W. Oechel, H. L. Qiu, A. F. Rahman, and D. a. Sims (2006), Monitoring drought effects on vegetation water content and fluxes in chaparral with the 970??nm water band index, *Remote Sens. Environ.*, *103*(3), 304–311, doi:10.1016/j.rse.2005.07.015.

Cleland, E. E., I. Chuine, A. Menzel, H. a. Mooney, and M. D. Schwartz (2007), Shifting plant phenology in response to global change, *Trends Ecol. Evol.*, *22*(7), 357–365, doi:10.1016/j.tree.2007.04.003.

Dandois, J. P., and E. C. Ellis (2010), Remote sensing of vegetation structure using computer vision, *Remote Sens.*, *2*(4), 1157–1176, doi:10.3390/rs2041157.

Dandois, J. P., and E. C. Ellis (2013), High spatial resolution three-dimensional mapping of vegetation spectral dynamics using computer vision, *Remote Sens. Environ.*, *136*, 259–276, doi:10.1016/j.rse.2013.04.005.

Darnell, A. R., N. J. Tate, and C. Brunsdon (2008), Improving user assessment of error implications in digital elevation models, *Comput. Environ. Urban Syst.*, *32*(4), 268–277, doi:10.1016/j.compenvurbsys.2008.02.003.

Delbart, N., T. Le Toan, L. Kergoat, and V. Fedotova (2006), Remote sensing of spring phenology in boreal regions: A free of snow-effect method using NOAA-AVHRR and SPOT-VGT data (1982-2004), *Remote Sens. Environ.*, *101*(1), 52–62, doi:10.1016/j.rse.2005.11.012.

Desmet, P. J. J. (1997), Effects Of Iinterpolation Errors On The Aanalysis Of DEMs, *Earth Surf. Process. Landforms*, *22*(June 1996), 563–580.

Dowling, T., A. Read, and J. Gallant (2009), Very high resolution DEM acquisition at low cost using a digital camera and free software, *18th World IMACS/MODSIM09 Congr.*, (July), 2479–2485.

Elmendorf, S. C. et al. (2012a), Global assessment of experimental climate warming on tundra vegetation: Heterogeneity over space and time, *Ecol. Lett.*, *15*(2), 164–175, doi:10.1111/j.1461-0248.2011.01716.x.

Elmendorf, S. C. et al. (2012b), Plot-scale evidence of tundra vegetation change and links to recent summer warming, *Nat. Clim. Chang.*, *2*(6), 453–457, doi:10.1038/nclimate1465.

Epstein, H. E., M. K. Raynolds, D. a Walker, U. S. Bhatt, C. J. Tucker, and J. E. Pinzon (2012), Dynamics of aboveground phytomass of the circumpolar Arctic tundra during the past three decades, *Environ. Res. Lett.*, *7*(1), 15506, doi:10.1088/1748-9326/7/1/015506.

Erdoğan, S. (2010), Modelling the spatial distribution of DEM error with geographically weighted regression: An experimental study, *Comput. Geosci.*, *36*(1), 34–43, doi:10.1016/j.cageo.2009.06.005.

Esri (2001), ArcGIS Geostatistical Analyst: Statistical Tools for Data Exploration, Modeling, and Advanced Surface Generation, , (August), 19.

ESRI (2013), Overview of Arc Hydro Terrain Preprocessing Workflows, , (February), 13.

Von Fischer, J. C., R. C. Rhew, G. M. Ames, B. K. Fosdick, and P. E. Von Fischer (2010), Vegetation height and other controls of spatial variability in methane emissions from the Arctic coastal tundra at Barrow, Alaska, *J. Geophys. Res. Biogeosciences*, *115*(3), 1–11, doi:10.1029/2009JG001283.

Fisher, P. (1998), Improved modeling of elevation error with Geostatistics, *Geoinformatica*, *2*(3), 215–233, doi:10.1023/A:1009717704255.

Fonstad, M. a., J. T. Dietrich, B. C. Courville, J. L. Jensen, and P. E. Carbonneau (2013), Topographic structure from motion: A new development in photogrammetric measurement, *Earth Surf. Process. Landforms*, *38*(4), 421–430, doi:10.1002/esp.3366.

Fraser, R. H., I. Olthof, T. C. Lantz, and C. Schmitt (2016), UAV Photogrammetry for Mapping Vegetation in the Low-Arctic, *Arct. Sci.*, *102*(June), 1–51, doi:10.1139/as-2016-0008.

Gamon, J. a, G. P. Kershaw, S. Williamson, and D. S. Hik (2012a), Microtopographic patterns in an arctic baydjarakh field: do fine-grain patterns enforce landscape stability?, *Environ. Res. Lett.*, *7*(1), 15502, doi:10.1088/1748-9326/7/1/015502.

Gamon, J. a., Y. Cheng, H. Claudio, L. MacKinney, and D. a. Sims (2006), A mobile tram system for systematic sampling of ecosystem optical properties, *Remote Sens. Environ.*, *103*(3), 246–254, doi:10.1016/j.rse.2006.04.006.

Gamon, J. a., K. F. Huemmrich, R. S. Stone, and C. E. Tweedie (2013), Spatial and temporal variation in primary productivity (NDVI) of coastal Alaskan tundra: Decreased vegetation growth following earlier snowmelt, *Remote Sens. Environ.*, *129*, 144–153, doi:10.1016/j.rse.2012.10.030.

Gamon, J. A., G. P. Kershaw, S. Williamson, and D. S. Hik (2012b), Microtopographic patterns in an arctic baydjarakh field: do fine-grain patterns enforce landscape stability?, *Environ. Res. Lett.*, *7*(1), 15502, doi:10.1088/1748-9326/7/1/015502.

Gao, J. (1997), Resolution and accuracy of terrain representation by grid DEMs at a micro-scale, *Int. J. Geogr. Inf. Sci.*, *11*(2), 199–212, doi:10.1080/136588197242464.

Gao, X., and a. R. Huete (2000), Validation of MODIS land surface reflectance and vegetation indices with multi-scale high spatial resolution data, *IGARSS 2000. IEEE 2000 Int. Geosci. Remote Sens. Symp. Tak. Pulse Planet Role Remote Sens. Manag. Environ. Proc. (Cat. No.00CH37120)*, 533–535, doi:10.1109/IGARSS.2000.861620.

Gitelson, A. a, Y. Zur, O. B. Chivkunova, and M. N. Merzlyak (2002), Assessing carotenoid content in plant leaves with reflectance spectroscopy., *Photochem. Photobiol.*, *75*(3), 272–281, doi:10.1562/0031-8655(2002)0750272ACCIPL2.0.CO2.

Gitelson, A. A., F. Verlag, Y. Gritz, and M. N. Merzlyak (2003), Relationships between leaf chlorophyll content and spectral reflectance and algorithms for non-destructive chlorophyll assessment in higher plant leaves, , *282*.

Goetz, S. J., A. G. Bunn, G. J. Fiske, and R. a Houghton (2005), Satellite-observed photosynthetic trends across boreal North America associated with climate and fire disturbance., *Proc. Natl. Acad. Sci. U. S. A.*, *102*(38), 13521–5, doi:10.1073/pnas.0506179102.

Gong, J., L. Zhllin, Q. Zhu, H. Sui, and Y. Zhou (2000), Effects of Various Factors on the Accuracy of DEMs : An Intensive Experimental Investigation, *Photogramm. Eng. Remote Sens.*, *66*(9), 1113–1117.

Goswami, S., J. a. Gamon, and C. E. Tweedie (2011), Surface hydrology of an arctic ecosystem: Multiscale analysis of a flooding and draining experiment using spectral reflectance, *J. Geophys. Res. Biogeosciences*, *116*(1), 1–14, doi:10.1029/2010JG001346.

Harwin, S., and A. Lucieer (2012), Assessing the accuracy of georeferenced point clouds produced via multi-view stereopsis from Unmanned Aerial Vehicle (UAV) imagery, *Remote Sens.*, *4*(6), 1573–1599, doi:10.3390/rs4061573.

Haugen, R.K., and Brown, J. (1980), Coastal-Inland Distributions of Summer Air Temperature and Precipitation in Northern Alaska, *Arct. Alp. Res.*, *12*(4), 403–412.

Healey, N. C., Oberbauer, S.F., Ahrends, H.E., Dierick, D., Welker, J.M., Leffler, A.J., Hollister, R.D., Vargas, S.A., Tweedie, C. E. (2014), A Mobile Instrumented Sensor Platform for Long-Term Terrestrial Ecosystem Analysis: An Example Application in an Arctic Tundra Ecosystem, *J. Environ. Informatics*, *24*(1), 1–10, doi:10.3808/jei.201400278.

Heimsath, A. M., and H. Farid (2002), Hillslope topography from unconstrained photographs, *Math. Geol.*, *34*(8), 929–952, doi:10.1023/A:1021364623017.

Helbig, M., J. Boike, M. Langer, P. Schreiber, B. R. K. Runkle, and L. Kutzbach (2013), Spatial and seasonal variability of polygonal tundra water balance: Lena River Delta, northern Siberia (Russia), *Hydrogeol. J.*, *21*(1), 133–147, doi:10.1007/s10040-012-0933-4.

Henry, G. H R and Molau, U. (1997), Tundra plants and climate change : the International Tundra Experiment (ITEX), , *3*, 1–9.

Henry, G., R. Hollister, I. S. Jónsdóttir, K. Klanderlud, U. Molau, S. F. Oberbauer, P. Webber, and P. Wookey (2013), The International Tundra Experiment: An Arctic Monitoring Network,

Hinzman, L. D., C. J. Deal, a. D. Mcguire, S. H. Mernild, I. V. Polyakov, and J. E. Walsh (2013), Trajectory of the Arctic as an integrated system, *Ecol. Appl.*, *23*(8), 1837–1868, doi:10.1890/11-1498.1.

Hollister, R. D. (2003), Response of Tundra Vegetation to Temperature: Implications for Forcasting Vegetation Change,

Hollister, R. D., and K. J. Flaherty (2010), Above- and below-ground plant biomass response to experimental warming in northern Alaska, *Appl. Veg. Sci.*, *13*(3), 378–387, doi:10.1111/j.1654-109X.2010.01079.x.

Hollister, R. D., P. J. Webber, and C. E. Tweedie (2005), The response of Alaskan arctic tundra to experimental warming: Differences between short- and long-term responses, *Glob. Chang. Biol.*, *11*(4), 525–536, doi:10.1111/j.1365-2486.2005.00926.x.

Hollister, R. D., P. J. Webber, and C. Bay (2014), Plant Response to Temperature in Northern Alaska : Implications for Predicting Vegetation Change PLANT RESPONSE TO TEMPERATURE IN NORTHERN ALASKA :, , *86*(6), 1562–1570.

Huemmrich, K. F. et al. (2010), Remote sensing of tundra gross ecosystem productivity and light use efficiency under varying temperature and moisture conditions, *Remote Sens. Environ.*, *114*(3), 481–489, doi:10.1016/j.rse.2009.10.003.

Huemmrich, K. F., J. Gamon, C. E. Tweedie, P. P. K. Campbell, D. Landis, and E. Middleton (2013), Arctic Tundra Vegetation Functional Types Based on Photosynthetic Physiology and Optical Properties, , 1–37.

Humphreys, E. R., and P. M. Lafleur (2011), sequestration in two low Arctic tundra ecosystems?, *Geophys. Res. Lett.*, *38*(9), 3–7, doi:10.1029/2011GL047339.

Hunter, G. j., and M. F. Goodchild (1997), Modeling the Uncertainty of Slope and Aspect Estimates Derived from Spatial Databases,

Hutchinson, M. F., T. Xu, and J. a Stein (2011), Recent Progress in the ANUDEM Elevation Gridding Procedure, *Geomorphometry*, 19–22.

Ide, R., and H. Oguma (2013), A cost-effective monitoring method using digital time-lapse cameras for detecting temporal and spatial variations of snowmelt and vegetation phenology in alpine ecosystems, *Ecol. Inform.*, *16*, 25–34, doi:10.1016/j.ecoinf.2013.04.003.

IPCC (2014), Climate Change 2014: Synthesis Report. Contribution of Working Groups I, II and III to the Fifth Assessment Report of the Intergovernmental Panel on Climate Change.

Jarihani, A. a., J. N. Callow, T. R. McVicar, T. G. Van Niel, and J. R. Larsen (2015), Satellite-derived Digital Elevation Model (DEM) selection, preparation and correction for hydrodynamic modelling

in large, low-gradient and data-sparse catchments, *J. Hydrol.*, *524*, 489–506, doi:10.1016/j.jhydrol.2015.02.049.

Javernick, L., J. Brasington, and B. Caruso (2014), Modeling the topography of shallow braided rivers using Structure-from-Motion photogrammetry, *Geomorphology*, *213*, 166–182, doi:10.1016/j.geomorph.2014.01.006.

Jia, G. J. (2003), Greening of arctic Alaska, 1981–2001, *Geophys. Res. Lett.*, *30*(20), 3–6, doi:10.1029/2003GL018268.

Jorgenson, M. T., M. Kanevskiy, Y. Shur, N. Moskalenko, D. R. N. Brown, K. Wickland, R. Striegl, and J. Koch (2015), Journal of Geophysical Research : Earth Surface, , 1–18, doi:10.1002/2015JF003602.Received.

Kasischke, E.S., et al. (2014), A Concise Experiment Plan for the Arctic-Boreal Vulnerability Experiment, *http://above.nasa.gov/acep/acep_final_pdf.pdf. Accessed 1/25/2015.*

Keenan, T. F. et al. (2014), Tracking forest phenology and seasonal physiology using digital repeat photography : a critical assessment, , *24*(6), 1478–1489.

Komarkova, V., and Webber, P. J. (1980), Two Low Arctic Vegetation Maps near Atkasook , Alaska, , *12*(4), 447–472.

Krivoruchko, K. (2004), Introduction to Modeling Spatial Processes Using Geostatistcal Analyst, *Esri*, 1–27.

Kurc, S. a., and L. M. Benton (2010), Digital image-derived greenness links deep soil moisture to carbon uptake in a creosotebush-dominated shrubland, *J. Arid Environ.*, *74*(5), 585–594, doi:10.1016/j.jaridenv.2009.10.003.

Laidler, G. J., P. M. Treitz, and D. M. Atkinson (2008), Remote Sensing of Arctic Vegetation : Relations between the NDVI , Spatial Resolution and Vegetation Cover on Boothia Peninsula , Nunavut Author (s): Gita J . Laidler , Paul M . Treitz and David M . Atkinson Published by : Arctic Institute of North Amer, , *61*(1), 1–13.

Lara, M. J., a. D. McGuire, E. S. Euskirchen, C. E. Tweedie, K. M. Hinkel, A. N. Skurikhin, V. E. Romanovsky, G. Grosse, W. R. Bolton, and H. Genet (2014), Polygonal tundra geomorphological change in response to warming alters future CO 2 and CH 4 flux on the Barrow Peninsula, *Glob. Chang. Biol.*, (August), n/a-n/a, doi:10.1111/gcb.12757.

Lassueur, T., S. Joost, and C. F. Randin (2006), Very high resolution digital elevation models: Do they improve models of plant species distribution?, *Ecol. Modell.*, *198*(1–2), 139–153, doi:10.1016/j.ecolmodel.2006.04.004.

Leberl, F., a Irschara, T. Pock, P. Meixner, M. Gruber, S. Scholz, and a Wiechert (2010), Point Clouds: Lidar versus 3D Vision, *Photogramm. Eng. Remote Sens.*, *76*(10), 1123–1134, doi:0099-1112/10/7610–1123.

Lefsky, M. a, W. B. Cohen, G. G. Parker, and J. David (2014), Lidar Remote Sensing for Ecosystem Studies, , *52*(1), 19–30.

Li, Z. (2014), Watershed modeling using arc hydro based on DEMs: a case study in Jackpine watershed, *Environ. Syst. Res.*, *3*(1), 11, doi:10.1186/2193-2697-3-11.

Liljedahl, A.K., Hinzman, L.D., Schulla, J. (2012), Ice-Wedge Polygon Type Controls Low-Gradient Watershed-Scale Hydrology,

Liljedahl, A. K. et al. (2016), Pan-Arctic ice-wedge degradation in warming permafrost and influence on tundra hydrology, *Nat. Geosci.*, *9*(April), 312–318, doi:10.1038/ngeo2674.

Lin, D. H., D. R. Johnson, C. Andresen, and C. E. Tweedie (2012), High spatial resolution decade-time scale land cover change at multiple locations in the Beringian Arctic (1948–2000s), *Environ. Res. Lett.*, *7*(2), 25502, doi:10.1088/1748-9326/7/2/025502.

Liu, H. Q., and A. Huete (1995), Feedback based modification of the NDVI to minimize canopy background and atmospheric noise, *IEEE Trans. Geosci. Remote Sens.*, *33*(2), 457–465, doi:10.1109/36.377946.

Liu, Z. L. Z., S. C. S. Cui, and Q. Y. Q. Yan (2008), Building extraction from high resolution satellite imagery based on multi-scale image segmentation and model matching, *2008 Int. Work. Earth Obs. Remote Sens. Appl.*, doi:10.1109/EORSA.2008.4620321.

Lucht, W. (2002), Climatic Control of the High-Latitude Vegetation Greening Trend and Pinatubo Effect, *Science (80-.).*, *296*(5573), 1687–1689, doi:10.1126/science.1071828.

Marzolff, I., J. B. Ries, and K. D. Albert (2002), Kite aerial photography for gully monitoring in sahelian landscapes, , 18–20.

McCune, B., and Grace, J. . (2002), Analysis of Ecological Communities, *MjM Softw. Des. Gleneden Beach, McKinney M.L*, *127*(January 2002), 247–260, doi:10.1016/S0022-0981(03)00091-1.

Menzel, a, and P. Fabian (1999), Growing season extended in Europe, *Nature*, *397*(6721), 659, doi:10.1038/17709.

Migliavacca, M. et al. (2011), Using digital repeat photography and eddy covariance data to model grassland phenology and photosynthetic CO2 uptake, *Agric. For. Meteorol.*, *151*(10), 1325–1337, doi:10.1016/j.agrformet.2011.05.012.

Myneni, R. B., C. D. Keeling, C. J. Tucker, G. Asrar, and R. R. Nemani (1997), Increased plant growth in the northern high latitudes from 1981 to 1991, *Nature*, *386*(6626), 698–702, doi:10.1038/386698a0.

Nelson, F. E., S. I. Outcalt, J. Brown, N. I. Shiklomanov, and K. M. Hinkel (1998), Spatial and Temporal Attributes of the Active-Layer Thickness Record, Barrow, Alaska, U.S.A., , (55), 797–802.

Nelson, S. and (2015), Circumpolar Active Layer Monitoring (CALM) Program, *Natl. Snow Ice Data Cent.*, 1–3.

Noh, M.-J., and I. M. Howat (2015a), Automated stereo-photogrammetric DEM generation at high latitudes: Surface Extraction with TIN-based Search-space Minimization (SETSM) validation and demonstration over glaciated regions, *GIScience Remote Sens.*, *1603*(June 2015), 1–20, doi:10.1080/15481603.2015.1008621.

Noh, M.-J., and I. M. Howat (2015b), Automated stereo-photogrammetric DEM generation at high latitudes: Surface Extraction with TIN-based Search-space Minimization (SETSM) validation and demonstration over glaciated regions, *GIScience Remote Sens.*, *1603*(June 2015), 1–20, doi:10.1080/15481603.2015.1008621.

Oberbauer, S. F. et al. (2007), Tundra CO2 fluxes in response to experimental warming across lattitudinal and moisture gradients, *Ecol. Monogr.*, *77*(2), 221–238, doi:10.1890/06-0649.

Oberbauer, S. F. et al. (2013a), Phenological response of tundra plants to background climate variation tested using the International Tundra Experiment,

Oberbauer, S. F. et al. (2013b), Phenological response of tundra plants to background climate variation tested using the International Tundra Experiment., *Philos. Trans. R. Soc. Lond. B. Biol. Sci.*, *368*(1624), 20120481, doi:10.1098/rstb.2012.0481.

Oberbauer, S. F. et al. (2013c), Phenological response of tundra plants to background climate variation tested using the International Tundra Experiment., *Philos. Trans. R. Soc. Lond. B. Biol. Sci.*, *368*(1624), 20120481, doi:10.1098/rstb.2012.0481.

Olivas, P. C., S. F. Oberbauer, C. E. Tweedie, W. C. Oechel, and A. Kuchy (2010), Responses of CO2 flux components of Alaskan Coastal Plain tundra to shifts in water table, *J. Geophys. Res. Biogeosciences*, *115*(4), 1–13, doi:10.1029/2009JG001254.

Osterkamp, T. E., M. . Jorgenson, E. A. G. Schuur, Y. L. Shur, M. . Kanevskiy, J. G. Vogel, and V. E. Tumskoy (2009), Physical and Ecological Changes Associated with Warming Permafrost and Thermokarst in Interior Alaska, *Permafr. Periglac. Process.*, *136*(January), 107–136, doi:10.1002/ppp.

Painter, S. L., J. D. Moulton, and C. J. Wilson (2012), Modeling challenges for predicting hydrologic response to degrading permafrost, *Hydrogeol. J.*, *21*(Hydrogeology of Cold Regions), 221–224, doi:10.1007/s10040-012-0917-4.

Park, H., Y. Kim, and J. S. Kimball (2016), Widespread permafrost vulnerability and soil active layer increases over the high northern latitudes inferred from satellite remote sensing and process model assessments, *Remote Sens. Environ.*, *175*, 349–358, doi:10.1016/j.rse.2015.12.046.

Peichl, M., O. Sonnentag, and M. B. Nilsson (2014), Bringing Color into the Picture: Using Digital Repeat Photography to Investigate Phenology Controls of the Carbon Dioxide Exchange in a Boreal Mire, *Ecosystems*, *18*(1), 115–131, doi:10.1007/s10021-014-9815-z.

Penuelas, J., I. Filella, J. A. Gamon, B. Y. J. Penuelas, I. Filella, and A. Gamon (1995), Assessment of photosynthetic radiation-use efficiency with spectral reflectance, , *131*(3), 291–296.

Post, E. et al. (2009), Ecological dynamics across the Arctic associated with recent climate change., *Science*, *325*(5946), 1355–1358, doi:10.1126/science.1173113.

Raaflaub, L. D., and M. J. Collins (2006), The effect of error in gridded digital elevation models on the estimation of topographic parameters, *Environ. Model. Softw.*, *21*(5), 710–732, doi:10.1016/j.envsoft.2005.02.003.

Rango, A., A. Laliberte, and C. Winters (2008), Role of aerial photos in compiling a long-term remote sensing data set, *J. Appl. Remote Sens.*, *2*(1), 23541, doi:10.1117/1.3009225.

Raynolds, M. K., J. C. Comiso, D. A. Walker, and D. Verbyla (2008), Relationship between satellite-derived land surface temperatures, arctic vegetation types, and NDVI, *Remote Sens. Environ.*, *112*(4), 1884–1894, doi:10.1016/j.rse.2007.09.008.

Richardson, A. D., J. P. Jenkins, B. H. Braswell, D. Y. Hollinger, S. V. Ollinger, and M. L. Smith (2007), Use of digital webcam images to track spring green-up in a deciduous broadleaf forest, *Oecologia*, *152*(2), 323–334, doi:10.1007/s00442-006-0657-z.

Richardson, A. D., B. H. Braswell, D. Y. Hollinger, J. P. Jenkins, and S. V. Ollinger (2009), Near-surface remote sensing of spatial and temporal variation in canopy phenology, *Ecol. Appl.*, *19*(6), 1417–1428, doi:10.1890/08-2022.1.

Richardson, A. D., T. F. Keenan, M. Migliavacca, Y. Ryu, O. Sonnentag, and M. Toomey (2013), Climate change, phenology, and phenological control of vegetation feedbacks to the climate system, *Agric. For. Meteorol.*, *169*, 156–173, doi:10.1016/j.agrformet.2012.09.012.

Rondeaux, G., M. Steven, and F. Baret (1996), Optimization of Soil-Adjusted Vegetation Indices, , *107*(August 1994), 95–107.

Rosnell, T., and E. Honkavaara (2012), Point cloud generation from aerial image data acquired by a quadrocopter type micro unmanned aerial vehicle and a digital still camera, *Sensors*, *12*(1), 453–480, doi:10.3390/s120100453.

Saitoh, T. M., S. Nagai, N. Saigusa, H. Kobayashi, R. Suzuki, K. N. Nasahara, and H. Muraoka (2012), Assessing the use of camera-based indices for characterizing canopy phenology in relation to gross primary production in a deciduous broad-leaved and an evergreen coniferous forest in Japan, *Ecol. Inform.*, *11*, 45–54, doi:10.1016/j.ecoinf.2012.05.001.

Schuur, E. et al. (2008), Vulnerability of Permafrost Carbon to Climate Change : Implications for the Global Carbon Cycle, *Bioscience*, *58*(8), 701–714.

Schwartz, M. D. (1998), Green-wave phenology, *Nature*, *394*, 839–840, doi:10.1038/29670.

Screen, J. a, and I. Simmonds (2010), The central role of diminishing sea ice in recent Arctic temperature amplification., *Nature*, *464*(7293), 1334–1337, doi:10.1038/nature09051.

Shaver, G. R., L. E. Street, E. B. Rastetter, M. T. Van Wijk, and M. Williams (2007), Functional convergence in regulation of net CO_2 flux in heterogeneous tundra landscapes in Alaska and Sweden, *J. Ecol.*, *95*(4), 802–817, doi:10.1111/j.1365-2745.2007.01259.x.

Sims, D. A., and J. A. Gamon (2002), Relationships between leaf pigment content and spectral reflectance across a wide range of species , leaf structures and developmental stages, , *81*, 337–354.

Smith, L. C., Y. Sheng, G. M. Macdonald, and L. D. Hinzman (2005), Disappearing Arctic lakes, , *XXX*(June), 2005.

Snavely, N., S. M. Seitz, and R. Szeliski (2008), Modeling the world from Internet photo collections, *Int. J. Comput. Vis.*, *80*(2), 189–210, doi:10.1007/s11263-007-0107-3.

Solano, R., K. Didan, A. Jacobson, and A. Huete (2010), MODIS Vegetation Index User ' s Guide (MOD13 Series), , *2010*(May).

Sommerkorn, M. (2008), Micro-topographic patterns unravel controls of soil water and temperature on soil respiration in three Siberian tundra systems, *Soil Biol. Biochem.*, *40*(7), 1792–1802, doi:10.1016/j.soilbio.2008.03.002.

Steinwand, D. A., J. A. Hutchinson, and J. P. Snyder (1995), Map Projections for Global and Continental Data Sets and an Analysis of Pixel Distortion Caused by Reprojection, *Photogrammatic Eng. Remote Sens.*, *61*(12), 1487–1497.

Stewart, K. J., P. Grogan, D. S. Coxson, and S. D. Siciliano (2014), Topography as a key factor driving atmospheric nitrogen exchanges in arctic terrestrial ecosystems, *Soil Biol. Biochem.*, *70*(3), 96–112, doi:10.1016/j.soilbio.2013.12.005.

Stow, D. a. et al. (2004), Remote sensing of vegetation and land-cover change in Arctic Tundra Ecosystems, *Remote Sens. Environ.*, *89*(3), 281–308, doi:10.1016/j.rse.2003.10.018.

Streletskiy, D. A., N. I. Shiklomanov, F. E. Nelson, and A. E. Klene (2007), 13 Years of Observations at Alaskan CALM Sites: Long-term Active Layer and Ground Surface Temperature Trends, *Proc. 9th Int. Conf. Permafr.*, 1–6.

Sullivan, P. F., S. J. T. Arens, R. A. Chimner, and J. M. Welker (2008), Temperature and microtopography interact to control carbon cycling in a high arctic fen, *Ecosystems*, *11*(1), 61–76, doi:10.1007/s10021-007-9107-y.

Sumerling, G. (2011), Lidar Analysis in ArcGIS ® 10 for Forestry Applications, *ESRI White Pap.*, (January), 53.

Tape, K., M. Sturm, and C. Racine (2006), The evidence for shrub expansion in Northern Alaska and the Pan-Arctic, *Glob. Chang. Biol.*, *12*(4), 686–702, doi:10.1111/j.1365-2486.2006.01128.x.

Throckmorton, H. M. et al. (2016), Active layer hydrology in an arctic tundra ecosystem: Quantifying water sources and cycling using water stable isotopes, *Hydrol. Process.*, *4986*(August), 4972–4986, doi:10.1002/hyp.10883.

Torre Jorgenson, M. et al. (2013), Reorganization of vegetation, hydrology and soil carbon after permafrost degradation across heterogeneous boreal landscapes, *Environ. Res. Lett.*, *8*(3), 35017, doi:10.1088/1748-9326/8/3/035017.

Triggs, B., P. F. McLauchlan, R. I. Hartley, and A. W. Fitzgibbon (2000), Bundle Adjustment — A Modern Synthesis, *Vis. Algorithms Theory Pract.*, *1883*, 298–372, doi:10.1007/3-540-44480-7_21.

Tucker, C. J. (1978), Red and Photographic Infrared Linear Combinations for Monitoring Vegetation,

Tucker, C. J. (1999), Higher Northern Latitude NDVI and Growing Season Trends from 1982 to 1999,

Tucker, C. J., and P. J. Sellers (2007), Satellite remote sensing of primary production, *Int. J. Remote Sens.*, *7*(11), 1395–1416, doi:10.1080/01431168608948944.

Usery, E. L., M. P. Finn, J. D. Cox, S. Ruhl, M. Bearden, E. L. Usery, M. P. Finn, J. D. Cox, and T. Beard (2003), Projecting global datasets to achieve equal areas, , *30*(1), 69–79.

Ustin, S. L., and J. A. Gamon (2010), Tansley review Remote sensing of plant functional types, , 795–816.

Vaze, J., J. Teng, and G. Spencer (2010), Impact of DEM accuracy and resolution on topographic indices, *Environ. Model. Softw.*, *25*(10), 1086–1098, doi:10.1016/j.envsoft.2010.03.014.

Villarreal, S., R. D. Hollister, D. R. Johnson, M. J. Lara, P. J. Webber, and C. E. Tweedie (2012), Tundra vegetation change near Barrow, Alaska (1972–2010), *Environ. Res. Lett.*, *7*(1), 15508, doi:10.1088/1748-9326/7/1/015508.

Vorosmarty, C. J., a. D. McGuire, and J. E. Hobbie (2010), Scaling Studies in Arctic System Science and Policy Support: A Call to Research, *U.S. Arct. Res. Comm.*, 76 pages.

Vörösmarty, C. J., L. D. Hinzman, B. J. Peterson, D. H. Bromwich, L. C. Hamilton, J. Morison, V. E. Romanovsky, M. Sturm, R. S. Webb, and D. L. Kane (2001), The Hydrologic Cycle and its Role in Arctic and Global Environmental Change: A Rationale and Strategy for Synthesis Study The Hydrologic Cycle and its Role in Arctic and Global Environmental Change, *NSF-ARCSS Hydrol. Work. Steer. Comm.*, *84*(September).

Walker, D. a et al. (2012), Environment, vegetation and greenness (NDVI) along the North America and Eurasia Arctic transects, *Environ. Res. Lett.*, *7*(1), 15504, doi:10.1088/1748-9326/7/1/015504.

Walker, M., and C. Wahren (2006), Plant community responses to experimental warming across the tundra biome, *Proc. …*, *103*(5), 1342–6, doi:10.1073/pnas.0503198103.

Ward, R. D., N. G. Burnside, C. B. Joyce, and K. Sepp (2013), The use of medium point density LiDAR elevation data to determine plant community types in Baltic coastal wetlands, *Ecol. Indic.*, *33*, 96–104, doi:10.1016/j.ecolind.2012.08.016.

Webber, P. J., and M. D. Walker (1991), The International Tundra Experiment (ITEX): Resolution, , 1990.

Wehr, A., and U. Lohr (1999), Airborne laser scanning—an introduction and overview, *ISPRS J. Photogramm. Remote Sens.*, *54*(2–3), 68–82, doi:10.1016/S0924-2716(99)00011-8.

Westergaard-Nielsen, A., M. Lund, B. U. Hansen, and M. P. Tamstorf (2013), Camera derived vegetation greenness index as proxy for gross primary production in a low Arctic wetland area, *ISPRS J. Photogramm. Remote Sens.*, *86*, 89–99, doi:10.1016/j.isprsjprs.2013.09.006.

Westoby, M. J., J. Brasington, N. F. Glasser, M. J. Hambrey, and J. M. Reynolds (2012), "Structure-from-Motion" photogrammetry: A low-cost, effective tool for geoscience applications, *Geomorphology*, *179*, 300–314, doi:10.1016/j.geomorph.2012.08.021.

Wilson, J. P. (2012), Digital terrain modeling, *Geomorphology*, *137*(1), 107–121, doi:10.1016/j.geomorph.2011.03.012.

Wu, S., J. Li, and G. H. Huang (2008), A study on DEM-derived primary topographic attributes for hydrologic applications: Sensitivity to elevation data resolution, *Appl. Geogr.*, *28*(3), 210–223, doi:10.1016/j.apgeog.2008.02.006.

Zeng, H., G. Jia, and H. Epstein (2011), Recent changes in phenology over the northern high latitudes detected from multi-satellite data, *Environ. Res. Lett.*, *6*(4), 45508, doi:10.1088/1748-9326/6/4/045508.

Zhang, Z., D. L. Kane, and L. D. Hinzman (2000), Development and application of a spatially-distributed arctic hydrological and thermal process model (ARHYTHM), *Hydrol. Process.*, *14*(6), 1017–1044, doi:10.1002/(SICI)1099-1085(20000430)14:6<1017::AID-HYP982>3.0.CO;2-G.

Zona, D., D. A. Lipson, R. C. Zulueta, S. F. Oberbauer, and W. C. Oechel (2011), Microtopographic controls on ecosystem functioning in the Arctic Coastal Plain, *J. Geophys. Res. Biogeosciences*, *116*(3), 1–12, doi:10.1029/2009JG001241.

Chapter 3: Plot-level Seasonal and Inter-annual Phenological Varibility is Greatest in Low-Arctic and Wet Sites Across the North Slope of Alaska

3.1 INTRODUCTION

The Arctic is experiencing among the most dramatic impacts from climate change on the planet (*ACIA*, 2004). Observed large-scale responses include, but are not limited to, loss of sea ice and snow cover, sea level rise, enhanced coastal erosion, increases in near-surface air temperature and satellite-derived green biomass, permafrost thaw and degradation, subsidence and shifts in vegetation (e.g. shrub expansion) (*IPCC*, 2014). Additionally, many of these changes have the potential to trigger positive feedbacks with other components of the Earth System, such as the mobilization of soil organic carbon resulting from the potential warming and melting of permafrost dominated landscapes. These effects could alter surface energy budgets (*Chapin et al.*, 2005) and land-atmosphere interactions of sink-source dynamics of trace gasses across the Arctic which can ultimately have a tremendous impact on the overall global climate system, thus improving our understanding of the magnitude of these changes occurring at multiple spatial and temporal scales is imperative for advancing our knowledge and predictive power of the future state of the Arctic and Earth processes.

Plant phenology is the observation of the timing of shifts in a plants life cycle and how these particular events are influenced by seasonal and inter-annual climate-induced variations. In the Arctic, plant phenology is sensitive to climatic variability (*Hollister et al.*, 2014), and has been identified as an indicator of climatic change impacts (*Oberbauer et al.*, 2013). Plot level phenological studies have provided great insight into species and functional plant type seasonal trends such as start of season (SOS), end of season (EOS), peak of season (POS), timing of snowmelt, and timing of senescence but have been generally limited in spatial coverage (*Hollister et al.*, 2005; *Oberbauer et al.*, 2013). These processes vary between ecosystems (*Walker et al.*, 2006) and land cover classes as seen across multiple plot-level warming studies such as the International Tundra Experiment (ITEX) (*Elmendorf et al.*, 2012b) and across spatial scales (*Elmendorf et al.*, 2012a) and in turn all respond differently to changing landscape characteristics such as seen from surface hydrology studies (*Goswami et al.*, 2011), permafrost degradation (*Jorgenson et al.*, 2013) and subsidence (*Streletskiy et al.*, 2007). Generally, however, plot level monitoring of vegetation phenology remains time consuming, expensive and logistically

challenging, especially in the Arctic. Linking plot-level research to the regional and landscape scales has been challenging due to the lack of adequate low/mid-altitude sampling platforms, logistical constraints and the lack of cross-scale validation of research methodologies.

Satellite remote sensing has provided an outstanding capacity to detect change at the landscape scale (*Stow et al.*, 2004; *Lin et al.*, 2012; *Andresen and Lougheed*, 2015), and shifts in greening trends at regional to circum-arctic scales (*Goetz et al.*, 2005; *Tape et al.*, 2006; *Walker et al.*, 2012; *Bhatt et al.*, 2013). However, image capture and interpretation, and change detection can be challenged by cloud cover (*Stow et al.*, 2004), the presence of standing water (*Goswami et al.*, 2011), the short growing season (~90 days) and low sun angles (*Buchhorn et al.*, 2013). The spatial resolution of most satellite platforms (i.e. 2- 250 meters per pixel) limits the ability to detect small-scale (e.g. cm) variability associated with microtopographic variability (*Vargas et al., in prep*) and the related differences in plant community composition associated with such variability (*Shaver et al.*, 2007; *Villarreal et al.*, 2012) Additionally, the dynamic and spatially heterogeneous arctic landscape has shown variability in responses to environmental change at the species and site level (*Oberbauer et al.*, 2013), which suggests a need for improved scaling of spatial resolution, high-frequency, phenology and affiliated environmental data to improve upon long-term ecological studies such as the International Tundra Experiment (ITEX) (*Webber and Walker*, 1991; *Henry et al.*, 2013). Without such advancement, ascertaining the species or plant community-specific mechanisms associated with regional to circum-arctic trends and variability will remain difficult to discern.

Clearly, the development and innovation of mid-scale remote sensing methods have the greatest potential to link understanding of phenological trends at plot and regional to circum-arctic scales and improve validation of satellite-based sensing (*Gamon et al.*, 2013; *Westergaard-Nielsen et al.*, 2013). Networks of low-cost sensors and other remote sensing platforms have the capacity to complement satellite derived measurements if deployed in an extensible manner (*Goswami et al.*, 2011; *Gamon et al.*, 2013; *Healey et al.*, 2014; *Andresen et al.*, 2014; *Vargas et al. in prep*). Additionally, repeat photography from inexpensive consumer grade digital camera traps can be used to calculate a range of spectral indices (e.g. green excess (GI) and green chromatic coordinate (% G)), and have a proven capacity to capture phenological dynamics in numerous ecosystems (*Richardson et al.*, 2009; *Saitoh et al.*, 2012; *Ide and Oguma*, 2013; *Westergaard-Nielsen et al.*, 2013; *Peichl et al.*, 2014; *Toomey et al.*, 2015; *Beamish et al.*, 2016). However, among the few

studies focused on capturing phenology using vegetation indices derived from RGB cameras, none have explored their performance in high-arctic tundra ecosystems from either small format aerial photography systems (SFAP) or repeat photography (Pheno-cams). Moreover, few studies appear to have explored how indices of vegetation properties differ between those derived from digital photography platforms and those derived from hyperspectral spectrometers. These systems vary markedly in both cost and suitability for mid-scale sampling and have the potential to bridge the gap between traditional plot-level and landscape scales studies.

3.2 OBJECTIVES

The primary goal of this study is to assess the utility of low-cost remote sensing platforms and sensors, specifically digital time-lapse and still-shot cameras, for conducting mid-scale high spatiotemporal sampling of tundra plant communities in northern Alaska. *Beamish et al.*, 2016 demonstrated the applicability of using the latter approach on small spatial (m^2 plots) and temporal (1 growing season) scales, for monitoring of tundra vegetation. However, the study at hand focused on evaluating the effectiveness of novel Pheno-cams, which offer a time-efficient approach, and a kite aerial photography (KAP) system, which offer a larger spatial coverage, in their capacity to assess seasonal and inter-annual variability of greening trends for dominant vegetation communities across two tundra landscapes and over the span of 6 years. We aimed to answer the following questions:

1) Can digital photography and their corresponding RGB indices capture the seasonal and inter-annual variability of vegetation community greening trends for dominant vegetation communities? 2) How do digital RGB indices compare to those derived from traditional remote sensing platforms and what are the advantages and disadvantages of each? 3) Can tundra surface characteristics be used to predict greening trends and variability for specific plant communities?

3.3 MATERIALS AND METHODS

3.3.1 Study area

This study was conducted at two sites, located on the Coastal Plain of the North Slope of Alaska near the towns of Utqiaġvik (Barrow) (71°18'N, 156°40'W) and 100 km south of Utqiaġvik near Atqasuk (70°29'N, 157°25'W) (Figure 3.1). At these locations, Mobile Instrumented Sensor Platform (MISP) transects (2 x 50 meters) were established as a contribution to the US Arctic

Observing Network (AON) (Figures 3.2 & 3.3) (*Healey et al.*, 2014). Each 50 meter transect was divided into smaller 1 x 2 meter plots and marked with white wooden boards secured to the tundra with 12" metal stakes. These boards served as ground control points (GCPs) for geo-rectification of all kite aerial imagery during image processing and were located using differential global positioning system (DGPS) (Figures 3.2 and 3.3).

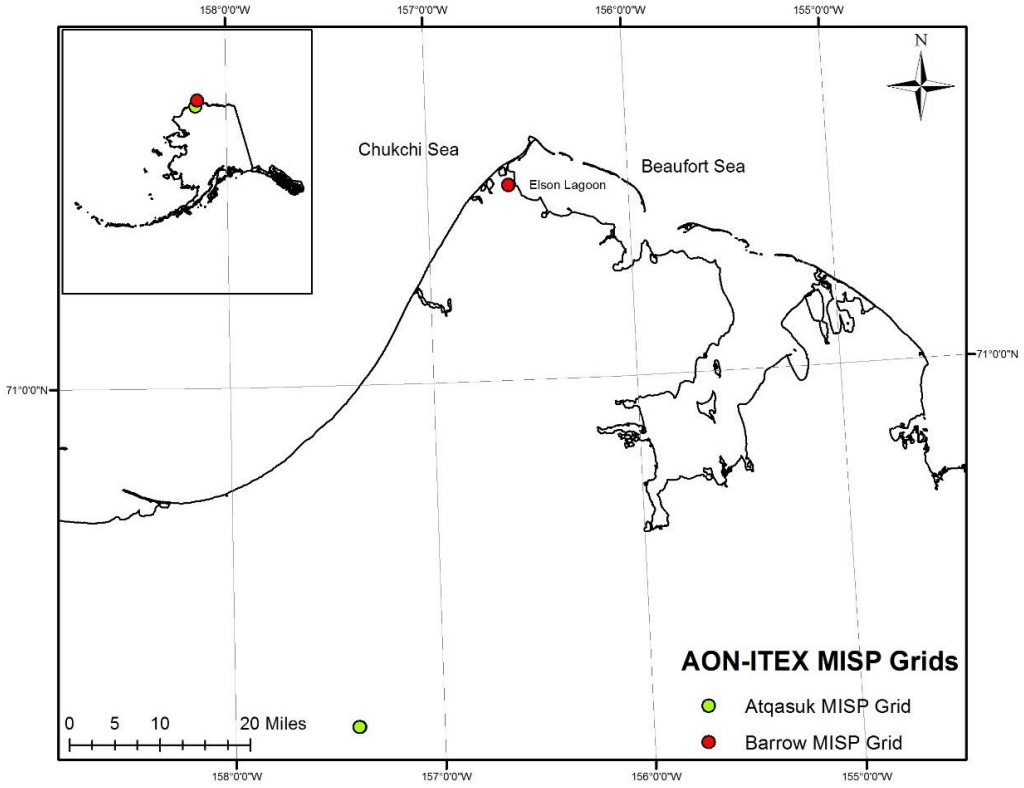

Figure 3.1: Map displaying location of MISP transects located on the north slope of Alaska. Atqasuk is about 100 km south of Utqiaġvik (Barrow).

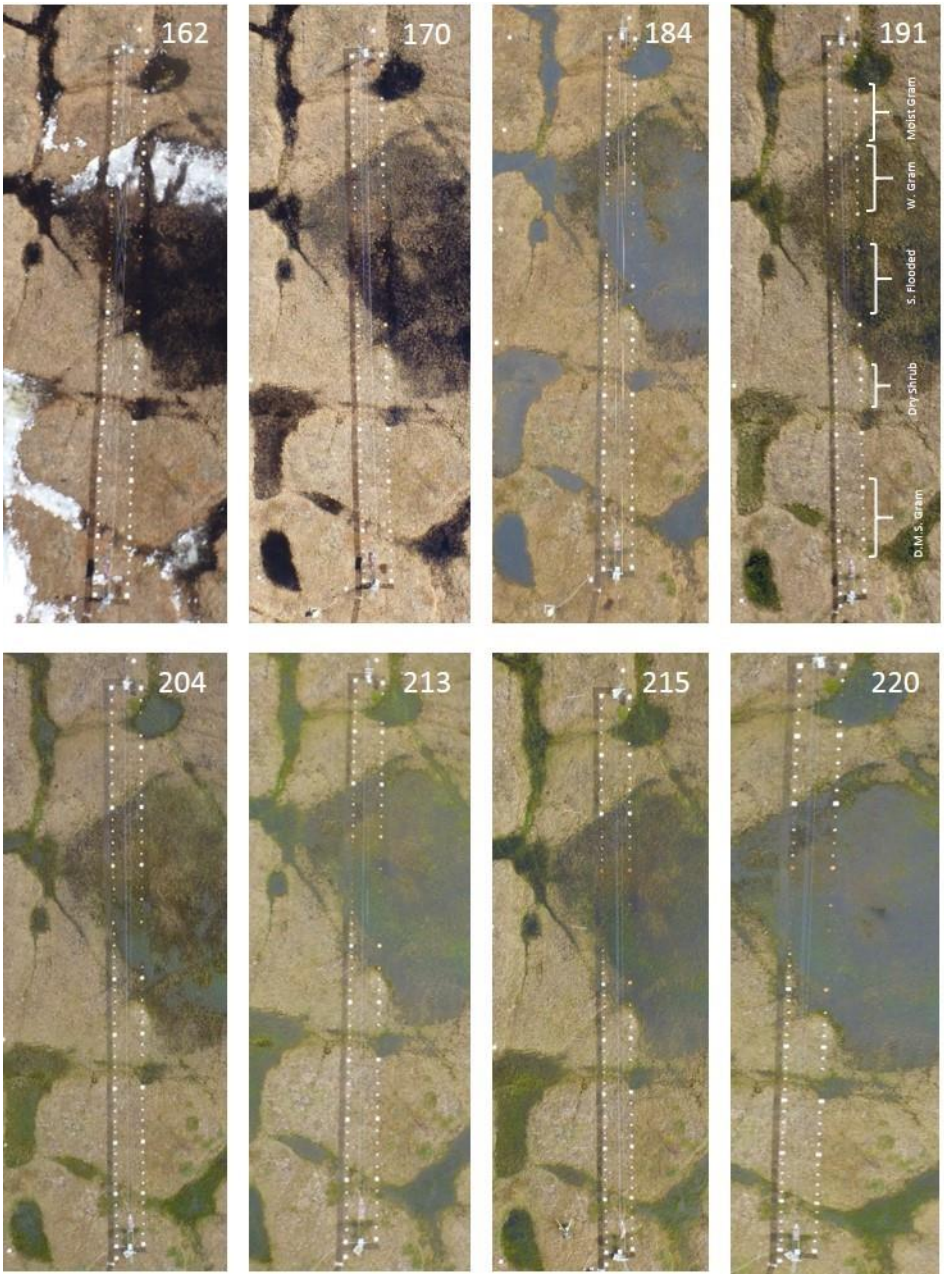

Figure 3.2: KAP depicting the primary seasonal stages of various vegetation classes and soil moistures sampled within the MISP transect in Utqiaġvik for the 2013 summer. Day of year (DOY) is displayed on the top corner of each image and grouped vegetation classes are seen in the top right aerial image. Major phenological events are highlighted such as DOY 162 (snow cover), DOY 184 (snowmelt flooding), DOY 191-215 (green-up) and DOY 220 (rain event flooding).

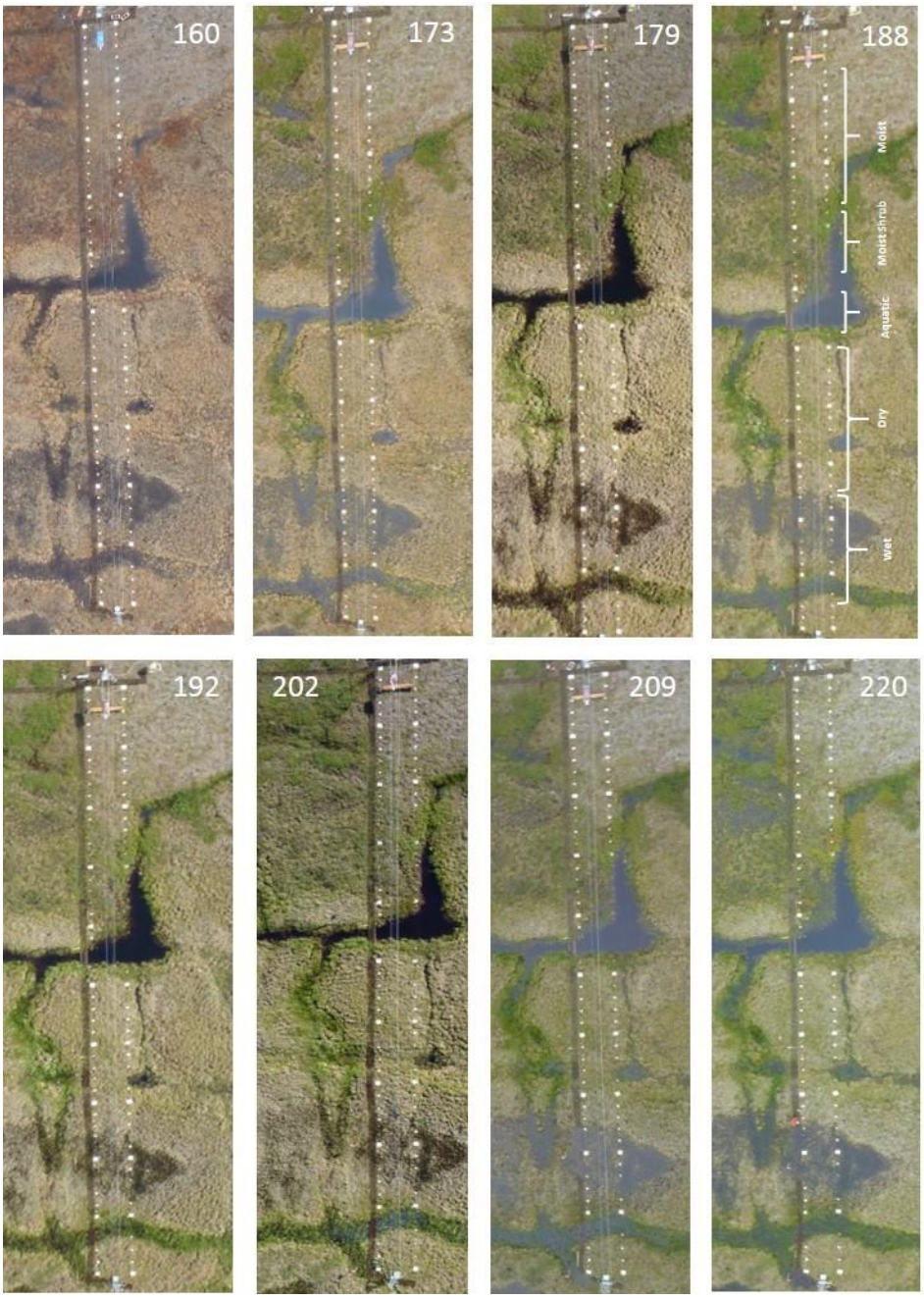

Figure 3.3: KAP depicting the primary seasonal stages of various vegetation classes and soil moistures sampled within the MISP transect in Atqasuk for the 2013 summer. Day of year (DOY) is displayed on the top corner of each image and grouped vegetation classes are seen in the top right aerial image. Major phenological events are highlighted such as DOY 160 (start-of-season) and DOY 173-220 (green-up).

Atqasuk tends to be warmer than Utqiaġvik, where fog and clouds typically dissipate by early noon and weather patterns are more dynamic (*Haugen, R.K., and Brown*, 1980). Additionally, mean July temperature is 3.7°C in Utqiaġvik and 9 °C in Atqasuk and summer precipitation is approximately 57 mm and 55 mm respectively (*Oberbauer et al.*, 2007). This region is dominated by continuous permafrost with a shallow seasonal thaw-depth in Utqiaġvik and shallow to intermediate depth in Atqasuk. Common landscape features include vegetated thaw lake basins, ice-wedge polygons ponds, low-gradient streams, hummock slopes, high and low-centered polygonal tundra, dry heath and wet meadow plant communities (*Brown et al.*, 1980). The Atqasuk landscape is predominantly characterized by dry heath and wet meadow plant communities yet they are more distinct than those found in Utqiaġvik, forming tussock tundra or complex composition of vegetation species. Table 3.1 depicts the soil moisture-defined vegetation classes (from *Lin et al.*, 2012; *Andresen et al., in prep.*), corresponding dominant species, and key parameters for each MISP transect.

Table 3.1: Summary of the two MISP transects present at Utqiaġvik and Atqasuk. The vegetation types and classes, wetland names, dominant species and landform types selected were based on Lin et al. (2011), Webber, (1980), Healey et al., (2014), and Andresen et al. in prep.

Parameters	Barrow					Atqasuk				
Vegetation Type	Dry Heath/ Mesic Heath		Moist Meadow	Wet Meadow		Dry Heath/ Mesic Heath	Moist Meadow		Wet Meadow	
Wetland Name	Dry dwarf shrub graminoid tundra	Dry-moist dwarf shrub graminoid tundra	Moist graminoid tundra	Seasonally flooded gramonoid tundra	Wet graminoid tundra	Dry shrub graminoid tundra	Moist graminoid tundra	Moist shrub graminoid tundra	Wet graminoid tundra	Aquatic graminoid tundra
Vegetation Class	Dry shrub	Dry-moist shrub-gram	Moist gram	Seasonally flooded	Wet gram	Dry	Moist	Moist shrub	Wet	Aquatic
Dominant Species	*Salix pulchra, Lazula arctica*	*Eriophorum spp.*	*Carex aquatilis/stans*	*pleaurocarpous mosses/ Arctophila fulva*	*Arctophila fulva*	*Cassiope tetragona*	*Vaccinium Vitis-idaea*	*Salix pulchra*	*Carex aquatilis*	*Arctophila fulva*
Landform Type	High center polygon/ Stabilized sand dune	High center polygon	Low center polygon/ low land	Marsh	Pond/lake	Stabilized sand dune/ snow patch	High center polygon	Low center polygon/low land	Marsh	Pond/lake
Mean Peak Season VWC (%)	42	35.4	55.8	70.5	63.5	30.6	31.03	40.1	59.3	49.8
Elevation (MASL)	3					30				
Mean Annual Temperature (°C)	-12.6					-11.9				
Mean July Temperature (°C)	3					7.2				
Average Maximum Thaw Depth (cm)	35-39					36-75+				

3.3.2 Data collection

3.3.2.1 Broad-band spectral reflectance

In-situ spectral reflectance data were generally collected once per week across all 50 plots for each MISP transect using a dual channel portable broadband field spectrometer (UniSpec DC,

PP Systems, Amesbury MA, USA). In addition to sampling of each plot during field acquisition, three additional measurements were taken over a white reference panel (Spectralon, LabSphere, North Sutton, New Hampshire, USA) to assist in cross-calibration of data and correct for changing light conditions as this can have an effect on the data being collected (*Gamon et al.*, 2006). This is an important consideration when working in arctic coastal landscapes, where light conditions tend to fluctuate frequently due to persistent broken cloud cover and strong winds (*Stow et al.*, 2004).

The UniSpec DC samples between the 310 to 1100 nm wavelength range and all raw radiance and irradiance measurements were post-processed to yield reflectance values from which fourteen published and well-recognized surface hydrology and vegetation indices were computed and further explored (*Tucker*, 1978; *Liu and Huete*, 1995; *Penuelas et al.*, 1995; *Rondeaux et al.*, 1996; *Sims and Gamon*, 2002; *Gitelson et al.*, 2002; *Gitelson et al.*, 2003; *Claudio et al.*, 2006; *Goswami et al.*, 2011) (Table 3.2).

In order to facilitate efficient and repeatable sampling each spectrometer fiber optic and corresponding field-of-view restrictor (approx. 20°) was strategically mounted on a tri-pod boom and surface reflectance measurements were manually acquired weekly to bi-weekly (weather depending) along each meter over each plot of the MISP transects during the summer growing seasons (early June to late August) from 2010-2015. All scans were acquired with a levelled tripod situated at the edge of the grid and with the boom holding the downward pointing spectrometer fiber situated over the center point of the plots at a height of approximately 1.62 meters. The resulting ground-based sampling footprint for each plot/scan was approximately 0.6 meters. During the 2010 field season, measurements were only recorded two times during August close to peak growing season due to logistical limitations.

Table 3.2: List of indices used in this study with corresponding equations and references. Digital camera formulas refer to the camera color channel information (digital numbers; DNs) while the spectrometer-derived formulas pertain to the reflectance wavelength value (nm).

Platform	Index Name	Index	Formula	Reference
Digital Camera	Green Excess	GEI	$2 * G_{DN} - (R_{DN}+B_{DN})$	Richardson et al., 2007
Digital Camera	Red digital number	Red DN	R_{DN}	Richardson et al., 2007
Digital Camera	Green digital number	Green DN	G_{DN}	Richardson et al., 2007
Digital Camera	Blue digital number	Blue DN	B_{DN}	Richardson et al., 2007
Digital Camera	Total digital number	Total RGB	$(R_{DN} + G_{DN} + B_{DN})/3$	Richardson et al., 2007
Digital Camera	Percent red	%R	$(R_{DN})/(R_{DN}+G_{DN}+B_{DN})$	Richardson et al., 2007
Digital Camera	Percent green	%G	$(G_{DN})/(R_{DN}+G_{DN}+B_{DN})$	Richardson et al., 2007
Digital Camera	Percent blue	%B	$(B_{DN})/(R_{DN}+G_{DN}+B_{DN})$	Richardson et al., 2007
Digital Camera	Lightness	L*	**See Reference	Paschos, 2001
Digital Camera	A-red-green	A*	**See Reference	Paschos, 2001
Digital Camera	B-blue-yellow	B*	**See Reference	Paschos, 2001
Digital Camera	AnyColor	AnyColor	**See Reference	Paschos, 2001
Digital Camera	Hue	Hue	**See Reference	Paschos, 2001
Digital Camera	Saturation	Saturation	**See Reference	Paschos, 2001
Digital Camera	Value	Value	**See Reference	Paschos, 2001
Digital Camera	nNDVI	nNDVI	$(R_{DN}-G_{DN})/(R_{DN}+G_{DN})$	Ramirez et al., in prep
Digital Camera	Test	TEST(L*A*)	A*(1+(L*)/(255))	Ramirez et al., in prep
Spectrometer	Carotenoid 1	CRI1	(1/R510)-(1/R550)	Gitelson et al., 2002
Spectrometer	Carotenoid 2	CRI2	(1/R510)-(1/R700)	Gitelson et al., 2002
Spectrometer	Gitelson 4	Gitelson4	(1/R550)-(1/R750)	Gitelson et al., 2003
Spectrometer	Gitelson 5	Gitelson5	(1/R700)-(1/R800)	Gitelson et al., 2003
Spectrometer	Greenness 1	Green1	(R554/R675)	Huemmrich K.H., personal communication
Spectrometer	Modified Normalized Difference Vegetation Index	MNDVI	(R750-R705)/(R750+R705-(2*R445))	Liu and Huete, 1995
Spectrometer	Modified Simple Ratio	MSR	(R750-R445)/(R705-R445)	Sims and Gamon, 2002
Spectrometer	Normalized Difference Soil Water Index- linear	NDSWI-lin	(R460-R1000)/(R460+R1000)	Goswami et al., 2011
Spectrometer	Normalized Difference Soil Water Index- log	NDSWI-log	(log(R1000) - log(R460))/(log(R1000) + log(R460))	Goswami et al., 2011
Spectrometer	Normalized Difference Vegetation Index	NDVI	(R800-R680)/(R800+R680)	Tucker, 1978
Spectrometer	Optimized Soil Adjusted Vegetation Index	OSAVI	1.16*(R800-R670)/(R800+R670+0.16)	Rondeaux et al., 1996
Spectrometer	Photochemical Reflectance Index 2	PRI 2	(R530-R550)/(R530+R550)	Sims and Gamon, 2002
Spectrometer	Structure Independent Pigment Index	SIPI	(R800-R450)/(R800-R650)	Peñuelas et al., 1995
Spectrometer	Water Band Index	WBI	(R900/R970)	Claudio et al., 2006

3.3.2.2 Kite aerial photography (KAP)

A single-camera rig system (SCRS) attached to a delta kite, similar to that used by *Andresen et al.*, 2014, was utilized to acquire aerial images of the MISP transects in both Utqiaġvik and Atqasuk (Figures 3.2 & 3.3). RGB images were acquired every one to two weeks depending on the weather conditions (e.g. wind speeds, rain, fog etc.) between early June and late August from 2010 to 2015, and were taken within 4 hours of solar noon (approximately 1 pm Alaska standard time; 2 hours before and 2 hours after) to maximize solar radiance and minimize

shadowing. All field acquisitions were taken from an altitude suitable for capturing the entire MISP transect in one image (~ 50-70 meters), which limited the need for image-stitching or mosaicking while preserving adequate spatial resolution for each image. To ensure coverage and avoid image distortion from high winds or condensation, hundreds of images were acquired "blindly" on each flight and the best two photographs were chosen to represent productivity (greening) for that particular day.

3.3.2.3 Pheno-cam imagery

Digital repeat photography (DRP) was also utilized to document seasonal and inter-annual trends at both MISP transects by using relatively low-cost time-lapse cameras (*Wingscapes WSCA02 BirdCam 2.0*). The cameras were mounted on-top of a meteorological tower with an average view angle from horizontal of -10° and centered on the middle of the transect. Imagery was acquired hourly in high-resolution true color (8 megapixel) red, green, and blue (RGB) during each growing season from 2011 to 2014, (Figures 3.4 & 3.5). The limited view angle from this system restricted total image coverage to 45 plots in both sites. Data for 2010 and 2015 are missing due to a lack of established infrastructure and logistical difficulties, respectively. Each camera was configured to acquire imagery with automatic exposure settings resulting in pixels representing relative brightness for each channel, rather than total radiance. These particular cameras were chosen for their time-lapse features, rugged design (e.g. freeze proof and water resistant), lightweight construction, and cost effectiveness (each cost approximately US $150).

Figure 3.4: DRP acquired from the Pheno-cams displaying the primary seasonal stages of the Utqiaġvik MISP transect during the 2013 growing season. Day of year (DOY) is displayed on the top right corner of each image and grouped vegetation classes are seen in image from DOY 191. The view-angle of this system is highlighted which limited the coverage of all plots equally (closer resulted with better coverage versus those that were further away).

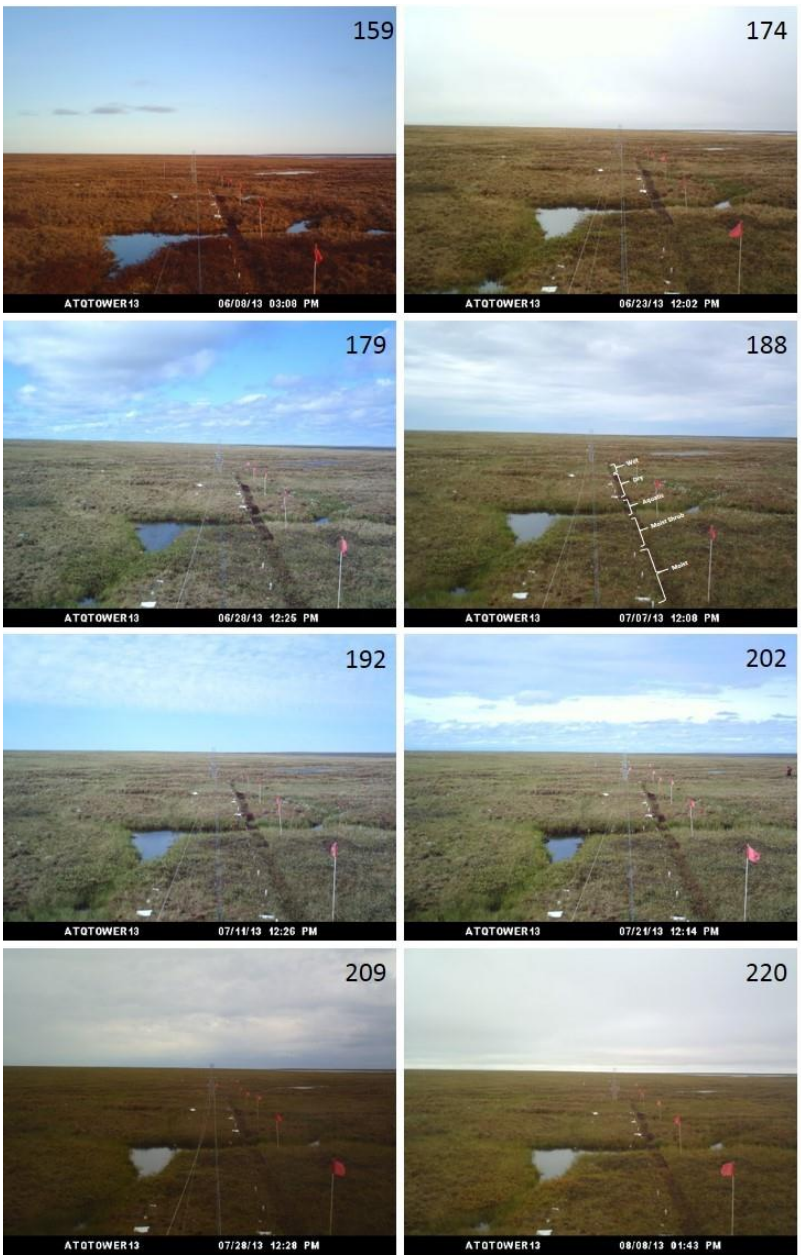

Figure 3.5: DRP acquired from the Pheno-cams displaying the primary seasonal stages of the Atqasuk MISP transect during the 2013 growing season. Day of year (DOY) is displayed on the top right corner of each image and grouped vegetation classes are seen in image from DOY 188. The view-angle of this system is highlighted which limited the coverage of all plots equally (closer resulted with better coverage versus those that were further away).

3.3.2.4 Ground-based surface measurements

A suite of ancillary data were acquired at least weekly during the snow-free period near the perimeter of the north side of each plot along both transects to minimize disturbance of the tundra vegetation within the plots. Volumetric soil water content (VWC) was obtained using a portable time-domain reflectometry (TDR) unit with the 12 cm rods (FieldScout TDR 300 Soil Moisture Meter; Spectrum Technologies, Inc., Plainfield, IL, USA). This instrument converts a measured electrical signal into percent soil moisture content using an equation valid over a wide-range of mineral soils. Soil temperature (°C) between 5 and 10 cm below each plot surface was measured using an inexpensive handheld digital thermometer (Commercial Waterproof Digital Thermometer; Taylor Precision Products, Inc., Oak Brook, IL, USA). Thaw depth was also monitored for each plot following a protocol developed for the *Circumpolar Active Layer Monitoring (CALM)* program (*Brown et al.*, 2000). Water table depth data was collected manually relative to the ground surface by inserting 15 cm long PVC tubes with holes drilled throughout into the tundra and below the active layer. A total of 22 tubes were installed along each transect at locations containing representative vegetation classes and corresponding soil moistures. Negative numbers indicated water levels below the ground surface and positive ones indicated pooling of surface water above the surface (*Goswami et al.*, 2011). Albedo data collected by the MISP robotic sensor platform and along the middle of each plot were also utilized for this study. Please see *Healey et al.*, (2014), for more details on data collection and processing.

3.4 DATA PROCESSING

3.4.1 Vegetation classification

As part of the AON-ITEX initiative, plant species cover was determined along both MISP transects during the summer of 2011 close to peak growing season by Grand Valley State University (GVSU) partners to the ITEX-AON project. Data were collected at 46 plots in Utqiaġvik and 42 plots in Atqasuk out of the total 50 plots. The reduced number of plots sampled reflects microtopographic, surface roughness, and logistical limitations associated with the sampling. A custom built metal frame was first leveled over each 2 x 1 meter plot and visual estimation of the percent cover of each species was made within each 10cm x 10cm grid cells nested within the 2 x 1 meter plot. This resulted in each plot having 190 subplots. The precision

of the sampling frame placement was limited due to microtopographic characteristics of the surface and the nature of sampling at such fine scales within a structurally complex ecosystem. To prevent the metal sampling frame from sinking into the tundra and to limit disturbance, the platform was designed to use the existing GCPs as support. Additionally, all subplot squares lined up perfectly with adjacent plots so that no ground sampling was missed or sampled more than once. Every effort was made so that repeat sampling is possible by installing small permanent markers within the plots that can be used to guide the frame placement in future years.

Species cover data were used to classify both transects into discrete plant communities using Hierarchical Cluster Analysis in PC-ORD 6 (MjM Software Design Gleneden Beach, OR, USA). SØrensen's similarity coefficient was employed with a flexible beta linkage method ($\beta = -0.25$) to minimize chaining (*McCune, B., and Grace*, 2002). A cutoff of less than 50% similarity for the Utqiaġvik communities and 55% for the Atqasuk plant communities was used to match these clusters with a high resolution (0.5 m) land cover classification map (*Andresen et al.* in prep.) derived from multiple World View 2 imagery. A total of 5 vegetation classes were identified at each site and are described in Table 3.1. At the Atqasuk MISP transect, it is important to note that the plots classified as *aquatic* are part of a large thermokarst trough that is connected to a drainage system adjacent to the MISP transect. Depending on the amount of snow from the previous winter, each summer showed different characteristics of plant composition within those three plots. When large amounts of water accumulated in the trough, greening tended to be low as few plants were able to grow above water level, however graminoids dominated these plots when water drained out and provided suitable conditions for plant growth.

3.4.2 RGB image processing

All digital images were manually sorted for quality by visually inspecting and removing any that displayed evidence of compromised relative brightness values caused by factors such as off nadir-view for the kite images, off focus or blurriness, and lens conditions that were altered by mist, fog, and/or condensation. For all years of this study, the two best images were selected from each flight date from the kite system as representative "snap-shots" of the plots on those particular sampling dates and times. For the Pheno-cam, daily median values of each spectral index were calculated from images acquired within 4 hours of solar noon to minimize impacts of shading and diurnal differences in irradiance. In some instances, images were not acquired and/or excluded

from the analysis due to low image quality (e.g. Pheno-cam view angle was shifted following high winds; image distortion; and the same problems reported above for KAP imagery etc.), which resulted in random gaps throughout the time series.

The selected images were then analyzed using the *Phenology Analyzer* software, which is a MATLAB application developed within the Systems Ecology Lab (SEL) and the Cyber-ShARE Center of Excellence at UTEP (Gesuri Ramirez et al., *patent pending*). This program allows for the selection of numerous Regions of Interest (ROI), with a range of customizable shapes and sizes and calculates red, green and blue channel intensity values, as well as a variety of RGB derived spectral indices for each given ROI (see Table 3.2, digital platforms). A total of 46 and 42 ROIs were created for each Pheno-cam image of the Utqiaġvik and Atqasuk MISP transects respectively (Figure 3.6). These ROIs correspond to the area sampled for species cover as described above. For KAP images, 48 ROIs at each transect were used for image analysis (Figure 3.7). Resulting spectral index values for each ROI were then exported as a text file and averaged to yield one value per plot per sampling day for KAP images and one value per plot per hour for the Pheno-cam images at both sites. In this study, we explored the GEI and green chromatic coordinate (percent green; %G) spectral indices (Table 3.2), which have proven utility for monitoring seasonal greening trends in various ecosystems including subalpine grasslands (*Migliavacca et al.*, 2011), forests (*Richardson et al.*, 2009; *Keenan et al.*, 2014), and low and high arctic tundra (*Westergaard-Nielsen et al.*, 2013, *Beamish et al.*, 2016).

Differences in RGB index values were assessed to enable inter-comparison between all camera systems using a grey color calibration card consisting of a brightness value of 127 in an 8-bit RGB scale 0-255. Images were repeatedly taken using each camera system simultaneously under the same light conditions and an average off-set factor from the gray scale value was determined for each channel. On average, the Pheno-cams displayed similar channel brightness variability with values of 115 ± 10, 128 ± 12 and 125 ± 10 for Red, Green, and Blue channels respectively. The kite system camera brightness values were 123 ± 10 for Red, 124 ± 11 for Green, and 128 ± 8 for the Blue channel. RGB channel intensities were then standardized across the different camera platforms in preparation for post processing (*Andresen, 2014).*

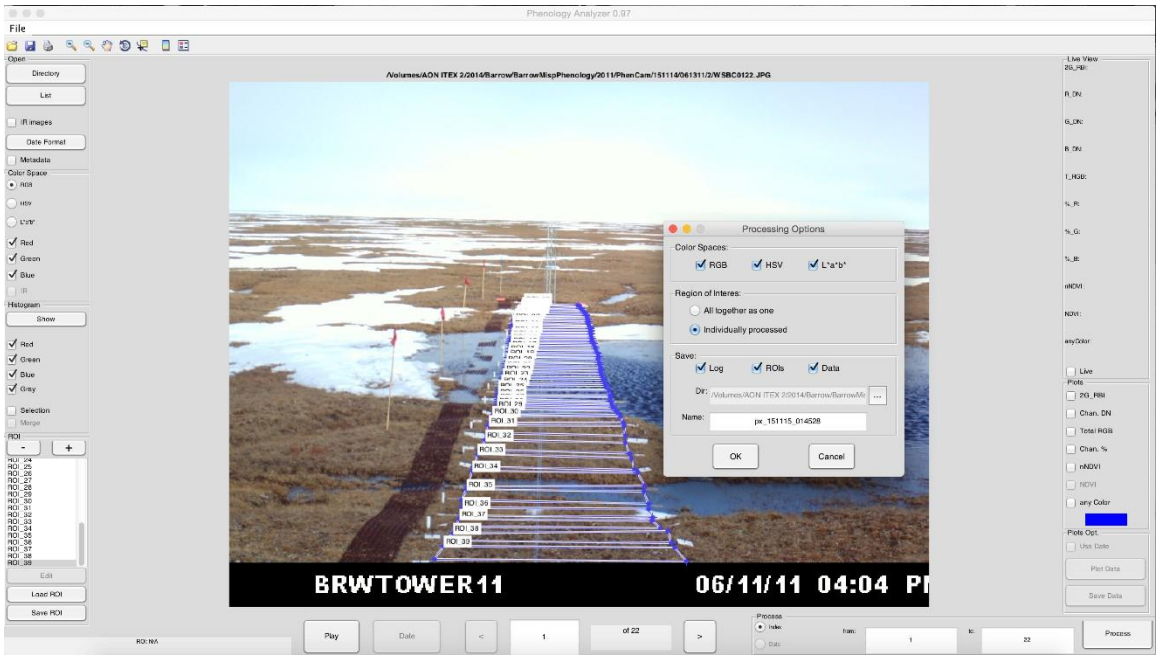

Figure 3.6: Example Pheno-cam image highlighting locations of ROIs across the Utqiaġvik MISP transect where spectral indices were extracted from for each sampling plot. All color spaces were explored using this approach (RGB, HSV and LAB).

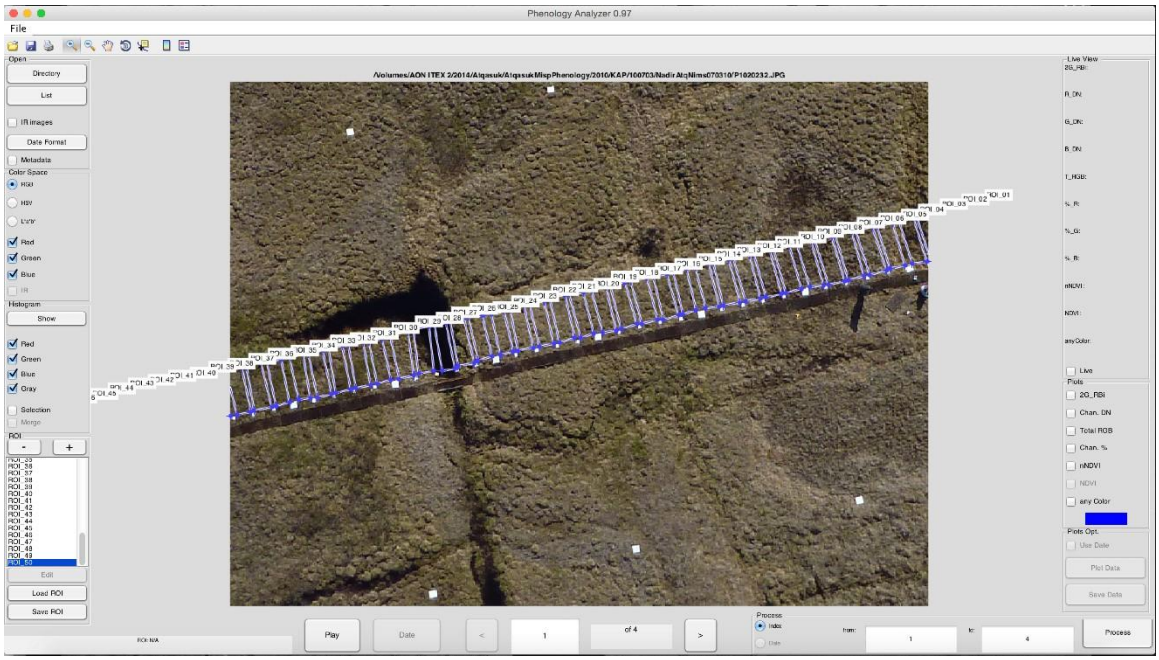

Figure 3.7: Example KAP image highlighting locations of ROIs across the Atqasuk MISP transect where spectral indices were extracted from for each sampling plot. All color spaces were explored using this approach (RGB, HSV and LAB).

3.4.3 Broad-band spectral reflectance processing

A custom-built software application, *rHyperSpec* (*Laney, 2012*), was utilized to process all broad-band reflectance data. This application was also developed in the SEL with an aim at reducing processing times and improving processing accuracy and visualization of multi-spectral data acquired specifically by the *PP Systems Unispec DC* spectrometer. Additionally, this package allows for a reduced number of post-processing steps and yields a gamut of spectral indices (see Table 3.2, spectrometer) commonly used within optical remote sensing. This software was utilized to process all raw data files for all sampling years and further explore and expand the application of optical sampling within the long term ITEX-AON monitoring program. Index values resulting from *rHyperSpec* were exported as a text file and averaged to yield one value per plot per sampling date.

3.5 DATA ANALYSIS

The main objective of this study was to assess the spectral outputs from digital cameras and compare them to outputs acquired from a ground-based spectrometer in order to explore the potential of these cost-effective alternatives (KAP and Pheno-cams) for monitoring and capturing seasonal and inter-annual phenology signals. Therefore, indices from each plot derived from all platforms were averaged by week of the year (WOY) and matched to corresponding vegetation classes calculated from the classification mentioned in section 3.4.1 in order to facilitate inter-comparison between datasets, which varied in temporal resolution and collection frequency. Additionally, these averages were used to minimize diurnal changes in light and weather conditions on vegetation. Statistical analyses focused on initially testing for normality of all data prior to determining correlations and regressions between all RGB derived indices and those acquired from the spectrometer. Specifically, NDVI was utilized as the reference index to which all other indices were compared as it has been shown to be a reliable indicator for estimating regional and continental scale changes in aboveground biomass and phenology in the Arctic (*Bhatt et al.*, 2010; *Zeng et al.*, 2011; *Walker et al.*, 2012). The Bonferroni correction was utilized to calculate an appropriate alpha value for each multivariate correlations and results were filtered to the appropriate significance level in order to reduce the possibility of type 1 errors from multiple comparisons (*Cabin et al.*, 2000). Pearson's correlations were calculated through *SAS JMP version 4.0.4* and *RStudio version 1.0.136* using the *cor*.test() function for all RGB and spectrometer indices across all vegetation classes (Table 3.3) and by vegetation class (Table 3.4), as well as between platforms across all classes (Table 3.5) and by vegetation class (Tables 3.6 and 3.7). Similarly, associations were tested between the ground-based surface measurements by vegetation classes (Table 3.10) and for all data (2011-2015) (Table 3.9) for both sites. In order to explore these trends further multiple linear regression (MLR) (*lm*() functions) was applied in an attempt to identify which surface measurements may drive seasonal trends and inter-annual differences in greenness the most (Tables 3.11 and 3.12). All data were plotted as a time series and fit with a smooth loess curve (Figures 3.8 - 3.13).

3.6 RESULTS

3.6.1 Timing of seasonal green-up

Plant growth, seasonal greening and peak greening signals were visually detectible with the naked-eye from the digital images acquired by both KAP and Pheno-cam sensors as seen from the 2013 summer field season examples in Figures 3.2, 3.3, 3.4 and 3.5. Early season images around day 163 from both platforms displayed some snow for the Utqiaġvik site and mostly brown and yellow leaf litter and standing water (mostly in Utqiaġvik) dominated the scenes over both transects. By day 170 the majority of the brown litter seemed to be taken over by green vegetation and surface water levels are shown to reduce in area in Utqiaġvik. A drastic green-up is seen around day 184 and continues through day 213 for the MISP grid in Utqiaġvik, while in Atqasuk green-up occurs earlier around day 173 and continues through day 209. A gradual yellowing is displayed around day 215 in Utqiaġvik and 220 in Atqasuk as seen from both KAP and Pheno-cam platforms, however images from the Pheno-cam seem to display these subtle changes better than the KAP system - probably due to the oblique view-angle. Similar trends and signals were seen across all sampling years for this study.

3.6.2 Seasonal and inter-annual greening patterns

Overall, both the KAP and Pheno-cam were able to detect similar seasonal green-up trends for all vegetation classes as specifically observed by the green RGB indices (GEI and %G) (Figures 3.8 and 3.9), which had the strongest correlations with NDVI compared to the majority of RGB calculated indices (Table 3.3 below). A large number of indices were excluded from further analysis because of the weak and non-significant correlations that resulted, thus the majority of analysis focused on the GEI and %G RGB indices. Additionally, each green index was able to detect variability among vegetation classes and across years in rates of greening and in some cases peak-greening for the majority of each growing season for both sites. Seasonal changes in greenness were more prominent and showed more seasonal and inter-annual variability when examined by vegetation class.

In Utqiaġvik, the GEI, %G and NDVI indices detected an incremental greening trajectory with the least seasonal and inter-annual variability for the drier vegetation classes (Figure 3.8). Those classes with higher soil moisture contents seemed to show higher greening values and more

seasonal and inter-annual variability. Peak greening is shown to occur around week 32 for all tundra classes as seen by all sensors, except for the drier communities, which showed faint changes in greenings towards the end of our sampling periods for each year. During 2014, all indices detected a sudden increase in greening around week 28 for seasonally flooded tundra, while in 2015 trends showed a sudden increase in greening around week 27 for all vegetation types, as seen from the KAP and spectrometer only.

Similar results were seen from the RGB and spectrometer greening trends in Atqasuk. The moist shrub vegetation classes exhibited the highest greening values with the most seasonal and inter-annual variability, however dry plant communities seemed to displayed more variability in greening and in some cases higher values when compared to those recorded in Utqiaġvik. During the 2011, 2012, and 2013 growing seasons all KAP indices were similar to NDVI trends in detecting low-greening for wet vegetation classes. The aquatic classes in Atqasuk showed various inter-annual trends as those seen during the 2011 and 2012 summers, where NDVI, GEI and %G observed high values of greening while during the 2013 and 2014 summers values were lowest among all classes.

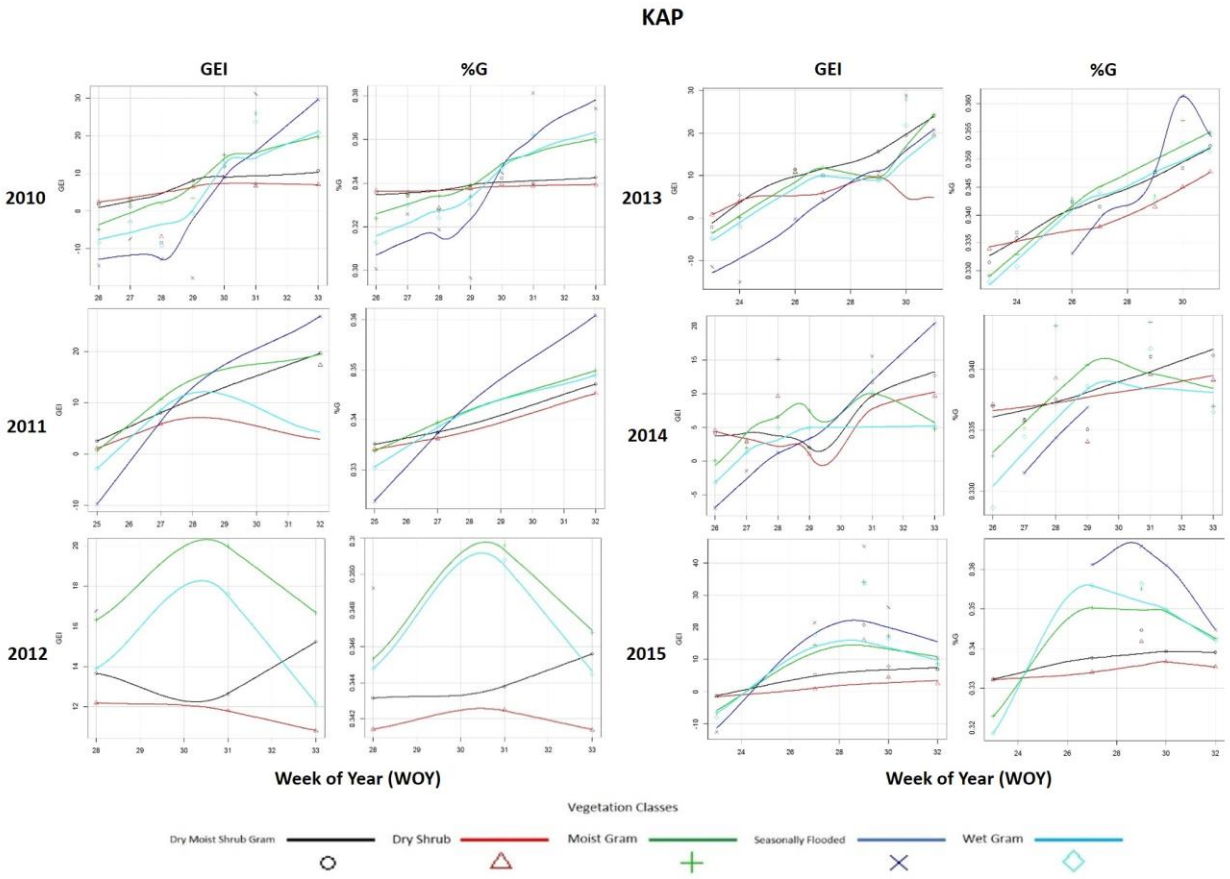

Figure 3.8a: Utqiaġvik MISP transect seasonal and inter-annual greening trends of all studied vegetation classes recorded from the KAP system (RGB GEI and %G) during 2010-2015 summers. Plots were fit with a smooth loess curve and the x-axis on all plots represents WOY (23-33).

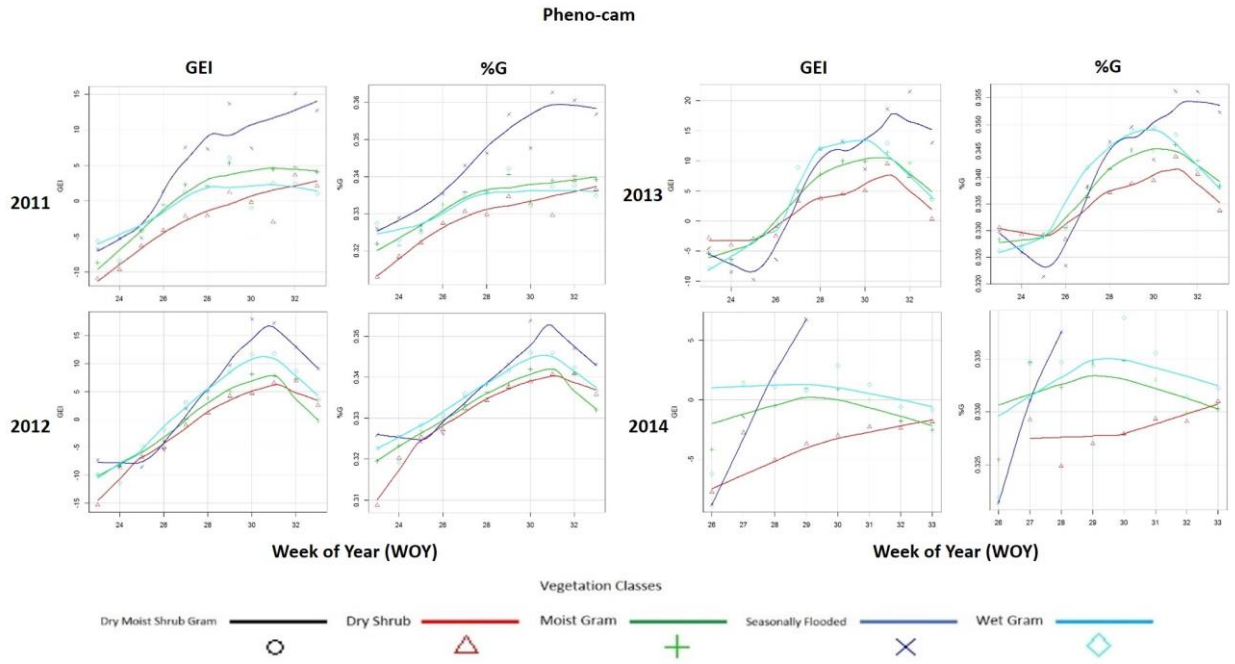

Figure 3.8b: Utqiaġvik MISP transect seasonal and inter-annual greening trends of all studied vegetation classes recorded from the Pheno-cam (RGB GEI and %G) during 2011-2014 summers. Plots were fit with a smooth loess curve and the x-axis on all plots represents WOY (23-33).

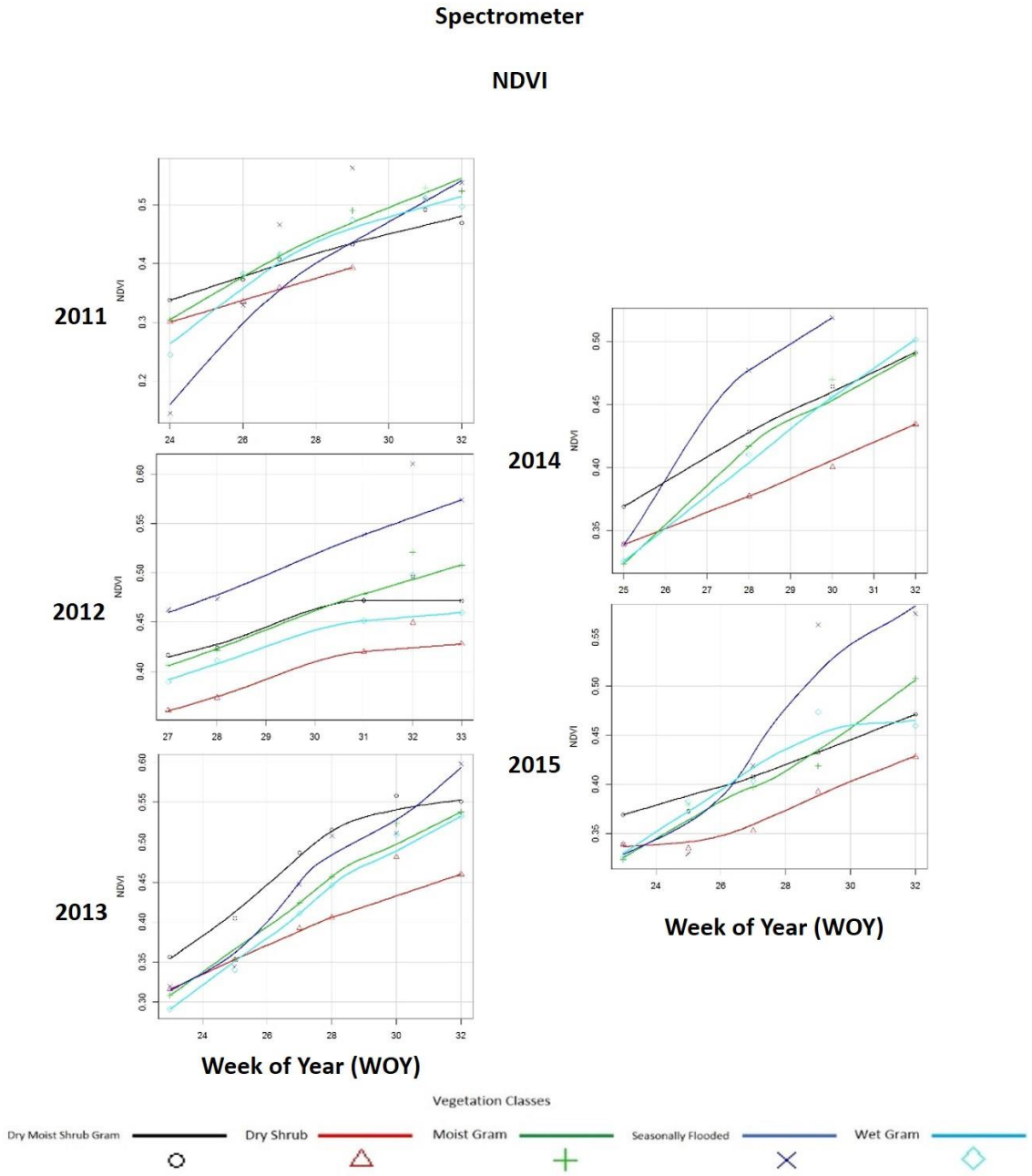

Figure 3.8c: Utqiaġvik MISP transect seasonal and inter-annual greening trends of all studied vegetation classes recorded from the spectrometer (NDVI) during 2011-2015 summers. Plots were fit with a smooth loess curve and the x-axis on all plots represents WOY (23-33).

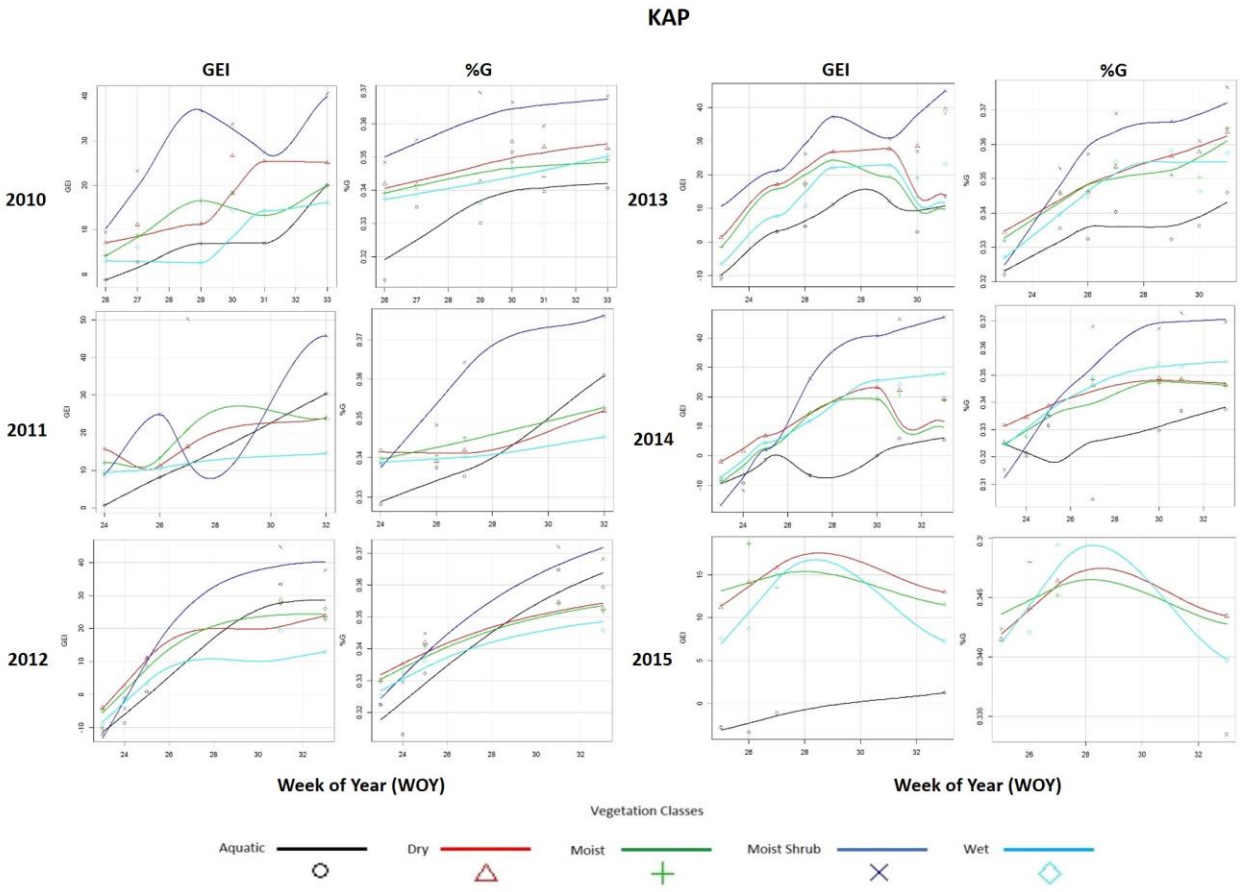

Figure 3.9a: Atqasuk MISP transect seasonal and inter-annual greening trends of all studied vegetation classes recorded from the KAP system (RGB GEI and %G) during 2010-2015 summers. Plots were fit with a smooth loess curve and the x-axis on all plots represents WOY (23-33).

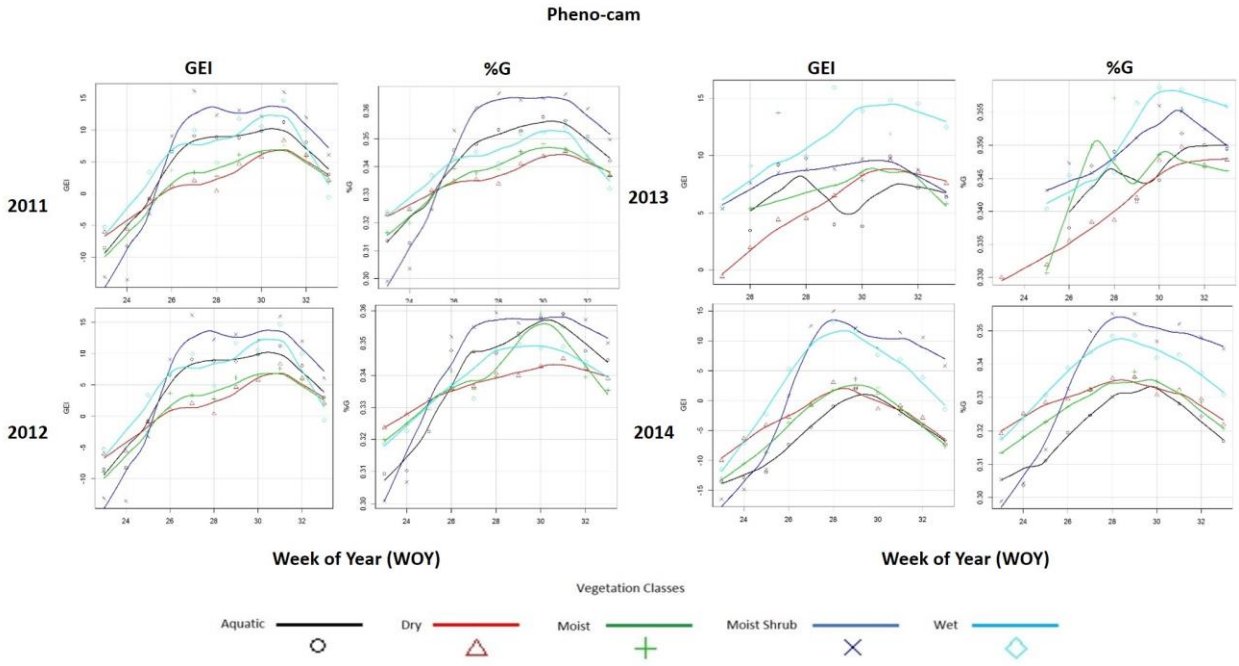

Figure 3.9b: Atqasuk MISP transect seasonal and inter-annual greening trends of all studied vegetation classes recorded from the Pheno-cam (RGB GEI and %G) during 2011-2014 summers. Plots were fit with a smooth loess curve and the x-axis on all plots represents WOY (23-33).

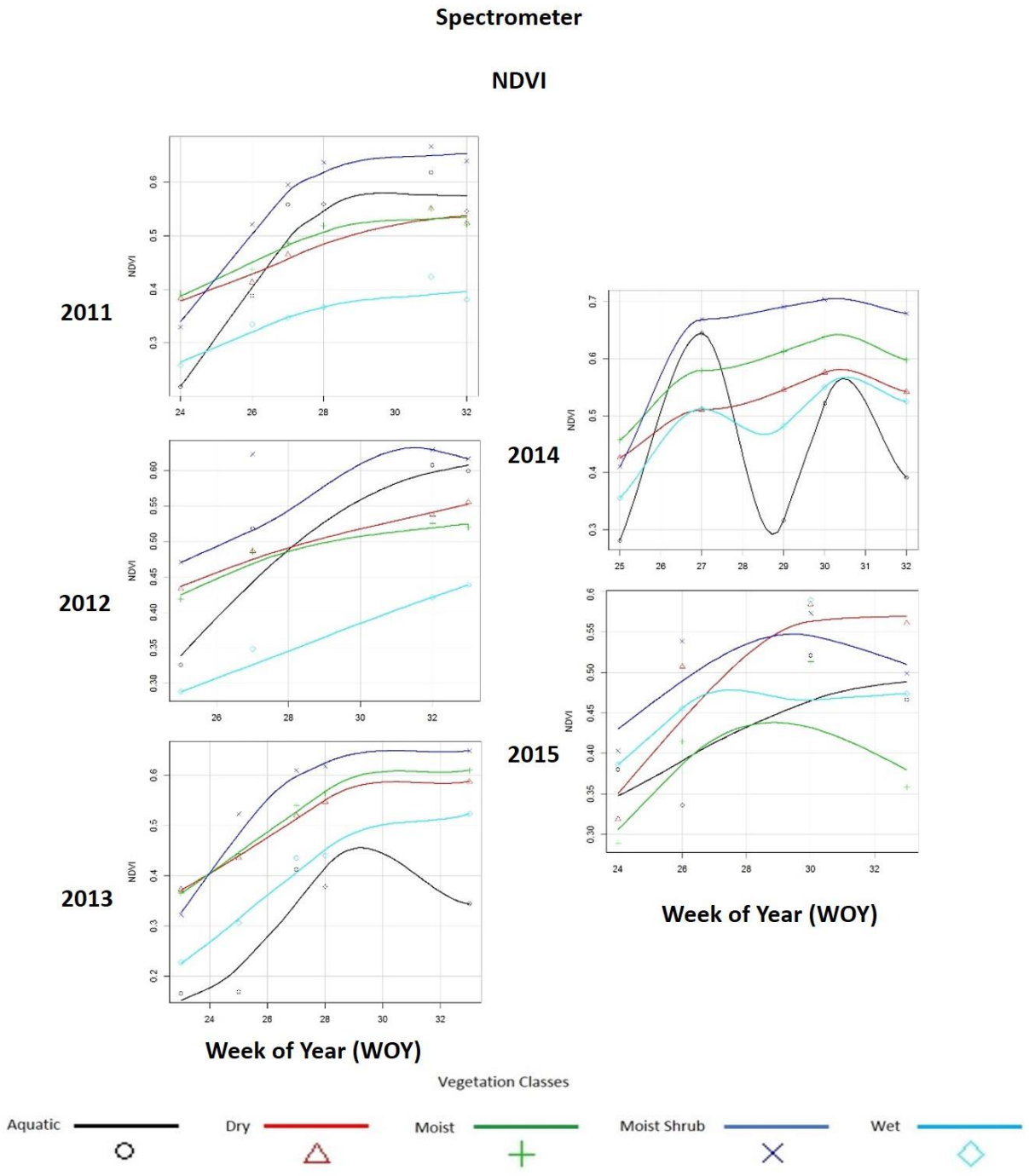

Figure 3.9c: Atqasuk MISP transect seasonal and inter-annual greening trends of all studied vegetation classes recorded from the spectrometer (NDVI) during 2011-2015 summers. Plots were fit with a smooth loess curve and the x-axis on all plots represents WOY (23-33).

Figures 3.10 and 3.11 depict the 5 year average of the RGB indices that were strongly correlated with NDVI and shows the seasonal greening trends from all approaches for both the Utqiaġvik and Atqasuk MISP transects. Across all years in Utqiaġvik and Atqasuk the wet vegetation classes seemed to be more productive than those classes with lower soil moisture values. In order to reduce multi-collinarity from the large number of correlations being examined, average Pearson's correlations were examined between GEI and %G and ground-based NDVI across all vegetation classes as a whole as well as by vegetation class within the MISP transects for both Utqiaġvik and Atqasuk. In Utqiaġvik across all classes, GEI correlated significantly strong with NDVI ($r= 0.76$, $p<0.0001$) while %G slightly less strong ($r= 0.68$, $p<0.0001$). However, %G resulted with stronger correlations with NDVI in Atqasuk ($r= 0.71$, $p<0.0001$) than GEI ($r= 0.68$, $p<0.0001$). When averages were taken from all resulting correlations at the vegetation class level, %G resulted with stronger correlations with NDVI in both Utqiaġvik and Atqasuk ($r= 0.78$, $p=0.006$; and $r= 0.72$, $p= 0.03$) respectively, than GEI ($r= 0.73$, $p= 0.017$; and $r= 0.07$, $p=0.03$).

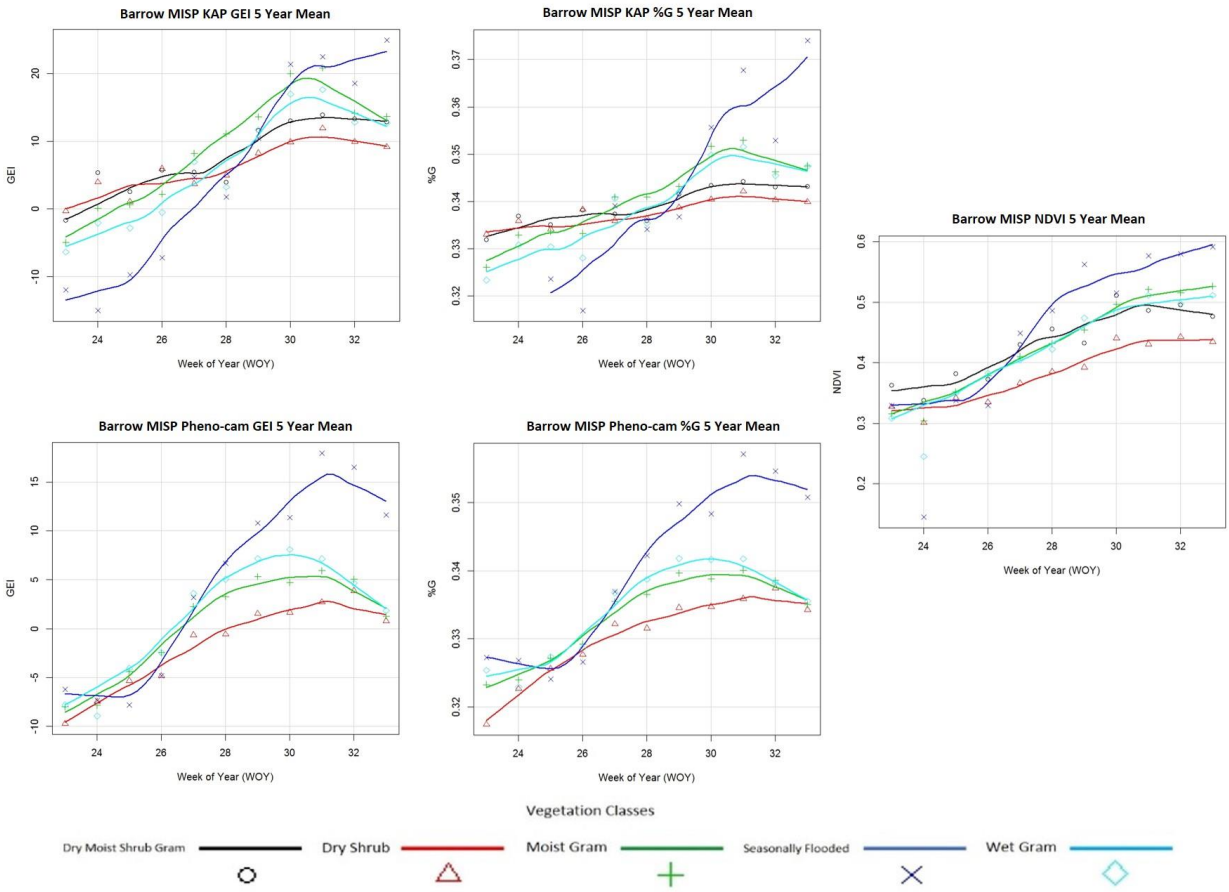

Figure 3.10: Utqiaġvik 5 year seasonal means of RGB-derived indices (GEI and %G) and spectrometer-derived NDVI for each vegetation class. Plots were fit with a smooth loess curve and the x-axis on all plots represents WOY (23-33).

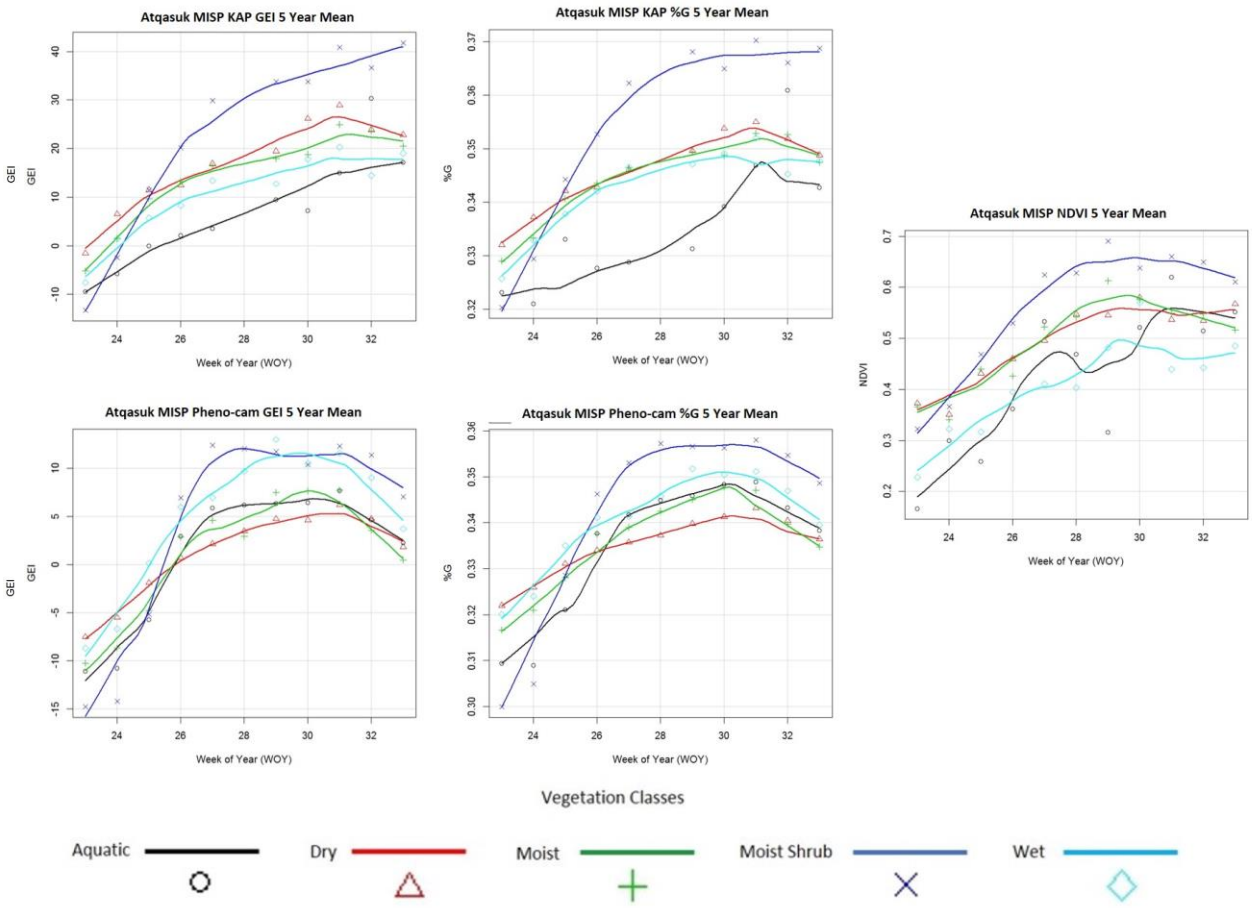

Figure 3.11: Atqasuk 5 year seasonal means of RGB-derived indices (GEI and %G) and spectrometer-derived NDVI for each vegetation class. Plots were fit with a smooth loess curve and the x-axis on all plots represents WOY (23-33).

3.6.3 Relationship strength between all indices and NDVI

The GEI and %G indices were able to detect subtle seasonal changes in greening throughout all years as seen from Figures 3.8a - 3.8c and 3.9a – 3.9c using both the KAP and Pheno-cam systems, which correlated well with NDVI values in Utqiaġvik. All correlations among GEI and %G and NDVI were strong resulting with r values greater than 0.7, $p < 0.05$. Moreover, several of the additional vegetation indices calculated from the spectrometer reflectance measurements also correlated strongly with NDVI across all classes, as seen from the Green, MNDVI and MSR indices in both Utqiaġvik and Atqasuk. Given the analysis at hand and the large number of correlations being explored, Table 3.3 summarizes the strongest and most significant

correlations (critical p-values adjusted using the Bonferroni correction) between all RGB derived indices and spectrometer-derived NDVI as well as between other spectrometer-derived indices and NDVI.

Table 3.3: Pearson's correlation results (critical p-values adjusted using the Bonferroni correction) between RGB and spectrometer-derived indices and NDVI specifically, for both the Utqiaġvik and Atqasuk MISP transects across all vegetation classes and data across all years.

Location	Platform	Index	r	p
Barrow	KAP	GEI	0.74	<0.0001
		%G	0.8	<0.0001
	Pheno-Cam	GEI	0.79	<0.0001
		%G	0.76	<0.0001
	UNISPEC	CRI1	0.74	<0.0001
		GREEN1	0.78	<0.0001
		MNDVI	0.94	<0.0001
		MSR	0.94	<0.0001
		OSAVI	0.56	<0.0001
		PRI2	-0.87	<0.0001
		SIPI	0.82	<0.0001
Atqasuk	KAP	GEI	0.79	<0.0001
		%G	0.82	<0.0001
	Pheno-Cam	GEI	0.56	<0.0001
		%G	0.6	<0.0001
	UNISPEC	CRI1	0.75	<0.0001
		GREEN1	0.85	<0.0001
		MNDVI	0.89	<0.0001
		MSR	0.9	<0.0001
		OSAVI	0.87	<0.0001
		PRI2	-0.86	<0.0001
		SIPI	0.91	<0.0001

When comparing correlations by vegetation classes, RGB indices and NDVI were generally stronger among %G and NDVI for the KAP system and between GEI and NDVI for the Pheno-cam systems at both sites, even though the results are subtle between both RGB platforms as seen in Table 3.4 below. In Utqiaġvik, correlations between KAP indices and NDVI were generally stronger for classes containing higher soil moisture content (e.g. moist gram- GEI (r=

0.67, p<0.05) and %G (r= 0.81, p<0.0001), seasonally flooded- GEI (r= 0.78, p<0.0001) and %G (r= 0.86, p<0.0001), and wet gram- GEI (r= 0.79, p<0.0001) and %G (r= 0.85, p<0.0001)) compared to drier classes (e.g. dry shrub- GEI (r=0.58, p<0.05) and %G (r= 0.71, p<0.05) and dry/moist shrub/gram- GEI (r= 0.66, p<0.05) and %G (r= 0.79, p<0.05)). The Pheno-cam in Utqiaġvik on the other hand did not capture marked differences between classes spanning a soil moisture gradient, however strong correlations resulted across classes nonetheless (i.e. dry shrub- GEI (r= 0.8, p<0.0001) and %G (r= 0.75, p<0.0001), moist gram- GEI (r= 0.78, p<0.0001) and %G (r= 0.78, p<0.0001), seasonally flooded- GEI (r= 0.81, p<0.0001) and %G (r= 0.74, p<0.0001), and wet gram- GEI (r= 0.71, p<0.0001) and %G (r= 0.74, p<0.0001)). Soil moisture also appeared to be related to site greening in Atqasuk, as seen from the strong associations between KAP GEI and %G and NDVI (Table 3.4). In Atqasuk, correlations between NDVI and KAP derived GEI in the moist shrub class resulted with a GEI r= 0.85, p<0.0001, %G r= 0.9, p<0.0001, while the wet class yielded a GEI r= 0.71, p<0.05 and %G r= 0.82, p<0.0001. The moist class resulted with a GEI r= 0.58, p<0.05 and %G 0.63, p<0.05. The dry vegetation class resulted with a GEI r=0.73 p<0.0001 and %G r= 0.79, p<0.0001. The Pheno-cam derived indices displayed lower correlations with NDVI values across all vegetation classes in Atqasuk when compared to the KAP system. The moist shrub class showed GEI r= 0.91, p<0.0001, and %G r= 0.88, p<0.0001, while the wet class yielded a GEI r= 0.65, p<0.05 and %G r= 0.61, p<0.05. The moist class resulted with a GEI r= 0.49, p<0.05 and %G r= 0.5, p<0.05. The dry vegetation class resulted with a GEI r= 0.65, p<0.05 and %G r= 0.65, p<0.05. It is important to note that the nNDVI index derived from the RGB images also had significant correlations with spectrometer-derived NDVI as seen mainly in the Atqasuk transect, specifically from the KAP system for the moist shrub (r= 0.8, p<0.0001) and moist classes (r= 0.72, p<0.05).The HUE index also corresponded well with NDVI from the KAP system for the dry (r= 0.73, p<0.05) and moist vegetation classes (r= 0.79, p<0.0001).

Associations between spectrometer-derived indices and NDVI were also explored at the vegetation class scale (Table 3.4) and similar findings were discovered to those across all classes as seen in Table 3.3 above. In Utqiaġvik, the dry moist shrub graminoid vegetation class displayed the strongest correlation between Green1 with NDVI with an r= 0.97, p<0.0001. Similarly, both the MNDVI and MSR were very strongly correlated with NDVI values resulting in r and p values of 0.94, <0.0001 and 0.93, <0.0001 respectively. Indices derived for the seasonally flooded class had the lowest correlations with NDVI but were strong nonetheless, with Green1 having an r of

0.71, p value of <0.0001, MNDVI having an r of 0.92, p value of <0.0001 and MSR with 0.93, p value of <0.0001. At the MISP transect in Atqasuk, strong correlations were also observed between spectrometer-derived indices and NDVI across all vegetation classes. The strongest correlations were recorded for the moist shrub class between NDVI and Green1 ($r=0.96$, $p<0.0001$), MNDVI ($r= 0.93$, $p<0.0001$), and MSR ($r= 0.89$, $p<0.0001$). The wet plots were lowest of all but still resulted with strong correlations between NDVI and Green1 ($r= 0.82$, $p<0.0001$), MNDVI ($r= 0.85$, $p<0.0001$), and MSR ($r= 0.91$, $p<0.0001$) (Table 3.4).

Table 3.4: Pearson's correlation results (critical p-values adjusted using the Bonferroni correction) between all indices (RGB and spectrometer-derived) and NDVI values for both the Utqiaġvik and Atqasuk MISP transects across each vegetation class.

Location	Veg Class	Platform	Index	r	P
Barrow	DMSGram	KAP	GEI	0.66	<0.05
			%G	0.79	<0.05
		UNISPEC	CRI1	0.81	<0.0001
			GITELSON5	0.85	<0.0001
			GREEN1	0.97	<0.0001
			MNDVI	0.94	<0.0001
			MSR	0.93	<0.0001
	Dry Shrub	KAP	GEI	0.58	<0.05
			%G	0.71	<0.05
		Pheno-Cam	GEI	0.8	<0.0001
			%G	0.75	<0.0001
		UNISPEC	CRI1	0.84	<0.0001
			GITELSON5	0.88	<0.0001
			GREEN1	0.9	<0.0001
			MNDVI	0.94	<0.0001
			MSR	0.94	<0.0001
	Moist Gram	KAP	GEI	0.67	<0.05
			%G	0.81	<0.0001
		Pheno-Cam	GEI	0.78	<0.0001
			%G	0.78	<0.0001
		UNISPEC	CRI1	0.75	<0.0001
			GITELSON5	0.7	<0.0001
			GREEN1	0.89	<0.0001
			MNDVI	0.93	<0.0001
			MSR	0.95	<0.0001
	Seasonally Flooded	KAP	GEI	0.78	<0.0001
			HUE	-0.75	<0.05
			%G	0.86	<0.0001
		Pheno-Cam	GEI	0.81	<0.0001
			%G	0.74	<0.0001
		UNISPEC	CRI1	0.81	<0.0001
			GREEN1	0.71	<0.0001
			MNDVI	0.92	<0.0001
			MSR	0.93	<0.0001
	Wet Gram	KAP	GEI	0.79	<0.0001
			%G	0.85	<0.0001
		Pheno-Cam	GEI	0.71	<0.0001
			%G	0.74	<0.0001
		UNISPEC	CRI1	0.75	<0.0001
			GREEN1	0.81	<0.0001
			MNDVI	0.96	<0.0001
			MSR	0.95	<0.0001
Location	Veg Class	Platform	Index	r	P
Atqasuk	Moist Shrub	KAP	GEI	0.85	<0.0001
			nNDVI	0.8	<0.0001
			%G	0.9	<0.0001
		Pheno-Cam	GEI	0.91	<0.0001
			%G	0.88	<0.0001
		UNISPEC	CRI1	0.82	<0.0001
			GITELSON5	0.67	<0.0001
			GREEN1	0.96	<0.0001
			MNDVI	0.93	<0.0001
			MSR	0.89	<0.0001
	Dry	KAP	GEI	0.73	<0.0001
			HUE	0.73	<0.05
			%G	0.79	<0.0001
		Pheno-Cam	GEI	0.65	<0.05
			%G	0.65	<0.05
		UNISPEC	CRI1	0.66	<0.0001
			GITELSON5	0.6	<0.05
			GREEN1	0.83	<0.0001
			MNDVI	0.89	<0.0001
			MSR	0.91	<0.0001
	Moist	KAP	GEI	0.58	<0.05
			HUE	0.79	<0.0001
			nNDVI	0.72	<0.05
			%G	0.63	<0.05
		Pheno-Cam	GEI	0.49	<0.05
			%G	0.5	<0.05
		UNISPEC	CRI1	0.73	<0.0001
			GREEN1	0.84	<0.0001
			MNDVI	0.94	<0.0001
			MSR	0.91	<0.0001
	Wet	KAP	GEI	0.71	<0.05
			%G	0.82	<0.0001
		Pheno-Cam	GEI	0.65	<0.05
			%G	0.61	<0.05
		UNISPEC	CRI1	0.76	<0.0001
			GREEN1	0.82	<0.0001
			MNDVI	0.85	<0.0001
			MSR	0.91	<0.0001

3.6.4 Relationship strength between RGB-derived and spectrometer-derived indices

Based on the Pearson's correlations results, not only did the GEI and %G indices appear to correlate very well with NDVI across all years (Table 3.3) and by vegetation classes as seen in Table 3.4 above, they also correlated well with a number of other spectrally-indices for all data years and across all classes as seen in Table 3.5 below. For the MISP transect in Utqiaġvik, KAP %G index had strong correlations with Green1 ($r= 0.81$, $p<0.0001$), MNDVI ($r= 0.74$, $p<0.0001$), MSR ($r= 0.76$, $p<0.0001$), PRI2 ($r= -0.76$, $p<0.0001$), and SIPI ($r= 0.63$, $p<0.0001$). KAP GEI on the other hand only showed strong correlations with MNDVI ($r= 0.66$, $p<0.0001$) and MSR ($r= 0.68$, $p<0.0001$).The Pheno-cam GEI and %G index correlated with Green1 ($r= 0.73$, $p<0.0001$; $r= 0.77$, $p<0.0001$), MNDVI ($r= 0.85$, $p<0.0001$; $r= 0.81$, $p<0.0001$), and MSR ($r= 0.82$, $p<0.0001$; $r= 0.78$, $p<0.0001$). The majority of the strong correlations at the Utqiaġvik site were also strong at the Atqasuk transect, although other indices also showed strong correlations. The KAP GEI index had a number of strong associations particularly with CRI ($r= 0.66$, $p<0.0001$), Green1 ($r= 0.75$, $p<0.0001$), MNDVI ($r= 0.71$, $p<0.0001$), MSR ($r= 0.69$, $p<0.0001$), OSAVI ($r= 0.72$, $p<0.0001$), PRI ($r= -0.75$, $p<0.0001$), and SIPI ($r= 0.71$, $p<0.0001$). The correlations for KAP %G were slightly stronger than those for GEI for the same spectral indices - CRI ($r= 0.76$, $p<0.0001$), Green1 ($r= 0.8$, $p<0.0001$), MNDVI ($r= 0.75$, $p<0.0001$), MSR ($r= 0.74$, $p<0.0001$), OSAVI ($r= 0.68$, $p<0.0001$), PRI ($r= -0.77$, $p<0.0001$), and SIPI ($r= 0.73$, $p<0.0001$). The Pheno-cam-derived indices had fewer correlations with other spectral indices than those from the KAP system but GEI was strongly correlated with Green1 ($r= 0.7$, $p<0.0001$), MNDVI ($r= 0.59$, $p<0.0001$), and MSR ($r= 0.59$, $p<0.0001$). Significant correlations for the Pheno-cam %G index occurred with Green1 ($r= 0.72$, $p<0.0001$), MNDVI ($r= 0.59$, $p<0.0001$), MSR ($r= 0.59$, $p<0.0001$), and PRI ($r= -0.61$, $p<0.0001$) as summarized in Table 3.5 below.

Table 3.5: Cross-platform Pearson's correlation results (critical p-values adjusted using the Bonferroni correction) between RGB indices and all spectrometer-derived indices for both the Utqiaġvik and Atqasuk MISP transects across all vegetation classes.

Location	Platform	Index	by Index	r	p
Barrow	KAP	GEI	MNDVI	0.66	<0.0001
		GEI	MSR	0.68	<0.0001
		%G	GREEN1	0.81	<0.0001
		%G	MNDVI	0.74	<0.0001
		%G	MSR	0.76	<0.0001
		%G	PRI2	-0.76	<0.0001
		%G	SIPI	0.63	<0.0001
	Pheno-Cam	GEI	GREEN1	0.73	<0.0001
		GEI	MNDVI	0.85	<0.0001
		GEI	MSR	0.82	<0.0001
		%G	GREEN1	0.77	<0.0001
		%G	MNDVI	0.81	<0.0001
		%G	MSR	0.78	<0.0001
Atqasuk	KAP	GEI	CRI1	0.66	<0.0001
		GEI	GREEN1	0.75	<0.0001
		GEI	MNDVI	0.71	<0.0001
		GEI	MSR	0.69	<0.0001
		GEI	OSAVI	0.72	<0.0001
		GEI	PRI2	-0.75	<0.0001
		GEI	SIPI	0.71	<0.0001
		%G	CRI1	0.76	<0.0001
		%G	GREEN1	0.8	<0.0001
		%G	MNDVI	0.75	<0.0001
		%G	MSR	0.74	<0.0001
		%G	OSAVI	0.68	<0.0001
		%G	PRI2	-0.77	<0.0001
		%G	SIPI	0.73	<0.0001
	Pheno-Cam	GEI	GREEN1	0.7	<0.0001
		GEI	MNDVI	0.59	<0.0001
		GEI	MSR	0.59	<0.0001
		%G	GREEN1	0.72	<0.0001
		%G	MNDVI	0.59	<0.0001
		%G	MSR	0.59	<0.0001
		%G	PRI2	-0.61	<0.0001

To further explore the relationship between RGB-derived indices and spectrally-acquired indices, associations were applied at the vegetation class level across all years of the study. Associations are stronger among %G and spectrometer-derived indices for the KAP system and for GEI for the Pheno-cam system at both sites even though the differences in resulting correlations are subtle as seen in Tables 3.6 and 3.7. Similar to the associations between RGB and NDVI seen in Table 3.5, strong correlations resulted between RGB indices and spectrometer-derived indices

and were generally found for classes with higher soil moisture in Utqiaġvik as seen for KAP-derived indices (e.g. moist gram- %G vs. Green1 ($r= 0.87$, $p<0.0001$), %G vs PRI ($r= -0.78$, $p<0.0001$), HUE vs. WBI ($r= 0.89$, $p<0.0001$), seasonally flooded- HUE vs. Gitelson ($r= 0.79$, $p<0.0001$), %G vs. Green1 ($r= 0.82$, $p<0.0001$), %G vs. MNDVI ($r= 0.85$, $p<0.0001$), %G vs. MSR ($r= 0.84$, $p<0.0001$), HUE vs. NDSWI-lin ($r= 0.95$, $p<0.0001$) %G vs. OSAVI ($r= 0.78$, $p<0.0001$), HUE vs. PRI ($r= 0.8$, $p<0.0001$), %G vs. PRI ($r= -0.75$, $p<0.05$), and HUE vs. WBI ($r= 0.91$, $p<0.05$) and wet gram- %G vs. Green1 ($r= 0.81$, $p<0.0001$), %G vs. MNDVI ($r= 0.76$, $p<0.0001$), %G vs. MSR ($r= 0.76$, $p<0.05$), HUE vs. NDSWI-lin ($r= 0.93$, $p<0.0001$), %G vs. OSAVI ($r= 0.78$, $p<0.0001$), %G vs. PRI ($r= -0.8$, $p<0.0001$), %G vs. SIPI ($r= 0.78$, $p<0.0001$), and HUE vs. WBI ($r= 0.88$, $p<0.0001$)) compared to classes with lower soil moisture (e.g. dry shrub- %G vs. Green1 ($r= 0.81$, $p<0.0001$), %G vs. NDSWI-lin ($r= -0.76$, $p<0.0001$), and %G vs. OSAVI ($r= 0.75$, $p<0.05$). No significant results were found for correlations between RGB indices and spectrometer-derived ones for plots classified as dry/moist shrub/graminoid tundra classes for the MISP transect in Utqiaġvik.

For the Atqasuk transect, stronger correlations were also recorded for classes containing higher soil moisture. For Pheno-cam-derived indices correlations were strong for wet (GEI vs. OSAVI ($r= 0.68$, $p<0.05$) and nNDVI vs Gitelson ($r= 0.77$, $p<0.0001$)), moist (GEI vs. Green1 ($r= 0.52$, $p<0.0001$), and GEI vs. OSAVI ($r= 0.54$, $p<0.0001$)), and moist shrub tundra (nNDVI vs. CRI ($r= 0.7$, $p<0.0001$), GEI vs. Green1 ($r= 0.87$, $p<0.0001$), GEI vs. MNDVI ($r= 0.86$, $p<0.0001$), nNDVI vs. MNDVI ($r= 0.71$, $p<0.0001$), GEI vs. MSR ($r= 0.81$, $p<0.0001$), nNDVI vs. MSR ($r= 0.7$, $p<0.0001$), GEI vs. OSAVI ($r= 0.93$, $p<0.0001$), GEI vs. PRI ($r= -0.88$, $p<0.0001$), and GEI vs. SIPI ($r= 0.91$, $p<0.0001$)). For classes typical of lower soil moisture classes correlations were less strong (e.g. dry- HUE vs. Gitelson ($r= -0.79$, $p<0.0001$), GEI vs. Green1 ($r= 0.7$, $p<0.0001$) and GEI vs. OSAVI ($r= 0.75$, $p<0.0001$), and no significant correlations were found for plots classified as aquatic (Tables 3.6 and 3.7).

Table 3.6: Cross-platform Pearson's correlation results (critical p-values adjusted using the Bonferroni correction) between RGB indices and spectrometer-derived indices for the Utqiaġvik MISP transect across each vegetation class.

Location	Veg Class	Platform	Index	by Index	r	p
Barrow	Dry Shrub	KAP	%G	GREEN1	0.81	<0.0001
			%G	NDSWI-lin	-0.76	<0.0001
			%G	OSAVI	0.75	<0.05
		Pheno-Cam	GEI	GITELSON5	0.74	<0.0001
			GEI	GREEN1	0.77	<0.0001
			%G	GREEN1	0.71	<0.0001
			GEI	MNDVI	0.8	<0.0001
			%G	MNDVI	0.74	<0.0001
			GEI	MSR	0.8	<0.0001
			%G	MSR	0.73	<0.0001
			GEI	OSAVI	0.77	<0.0001
			%G	OSAVI	0.72	<0.0001
	Moist Gram	KAP	GEI	GREEN1	0.77	<0.0001
			%G	GREEN1	0.87	<0.0001
			%G	PRI2	-0.78	<0.0001
			HUE	WBI	0.89	<0.0001
		Pheno-Cam	GEI	GREEN1	0.75	<0.0001
			%G	GREEN1	0.76	<0.0001
			GEI	MNDVI	0.81	<0.0001
			%G	MNDVI	0.8	<0.0001
			GEI	MSR	0.8	<0.0001
			%G	MSR	0.79	<0.0001
			GEI	OSAVI	0.74	<0.0001
			%G	OSAVI	0.74	<0.0001
	Seasonally Flooded	KAP	HUE	GITELSON5	0.79	<0.0001
			GEI	GREEN1	0.75	<0.05
			%G	GREEN1	0.82	<0.0001
			GEI	MNDVI	0.77	<0.0001
			%G	MNDVI	0.85	<0.0001
			GEI	MSR	0.75	<0.0001
			%G	MSR	0.84	<0.0001
			HUE	NDSWI-lin	0.95	<0.0001
			%G	OSAVI	0.78	<0.0001
			HUE	PRI2	0.8	<0.0001
			%G	PRI2	-0.75	<0.05
			HUE	WBI	0.91	<0.05
		Pheno-Cam	GEI	GREEN1	0.75	<0.0001
			%G	GREEN1	0.78	<0.0001
			GEI	MNDVI	0.89	<0.0001
			%G	MNDVI	0.8	<0.0001
			GEI	MSR	0.86	<0.0001
			%G	MSR	0.77	<0.0001
			GEI	OSAVI	0.73	<0.0001
	Wet Gram	KAP	%G	GREEN1	0.81	<0.0001
			%G	MNDVI	0.76	<0.0001
			%G	MSR	0.76	<0.05
			HUE	NDSWI-lin	0.93	<0.0001
			GEI	OSAVI	0.75	<0.05
			%G	OSAVI	0.78	<0.0001
			GEI	PRI2	-0.77	<0.0001
			%G	PRI2	-0.8	<0.0001
			GEI	SIPI	0.74	<0.05
			%G	SIPI	0.78	<0.0001
			HUE	WBI	0.88	<0.0001
		Pheno-Cam	GEI	MNDVI	0.75	<0.0001
			%G	MNDVI	0.78	<0.0001
			GEI	MSR	0.74	<0.0001
			%G	MSR	0.77	<0.0001
			GEI	OSAVI	0.83	<0.0001
			%G	OSAVI	0.85	<0.0001

Table 3.7: Cross-platform Pearson's correlation results (critical p-values adjusted using the Bonferroni correction) between RGB indices and spectrometer-derived indices for the Atqasuk MISP transect across each vegetation class.

Location	Veg Class	Platform	Index	by Index	r	p
Atqasuk	Moist Shrub	KAP	%G	CRI1	0.75	<0.0001
			GEI	GREEN1	0.84	<0.0001
			nNDVI	GREEN1	0.77	<0.0001
			%G	GREEN1	0.88	<0.0001
			GEI	MNDVI	0.76	<0.0001
			HUE	MNDVI	0.79	<0.0001
			nNDVI	MNDVI	0.87	<0.0001
			%G	MNDVI	0.83	<0.0001
			HUE	MSR	0.79	<0.0001
			nNDVI	MSR	0.86	<0.0001
			%G	MSR	0.79	<0.0001
			GEI	NDSWI-lin	-0.73	<0.0001
			GEI	OSAVI	0.88	<0.0001
			%G	OSAVI	0.86	<0.0001
			GEI	PRI2	-0.81	<0.0001
			%G	PRI2	-0.83	<0.0001
			GEI	SIPI	0.76	<0.0001
			%G	SIPI	0.79	<0.0001
		Pheno-Cam	nNDVI	CRI1	0.7	<0.0001
			GEI	GREEN1	0.87	<0.0001
			%G	GREEN1	0.86	<0.0001
			GEI	MNDVI	0.86	<0.0001
			nNDVI	MNDVI	0.71	<0.0001
			%G	MNDVI	0.81	<0.0001
			GEI	MSR	0.81	<0.0001
			nNDVI	MSR	0.7	<0.0001
			%G	MSR	0.76	<0.0001
			GEI	NDSWI-lin	-0.7	<0.0001
			%G	NDSWI-lin	-0.7	<0.0001
			GEI	OSAVI	0.93	<0.0001
			%G	OSAVI	0.94	<0.0001
			GEI	PRI2	-0.88	<0.0001
			%G	PRI2	-0.87	<0.0001
			GEI	SIPI	0.91	<0.0001
			%G	SIPI	0.89	<0.0001
	Dry	KAP	HUE	GREEN1	0.74	<0.0001
			HUE	MNDVI	0.86	<0.0001
			HUE	MSR	0.84	<0.0001
			GEI	OSAVI	0.8	<0.0001
			%G	OSAVI	0.82	<0.0001
			%G	SIPI	0.75	<0.0001
		Pheno-Cam	HUE	GITELSON5	-0.79	<0.0001
			GEI	GREEN1	0.7	<0.0001
			GEI	OSAVI	0.75	<0.0001
			%G	OSAVI	0.72	<0.05
	Moist	KAP	HUE	CRI1	0.77	<0.0001
			HUE	GREEN1	0.82	<0.0001
			nNDVI	GREEN1	0.74	<0.05
			%G	GREEN1	0.73	<0.05
			HUE	MNDVI	0.82	<0.0001
			nNDVI	MNDVI	0.74	<0.05
			HUE	MSR	0.77	<0.0001
			HUE	PRI2	-0.83	<0.0001
			nNDVI	PRI2	-0.76	<0.0001
		Pheno-Cam	GEI	GREEN1	0.52	<0.0001
			%G	GREEN1	0.53	<0.0001
			GEI	OSAVI	0.54	<0.0001
			%G	OSAVI	0.56	<0.0001
	Wet	KAP	%G	CRI1	0.79	<0.0001
			%G	GREEN1	0.76	<0.0001
			GEI	MNDVI	0.73	<0.05
			%G	MNDVI	0.82	<0.0001
			%G	MSR	0.8	<0.0001
		Pheno-Cam	nNDVI	GITELSON5	0.77	<0.0001
			GEI	OSAVI	0.68	<0.05

3.6.5 Seasonal surface characteristics

Descriptive statistics of the ground-based surface data collected for this study are summarized in Table 3.8 below and visualized in Figure 3.12a – 3.12e for Utqiaġvik and Figure 3.13a – 3.13e for Atqasuk. Soil temperature at depths between 5-10 cm below the surface of the Utqiaġvik MISP transect appeared the warmest in 2012, 2014, and 2015 with maximum temperature values reaching 4.4 °C, 4.5 °C, and 6.6 °C, as well as mean temperatures around 2.2 °C, 1.9 °C, and 3.6 °C respectively. 2013 and 2014 had the highest VWC values with maximum reaching and stabilizing at 74.3% and 74.03% respectively as seen for the seasonally flooded vegetation classes. Based on mean seasonal VWC, 2013 was the wettest (55.41%) followed by 2014 with 55.26%. Thaw depth was also monitored throughout each growing season and 2013 seemed to experience the deepest depth of thaw at 40.38 cm followed by 2015 with 35.72 cm during the end of season. The depth of the water table was highest in 2014 (10.33 cm above ground surface) followed by 2012 (6.8 cm). 2015 had the lowest depth (-30.6 cm below ground surface) followed by 2012 (-29.1 cm). Surface albedo data was recorded between 2012 and 2014 with an automated system throughout each growing season by researchers from FIU and peak season values were greatest for the dry/moist shrub/gram vegetation classes with a value of 0.1.

Compared to the Utqiaġvik MISP transect, the Atqasuk MISP transect displayed higher soil temperatures, lower soil moisture content, deeper thaw depth, deeper water table depth, and a similar albedo. 2014 had the highest soil temperatures with maximum values reaching 11.4 °C followed by 2013 at 10.3 °C. The highest mean temperatures were observed during 2013 and 2010 (5.8 °C and 5.6 °C respectively). The lowest soil temperatures were recorded in 2012 and 2013 (0.6 °C and 0.3 °C respectively). All data were plotted as a time series and fit with a smoothing loess curve to facilitate visualization of seasonal patterns and between-year variability (Figures 3.16 and 3.17). 2013 displayed the highest VWC maximum values of 71.2% followed by 2014 (68.7%) for the moist shrub classes. When compared to the Utqiaġvik MISP transect, WTD was lower reaching the highest at 7.25 cm above the ground during 2013 and lowest in 2012 with -30.75 cm below the surface. The AL thaw depth was considerably deeper in Atqasuk than in Utqiaġvik reaching maximum depths of 113.5 cm for 2012 and 2013 towards the end of the growing season.

Table 3.8: Yearly statistics of the ground-based surface data taken along each transect.

Site	Enviro. Parameter	Stat	2010	2011	2012	2013	2014	2015
Barrow	Soil Temperature (°C)	Min	-1.066	0.1066	0.425	-0.7711	0.5125	1.48
		Median	0.8054	1.0296	2.32	1.0473	2	3.467
		Mean	0.6085	1.0201	2.205	0.8601	1.996	3.619
		Max	2.0716	1.8602	4.412	2.0182	4.5125	6.612
		Std. Dev.	0.8822	0.4806	1.0912	0.7573	0.9923	1.2713
	Soil Moisture (%)	Min	NA	3.538	9.213	30.43	16.89	NA
		Median	NA	49.783	52.884	55.48	55.26	NA
		Mean	NA	47.193	46.917	55.41	52.28	NA
		Max	NA	73.95	72.9	74.36	74.03	NA
		Std. Dev.	NA	21.4402	18.3847	13.6796	15.7404	NA
	AL Thaw Depth (cm)	Min	10.5	4.25	4.75	10.9	5.25	17.82
		Median	23.88	16.87	17.75	29.46	20.36	29.34
		Mean	23.23	16.75	19.15	26.96	19.02	28.43
		Max	35.38	29.81	36.69	40.38	29.69	35.72
		Std. Dev.	8.4251	7.9071	9.3739	8.4589	7.4027	4.8162
	WTD (cm)	Min	NA	-8.2	-29.1	-24.9	-21.2	-30.667
		Median	NA	-0.375	-11.75	-8.417	-1	-14
		Mean	NA	-1.153	-11.946	-8.554	-3.505	-12.725
		Max	NA	4.375	6.875	5.75	10.333	2.938
		Std. Dev.	NA	2.8845	8.6388	8.2467	8.9753	9.1954
	Albedo	Min	NA	NA	0.1084	0.1195	0.113	NA
		Median	NA	NA	0.1606	0.155	0.1624	NA
		Mean	NA	NA	0.1691	0.1552	0.1631	NA
		Max	NA	NA	0.233	0.1997	0.2072	NA
		Std. Dev.	NA	NA	0.0293	0.01779	0.0213	NA
Site	Enviro. Parameter	Stat	2010	2011	2012	2013	2014	2015
Atqasuk	Soil Temperature (°C)	Min	1.45	0.5214	0.6	0.3	0.5071	1.483
		Median	5.592	4.0077	3.773	6.002	3.93	4
		Mean	5.683	3.829	3.953	5.858	4.3597	4.461
		Max	9.6	7	8.5	10.31	11.465	9.33
		Std. Dev.	2.1205	1.8038	2.1526	2.5409	2.3689	2.0665
	Soil Moisture (%)	Min	NA	17.47	9.693	9.871	7.693	NA
		Median	NA	32.81	31.33	52.775	47.707	NA
		Mean	NA	38.48	35.195	46.835	46.324	NA
		Max	NA	60.19	61.45	71.217	68.767	NA
		Std. Dev.	NA	13.9389	15.0942	17.7381	16.9437	NA
	AL Thaw Depth (cm)	Min	23.52	7.25	6	6.583	2.5	17.75
		Median	46.91	35	30.6	41.571	37.7	44.35
		Mean	52.65	42.05	36.19	44.637	38.83	47.43
		Max	111	113	113.5	113.5	103.5	95
		Std. Dev.	2.5675	27.7429	26.0401	26.3075	26.0507	21.7717
	WTD (cm)	Min	NA	-16.25	-30.75	-28.4	-28.5	-28
		Median	NA	0	-17.2	-11.75	-5.95	-15.5
		Mean	NA	-2.6	-16.995	-11.55	-8.125	-16.577
		Max	NA	4.7	1.875	7.25	6.25	3.875
		Std. Dev.	NA	4.4563	8.181	11.0461	9.8323	9.04553
	Albedo	Min	NA	NA	0.1285	0.0659	0.009526	NA
		Median	NA	NA	0.1572	0.14132	0.1346	NA
		Mean	NA	NA	0.1655	0.13255	0.1352	NA
		Max	NA	NA	0.2416	0.17919	0.1848	NA
		Std. Dev.	NA	NA	0.0296	0.0331	0.03121	NA

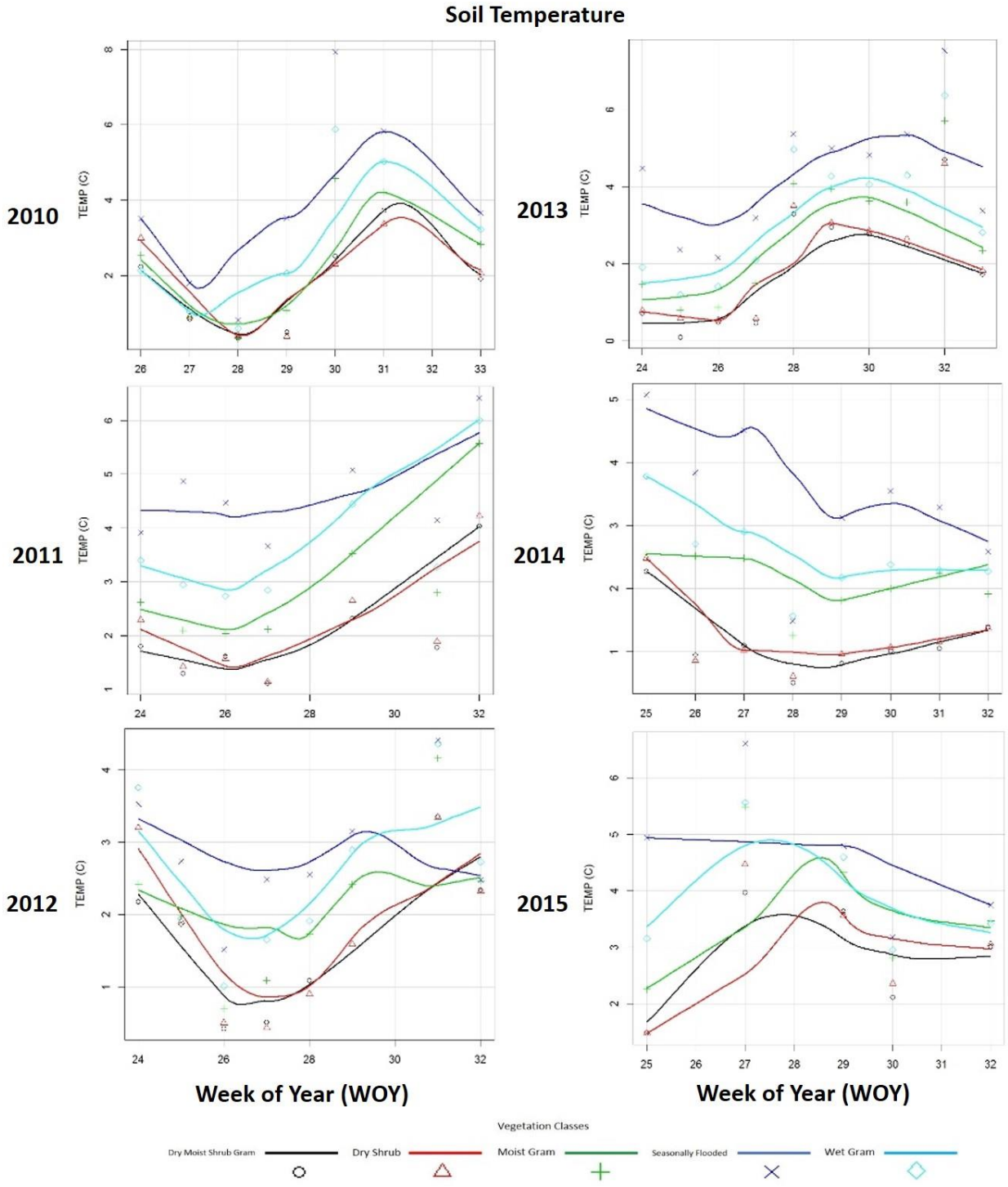

Figure 3.12a: Seasonal and inter-annual soil temperature (at ~5cm depth (°C)) averaged across each vegetation class located within the MISP transect in Utqiaġvik. Plots were fit with a smooth loess curve and the x-axis on all plots represents WOY (~23-33).

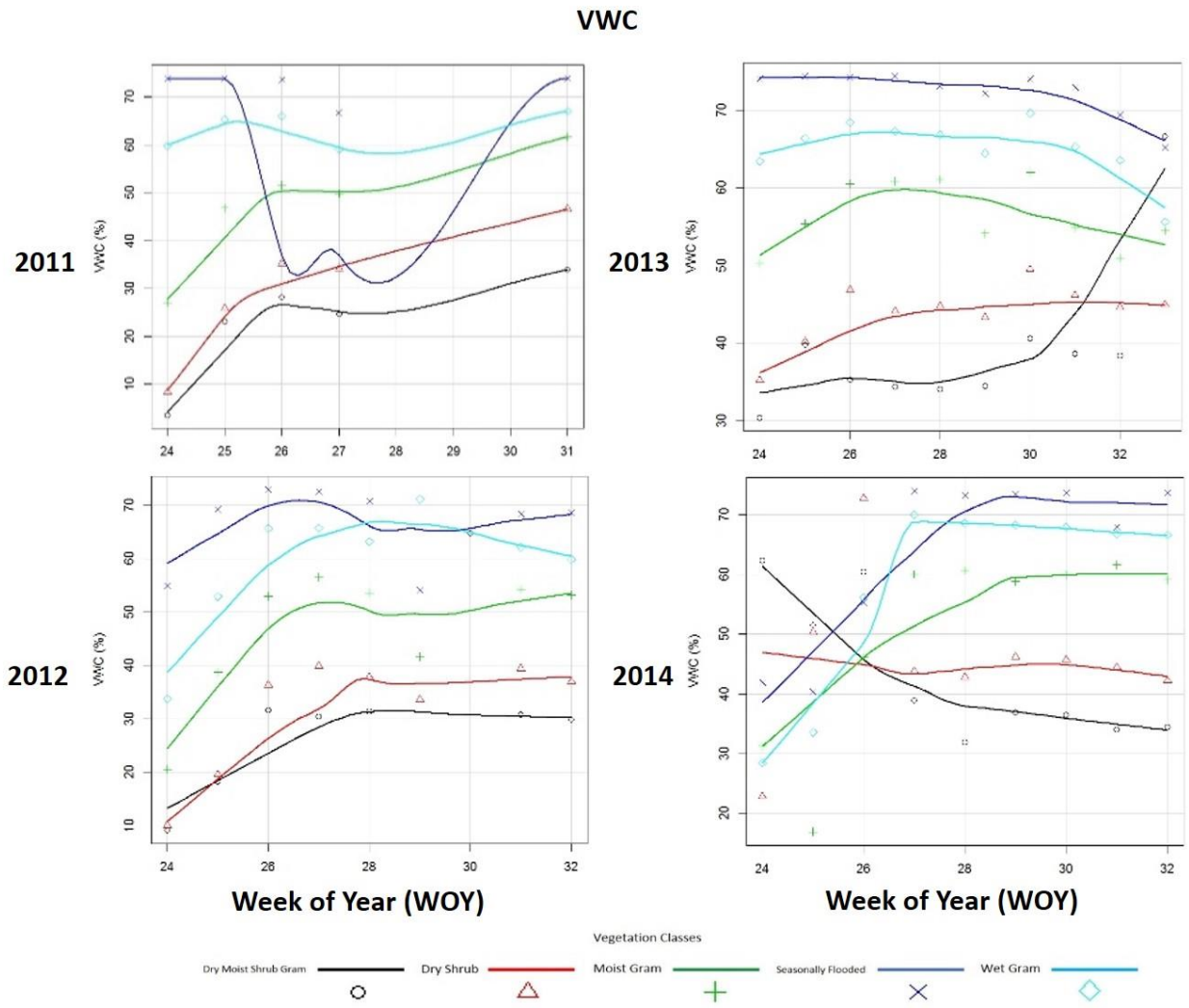

Figure 3.12b: Seasonal and inter-annual percent volumetric water content (VWC) averaged across each vegetation class located within the MISP transect in Utqiaġvik. Plots were fit with a smooth loess curve and the x-axis on all plots represents WOY (~23-33).

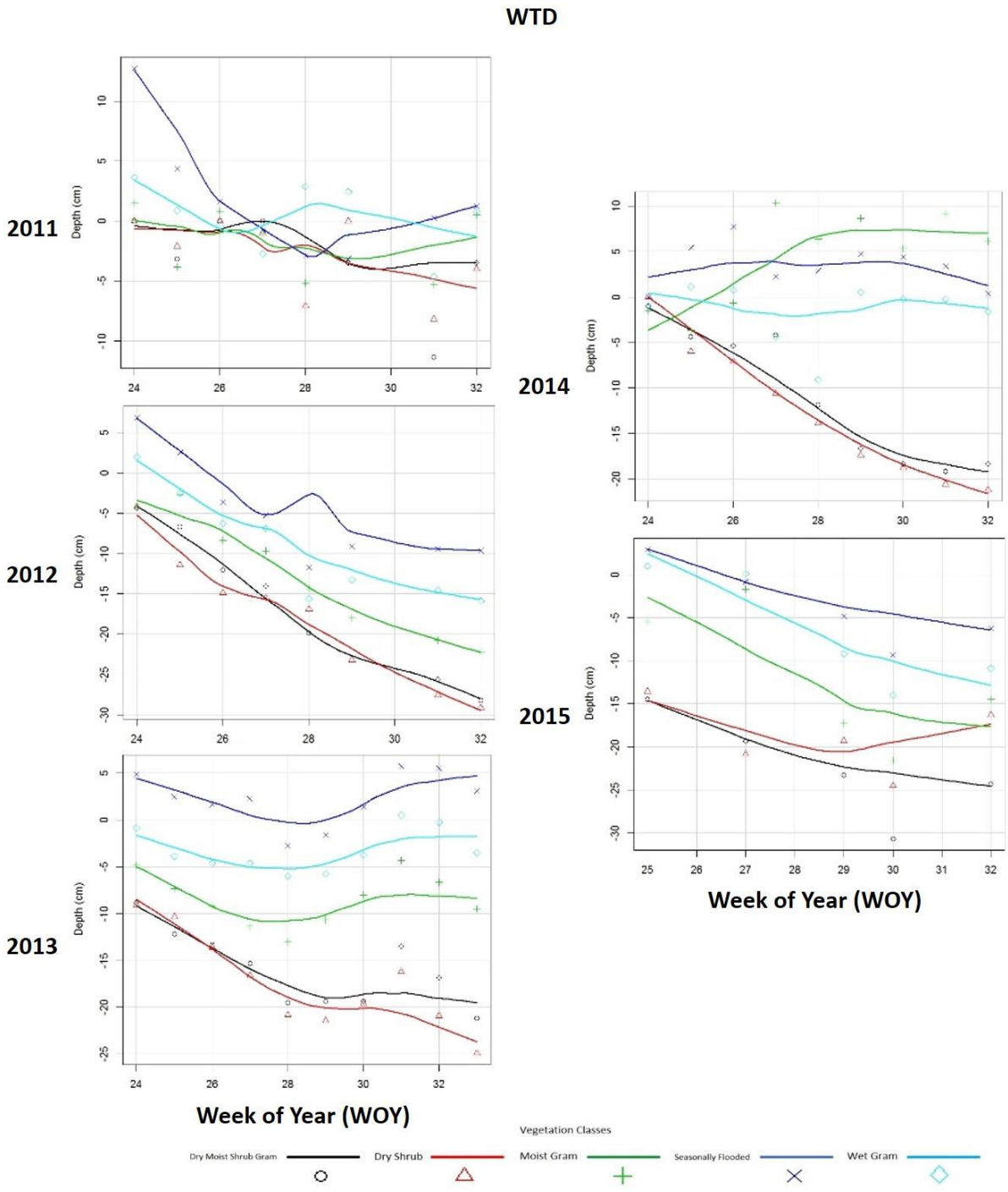

Figure 3.12c: Seasonal and inter-annual water table depth (WTD (cm)) averaged across each vegetation class located within the MISP transect in Utqiaġvik. The ground level is

represented at depth 0 cm. Plots were fit with a smooth loess curve and the x-axis on all plots represents WOY (~23-33).

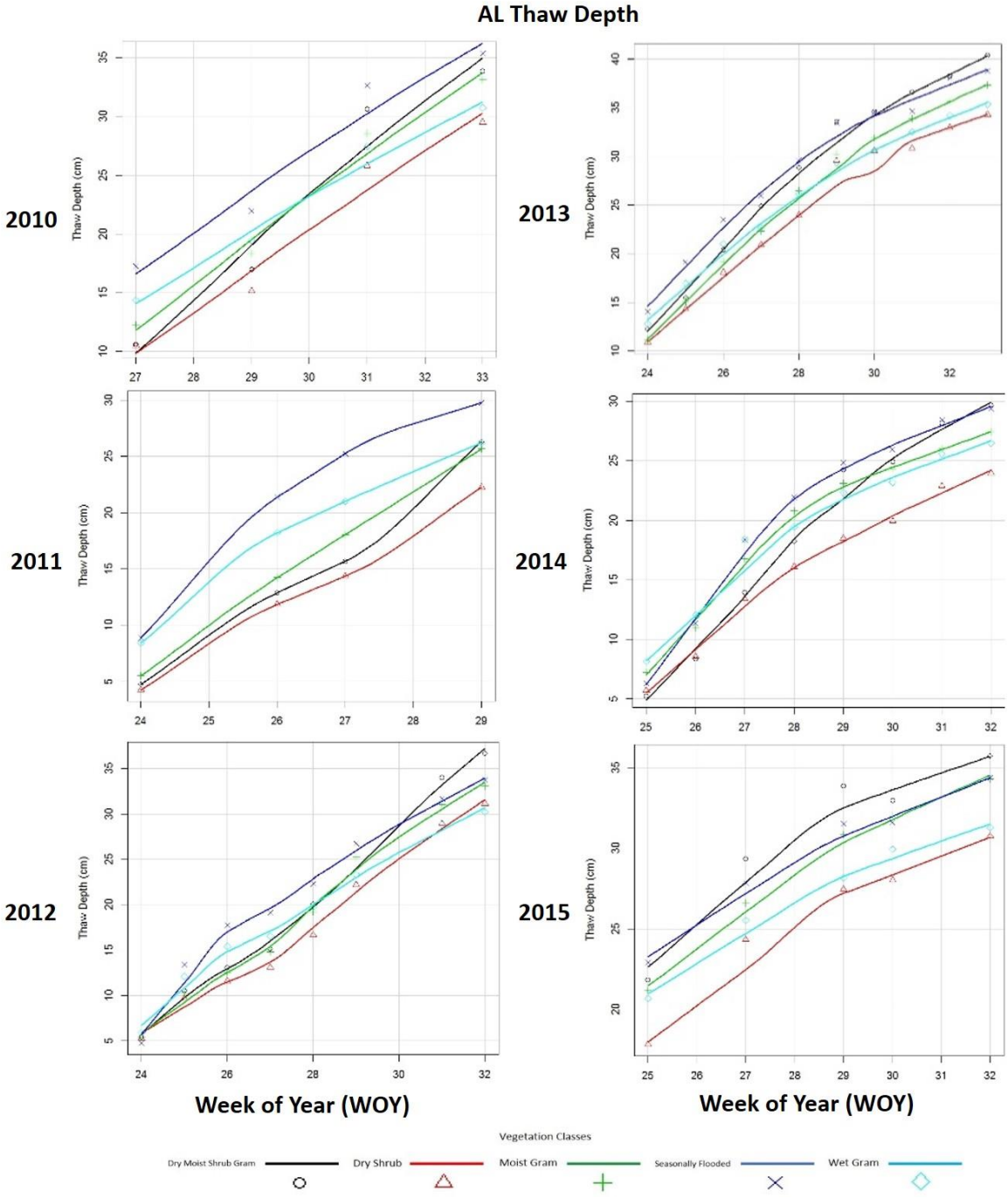

Figure 3.12d: Seasonal and inter-annual active layer thaw depth (AL (cm)) averaged across each vegetation class located within the MISP transect in Utqiaġvik. Plots were fit with a smooth loess curve and the x-axis on all plots represents WOY (~23-33).

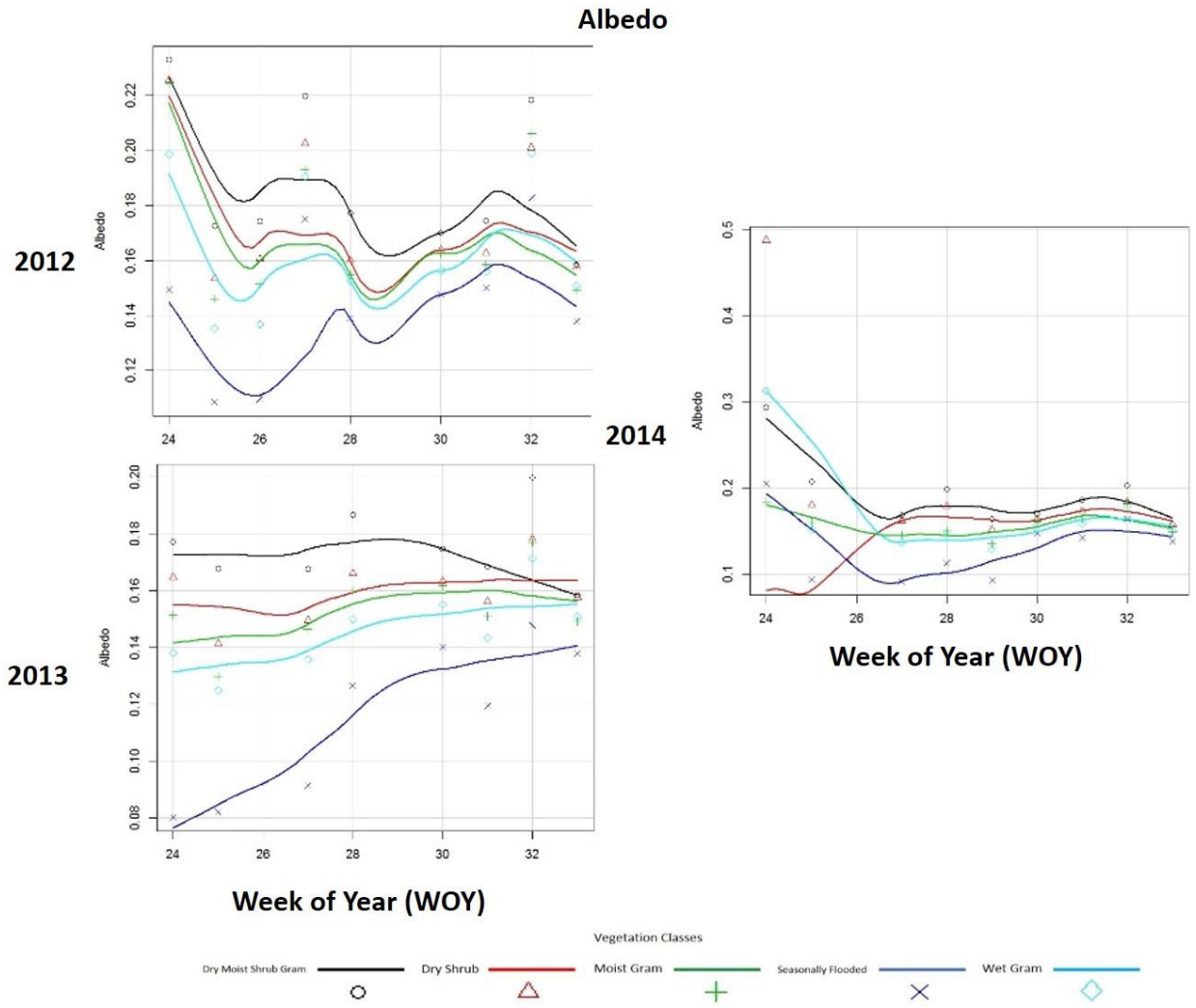

Figure 3.12e: Seasonal and inter-annual surface albedo averaged across each vegetation class located within the MISP transect in Utqiaġvik. Plots were fit with a smooth loess curve and the x-axis on all plots represents WOY (~23-33).

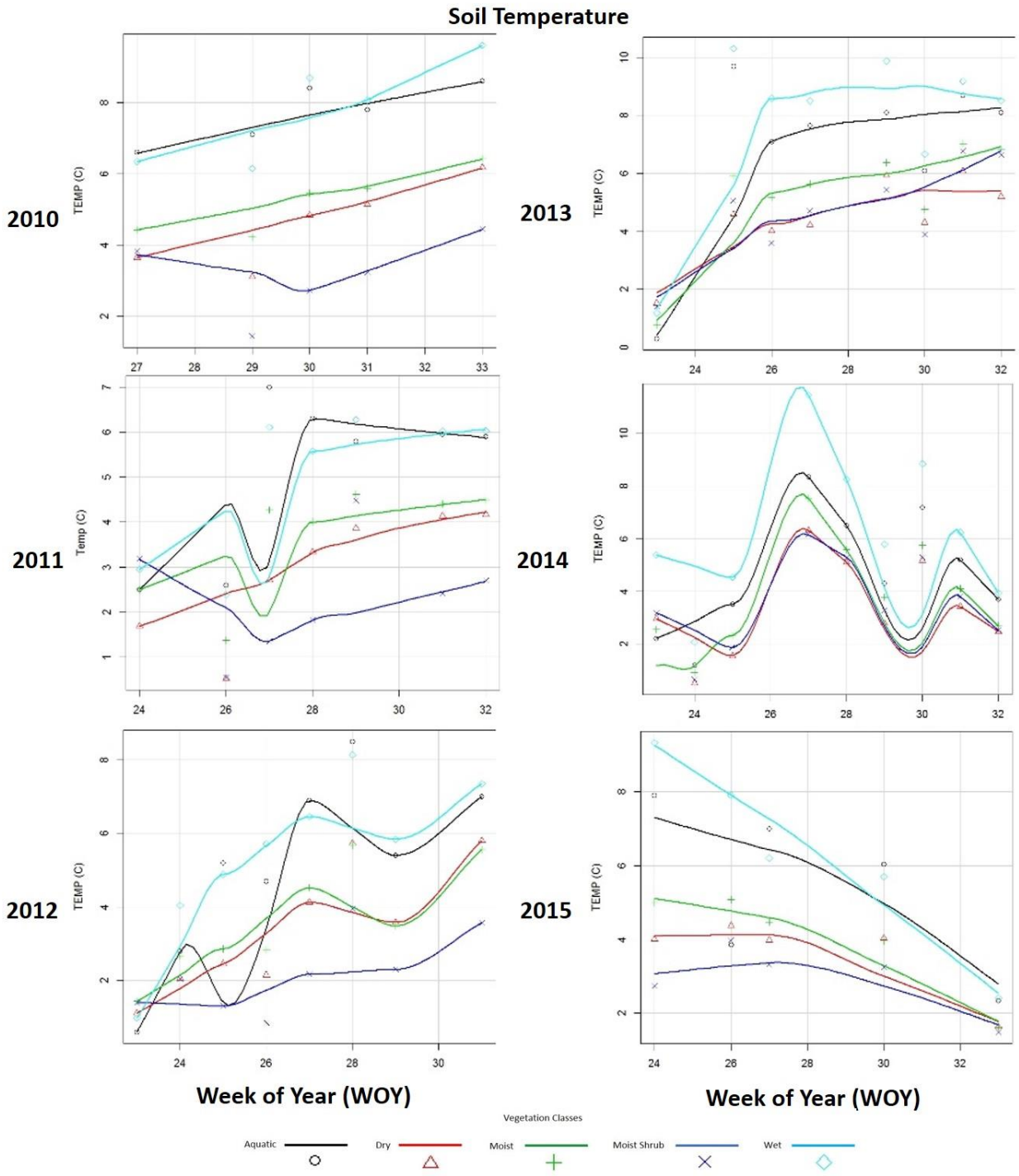

Figure 3.13a: Seasonal and inter-annual soil temperature (at ~5cm depth (°C)) averaged across each vegetation class located within the MISP transect in Atqasuk. Plots were fit with a smooth loess curve and the x-axis on all plots represents WOY (~23-33).

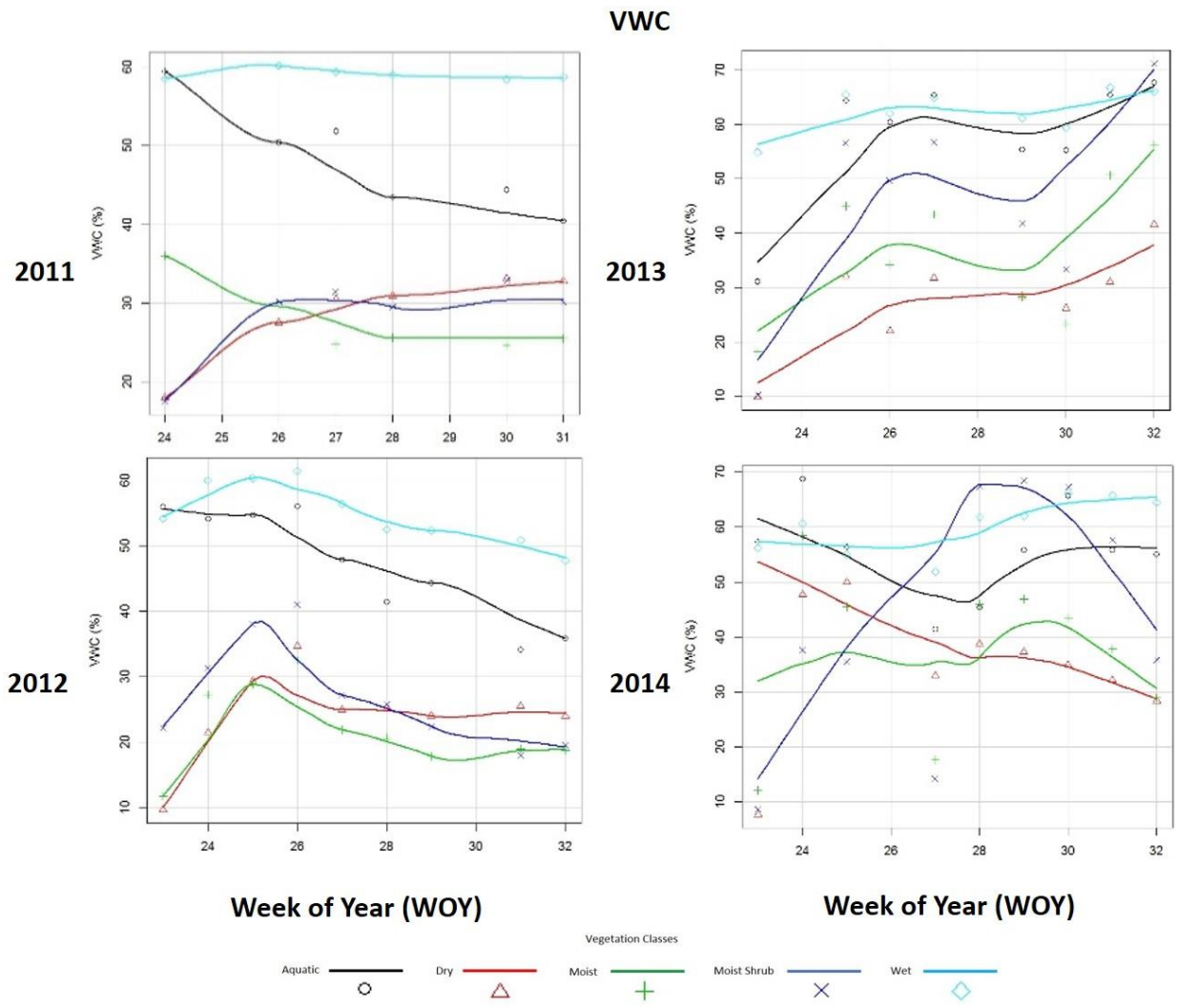

Figure 3.13b: Seasonal and inter-annual percent volumetric water content (VWC) averaged across each vegetation class located within the MISP transect in Atqasuk. Plots were fit with a smooth loess curve and the x-axis on all plots represents WOY (~23-33).

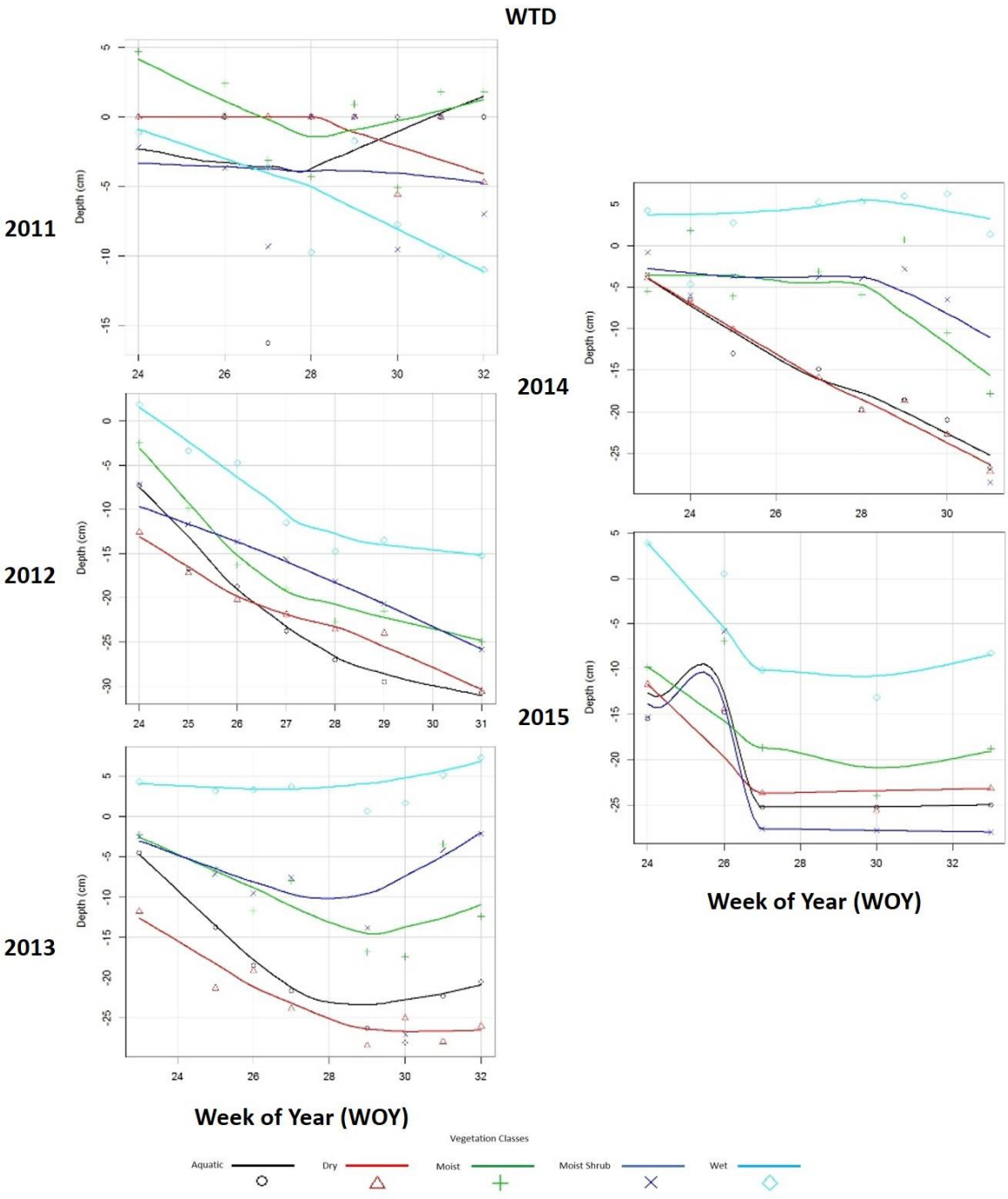

Figure 3.13c: Seasonal and inter-annual water table depth (WTD (cm)) averaged across each vegetation class located within the MISP transect in Atqasuk. The ground level is represented at depth 0 cm. Plots were fit with a smooth loess curve and the x-axis on all plots represents WOY (~23-33).

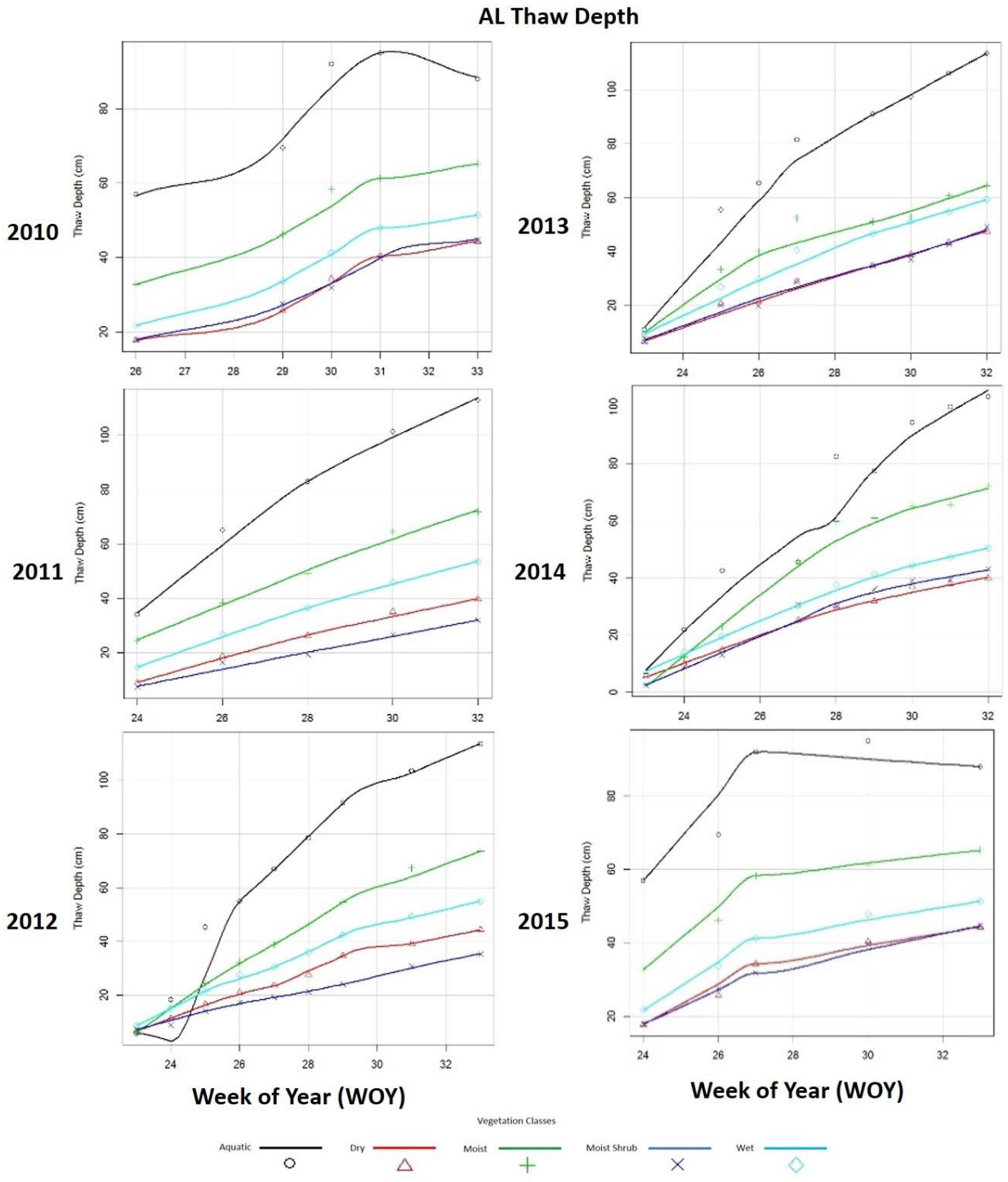

Figure 3.13d: Seasonal and inter-annual active layer thaw depth (AL (cm)) averaged across each vegetation class located within the MISP transect in Atqasuk. Plots were fit with a smooth loess curve and the x-axis on all plots represents WOY (~23-33).

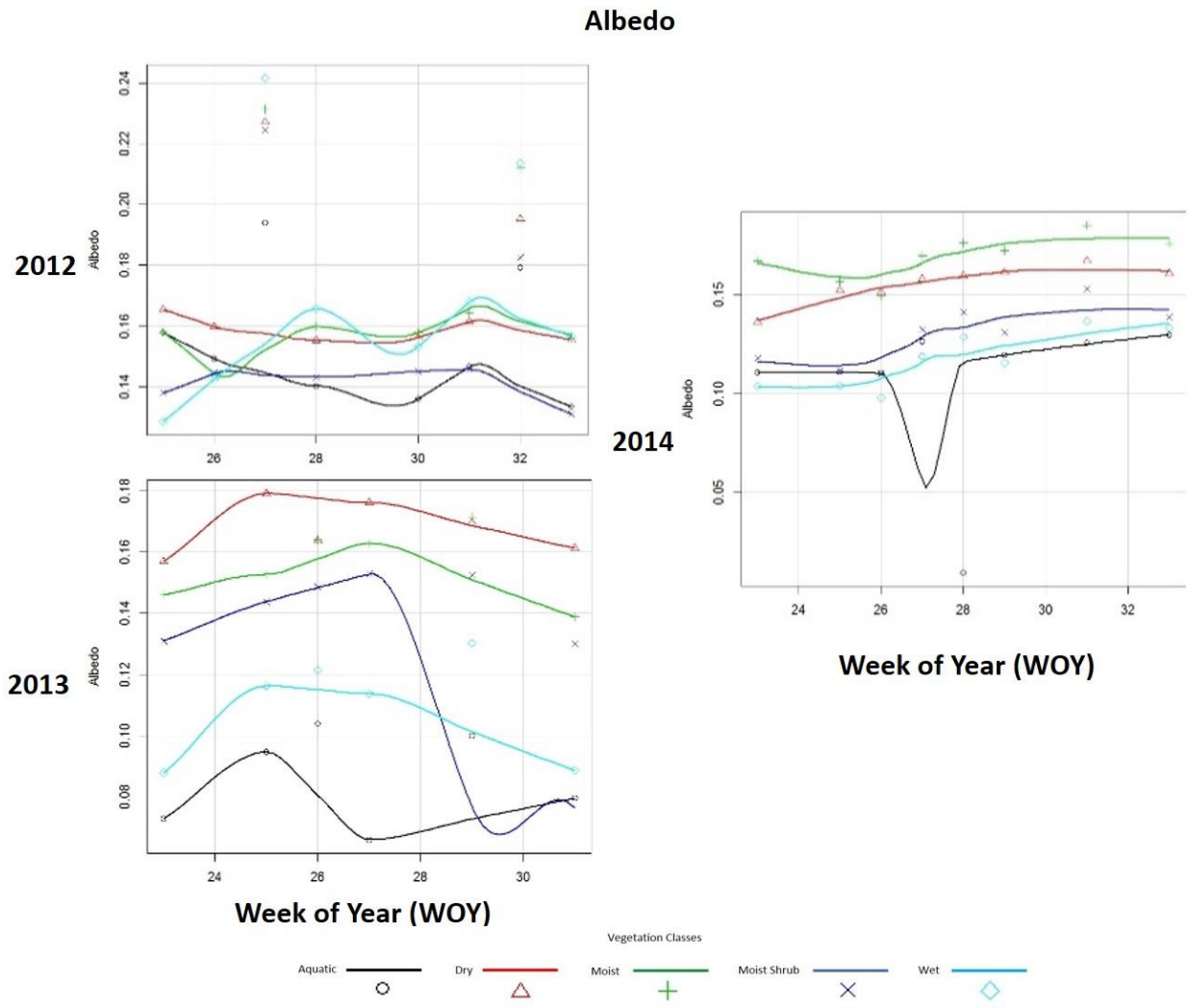

Figure 3.13e: Seasonal and inter-annual surface albedo averaged across each vegetation class located within the MISP transect in Atqasuk. Plots were fit with a smooth loess curve and the x-axis on all plots represents WOY (~23-33).

Relationships among the surface measurements were explored with the goal of avoiding multicollinearity prior to applying multiple linear regression analysis that included spectrometer-derived datasets. These relationships are summarized in Table 3.9 for all years of data collection for all vegetation classes. Table 3.10 summarizes correlations between land surface data by vegetation class for all years of data collection. No significant correlations were found between the ground based measurements, suggesting data is suitable for exploring further.

Table 3.9: Pearson's correlation results (critical p-values adjusted using the Bonferroni correction) between ground-based surface measurements across all vegetation classes for all years of data.

Location	Index	by Index	r	p
Barrow	Albedo	AL thaw depth	-0.01	0.910
	Albedo	VWC	-0.63	<0.0001
	Albedo	Soil temp	-0.21	0.0258
	Albedo	WTD	-0.46	<0.0001
	AL thaw depth	VWC	0.35	<0.0001
	AL thaw depth	Soil temp	0.42	<0.0001
	AL thaw depth	WTD	-0.36	<0.0001
	VWC	WTD	0.36	<0.0001
	VWC	Soil temp	0.38	<0.0001
	Soil temp	WTD	0.26	<0.0001
Atqasuk	Albedo	AL thaw depth	0.06	0.607
	Albedo	VWC	-0.49	<0.0001
	Albedo	Soil temp	-0.21	0.0640
	Albedo	WTD	-0.43	<0.0001
	AL thaw depth	VWC	0.23	<0.05
	AL thaw depth	Soil temp	0.52	<0.0001
	AL thaw depth	WTD	-0.40	<0.0001
	VWC	WTD	0.24	<0.05
	VWC	Soil temp	0.45	<0.0001
	Soil temp	WTD	-0.04	0.6

Table 3.10: Pearson's correlation results (critical p-values adjusted using the Bonferroni correction) between ground-based surface measurements across each vegetation class for all years of data.

Location	Veg Class	Index	by Index	r	p
Barrow	DMSGram	AL thaw depth	Soil temp	0.57	<0.0001
		AL thaw depth	WTD	-0.80	<0.0001
	Dry Shrub	AL thaw depth	Soil temp	0.51	<0.0001
		AL thaw depth	WTD	-0.77	<0.0001
	Moist Gram	AL thaw depth	VWC	0.50	<0.0001
		AL thaw depth	Soil temp	0.54	<0.0001
	Seasonally Flooded	AL thaw depth	WTD	-0.48	<0.001
	Wet Gram	AL thaw depth	Soil temp	0.42	<0.001
Location	Veg Class	Index	by Index	r	P
Atqasuk	Moist Shrub	AL thaw depth	Soil temp	0.57	<0.0001
		AL thaw depth	WTD	-0.47	<0.001
	Dry	AL thaw depth	Soil temp	0.62	<0.0001
		AL thaw depth	WTD	-0.65	<0.0001
		Soil temp	WTD	-0.53	<0.0001
	Moist	AL thaw depth	Soil temp	0.59	<0.0001
	Wet	AL thaw depth	Soil temp	0.45	<0.001

3.6.6 Relationships between greening and ground-based measurements

Based on the analysis applied thus far, it can be concluded that RGB indices and spectrometer-derived indices are similar in their capacity to detect changes in seasonal and inter-annual greening of a range of arctic coastal plain vegetation classes. To explore how these indices are affected by environmental factors such as soil moisture, soil temperature, active layer thaw depth, water table depth, and albedo, multiple linear regression was used to identify how well the ground-based measurements can predict each green index across all class and for each class individually (Tables 3.11 and 3.12). In Utqiaġvik, it seemed like the active layer thaw depth was the strongest

predictor ($p<0.001$) of all RGB indices (KAP GEI and %G; Pheno-cam GEI and %G) and most spectrometer-derived indices (NDVI, MNDVI, MSR, OSAVI, and SIPI), followed by albedo ($p<0.01$) for all spectrometer-derived indices and KAP indices, and $p<0.05$ for Pheno-cam. While in Atqasuk, albedo resulted to be the strongest predictor ($p<0.001$) of all RGB indices (KAP GEI and %G; Pheno-cam GEI and %G) and most spectrometer-derived indices (NDVI, MNDVI, MSR, OSAVI, and SIPI). WTD seemed to predict all spectrometer-derived indices with high confidence ($p<0.05$) but not for any of the RGB derived indices. When analyzing the MLR results by vegetation class it seemed that all ground-based measurements can predict greening values better for classes that contain moist to wet soil moisture content versus those plots with dry to moist classes as seen at both sites.

Table 3.11: Multiple linear regression results between all RGB and spectrometer-derived indices and ground-based surface measurements (i.e. VWC, soil temperature, active layer thaw depth, WTD, and albedo) data for each Utqiaġvik MISP transect vegetation class.

Location	Veg Class	Platform	Index	Adj. R^2	p
Barrow	DMSGram	KAP	GEI	0.29	0.3063
			%G	0.39	0.2369
		UNISPEC	CRI1	0.59	0.03879
			GREEN1	0.89	<0.0001
			MNDVI	0.9	<0.0001
			MSR	0.91	<0.0001
			NDVI	0.85	<0.001
			OSAVI	0.79	<0.001
			PRI2	0.41	0.1107
			SIPI	0.411	0.116
	Dry Shrub	KAP	GEI	0.67	0.07481
			%G	0.75	0.04963
		Pheno-Cam	GEI	0.64	<0.0001
			%G	0.58	<0.001
		UNISPEC	CRI1	0.56	0.0467
			GREEN1	0.89	<0.0001
			MNDVI	0.79	<0.001
			MSR	0.79	<0.001
			NDVI	0.95	<0.0001
			OSAVI	0.92	<0.0001
			PRI2	0.52	0.06156
			SIPI	0.51	0.067
	Moist Gram	KAP	GEI	0.74	0.05075
			%G	0.87	0.0141
		Pheno-Cam	GEI	0.84	<0.0001
			%G	0.84	<0.0001
		UNISPEC	CRI1	0.61	0.03201
			GREEN1	0.82	<0.001
			MNDVI	0.93	<0.0001
			MSR	0.92	<0.0001
			NDVI	0.96	<0.0001
			OSAVI	0.91	<0.0001
			PRI2	0.56	0.04797
			SIPI	0.52	0.06321
	Seasonally Flooded	KAP	GEI	0.99	<0.0001
			%G	0.95	<0.001
		Pheno-Cam	GEI	0.86	<0.0001
			%G	0.75	<0.0001
		UNISPEC	CRI1	-0.14	0.6369
			GREEN1	0.84	<0.001
			MNDVI	0.95	<0.0001
			MSR	0.95	<0.0001
			NDVI	0.78	<0.001
			OSAVI	0.89	<0.0001
			PRI2	0.38	0.1345
			SIPI	0.41	0.1144
	Wet Gram	KAP	GEI	0.8	0.0301
			%G	0.84	0.01986
		Pheno-Cam	GEI	0.78	<0.0001
			%G	0.78	<0.0001
		UNISPEC	CRI1	0.22	0.2544
			GREEN1	0.84	<0.001
			MNDVI	0.91	<0.0001
			MSR	0.9	<0.0001
			NDVI	0.91	<0.0001
			OSAVI	0.85	<0.001
			PRI2	0.43	0.106
			SIPI	0.5	0.0733

Table 3.12: Multiple linear regression results between all RGB and spectrometer-derived indices and ground-based surface measurements (i.e. VWC, soil temperature, active layer thaw depth, WTD, and albedo) data for each Atqasuk MISP transect vegetation class.

Location	Veg Class	Platform	Index	Adj. R^2	p
Atqasuk	Moist Shrub	KAP	GEI	0.89	0.001301
			%G	0.89	0.001254
		Pheno-Cam	GEI	0.61	0.009135
			%G	0.66	<0.001
		UNISPEC	CRI1	0.87	0.249
			GREEN1	0.99	0.0528
			MNDVI	0.99	0.0619
			MSR	0.97	0.124
			NDVI	0.98	0.09573
			OSAVI	0.83	0.2827
			PRI2	0.99	0.05779
			SIPI	0.46	0.4866
	Dry	KAP	GEI	0.88	<0.001
			%G	0.86	<0.001
		Pheno-Cam	GEI	0.7	0.002671
			%G	0.69	<0.001
		UNISPEC	CRI1	0.86	0.255
			GREEN1	0.8	0.308
			MNDVI	0.98	0.0873
			MSR	0.99	0.0737
			NDVI	0.98	0.08976
			OSAVI	0.84	0.2771
			PRI2	0.95	0.1485
			SIPI	0.87	0.2511
	Moist	KAP	GEI	0.96	<0.0001
			%G	0.96	<0.0001
		Pheno-Cam	GEI	0.67	0.004295
			%G	0.77	<0.0001
		UNISPEC	CRI1	0.9	0.222
			GREEN1	0.89	0.23
			MNDVI	0.86	0.255
			MSR	0.89	0.227
			NDVI	0.91	0.2047
			OSAVI	0.98	0.09072
			PRI2	0.90	0.215
			SIPI	0.99	0.0240
	Wet	KAP	GEI	0.96	<0.0001
			%G	0.94	<0.0001
		Pheno-Cam	GEI	0.77	<0.0001
			%G	0.81	<0.0001
		UNISPEC	CRI1	0.86	0.258
			GREEN1	0.86	0.255
			MNDVI	0.69	0.375
			MSR	0.84	0.27
			NDVI	0.98	0.09839
			OSAVI	0.99	0.02057
			PRI2	0.92	0.1919
			SIPI	0.46	0.486
	Aquatic	KAP	GEI	0.41	0.224
			%G	-0.08	0.574
		Pheno-Cam	GEI	0.55	0.03794
			%G	0.57	0.0298
		UNISPEC	CRI1	-0.24	0.789
			GREEN1	0.39	0.076
			MNDVI	0.76	<0.001
			MSR	0.82	<0.001
			NDVI	0.47	0.0318
			OSAVI	0.31	0.106
			PRI2	0.68	0.00903
			SIPI	0.09	0.4033

3.7 DISCUSSION

The focus of this study was to test the capacity of mid-scale remote sensing sensors to monitor plant phenology of arctic tundra vegetation classes across multiple locations. Specifically, inexpensive digital cameras (e.g. Pheno-cams and kite-based cameras) were assessed and data were compared to high-resolution spectrometer-derived ground-based data in order to gauge applicability of filling the gaps between plot-level research studies and landscape satellite-derived signals. Improving upon the validation of research methodologies acquired at multiple spatial scales is imperative to improve or understanding of changing arctic landscapes and their potential impacts on global processes.

3.7.1 Differences among sampling sensors

All sensors utilized in this study seemed to be sensitive to seasonal and inter-annual plant phenology across a number of vegetation classes in northern Alaska and over a span of 6 years. When comparing the two RGB sensors, the KAP platform resulted with stronger correlations for the majority of wet vegetation classes versus those derived from the Pheno-cam. This might be due to the oblique view-angle of the Pheno-cams which could limit the capture of microtopographic characters of the tundra surface, especially the low-lying troughs and ponds. Additionally, solar illumination and sensor viewing geometries (e.g. bidirectional reflectance distribution function (BRDF)) can have a large effect on measured surface reflectance of various arctic plant communities therefore a closer examination of this is needed. This function defines how light is reflected and depends on the sensor angle relative to the surface as well as to the angle of incoming light relative to the surface (*Buchhorn et al.*, 2016). Related to this, is the KAP system and UNISPEC fibers ability to capture these areas better given the advantage of the NADIR view angle of the sensors which suggests that each approach can be used for particular cases (i.e. Pheno-cams might be better for species-level sampling of arctic tundra communities, while KAP might be better for landscape-level sampling). Another possible reason for the differences between these sensors could be the spectral range or resolution of each as the Pheno-cams were 8MP while the camera used on the KAP platform was 12MP. Additionally, light saturation might also play in important role as fluctuating light conditions in the high arctic is common and can potentially alter the signals being observed by the sensors. A white panel for calibration of RGB imagery might be

used in future studies to assist with correcting for this possible source of error (*Richardson et al.*, 2007).

Both RGB systems were relatively inexpensive (between $150- $500) when compared to the spectrometer cost (~$30K) and simple to execute with little knowledge of remote sensing and required limited maintenance over the course of the study. The Pheno-cams have the advantage of automation and high sampling frequencies that could potentially assist with capturing the small-scale changes in species-specific signals (i.e. bud-burst, flowering, senescence etc.) rather than the subtle changes seen across the landscape in these ecosystems. Previous studies across the high and low arctic have utilized commercial grade digital cameras to assess seasonal and inter-annual greening trends and have provided an insight into the potential of using these sensors (*Westergaard-Nielsen et al.*, 2013; *Andresen,* 2014; *Beamish et al.*, 2016). This study expands upon these approaches by applying methods to multiple vegetation classes spanning multiple sites and ranging over 6 years of data.

3.7.2 Differences between sites and years

Overall it seemed like all sensors were able to capture greening trends better for vegetation classes containing wetter soil moisture, while plots that were dry were more variable and harder to predict as seen in both Utqiaġvik and Atqasuk. Given the characteristics and structure of the landscape, the warmer surface temperatures, and the resulting deeper active layer thaw depths, Atqasuk could potentially be considered a predictor for Utqiaġvik, representing the future state of areas similar to Utqiaġvik. With this in mind and considering most signals were stronger in Atqasuk, these sensors might be capable of monitoring future changes better at locations that exhibit these types of characteristics. The Utqiaġvik sites resulted with the highest greening values from the seasonally flooded vegetation classes, while in Atqasuk it was for the moist shrub vegetation classes as captured by all approaches for mostly all growing seasons. The moist shrub plots in Atqasuk are mostly dominated by *salix* spp. shrubs which flourish throughout the growing season causing high increases in greening. The vegetation present at these plots could be representative of the future shrub expansion seen across northern Alaska (*Jia*, 2003) and continued monitoring of these particular types of vegetation classes can provide a better insight into the future state of colder dominated areas such as Utqiaġvik.

3.7.3 Differences between vegetation classes

Wetter classes typically contain erect graminoid species with a higher leaf area index than dry classes and showed a greater variability in greenness between years at both sites. Interestingly though, the Atqasuk dry plots seemed to display higher greening trends than comparable plots in Utqiaġvik. The aquatic classes in Atqasuk displayed drastic inter-annual fluctuations in greening trends as observed by all sensors. This could have a direct correlation with available soil moisture at these particular plots as they fall within a thermokarst trough and some years might experience draining. The 2011 and 2012 summers in Atqasuk exhibited 42.43% and 35.02% mean peak season VWC respectively, while the 2013 and 2014 summers showed higher contents at 62.74% and 58.86%. Lower VWC within these plots would allow for more 'viewable' vegetation cover by graminoids and can potentially explain the higher greening values, whereas standing water in troughs obscures underlying vegetation in RGB imagery and lowers a greening signal.

Overall, the wetter classes seemed to be the most productive over the growing seasons and DRP and KAP were able to predict greening trends in these classes better than in dry classes in Utqiaġvik, while in Atqasuk the dry classes seemed more productive than similar classes in Utqiaġvik. This might be due to the colder surface temperatures experienced over the high centered polygons or dry classes in Utqiaġvik when compared to Atqasuk where they experience much warmer temperatures and can ultimately have an effect on productivity (*Gamon et al.*, 2012).

Key findings from this study suggest that cost-effective alternative digital imaging and remote sensing methods are suitable for monitoring plot-level phenological dynamics of arctic tundra ecosystems and can be used in conjunction to other spectral imaging approaches to facilitate or understanding of the future state of the Arctic and Earth systems. Each approach resulted with different capacities at particular spatial scales and using all approaches together might assist with filling gap of the lack of cross-scale validation of research methodologies.

3.8 CONCLUSION

This chapter explored the use of inexpensive remote sensing alternatives for monitoring plot-level phenology across a small-spatial scales at two locations on the Coastal Plain of the North Slope of Alaska. Signals from these approaches were compared to those acquired from traditional remote sensing spectral reflectance approaches such as those from ground-based spectrometers

(e.g. NDVI). Findings suggest that these low-cost systems have the ability to document seasonal and inter-annual plant phenology across various vegetation classes. Additionally, not only did the RGB-derived indices correlate strongly with NDVI but they also resulted in strong linear relationships with other spectrometer-derived indices (e.g. Green, MNDVI, and MSR). These results suggest that a closer look into the spectral bands being used to calculate each index is necessary as there is high chance of collinearity between each index that can ultimately be causing the high correlations. Moreover, these findings also highlight the need for better understanding of sensor view angles in addition to sun-angles and light conditions and their effects on not only the vegetation but also the signals being observed from the various sensors.

In addition to the KAP and Pheno-cams ability to capture seasonal and inter-annual greening trends across multiple arctic vegetation classes, these systems have the added benefit of being low-cost and require minimal user knowledge of spectral radiometric approaches, which is an added advantage over traditional alternative remote sensing methods even though further research is needed to better quantify their full potential.

3.9 REFERENCES

Aber, J. S., R. J. Sobieski, D. a Distler, and M. C. Nowak (1999), Kite Aerial Photography for Environmental Site Investigations, , *102*(1), 57–67, doi:10.2307/3628217.

Aber, J. S., S. W. Aber, and F. Pavri (2002), Unmanned Small-Format Aerial Photography From Kites for Acquiring Large-Scale , High-Resolution , Multiview-Angle Imagery, *Int. Arch. Photogramm. Remote Sens. Spat. Inf. Sci.*, *34*(1), 1–6.

Aber, J. S., D. Eberts, and S. W. Aber (2005), Applications of kite aerial photography: Biocontrol of salt cedar (Tamarix) in the western United States, *Trans. Kansas Acad. Sci.*, *108*(1 & 2), 63–66, doi:10.1660/0022-8443(2005)108[0063:AOKAPB]2.0.CO;2.

ACIA (2004a), Impacts of a Warming Arctic: Arctic Climate Impact Assessment, *Cambridge Univ. Press*, 1046, doi:10.2277/0521617782.

ACIA (2004b), Impacts of a Warming Arctic: Arctic Climate Impact Assessment, *Cambridge Univ. Press*, 1046, doi:10.2277/0521617782.

Andresen, C. G. (2014), Monitoring and understanding decadal scale changes in hydrology, productivity and carbon balance in Arctic tundra ponds, , 108.

Andresen, C. G., and V. L. Lougheed (2015), Disappearing Arctic tundra ponds: Fine-scale analysis of surface hydrology in drained thaw lake basins over a 65 year period (1948–2013), , 1–14, doi:10.1002/2014JG002778.Received.

Andresen, C. G., S. A. Vargas, V. L. Lougheed, and C. E. Tweedie (2014), Kite-based Aerial Photography (KAP): A Low Cost, Effective Tool for Wetland Research, *Wetl. Sci. Pract.*, *Dec*(December), 28–31.

Arft, a. M. et al. (1999), Responses of Tundra plants to experimental warming: Meta-analysis of the International Tundra Experiment, *Ecol. Monogr.*, *69*(4), 491–511, doi:10.1890/0012-9615(1999)069[0491:ROTPTE]2.0.CO;2.

Bangen, S. G., J. M. Wheaton, N. Bouwes, B. Bouwes, and C. Jordan (2014), A methodological intercomparison of topographic survey techniques for characterizing wadeable streams and rivers, *Geomorphology*, *206*, 343–361, doi:10.1016/j.geomorph.2013.10.010.

Battersby, S. E., D. “daan” Strebe, and M. P. Finn (2016), Shapes on a plane: evaluating the impact of projection distortion on spatial binning, *Cartogr. Geogr. Inf. Sci.*, *406*(May), 1–12, doi:10.1080/15230406.2016.1180263.

Beamish, A. L., W. Nijland, M. Edwards, N. C. Coops, and G. H. R. Henry (2016), Phenology and vegetation change measurements from true colour digital photography in high Arctic tundra, *NRC Res. Press*, *49*(May), 33–49.

Bhardwaj, A., L. Sam, A. Bhardwaj, and F. J. Martín-Torres (2016), LiDAR remote sensing of the cryosphere: Present applications and future prospects, *Remote Sens. Environ.*, *177*, 125–143, doi:10.1016/j.rse.2016.02.031.

Bhatt, U. S. et al. (2010), Circumpolar Arctic tundra vegetation change is linked to sea ice decline, *Earth Interact.*, *14*(8), doi:10.1175/2010EI315.1.

Bhatt, U. S., D. a. Walker, M. K. Raynolds, P. a. Bieniek, H. E. Epstein, J. C. Comiso, J. E. Pinzon, C. J. Tucker, and I. V. Polyakov (2013), Recent declines in warming and vegetation greening trends over pan-arctic tundra, *Remote Sens.*, *5*(9), 4229–4254, doi:10.3390/rs5094229.

Biasi, C., W. Wanek, O. Rusalimova, C. Kaiser, C. Biasi, W. Wanek, C. Kaiser, H. Meyer, and A. Richter (2017), Microtopography and Plant-Cover Controls on Nitrogen Dynamics in Hummock Tundra Ecosystems in Siberia Meyer , Pavel Barsukov and Andreas Richter Published by : INSTAAR , University of Colorado Stable URL : http://www.jstor.org/stable/4095862 REFERENCES Li, , *37*(4), 435–443.

Boelman, N. T., M. Stieglitz, H. M. Rueth, M. Sommerkorn, K. L. Griffin, G. R. Shaver, and J. a Gamon (2003), Response of NDVI, biomass, and ecosystem gas exchange to long-term warming and fertilization in wet sedge tundra., *Oecologia*, *135*(3), 414–421, doi:10.1007/s00442-003-1198-3.

Boelman, N. T., L. Gough, J. R. McLaren, and H. Greaves (2011a), Does NDVI reflect variation in the structural attributes associated with increasing shrub dominance in arctic tundra?, *Environ. Res. Lett.*, *6*(3), 35501, doi:10.1088/1748-9326/6/3/035501.

Boelman, N. T., L. Gough, J. R. McLaren, and H. Greaves (2011b), Does NDVI reflect variation in the structural attributes associated with increasing shrub dominance in arctic tundra?, *Environ. Res. Lett.*, *6*, 35501, doi:10.1088/1748-9326/6/3/035501.

Bradley, N. L., C. A. Leopold, J. Ross, and W. Huffaker (1999), Phenological changes reflect climate change in Wisconsin., *Proc. Natl. Acad. Sci. U. S. A.*, *96*(August), 9701–9704, doi:10.1073/pnas.96.17.9701.

Brown, J., P. C. Miller, L. L. Tieszen, and F. L. Bunnell (1980), *An Arctic Ecosystem: The Coastal Tundra at Barrow, Alaska*.

Brown, J., F. E. Nelson, and K. M. Hinkel (2000), The circumpolar active layer monitorign (CALM) program research designs and initial results, *Polar Geogr.*, *3*(May 2012), 162–165.

Cabin, R. J., R. J. Mitchell, E. Siemann, D. Wedin, and K. S. N. Bio (2000), To Bonferroni or Not to Bonferroni : When and How Are the Questions Published by : Wiley on behalf of the Ecological Society of America Stable URL : http://www.jstor.org/stable/20168454 How Are the Questions To Bonferroni or Not to Bonferroni : When and, , *81*(3), 246–248.

Carlisle, B. H. (2005), Modelling the spatial distribution of DEM error, *Trans. GIS*, *9*(4), 521–540, doi:10.1111/j.1467-9671.2005.00233.x.

Carter, J., Schmid, K., Waters, K., Betzhold, L., Hadley, B., Mataosky, R., Halleran, J. (2012), Lidar 101 : An Introduction to Lidar Technology , Data , and Applications, *NOAA Coast. Serv. Cent.*, (November), 76.

Chapin, F. S. et al. (2005), Role of Land-Surface Changes in Arctic Summer Warming, *Science (80-.).*, *657*(2005), 9–13, doi:10.1126/science.1117368.

Chaplot, V., F. Darboux, H. Bourennane, S. Leguédois, N. Silvera, and K. Phachomphon (2006), Accuracy of interpolation techniques for the derivation of digital elevation models in relation to landform types and data density, *Geomorphology*, *77*(1–2), 126–141, doi:10.1016/j.geomorph.2005.12.010.

Chen, C., and T. Yue (2010), A method of DEM construction and related error analysis, *Comput. Geosci.*, *36*(6), 717–725, doi:10.1016/j.cageo.2009.12.001.

Claudio, H. C., Y. Cheng, D. a. Fuentes, J. a. Gamon, H. Luo, W. Oechel, H. L. Qiu, A. F. Rahman, and D. a. Sims (2006), Monitoring drought effects on vegetation water content and fluxes in chaparral with the 970??nm water band index, *Remote Sens. Environ.*, *103*(3), 304–311, doi:10.1016/j.rse.2005.07.015.

Cleland, E. E., I. Chuine, A. Menzel, H. a. Mooney, and M. D. Schwartz (2007), Shifting plant phenology in response to global change, *Trends Ecol. Evol.*, *22*(7), 357–365, doi:10.1016/j.tree.2007.04.003.

Dandois, J. P., and E. C. Ellis (2010), Remote sensing of vegetation structure using computer vision, *Remote Sens.*, *2*(4), 1157–1176, doi:10.3390/rs2041157.

Dandois, J. P., and E. C. Ellis (2013), High spatial resolution three-dimensional mapping of vegetation spectral dynamics using computer vision, *Remote Sens. Environ.*, *136*, 259–276, doi:10.1016/j.rse.2013.04.005.

Darnell, A. R., N. J. Tate, and C. Brunsdon (2008), Improving user assessment of error implications in digital elevation models, *Comput. Environ. Urban Syst.*, *32*(4), 268–277, doi:10.1016/j.compenvurbsys.2008.02.003.

Delbart, N., T. Le Toan, L. Kergoat, and V. Fedotova (2006), Remote sensing of spring phenology in boreal regions: A free of snow-effect method using NOAA-AVHRR and SPOT-VGT data (1982-2004), *Remote Sens. Environ.*, *101*(1), 52–62, doi:10.1016/j.rse.2005.11.012.

Desmet, P. J. J. (1997), Effects Of Iinterpolation Errors On The Aanalysis Of DEMs, *Earth Surf. Process. Landforms*, *22*(June 1996), 563–580.

Dowling, T., A. Read, and J. Gallant (2009), Very high resolution DEM acquisition at low cost using a digital camera and free software, *18th World IMACS/MODSIM09 Congr.*, (July), 2479–2485.

Elmendorf, S. C. et al. (2012a), Global assessment of experimental climate warming on tundra vegetation: Heterogeneity over space and time, *Ecol. Lett.*, *15*(2), 164–175, doi:10.1111/j.1461-0248.2011.01716.x.

Elmendorf, S. C. et al. (2012b), Plot-scale evidence of tundra vegetation change and links to recent summer warming, *Nat. Clim. Chang.*, *2*(6), 453–457, doi:10.1038/nclimate1465.

Epstein, H. E., M. K. Raynolds, D. a Walker, U. S. Bhatt, C. J. Tucker, and J. E. Pinzon (2012), Dynamics of aboveground phytomass of the circumpolar Arctic tundra during the past three decades, *Environ. Res. Lett.*, *7*(1), 15506, doi:10.1088/1748-9326/7/1/015506.

Erdoğan, S. (2010), Modelling the spatial distribution of DEM error with geographically weighted regression: An experimental study, *Comput. Geosci.*, *36*(1), 34–43, doi:10.1016/j.cageo.2009.06.005.

Esri (2001), ArcGIS Geostatistical Analyst: Statistical Tools for Data Exploration, Modeling, and Advanced Surface Generation, , (August), 19.

ESRI (2013), Overview of Arc Hydro Terrain Preprocessing Workflows, , (February), 13.

Von Fischer, J. C., R. C. Rhew, G. M. Ames, B. K. Fosdick, and P. E. Von Fischer (2010), Vegetation height and other controls of spatial variability in methane emissions from the Arctic coastal tundra at Barrow, Alaska, *J. Geophys. Res. Biogeosciences*, *115*(3), 1–11, doi:10.1029/2009JG001283.

Fisher, P. (1998), Improved modeling of elevation error with Geostatistics, *Geoinformatica*, *2*(3), 215–233, doi:10.1023/A:1009717704255.

Fonstad, M. a., J. T. Dietrich, B. C. Courville, J. L. Jensen, and P. E. Carbonneau (2013), Topographic structure from motion: A new development in photogrammetric measurement, *Earth Surf. Process. Landforms*, *38*(4), 421–430, doi:10.1002/esp.3366.

Fraser, R. H., I. Olthof, T. C. Lantz, and C. Schmitt (2016), UAV Photogrammetry for Mapping Vegetation in the Low-Arctic, *Arct. Sci.*, *102*(June), 1–51, doi:10.1139/as-2016-0008.

Gamon, J. a, G. P. Kershaw, S. Williamson, and D. S. Hik (2012a), Microtopographic patterns in an arctic baydjarakh field: do fine-grain patterns enforce landscape stability?, *Environ. Res. Lett.*, *7*(1), 15502, doi:10.1088/1748-9326/7/1/015502.

Gamon, J. a., Y. Cheng, H. Claudio, L. MacKinney, and D. a. Sims (2006), A mobile tram system for systematic sampling of ecosystem optical properties, *Remote Sens. Environ.*, *103*(3), 246–254, doi:10.1016/j.rse.2006.04.006.

Gamon, J. a., K. F. Huemmrich, R. S. Stone, and C. E. Tweedie (2013), Spatial and temporal variation in primary productivity (NDVI) of coastal Alaskan tundra: Decreased vegetation growth following earlier snowmelt, *Remote Sens. Environ.*, *129*, 144–153, doi:10.1016/j.rse.2012.10.030.

Gamon, J. A., G. P. Kershaw, S. Williamson, and D. S. Hik (2012b), Microtopographic patterns in an arctic baydjarakh field: do fine-grain patterns enforce landscape stability?, *Environ. Res. Lett.*, *7*(1), 15502, doi:10.1088/1748-9326/7/1/015502.

Gao, J. (1997), Resolution and accuracy of terrain representation by grid DEMs at a micro-scale, *Int. J. Geogr. Inf. Sci.*, *11*(2), 199–212, doi:10.1080/136588197242464.

Gao, X., and a. R. Huete (2000), Validation of MODIS land surface reflectance and vegetation indices with multi-scale high spatial resolution data, *IGARSS 2000. IEEE 2000 Int. Geosci. Remote Sens. Symp. Tak. Pulse Planet Role Remote Sens. Manag. Environ. Proc. (Cat. No.00CH37120)*, 533–535, doi:10.1109/IGARSS.2000.861620.

Gitelson, A. a, Y. Zur, O. B. Chivkunova, and M. N. Merzlyak (2002), Assessing carotenoid content in plant leaves with reflectance spectroscopy., *Photochem. Photobiol.*, *75*(3), 272–281, doi:10.1562/0031-8655(2002)0750272ACCIPL2.0.CO2.

Gitelson, A. A., F. Verlag, Y. Gritz, and M. N. Merzlyak (2003), Relationships between leaf chlorophyll content and spectral reflectance and algorithms for non-destructive chlorophyll assessment in higher plant leaves, , *282*.

Goetz, S. J., A. G. Bunn, G. J. Fiske, and R. a Houghton (2005), Satellite-observed photosynthetic trends across boreal North America associated with climate and fire disturbance., *Proc. Natl. Acad. Sci. U. S. A.*, *102*(38), 13521–5, doi:10.1073/pnas.0506179102.

Gong, J., L. Zhllin, Q. Zhu, H. Sui, and Y. Zhou (2000), Effects of Various Factors on the Accuracy of DEMs : An Intensive Experimental Investigation, *Photogramm. Eng. Remote Sens.*, *66*(9), 1113–1117.

Goswami, S., J. a. Gamon, and C. E. Tweedie (2011), Surface hydrology of an arctic ecosystem: Multiscale analysis of a flooding and draining experiment using spectral reflectance, *J. Geophys. Res. Biogeosciences*, *116*(1), 1–14, doi:10.1029/2010JG001346.

Harwin, S., and A. Lucieer (2012), Assessing the accuracy of georeferenced point clouds produced via multi-view stereopsis from Unmanned Aerial Vehicle (UAV) imagery, *Remote Sens.*, *4*(6), 1573–1599, doi:10.3390/rs4061573.

Haugen, R.K., and Brown, J. (1980), Coastal-Inland Distributions of Summer Air Temperature and Precipitation in Northern Alaska, *Arct. Alp. Res.*, *12*(4), 403–412.

Healey, N. C., Oberbauer, S.F., Ahrends, H.E., Dierick, D., Welker, J.M., Leffler, A.J., Hollister, R.D., Vargas, S.A., Tweedie, C. E. (2014), A Mobile Instrumented Sensor Platform for Long-Term Terrestrial Ecosystem Analysis: An Example Application in an Arctic Tundra Ecosystem, *J. Environ. Informatics*, *24*(1), 1–10, doi:10.3808/jei.201400278.

Heimsath, A. M., and H. Farid (2002), Hillslope topography from unconstrained photographs, *Math. Geol.*, *34*(8), 929–952, doi:10.1023/A:1021364623017.

Helbig, M., J. Boike, M. Langer, P. Schreiber, B. R. K. Runkle, and L. Kutzbach (2013), Spatial and seasonal variability of polygonal tundra water balance: Lena River Delta, northern Siberia (Russia), *Hydrogeol. J.*, *21*(1), 133–147, doi:10.1007/s10040-012-0933-4.

Henry, G. H R and Molau, U. (1997), Tundra plants and climate change : the International Tundra Experiment (ITEX), , *3*, 1–9.

Henry, G., R. Hollister, I. S. Jónsdóttir, K. Klanderlud, U. Molau, S. F. Oberbauer, P. Webber, and P. Wookey (2013), The International Tundra Experiment: An Arctic Monitoring Network,

Hinzman, L. D., C. J. Deal, a. D. Mcguire, S. H. Mernild, I. V. Polyakov, and J. E. Walsh (2013), Trajectory of the Arctic as an integrated system, *Ecol. Appl.*, *23*(8), 1837–1868, doi:10.1890/11-1498.1.

Hollister, R. D. (2003), Response of Tundra Vegetation to Temperature: Implications for Forcasting Vegetation Change,

Hollister, R. D., and K. J. Flaherty (2010), Above- and below-ground plant biomass response to experimental warming in northern Alaska, *Appl. Veg. Sci.*, *13*(3), 378–387, doi:10.1111/j.1654-109X.2010.01079.x.

Hollister, R. D., P. J. Webber, and C. E. Tweedie (2005), The response of Alaskan arctic tundra to experimental warming: Differences between short- and long-term responses, *Glob. Chang. Biol.*, *11*(4), 525–536, doi:10.1111/j.1365-2486.2005.00926.x.

Hollister, R. D., P. J. Webber, and C. Bay (2014), Plant Response to Temperature in Northern Alaska : Implications for Predicting Vegetation Change PLANT RESPONSE TO TEMPERATURE IN NORTHERN ALASKA :, , *86*(6), 1562–1570.

Huemmrich, K. F. et al. (2010), Remote sensing of tundra gross ecosystem productivity and light use efficiency under varying temperature and moisture conditions, *Remote Sens. Environ.*, *114*(3), 481–489, doi:10.1016/j.rse.2009.10.003.

Huemmrich, K. F., J. Gamon, C. E. Tweedie, P. P. K. Campbell, D. Landis, and E. Middleton (2013), Arctic Tundra Vegetation Functional Types Based on Photosynthetic Physiology and Optical Properties, , 1–37.

Humphreys, E. R., and P. M. Lafleur (2011), sequestration in two low Arctic tundra ecosystems?, *Geophys. Res. Lett.*, *38*(9), 3–7, doi:10.1029/2011GL047339.

Hunter, G. j., and M. F. Goodchild (1997), Modeling the Uncertainty of Slope and Aspect Estimates Derived from Spatial Databases,

Hutchinson, M. F., T. Xu, and J. a Stein (2011), Recent Progress in the ANUDEM Elevation Gridding Procedure, *Geomorphometry*, 19–22.

Ide, R., and H. Oguma (2013), A cost-effective monitoring method using digital time-lapse cameras for detecting temporal and spatial variations of snowmelt and vegetation phenology in alpine ecosystems, *Ecol. Inform.*, *16*, 25–34, doi:10.1016/j.ecoinf.2013.04.003.

IPCC (2014), Climate Change 2014: Synthesis Report. Contribution of Working Groups I, II and III to the Fifth Assessment Report of the Intergovernmental Panel on Climate Change.

Jarihani, A. a., J. N. Callow, T. R. McVicar, T. G. Van Niel, and J. R. Larsen (2015), Satellite-derived Digital Elevation Model (DEM) selection, preparation and correction for hydrodynamic modelling

in large, low-gradient and data-sparse catchments, *J. Hydrol.*, *524*, 489–506, doi:10.1016/j.jhydrol.2015.02.049.

Javernick, L., J. Brasington, and B. Caruso (2014), Modeling the topography of shallow braided rivers using Structure-from-Motion photogrammetry, *Geomorphology*, *213*, 166–182, doi:10.1016/j.geomorph.2014.01.006.

Jia, G. J. (2003), Greening of arctic Alaska, 1981–2001, *Geophys. Res. Lett.*, *30*(20), 3–6, doi:10.1029/2003GL018268.

Jorgenson, M. T., M. Kanevskiy, Y. Shur, N. Moskalenko, D. R. N. Brown, K. Wickland, R. Striegl, and J. Koch (2015), Journal of Geophysical Research : Earth Surface, , 1–18, doi:10.1002/2015JF003602.Received.

Kasischke, E.S., et al. (2014), A Concise Experiment Plan for the Arctic-Boreal Vulnerability Experiment, *http://above.nasa.gov/acep/acep_final_pdf.pdf. Accessed 1/25/2015.*

Keenan, T. F. et al. (2014), Tracking forest phenology and seasonal physiology using digital repeat photography : a critical assessment, , *24*(6), 1478–1489.

Komarkova, V., and Webber, P. J. (1980), Two Low Arctic Vegetation Maps near Atkasook , Alaska, , *12*(4), 447–472.

Krivoruchko, K. (2004), Introduction to Modeling Spatial Processes Using Geostatistcal Analyst, *Esri*, 1–27.

Kurc, S. a., and L. M. Benton (2010), Digital image-derived greenness links deep soil moisture to carbon uptake in a creosotebush-dominated shrubland, *J. Arid Environ.*, *74*(5), 585–594, doi:10.1016/j.jaridenv.2009.10.003.

Laidler, G. J., P. M. Treitz, and D. M. Atkinson (2008), Remote Sensing of Arctic Vegetation : Relations between the NDVI , Spatial Resolution and Vegetation Cover on Boothia Peninsula , Nunavut Author (s): Gita J . Laidler , Paul M . Treitz and David M . Atkinson Published by : Arctic Institute of North Amer, , *61*(1), 1–13.

Lara, M. J., a. D. McGuire, E. S. Euskirchen, C. E. Tweedie, K. M. Hinkel, A. N. Skurikhin, V. E. Romanovsky, G. Grosse, W. R. Bolton, and H. Genet (2014), Polygonal tundra geomorphological change in response to warming alters future CO 2 and CH 4 flux on the Barrow Peninsula, *Glob. Chang. Biol.*, (August), n/a-n/a, doi:10.1111/gcb.12757.

Lassueur, T., S. Joost, and C. F. Randin (2006), Very high resolution digital elevation models: Do they improve models of plant species distribution?, *Ecol. Modell.*, *198*(1–2), 139–153, doi:10.1016/j.ecolmodel.2006.04.004.

Leberl, F., a Irschara, T. Pock, P. Meixner, M. Gruber, S. Scholz, and a Wiechert (2010), Point Clouds: Lidar versus 3D Vision, *Photogramm. Eng. Remote Sens.*, *76*(10), 1123–1134, doi:0099-1112/10/7610–1123.

Lefsky, M. a, W. B. Cohen, G. G. Parker, and J. David (2014), Lidar Remote Sensing for Ecosystem Studies, , *52*(1), 19–30.

Li, Z. (2014), Watershed modeling using arc hydro based on DEMs: a case study in Jackpine watershed, *Environ. Syst. Res.*, *3*(1), 11, doi:10.1186/2193-2697-3-11.

Liljedahl, A.K., Hinzman, L.D., Schulla, J. (2012), Ice-Wedge Polygon Type Controls Low-Gradient Watershed-Scale Hydrology,

Liljedahl, A. K. et al. (2016), Pan-Arctic ice-wedge degradation in warming permafrost and influence on tundra hydrology, *Nat. Geosci.*, *9*(April), 312–318, doi:10.1038/ngeo2674.

Lin, D. H., D. R. Johnson, C. Andresen, and C. E. Tweedie (2012), High spatial resolution decade-time scale land cover change at multiple locations in the Beringian Arctic (1948–2000s), *Environ. Res. Lett.*, *7*(2), 25502, doi:10.1088/1748-9326/7/2/025502.

Liu, H. Q., and A. Huete (1995), Feedback based modification of the NDVI to minimize canopy background and atmospheric noise, *IEEE Trans. Geosci. Remote Sens.*, *33*(2), 457–465, doi:10.1109/36.377946.

Liu, Z. L. Z., S. C. S. Cui, and Q. Y. Q. Yan (2008), Building extraction from high resolution satellite imagery based on multi-scale image segmentation and model matching, *2008 Int. Work. Earth Obs. Remote Sens. Appl.*, doi:10.1109/EORSA.2008.4620321.

Lucht, W. (2002), Climatic Control of the High-Latitude Vegetation Greening Trend and Pinatubo Effect, *Science (80-.).*, *296*(5573), 1687–1689, doi:10.1126/science.1071828.

Marzolff, I., J. B. Ries, and K. D. Albert (2002), Kite aerial photography for gully monitoring in sahelian landscapes, , 18–20.

McCune, B., and Grace, J. . (2002), Analysis of Ecological Communities, *MjM Softw. Des. Gleneden Beach, McKinney M.L*, *127*(January 2002), 247–260, doi:10.1016/S0022-0981(03)00091-1.

Menzel, a, and P. Fabian (1999), Growing season extended in Europe, *Nature*, *397*(6721), 659, doi:10.1038/17709.

Migliavacca, M. et al. (2011), Using digital repeat photography and eddy covariance data to model grassland phenology and photosynthetic CO2 uptake, *Agric. For. Meteorol.*, *151*(10), 1325–1337, doi:10.1016/j.agrformet.2011.05.012.

Myneni, R. B., C. D. Keeling, C. J. Tucker, G. Asrar, and R. R. Nemani (1997), Increased plant growth in the northern high latitudes from 1981 to 1991, *Nature*, *386*(6626), 698–702, doi:10.1038/386698a0.

Nelson, F. E., S. I. Outcalt, J. Brown, N. I. Shiklomanov, and K. M. Hinkel (1998), Spatial and Temporal Attributes of the Active-Layer Thickness Record, Barrow, Alaska, U.S.A., , (55), 797–802.

Nelson, S. and (2015), Circumpolar Active Layer Monitoring (CALM) Program, *Natl. Snow Ice Data Cent.*, 1–3.

Noh, M.-J., and I. M. Howat (2015a), Automated stereo-photogrammetric DEM generation at high latitudes: Surface Extraction with TIN-based Search-space Minimization (SETSM) validation and demonstration over glaciated regions, *GIScience Remote Sens.*, *1603*(June 2015), 1–20, doi:10.1080/15481603.2015.1008621.

Noh, M.-J., and I. M. Howat (2015b), Automated stereo-photogrammetric DEM generation at high latitudes: Surface Extraction with TIN-based Search-space Minimization (SETSM) validation and demonstration over glaciated regions, *GIScience Remote Sens.*, *1603*(June 2015), 1–20, doi:10.1080/15481603.2015.1008621.

Oberbauer, S. F. et al. (2007), Tundra CO2 fluxes in response to experimental warming across lattitudinal and moisture gradients, *Ecol. Monogr.*, *77*(2), 221–238, doi:10.1890/06-0649.

Oberbauer, S. F. et al. (2013a), Phenological response of tundra plants to background climate variation tested using the International Tundra Experiment,

Oberbauer, S. F. et al. (2013b), Phenological response of tundra plants to background climate variation tested using the International Tundra Experiment., *Philos. Trans. R. Soc. Lond. B. Biol. Sci.*, *368*(1624), 20120481, doi:10.1098/rstb.2012.0481.

Oberbauer, S. F. et al. (2013c), Phenological response of tundra plants to background climate variation tested using the International Tundra Experiment., *Philos. Trans. R. Soc. Lond. B. Biol. Sci.*, *368*(1624), 20120481, doi:10.1098/rstb.2012.0481.

Olivas, P. C., S. F. Oberbauer, C. E. Tweedie, W. C. Oechel, and A. Kuchy (2010), Responses of CO2 flux components of Alaskan Coastal Plain tundra to shifts in water table, *J. Geophys. Res. Biogeosciences*, *115*(4), 1–13, doi:10.1029/2009JG001254.

Osterkamp, T. E., M. . Jorgenson, E. A. G. Schuur, Y. L. Shur, M. . Kanevskiy, J. G. Vogel, and V. E. Tumskoy (2009), Physical and Ecological Changes Associated with Warming Permafrost and Thermokarst in Interior Alaska, *Permafr. Periglac. Process.*, *136*(January), 107–136, doi:10.1002/ppp.

Painter, S. L., J. D. Moulton, and C. J. Wilson (2012), Modeling challenges for predicting hydrologic response to degrading permafrost, *Hydrogeol. J.*, *21*(Hydrogeology of Cold Regions), 221–224, doi:10.1007/s10040-012-0917-4.

Park, H., Y. Kim, and J. S. Kimball (2016), Widespread permafrost vulnerability and soil active layer increases over the high northern latitudes inferred from satellite remote sensing and process model assessments, *Remote Sens. Environ.*, *175*, 349–358, doi:10.1016/j.rse.2015.12.046.

Peichl, M., O. Sonnentag, and M. B. Nilsson (2014), Bringing Color into the Picture: Using Digital Repeat Photography to Investigate Phenology Controls of the Carbon Dioxide Exchange in a Boreal Mire, *Ecosystems*, *18*(1), 115–131, doi:10.1007/s10021-014-9815-z.

Penuelas, J., I. Filella, J. A. Gamon, B. Y. J. Penuelas, I. Filella, and A. Gamon (1995), Assessment of photosynthetic radiation-use efficiency with spectral reflectance, , *131*(3), 291–296.

Post, E. et al. (2009), Ecological dynamics across the Arctic associated with recent climate change., *Science*, *325*(5946), 1355–1358, doi:10.1126/science.1173113.

Raaflaub, L. D., and M. J. Collins (2006), The effect of error in gridded digital elevation models on the estimation of topographic parameters, *Environ. Model. Softw.*, *21*(5), 710–732, doi:10.1016/j.envsoft.2005.02.003.

Rango, A., A. Laliberte, and C. Winters (2008), Role of aerial photos in compiling a long-term remote sensing data set, *J. Appl. Remote Sens.*, *2*(1), 23541, doi:10.1117/1.3009225.

Raynolds, M. K., J. C. Comiso, D. A. Walker, and D. Verbyla (2008), Relationship between satellite-derived land surface temperatures, arctic vegetation types, and NDVI, *Remote Sens. Environ.*, *112*(4), 1884–1894, doi:10.1016/j.rse.2007.09.008.

Richardson, A. D., J. P. Jenkins, B. H. Braswell, D. Y. Hollinger, S. V. Ollinger, and M. L. Smith (2007), Use of digital webcam images to track spring green-up in a deciduous broadleaf forest, *Oecologia*, *152*(2), 323–334, doi:10.1007/s00442-006-0657-z.

Richardson, A. D., B. H. Braswell, D. Y. Hollinger, J. P. Jenkins, and S. V. Ollinger (2009), Near-surface remote sensing of spatial and temporal variation in canopy phenology, *Ecol. Appl.*, *19*(6), 1417–1428, doi:10.1890/08-2022.1.

Richardson, A. D., T. F. Keenan, M. Migliavacca, Y. Ryu, O. Sonnentag, and M. Toomey (2013), Climate change, phenology, and phenological control of vegetation feedbacks to the climate system, *Agric. For. Meteorol.*, *169*, 156–173, doi:10.1016/j.agrformet.2012.09.012.

Rondeaux, G., M. Steven, and F. Baret (1996), Optimization of Soil-Adjusted Vegetation Indices, , *107*(August 1994), 95–107.

Rosnell, T., and E. Honkavaara (2012), Point cloud generation from aerial image data acquired by a quadrocopter type micro unmanned aerial vehicle and a digital still camera, *Sensors*, *12*(1), 453–480, doi:10.3390/s120100453.

Saitoh, T. M., S. Nagai, N. Saigusa, H. Kobayashi, R. Suzuki, K. N. Nasahara, and H. Muraoka (2012), Assessing the use of camera-based indices for characterizing canopy phenology in relation to gross primary production in a deciduous broad-leaved and an evergreen coniferous forest in Japan, *Ecol. Inform.*, *11*, 45–54, doi:10.1016/j.ecoinf.2012.05.001.

Schuur, E. et al. (2008), Vulnerability of Permafrost Carbon to Climate Change : Implications for the Global Carbon Cycle, *Bioscience*, *58*(8), 701–714.

Schwartz, M. D. (1998), Green-wave phenology, *Nature*, *394*, 839–840, doi:10.1038/29670.

Screen, J. a, and I. Simmonds (2010), The central role of diminishing sea ice in recent Arctic temperature amplification., *Nature*, *464*(7293), 1334–1337, doi:10.1038/nature09051.

Shaver, G. R., L. E. Street, E. B. Rastetter, M. T. Van Wijk, and M. Williams (2007), Functional convergence in regulation of net CO_2 flux in heterogeneous tundra landscapes in Alaska and Sweden, *J. Ecol.*, *95*(4), 802–817, doi:10.1111/j.1365-2745.2007.01259.x.

Sims, D. A., and J. A. Gamon (2002), Relationships between leaf pigment content and spectral reflectance across a wide range of species , leaf structures and developmental stages, , *81*, 337–354.

Smith, L. C., Y. Sheng, G. M. Macdonald, and L. D. Hinzman (2005), Disappearing Arctic lakes, , *XXX*(June), 2005.

Snavely, N., S. M. Seitz, and R. Szeliski (2008), Modeling the world from Internet photo collections, *Int. J. Comput. Vis.*, *80*(2), 189–210, doi:10.1007/s11263-007-0107-3.

Solano, R., K. Didan, A. Jacobson, and A. Huete (2010), MODIS Vegetation Index User ' s Guide (MOD13 Series), , *2010*(May).

Sommerkorn, M. (2008), Micro-topographic patterns unravel controls of soil water and temperature on soil respiration in three Siberian tundra systems, *Soil Biol. Biochem.*, *40*(7), 1792–1802, doi:10.1016/j.soilbio.2008.03.002.

Steinwand, D. A., J. A. Hutchinson, and J. P. Snyder (1995), Map Projections for Global and Continental Data Sets and an Analysis of Pixel Distortion Caused by Reprojection, *Photogrammatic Eng. Remote Sens.*, *61*(12), 1487–1497.

Stewart, K. J., P. Grogan, D. S. Coxson, and S. D. Siciliano (2014), Topography as a key factor driving atmospheric nitrogen exchanges in arctic terrestrial ecosystems, *Soil Biol. Biochem.*, *70*(3), 96–112, doi:10.1016/j.soilbio.2013.12.005.

Stow, D. a. et al. (2004), Remote sensing of vegetation and land-cover change in Arctic Tundra Ecosystems, *Remote Sens. Environ.*, *89*(3), 281–308, doi:10.1016/j.rse.2003.10.018.

Streletskiy, D. A., N. I. Shiklomanov, F. E. Nelson, and A. E. Klene (2007), 13 Years of Observations at Alaskan CALM Sites: Long-term Active Layer and Ground Surface Temperature Trends, *Proc. 9th Int. Conf. Permafr.*, 1–6.

Sullivan, P. F., S. J. T. Arens, R. A. Chimner, and J. M. Welker (2008), Temperature and microtopography interact to control carbon cycling in a high arctic fen, *Ecosystems*, *11*(1), 61–76, doi:10.1007/s10021-007-9107-y.

Sumerling, G. (2011), Lidar Analysis in ArcGIS ® 10 for Forestry Applications, *ESRI White Pap.*, (January), 53.

Tape, K., M. Sturm, and C. Racine (2006), The evidence for shrub expansion in Northern Alaska and the Pan-Arctic, *Glob. Chang. Biol.*, *12*(4), 686–702, doi:10.1111/j.1365-2486.2006.01128.x.

Throckmorton, H. M. et al. (2016), Active layer hydrology in an arctic tundra ecosystem: Quantifying water sources and cycling using water stable isotopes, *Hydrol. Process.*, *4986*(August), 4972–4986, doi:10.1002/hyp.10883.

Torre Jorgenson, M. et al. (2013), Reorganization of vegetation, hydrology and soil carbon after permafrost degradation across heterogeneous boreal landscapes, *Environ. Res. Lett.*, *8*(3), 35017, doi:10.1088/1748-9326/8/3/035017.

Triggs, B., P. F. McLauchlan, R. I. Hartley, and A. W. Fitzgibbon (2000), Bundle Adjustment — A Modern Synthesis, *Vis. Algorithms Theory Pract.*, *1883*, 298–372, doi:10.1007/3-540-44480-7_21.

Tucker, C. J. (1978), Red and Photographic Infrared Linear Combinations for Monitoring Vegetation,

Tucker, C. J. (1999), Higher Northern Latitude NDVI and Growing Season Trends from 1982 to 1999,

Tucker, C. J., and P. J. Sellers (2007), Satellite remote sensing of primary production, *Int. J. Remote Sens.*, *7*(11), 1395–1416, doi:10.1080/01431168608948944.

Usery, E. L., M. P. Finn, J. D. Cox, S. Ruhl, M. Bearden, E. L. Usery, M. P. Finn, J. D. Cox, and T. Beard (2003), Projecting global datasets to achieve equal areas, , *30*(1), 69–79.

Ustin, S. L., and J. A. Gamon (2010), Tansley review Remote sensing of plant functional types, , 795–816.

Vaze, J., J. Teng, and G. Spencer (2010), Impact of DEM accuracy and resolution on topographic indices, *Environ. Model. Softw.*, *25*(10), 1086–1098, doi:10.1016/j.envsoft.2010.03.014.

Villarreal, S., R. D. Hollister, D. R. Johnson, M. J. Lara, P. J. Webber, and C. E. Tweedie (2012), Tundra vegetation change near Barrow, Alaska (1972–2010), *Environ. Res. Lett.*, *7*(1), 15508, doi:10.1088/1748-9326/7/1/015508.

Vorosmarty, C. J., a. D. McGuire, and J. E. Hobbie (2010), Scaling Studies in Arctic System Science and Policy Support: A Call to Research, *U.S. Arct. Res. Comm.*, 76 pages.

Vörösmarty, C. J., L. D. Hinzman, B. J. Peterson, D. H. Bromwich, L. C. Hamilton, J. Morison, V. E. Romanovsky, M. Sturm, R. S. Webb, and D. L. Kane (2001), The Hydrologic Cycle and its Role in Arctic and Global Environmental Change: A Rationale and Strategy for Synthesis Study The Hydrologic Cycle and its Role in Arctic and Global Environmental Change, *NSF-ARCSS Hydrol. Work. Steer. Comm.*, *84*(September).

Walker, D. a et al. (2012), Environment, vegetation and greenness (NDVI) along the North America and Eurasia Arctic transects, *Environ. Res. Lett.*, *7*(1), 15504, doi:10.1088/1748-9326/7/1/015504.

Walker, M., and C. Wahren (2006), Plant community responses to experimental warming across the tundra biome, *Proc. …*, *103*(5), 1342–6, doi:10.1073/pnas.0503198103.

Ward, R. D., N. G. Burnside, C. B. Joyce, and K. Sepp (2013), The use of medium point density LiDAR elevation data to determine plant community types in Baltic coastal wetlands, *Ecol. Indic.*, *33*, 96–104, doi:10.1016/j.ecolind.2012.08.016.

Webber, P. J., and M. D. Walker (1991), The International Tundra Experiment (ITEX): Resolution, , 1990.

Wehr, A., and U. Lohr (1999), Airborne laser scanning—an introduction and overview, *ISPRS J. Photogramm. Remote Sens.*, *54*(2–3), 68–82, doi:10.1016/S0924-2716(99)00011-8.

Westergaard-Nielsen, A., M. Lund, B. U. Hansen, and M. P. Tamstorf (2013), Camera derived vegetation greenness index as proxy for gross primary production in a low Arctic wetland area, *ISPRS J. Photogramm. Remote Sens.*, *86*, 89–99, doi:10.1016/j.isprsjprs.2013.09.006.

Westoby, M. J., J. Brasington, N. F. Glasser, M. J. Hambrey, and J. M. Reynolds (2012), "Structure-from-Motion" photogrammetry: A low-cost, effective tool for geoscience applications, *Geomorphology*, *179*, 300–314, doi:10.1016/j.geomorph.2012.08.021.

Wilson, J. P. (2012), Digital terrain modeling, *Geomorphology*, *137*(1), 107–121, doi:10.1016/j.geomorph.2011.03.012.

Wu, S., J. Li, and G. H. Huang (2008), A study on DEM-derived primary topographic attributes for hydrologic applications: Sensitivity to elevation data resolution, *Appl. Geogr.*, *28*(3), 210–223, doi:10.1016/j.apgeog.2008.02.006.

Zeng, H., G. Jia, and H. Epstein (2011), Recent changes in phenology over the northern high latitudes detected from multi-satellite data, *Environ. Res. Lett.*, *6*(4), 45508, doi:10.1088/1748-9326/6/4/045508.

Zhang, Z., D. L. Kane, and L. D. Hinzman (2000), Development and application of a spatially-distributed arctic hydrological and thermal process model (ARHYTHM), *Hydrol. Process.*, *14*(6), 1017–1044, doi:10.1002/(SICI)1099-1085(20000430)14:6<1017::AID-HYP982>3.0.CO;2-G.

Zona, D., D. A. Lipson, R. C. Zulueta, S. F. Oberbauer, and W. C. Oechel (2011), Microtopographic controls on ecosystem functioning in the Arctic Coastal Plain, *J. Geophys. Res. Biogeosciences*, *116*(3), 1–12, doi:10.1029/2009JG001241.

Chapter 4: Spatial and Temporal Scaling of Surface Characteristics: A Case Study in a High Arctic Tundra Ecosystem

4.1 INTRODUCTION

Recent changes in the Earth's atmosphere and climate patterns are impacting other components of the Earth system (*IPCC*, 2014). Changes in arctic terrestrial landscape ecology and the composition, structure and function of ecosystems have the capacity to alter regional and global processes through feedbacks between physical and biogeochemical subsystems (*Hinzman et al.*, 2013). However, landscape ecology emphasizes broad spatial and temporal scales and the effects of the geographical patterns exhibited within any given ecosystem can also vary drastically from one location to the next (e.g. processes and patterns exhibited at one spatial scale may not be significant or predictive at another spatial scale). Tundra landscapes are spatially heterogeneous areas and their structure, or spatial relationships within the ecosystem, their function (e.g. interactions between the spatial elements of the landscape), and the related ecosystem change to the structure and function are temporally and spatially scale dependent (*Turner*, 1989). Remote sensing and the field of spectroscopy has provided essential tools that have shown the capacity to document biophysical environmental parameters such as vegetation productivity extracted from reflectance measurements acquired at multiple spatial scales (i.e. field, airborne and satellite platforms) using vegetation indices such as the normalized difference vegetation index (NDVI) (*Vierling et al.*, 1997; *Sims and Gamon*, 2002; *Boelman et al.*, 2003; *Stow et al.*, 2004; *Huemmrich et al.*, 2010; *Epstein et al.*, 2012; *Huemmrich et al.*, 2013). However considerable differences exists between observations acquired from multiple platforms using multiple indices (i.e. mean simple ratio (MSR), and modified normalized difference vegetation index (MNDVI)) as each is calculated from slightly different wavelengths and bands depending on the sensor being employed (*Stow et al.*, 2004), which might lead to misinterpretation (Figure 4.1).

Due to the characteristic heterogeneity of tundra landscapes, scaling of ecosystem processes from one spatial scale (i.e. meters) to another (hundreds of kilometers) is dynamic and has limited research efforts focused on employing optical remote sensing for monitoring landscape ecology in tundra ecosystems. Additionally, the short growing seasons and related phenological dynamics, persistent clouds cover, standing water and drastic light fluctuations typical of high-arctic tundra ecosystems have also limited cross-platform remote sensing efforts (Stow et al. 2004).

Moreover, there is a lack of cross-comparison between observations acquired from different spatiotemporal scales specifically looking into the effect of using similar wavelengths and spectral bands from different sensors to calculate representative indices that quantify biophysical properties of vegetation dynamics such as NDVI, leaf area index (LAI) and biomass estimation across multiple predominant vegetation classes. Research efforts focused on this might be key to improving our understanding of the magnitude and scale of change facing the Arctic and thus the effects reciprocated to global processes (*Vorosmarty et al.*, 2010).

As described in the previous two chapters, the Arctic plays an important role within the Earth System and climate warming may trigger the loss of large amounts of soil organic carbon from permafrost dominated landscape to the atmosphere, which could enhance greenhouse warming. The magnitude of responses to these changes are relatively poorly understood for most arctic landscapes and despite advances in remote sensing and other technological advances, linking research results from plot to regional scales remains a challenge. These challenges underpin the primary motivation for this dissertation. In chapter 2, inter-comparison of KAP and LiDAR systems showed that KAP has a strong potential for use in DEM modeling of tundra landscapes, especially in polygonised tundra landscapes that are prone to thermokarst. Chapter 3 focused on the assessment of KAP and Pheno-cam RGB-derived indices and demonstrated the capacity for these low-cost systems to document phenological trends along plot-level MISP transects. Given this success, this chapter further examines the capacity of low-cost digital cameras to document vegetation phenological trends and produce a DEM spanning a larger spatial scale. This study sampled vegetation phenology at the same plot-level scale of the MISP transects in disjoint plots distributed sparsely across a larger landscape area in high and low arctic tundra near Utqiaġvik and Atqasuk respectively. At each study location, the area of study is comparable to that of a raw data pixel acquired by many globally orbiting satellites such as MODIS, which has become amongst the most widely used satellite platforms for the assessment of ecosystem properties at regional to global scales (MODIS NDVI) (*Gao and Huete*, 2000; *Bhatt et al.*, 2010; *Gamon et al.*, 2013).

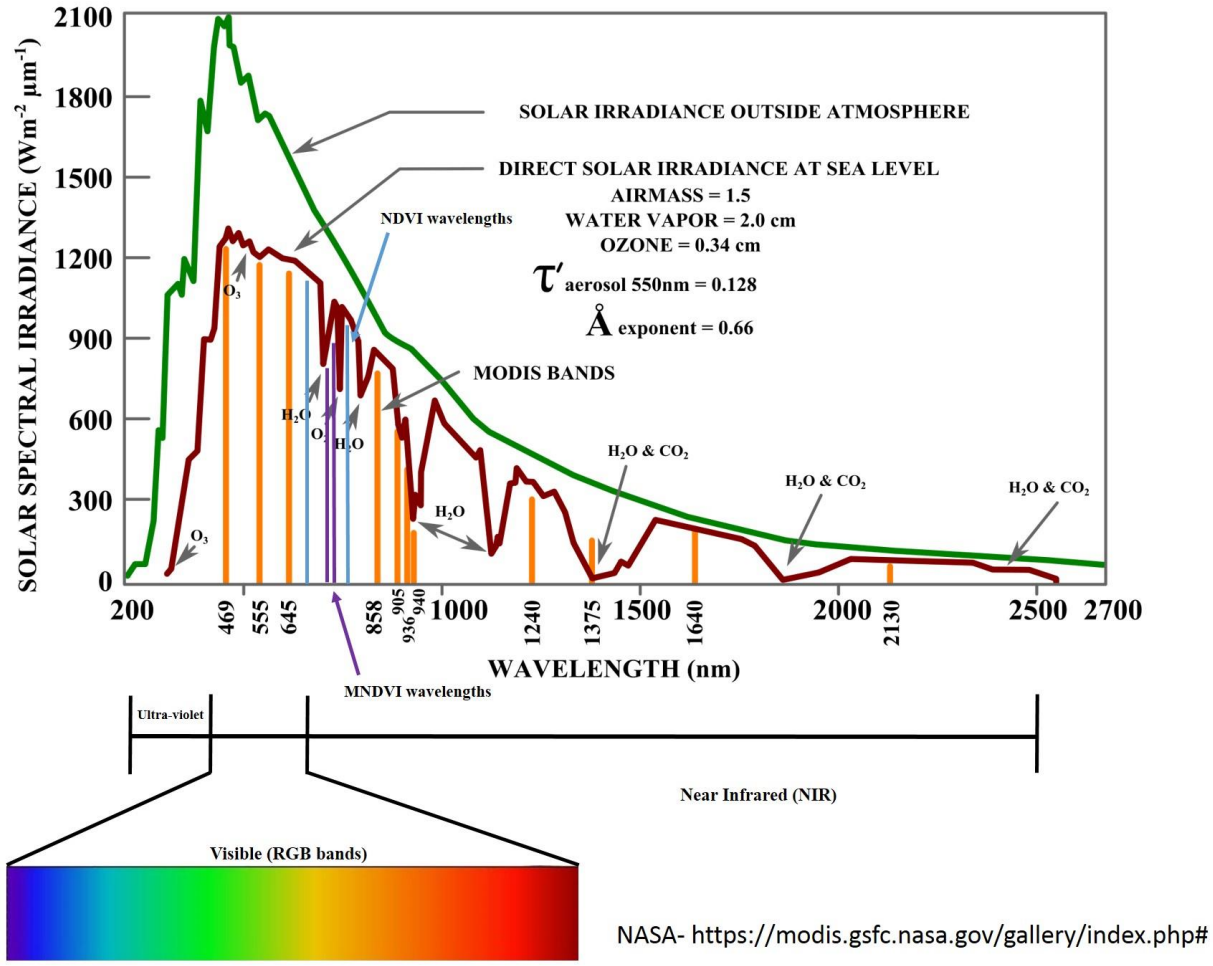

Figure 4.1 Depiction of the electromagnetic spectrum and solar irradiance with corresponding wavelength ranges highlighting the bands used to calculate spectral indices within this study. MODIS bands are shown in orange, while NDVI and MNDVI wavelengths are shown in blue and purple respectively. Solar spectral irradiance incident on the top of the atmosphere (green curve) and transmitted through the atmosphere to the Earth's surface (brown curve) is also shown. Major absorption bands in the atmosphere are clearly apparent.

4.2 OBJECTIVES

The overall objective of this study was to both 1) expand on, and integrate findings from the previous two chapters and explore the potential of Kite Aerial Photography (KAP) to be used for scaling Digital Elevation Models and seasonal greening trends to the landscape scale (1 km^2); and 2) explore the relationship between seasonal greening trends and vegetation type and surface microtopography. This chapter addresses the scalability of plot-level phenological dynamics and land surface structure datasets to the landscapes level.

4.2.1 Materials and methods

The majority of field sampling and data analysis methods utilized in chapters 2 and 3 were adopted for this study to facilitate inter-comparison of phenological dynamics and landscape characteristics across multiple spatial and temporal scales, vegetation types, soil moisture regimes and geographical locations. Therefore, this chapter will focus on presenting data collection, processing, analysis, and results for that of the CALM grid plots (referred to as CALM grids from here on out) in both Utqiaġvik and Atqasuk. For details on the MISP transects and related approaches, please refer to chapter 3.

4.2.2 Study area

This investigation was conducted at two locations near Utqiaġvik (71°18'N, 156°40'W) and Atqasuk (70°29'N, 157°25'W) on the North Slope of Alaska, as a contribution to the Arctic Observing Network's International Tundra Experiment (AON-ITEX). At these locations the Circumpolar Active Layer Monitoring (CALM) grids, formerly known as the Arctic System Science (ARCSS) grids, were established in the mid-1990s in an effort to monitor changes in the active layer of tundra landscapes. Both grids measure 1000 meters by 1000 meters (1 km^2 or 100 hectares), with nodes spaced on a 100 meter grid (*Brown et al.*, 2000). During the summers of 2011 and 2012, 1 x 1 meter plots were established approximately 3 x 3 meters to the south and west of each CALM node. The central aim of this study was to build a capacity to monitor plot level plant community composition and structure across a spatial domain typically sampled by a global orbiting satellite platform (e.g. MODIS). Using geographical information systems (GIS) a subset of 30 plots was chosen from each CALM grid in Utqiaġvik and Atqasuk. These plots spanned a large area within the CALM grid, were logistically feasible to sample periodically, and represented a wide range of plant community types and landscape geography encountered within the greater study areas (Figures 4.1 and 4.2). This study also utilized the Mobile Instrumented Sensor Platform (MISP) transects (2 x 50 meters) (from chapter 3) established at both sampling locations in 2011, which consisted of contiguous 2 x 1 meter plots and a range of vegetation types found throughout the CALM grid. Figures 4.3 and 4.4 display plot-level images (PLIs) of plots containing dominant vegetation classes for both CALM grids. Table 4.1 below summarizes the vegetation types and classes (from *Lin et al.*, 2012; *Andresen et al.*, in prep), dominant species and landform types present at each MISP transect and CALM grids.

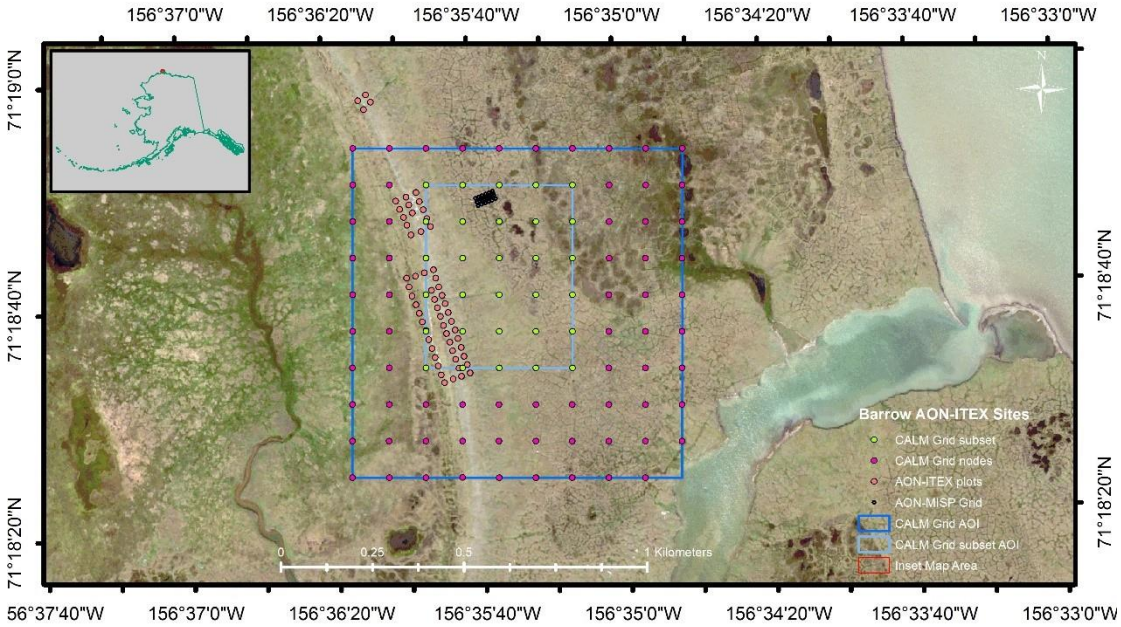

Figure 4.2: True color World View 2 image captured during the summer of 2013 displaying location of the Utqiaġvik AON-ITEX sites including ITEX warming plots, MISP transect, CALM grid, with corresponding nodes and areas of interest.

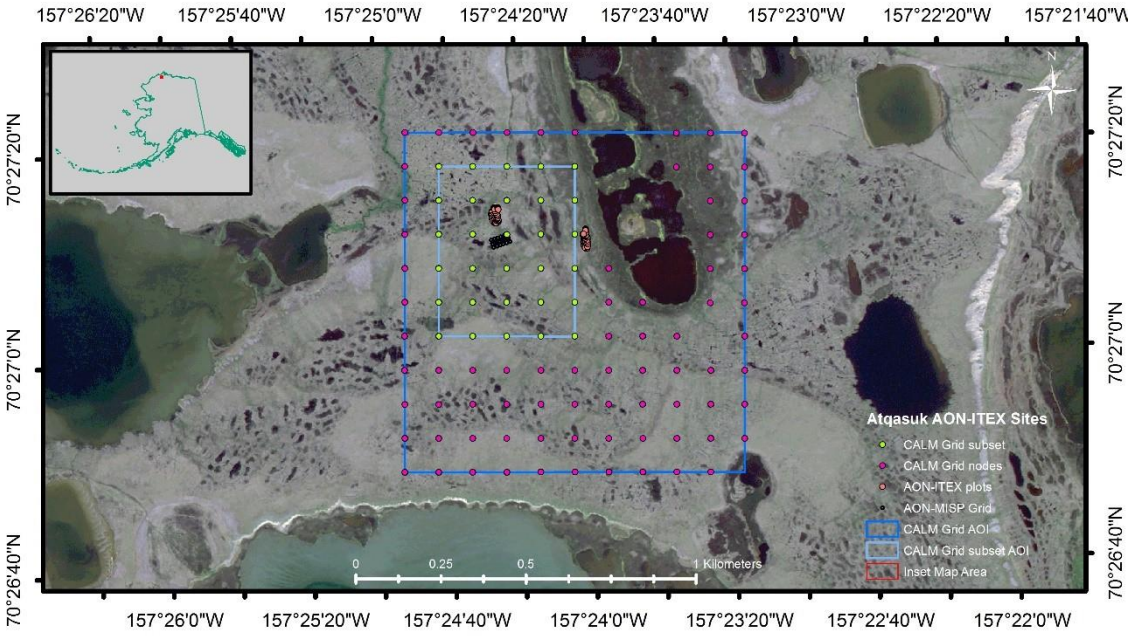

Figure 4.3: True color World View 2 image captured during the summer of 2013 displaying location of the Atqasuk AON-ITEX sites including ITEX warming plots, MISP transect, CALM grid, with corresponding nodes and areas of interest.

Table 4.1: Summary of the MISP transects and CALM plots present at Utqiaġvik and Atqasuk. The vegetation types and classes, wetland names, dominant species and landform types selected were based on Lin et al. (2011), Webber, (1980), Healey et al., (2014), and Andresen et al. in prep.

Parameters	Barrow					Atqasuk				
Vegetation Type	Dry Heath/ Mesic Heath		Moist Meadow	Wet Meadow		Dry Heath/ Mesic Heath	Moist Meadow		Wet Meadow	
Wetland Name	Dry dwarf shrub graminoid tundra	Dry-moist dwarf shrub graminoid tundra	Moist graminoid tundra	Seasonally flooded gramonoid tundra	Wet graminoid tundra	Dry shrub graminoid tundra	Moist graminoid tundra	Moist shrub graminoid tundra	Wet graminoid tundra	Aquatic graminoid tundra
Vegetation Class	Dry shrub	Dry-moist shrub-gram	Moist gram	Seasonally flooded	Wet gram	Dry	Moist	Moist shrub	Wet	Aquatic
Dominant Species	*Salix pulchra, Lazula arctica*	*Eriophorum spp.*	*Carex aquatilis/stans*	*pleaurocarpous mosses/ Arctophila fulva*	*Arctophila fulva*	*Cassiope tetragona*	*Vaccinium Vitis-idaea*	*Salix pulchra*	*Carex aquatilis*	*Arctophila fulva*
Landform Type	High center polygon/ Stabilized sand dune	High center polygon	Low center polygon/ low land	Marsh	Pond/lake	Stabilized sand dune/ snow patch	High center polygon	Low center polygon/low land	Marsh	Pond/lake
Mean Peak Season VWC (%)	42	35.4	55.8	70.5	63.5	30.6	31.03	40.1	59.3	49.8
Elevation (MASL)	3					30				
Mean Annual Temperature (°C)	-12.6					-11.9				
Mean July Temperature (°C)	3					7.2				
Average Maximum Thaw Depth (cm)	35-39					36-75+				

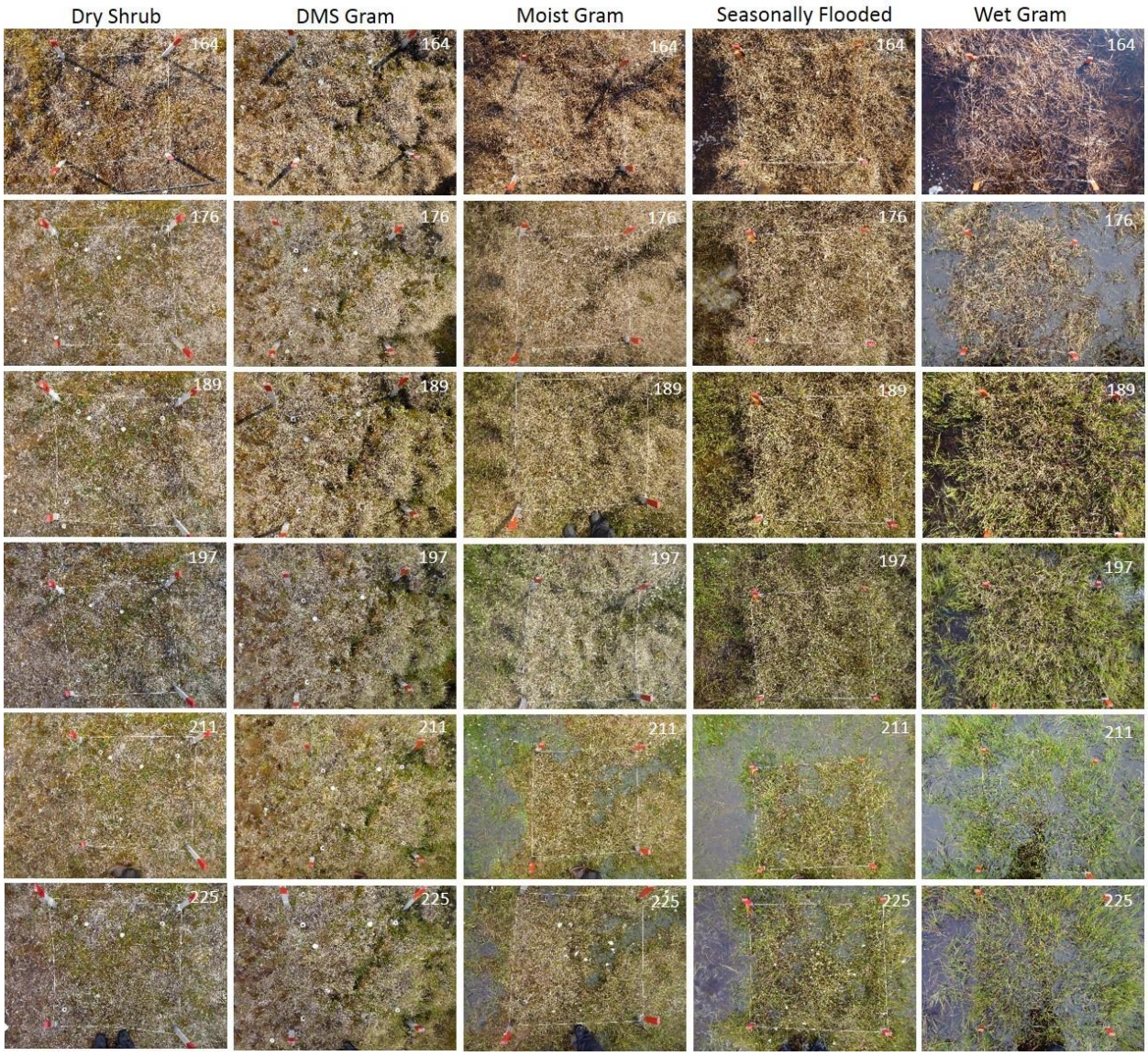

Figure 4.4: Utqiaġvik CALM grid PLIs depicting the primary seasonal stages of the various vegetation classes and corresponding soil moisture contents present at representative plots. Day of year (DOY) is displayed on the top right corner of each image. Major phenological events are highlighted such as green-up (DOY 189-211) for all classes, drying (DOY 189-197) for seasonally flooded and wet gram classes and flooding (DOY 211) also for the seasonally flooded and wet gram classes plus the moist gram class.

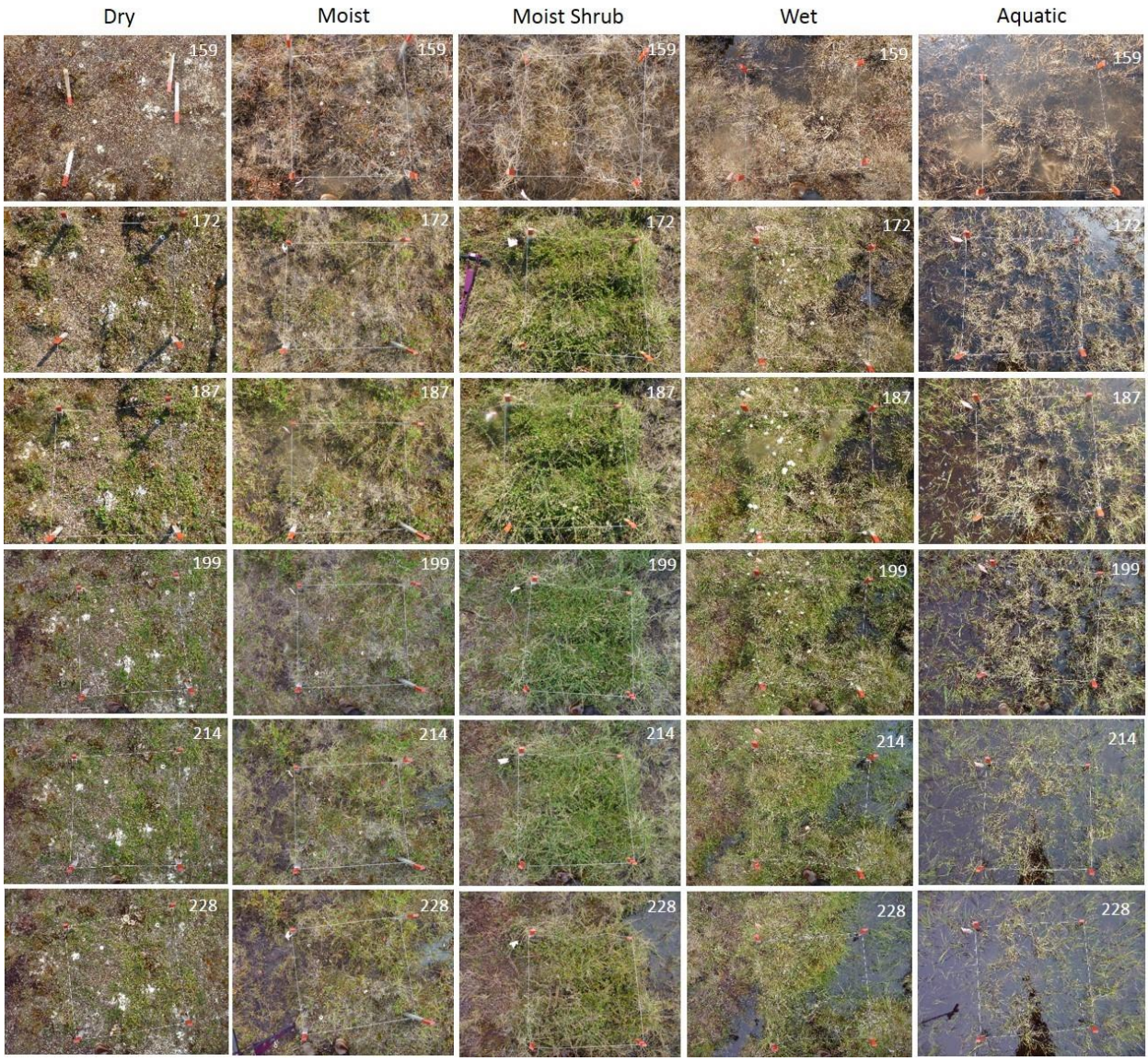

Figure 4.5: Atqasuk CALM grid PLIs depicting the primary seasonal stages of the various vegetation classes and corresponding soil moisture contents present at representative plots. Day of year (DOY) is displayed on the top right corner of each image. Major phenological events are highlighted such as green-up (DOY 172-214) for all classes except the aquatic and flooding (DOY 214) for all classes but dry.

The dominant plant communities of the Utqiaġvik area consist mostly of dry high-centered polygons characterized by mosses and lichens and wet, low-lying troughs mostly dominated by graminoids, giving the landscape its typical patterned array. Utqiaġvik is considered to be located

in a high Arctic climate zone which often displays short cool summers with fluctuating air temperatures between 0.8°C and 3.7°C on average (*Hollister*, 2003; *Oberbauer et al.*, 2013b). The snow free period varies between early June and early September and summers are typically foggy, cloudy and humid with an average summer precipitation of approximately 19 mm (*Brown et al.*, 1980; *Hollister*, 2003). Utqiaġvik exhibits a lower diversity of vegetation compared to Atqasuk, most likely due to the harsh climate (*Komarkova, V., and Webber*, 1980). The Atqasuk landscape is also dominated by dry heath and wet meadow plant communities, however these are more distinct (i.e. tussock tundra) than in Utqiaġvik as far as species composition and abundance. Atqasuk is characterized as a low arctic climate zone and consists of moderate summers with air temperature ranging between 3.2°C and 8.7°C and average summer precipitation of 26 mm, resulting in a higher vegetation diversity relative to Utqiaġvik (*CAVM Team,* 2003).

4.2.3 Data collection

4.2.3.1 CALM Vegetation Phenology

4.2.3.1.1 Broad-band spectral reflectance

A dual-channel mobile field spectrometer (UniSpec DC, PP Systems, Amesbury MA, USA) was utilized by Systems Ecology Laboratory (SEL) researchers to acquire plot level reflectance measurements of all 30 CALM grid plots for both Utqiaġvik and Atqasuk. Sampling approaches at both locations followed that of chapter 3 across the MISP transects, and took place during the summer growing seasons between 2010 and 2015, although exact start dates varied due to the onset of snowmelt and logistical limitations typically experienced when working in this region. The CALM grid plots were sampled every other week between early June and mid-August. Sampling took place from the north edge of each plot to minimize disturbance of the plot due to shading from sun-angles as well as to avoid stepping inside each plot. The radiance fore-optic was mounted onto a tripod boom positioned looking down at the target approximately 1.62 meters above the tundra surface yielding a sampling surface area of approximately 0.6 meters, and was aimed towards the center of each plot. Similarly, the irradiance fore-optic was also mounted onto the boom but looking up at incoming radiation. A white reference standard panel (Spectralon, LabSphere, North Sutton, New Hampshire, USA) was also utilized during field data acquisition to assist in cross-calibration of data and correct for changing light conditions that might affect

radiance and irradiance measurements. All reflectance spectra yielded data in the 300 to 1100 nm wavelength range from which an assortment of vegetation and water indices were calculated for each plot (e.g. Normalized Difference Vegetation Index (NDVI) and Water Band Index (WBI); Table 4.2). Indices such as these offer metrics for detecting structural and physiological properties and seasonal change in vegetation (*Ustin and Gamon*, 2010).

Table 4.2: List of indices used in this study with corresponding equations and references. Digital camera formulas refer to the camera color channel information (digital numbers; DNs) while the spectrometer-derived formulas pertain to the reflectance wavelength value (nm).

Platform	Index Name	Index	Formula	Reference
Digital Camera	Green Excess	GEI	$2 * G_{DN} - (R_{DN}+B_{DN})$	Richardson et al., 2007
Digital Camera	Red digital number	Red DN	R_{DN}	Richardson et al., 2007
Digital Camera	Green digital number	Green DN	G_{DN}	Richardson et al., 2007
Digital Camera	Blue digital number	Blue DN	B_{DN}	Richardson et al., 2007
Digital Camera	Total digital number	Total RGB	$(R_{DN} + G_{DN} + B_{DN})/3$	Richardson et al., 2007
Digital Camera	Percent red	%R	$(R_{DN})/(R_{DN}+G_{DN}+B_{DN})$	Richardson et al., 2007
Digital Camera	Percent green	%G	$(G_{DN})/(R_{DN}+G_{DN}+B_{DN})$	Richardson et al., 2007
Digital Camera	Percent blue	%B	$(B_{DN})/(R_{DN}+G_{DN}+B_{DN})$	Richardson et al., 2007
Digital Camera	Lightness	L*	**See Reference	Paschos, 2001
Digital Camera	A-red-green	A*	**See Reference	Paschos, 2001
Digital Camera	B-blue-yellow	B*	**See Reference	Paschos, 2001
Digital Camera	AnyColor	AnyColor	**See Reference	Paschos, 2001
Digital Camera	Hue	Hue	**See Reference	Paschos, 2001
Digital Camera	Saturation	Saturation	**See Reference	Paschos, 2001
Digital Camera	Value	Value	**See Reference	Paschos, 2001
Digital Camera	nNDVI	nNDVI	$(R_{DN}-G_{DN})/(R_{DN}+G_{DN})$	Ramirez et al., in prep
Digital Camera	Test	TEST(L*A*)	A*(1+(L*)/(255))	Ramirez et al., in prep
Spectrometer	Carotenoid 1	CRI1	(1/R510)-(1/R550)	Gitelson et al., 2002
Spectrometer	Carotenoid 2	CRI2	(1/R510)-(1/R700)	Gitelson et al., 2002
Spectrometer	Gitelson 4	Gitelson4	(1/R550)-(1/R750)	Gitelson et al., 2003
Spectrometer	Gitelson 5	Gitelson5	(1/R700)-(1/R800)	Gitelson et al., 2003
Spectrometer	Greenness 1	Green1	(R554/R675)	Huemmrich K.H., personal communication
Spectrometer	Modified Normalized Difference Vegetation Index	MNDVI	(R750-R705)/(R750+R705-(2*R445))	Liu and Huete, 1995
Spectrometer	Modified Simple Ratio	MSR	(R750-R445)/(R705-R445)	Sims and Gamon, 2002
Spectrometer	Normalized Difference Soil Water Index- linear	NDSWI-lin	(R460-R1000)/(R460+R1000)	Goswami et al., 2011
Spectrometer	Normalized Difference Soil Water Index- log	NDSWI-log	(log(R1000) - log(R460))/(log(R1000) + log(R460))	Goswami et al., 2011
Spectrometer	Normalized Difference Vegetation Index	NDVI	(R800-R680)/(R800+R680)	Tucker, 1978
Spectrometer	Optimized Soil Adjusted Vegetation Index	OSAVI	1.16*(R800-R670)/(R800+R670+0.16)	Rondeaux et al., 1996
Spectrometer	Photochemical Reflectance Index 2	PRI 2	(R530-R550)/(R530+R550)	Sims and Gamon, 2002
Spectrometer	Structure Independent Pigment Index	SIPI	(R800-R450)/(R800-R650)	Peñuelas et al., 1995
Spectrometer	Water Band Index	WBI	(R900/R970)	Claudio et al., 2006

4.2.3.1.2 Plot-level RGB photography

Given that the CALM grid plots were spatially distributed, sampling of these plots required a slightly different approach than that employed for the KAP and Pheno-cam systems. For example, the KAP system has successfully been used to cover large areas (>400 meters), however it has also been limited by the typically harsh weather conditions (e.g. high gusty winds, rain and fog). Therefore, PLIs were taken by SEL researchers over each CALM grid plot approximately once every 2 weeks during the summer sampling period between 2012 through 2015. Images were taken from the north side and directly above each plot to avoid casting a shadow and to minimize disturbance adjacent to plots (Figure 4.3 and 4.4). All images were taken using the same digital point-and-shoot camera utilized by the KAP system.

4.2.3.1.3 Ground-based surface measurements

A suite of ground-based surface measurements were taken by SEL researchers from the perimeter of the north side of each CALM grid plot, similarly to the MISP field collection approach. Soil moisture percentage or volumetric water content (VWC) was obtained using a portable time-domain reflectometry (TDR) unit, coupled with 12 cm rods (FieldScout TDR 300 Soil Moisture Meter; Spectrum Technologies, Inc., Plainfield, IL, USA). This particular instrument converts a measured electrical signal into percent soil moisture content using an equation valid over a wide-range of mineral soils. Soil temperature in degree Celsius (°C) was measured between 5 and 10 cm below the surface of the tundra using an inexpensive handheld digital thermometer (Commercial Waterproof Digital Thermometer; Taylor Precision Products, Inc., Oak Brook, IL, USA). The active layer (AL) thaw depth in meters was also monitored and measured using a CALM depth probe (*Brown et al.*, 2000). Water Table depth data were not collected across the CALM plot.

4.2.3.2 Utqiaġvik CALM grid elevation

4.2.3.2.1 Airborne photography and digital photogrammetry

The capacity of the kite to cover larger areas (1km^2) was a difficult task given the characteristic low-lying clouds that dominate most of the snow-free summers in Utqiaġvik. Additionally, control of the kite platform diminished with increased height and wind speed, which posed a great limitation for attempting to cover the entire CALM grid. Therefore, hundreds of

digital true-color red, green and blue (RGB) airborne images of the entire Utqiaġvik CALM grid were acquired by SEL researchers from a helicopter at an average flying height of 380 meters above the tundra surface in late August 2013. All images were acquired every five to ten seconds to ensure at least 60% overlap between images using a *Panasonic Lumix (DMC-TS3)* (12 megapixel) point-and-shoot digital camera, the same unit used for the BE DEM site study described in Chapter 2 and for collecting PLIs of the CALM grid plots. To enhance georectification of images for 3D scene reconstruction and dense Point Cloud (PC) production, 211 Ground Control Points (GCPs) were used within the study area (see www.barrowmapped.org). Precise locations for each GCP were measured using post-processed kinematic surveys performed with a DGPS unit (*Trimble R7 receiver, a Zephyr Geodetic antenna, and a TSC2 survey controller*).

4.2.3.2.2 Airborne Light Detection and Ranging (A-LiDAR)

The same A-LiDAR dataset used for chapter 2 was utilized to further explore elevation characteristics across the CALM grid. This acquisition was made by the Next-Generation Ecosystem Experiments (NGEE) research group and executed by *AeroMetric, Inc.*, under contract to the Earth and Natural Sciences Division of the Los Alamos National Laboratory (LANL) in mid July 2013. Please refer to chapter 2 for more details on data collection and field metadata information.

4.2.3.2.3 Stereo Satellite Imagery (SSI)

The SSI-derived DEM used in this study was clipped from version 1 of the ArcticDEM released on September 1, 2016. The ArcticDEM is a public-private effort coordinated by The Polar Geospatial Center (PGC) in collaboration with the National Geospatial-Intelligence Agency (NGA), National Science Foundation (NSF) and several other institutions. The ArcticDEM has been developed from several years of high- resolution (0.5 meter) panchromatic imagery acquired throughout the year (including the snow-covered and snow-free period) by the Worldview 1, Worldview 2, and Worldview 3 optical satellites maintained by DigitalGlobe (*Noh and Howat*, 2015).

4.3 DATA PROCESSING

4.3.1 Vegetation Phenology

4.3.1.1 Vegetation classification

As part of the AON-ITEX initiative, plant community composition and structure data were collected for all CALM grid plots by Grand Valley State University (GVSU) researchers whom are partners to the AON-ITEX initiative. These data differed slightly from that collected across the MISP transects (e.g. plant species cover) and were also sampled inter-annually during the summers of 2010, 2012, 2013, 2014, and 2015. A similar yet smaller point frame (70 cm) was placed over each CALM plot and plant species was recorded at each location. The height of the species was analyzed visually and measured using a ruler relative to the ground at that location. The point frame grids were spaced 7 cm apart and started at 3.5 cm from the edge of the frame. All hits and all the species that were encountered were recorded. Occasionally, it was difficult to distinguish which species was on the ground because there were several intertwined individuals within the canopy, therefore preference was given to vascular plants, then lichens, and then mosses. Due to limitation of field identification many species were lumped into larger taxa. Please refer to chapter 2 for more details on the plot sampling frame and approach used across the MISP transects located in Utqiaġvik and Atqasuk as well.

The same data processing workflows used for Chapter 3 were applied to the CALM plant community data and were used to classify all CALM plots into discrete plant communities using Hierarchical Cluster Analysis in PC-ORD 6 (MjM Software Design Gleneden Beach, OR, USA). SØrensen's similarity coefficient was employed consisting of a flexible beta linkage method (β = -0.25) for chaining minimization purposes (*McCune and Grace 2002*). A cutoff of less than 50% similarity for the Utqiaġvik communities and 55% for the Atqasuk plant communities was used to match these clusters with high resolution (0.5 m) vegetation maps (*Andresen et al.* in prep.) derived from multiple high-resolution World View 2 imagery. This approach was used for all years of data, and resulted in 5 dominant vegetation classes at each site and are described in Table 4.1.

4.3.1.2 Broad-band spectral reflectance processing

All broad-band reflectance data was processed using the same custom built software application used in chapter 3 (*rHyperSpec, Laney,* 2012). This tool was developed by researchers

at the SEL with an aim at reducing data processing times and improving processing accuracy and data visualization of multi-spectral data acquired specifically by the *PP Systems Unispec DC* spectrometer. This software was the main source utilized to process all broad-band reflectance data collected for all years from both locations. Additionally, this package allows for reduced post-processing steps and yields a gamut of spectral indices (see Table 4.2, *spec*) commonly used within optical remote sensing. This tool was not only used to process all raw data files from all sampling years but also to further explore and expand the application of optical sampling within the long term ITEX-AON monitoring program. Index values resulting from *rHyperSpec* were exported as a text file and averaged to yield one value per plot per sampling date.

4.3.1.3 RGB image processing

All plot-level images were visually inspected for quality and any that were considered subpar were removed. All images of the CALM grid plots were acquired within 3 hours of solar noon and only one final image per acquisition date was selected for analysis. All PLIs were manually processed individually to maximize the integrity of image to image registration and ensure the same ROI was being analyzed for each. One ROI was developed for each CALM plot at both sites. All images were processed using the *Phenology Analyzer* software, developed within the Systems Ecology Laboratory (SEL) at the University of Texas at El Paso (UTEP) (*Ramirez, et al.* patent pending) as described in more detail in chapter 3. Regions of interest (ROI) were created for each final image selected across each individual plot and for all CALM grid plots.

4.3.2 Utqiaġvik CALM grid PC processing

4.3.2.1 Airborne photography (A-Photography)

All A-Photography images were visually checked for quality by removing those that were considered sub-par (i.e. blurry, distorted brightness values, cloud cover, condensation etc.). Following initial sweep, 336 images were ingested into *Agisoft Photoscan Pro* (version 10.2.2), for the purpose of aligning overlapping images using the GCP reference data, followed by feature extraction from each individual image, then tie point assembly and lastly for dense point cloud production. The analysis report from the photogrammetric software approximated a PC resolution of 0.1 meters, derived from 17,507 tie points. The resulting raw PC contained 16,737,370 points yielding a point density of approximately 16.7 points/ m^2. Lastly, due to the size of the raw dense

PC it was parsed into smaller tiles and exported as ASCII text files referenced to the WGS84 datum.

4.3.2.2 Airborne LiDAR

The same PC processing approach applied in chapter 2 was utilized for this chapter and consisted of clipping the parsed tile corresponding to the CALM grid that contained all laser returns. The resulting PC contained 14,571,378 points, giving a mean point density of approximately 14.57 points/m^2 for the CALM study area.

4.4 DATA ANALYSIS

ArcMap (version 10.2.2) was utilized to perform the majority of post-processing steps such as clipping data to the study area boundary, merging all scans, projecting data, and performing geostatistical analysis on and surface interpolation of the data. Each method collected data referenced to different horizontal and vertical datums, therefore all datasets were transformed to the same horizontal and vertical (NAD 83, UTM zone 4) datum in order to establish a similar baseline for all datasets. Thus, the vertical datum for the A-LiDAR dataset was converted from NAVD88 to NAD83 using the *National Oceanic and Atmospheric Administration's (NOAA) Vertical Datum Transformation* program (version 3.4, http://vdatum.noaa.gov). *Trimble Business Center* (version 2.6) was used to process all DGPS ground survey data (i.e. GCPs).

As mentioned above, field data collection, processing and analysis methods used for this study mimic those used in chapters 2 and 3, which evaluated the effectiveness of KAP for the derivation of DEMs at the Utqiaġvik BE DEM study site and the cross-platform inter-comparison of vegetation phenology indices at the Utqiaġvik and Atqasuk MISP transects respectively. All results presented here pertain to those of the CALM grid plots from both Utqiaġvik and Atqasuk and the cross-site analysis between the MISP and CALM phenology data at each location. Results from the Utqiaġvik BE DEM site presented in Chapter 2 are also compared to the results generated below for the Utqiaġvik CALM grid DEM.

For the phenology study, all green index values from each plot derived from all RGB and spectral platforms were averaged by week of year (WOY) and matched to corresponding vegetation classes generated from the classification described in Section 4.3.1.1 above. The Bonferroni correction was utilized to calculate an appropriate alpha value for each multivariate

correlations and results were filtered to the appropriate significance level in order to reduce the possibility of type 1 errors from multiple comparisons (*Cabin et al.*, 2000). Pearson's correlations were calculated through *SAS JMP version 4.0.4* and *RStudio version 1.0.136* using the *cor*.test() function between all CALM RGB and NDVI indices and for inter-comparison of all data and vegetation classes and are summarized in Table 4.3 and Table 4.4. Furthermore, associations were tested between the ground-based surface parameters for all data (2011-2015) (Table 4.7) at both sites. In order to explore these trends further, multiple linear regression (MLR) was applied in an attempt to identify which ground-based measurements may influence changes in seasonal and inter-annual greenness. All data were plotted as a time series and fit with a smooth loess curve, however data gaps did occur and in those instances trends were fit linearly to facilitate visualization (Figures 4.5- 4.10). Correlations between MISP and CALM plots were explored for all years of data for Utqiaġvik and Atqasuk locations separately (section 4.5.7). Please refer to chapter 2 for a more detailed description on PC analysis, DEM interpolation and DEM analysis methodologies applied to the CALM grid.

4.5 RESULTS

4.5.1 Timing of seasonal green-up

Seasonal and peak greening signals were visually detectible from the PLIs (Figures 4.3 and 4.4), each displaying different degrees of clarity. Early season plot images taken around day 164 reveal some greenness for the dry shrub and dry moist shrub/graminoid veg classes within the Utqiaġvik CALM grid plots, while very little to no green vegetation is seen for the other three classes. This signal is not as obvious from the KAP and Pheno-cams images over the MISP transect around the same sampling date. Day 176 typically showed a slight increase in greening within all plots that occurred around the same time surface water coverage across all vegetation classes diminished at the Utqiaġvik MISP plots. A large increase in greening occurs around day 189 across all classes within the Utqiaġvik CALM grid plots and continually increases until day 211. Green-up is seen to occur earlier (day 172) across all vegetation classes for the Atqasuk CALM grid plots and gradually continues through day 214. This was also observed from the KAP and Pheno-cam images of the MISP transects across all classes at both Utqiaġvik and Atqasuk. Senescence of dry/moist vegetation classes is seen to occur between day 197 and 211, while moist and wet classes seem to continue increasing in greenness as seen from the Utqiaġvik plot images. In Atqasuk,

initiation of senescence was delayed until between day 214 and 228, which is later in the growing season than was observed for Utqiaġvik and can also be observed from the KAP and Pheno-cam time series imagery over the MISP transects. Utqiaġvik CALM plot images displayed a more distinct change in greening over classes containing higher soil moisture content. While in Atqasuk, the CALM plots characterized as moist and moist shrub seemed to show more prominent changes in greening than those containing drier or too wet soil moistures. These same trends were also observed across the wet classes for both Utqiaġvik and Atqasuk MISP transects.

4.5.2 CALM grid seasonal greening patterns

Analysis of PLIs of the CALM plots seemed to display similar seasonal trends in greening changes (Figure 4.5a - 4.5b and 4.6a – 4.6b), as visually observed and described in section 4.5.1 above. Similar to the approach taken for the MISP correlations (chapter 3), a large number of indices were excluded from further analysis because of the weak and non-significant correlations that resulted, thus the majority of analysis focused on the GEI, %G, and nNDVI RGB-derived indices and NDVI, MNDVI, MSR, Green spectrometer-derived indices which resulted with the strongest correlations across most vegetation classes. In some cases the TEST and a* indices derived from the RGB cameras as well as SIPI and OSAVI from the spectrometer were also included in further analysis as they resulted with strong correlations with NDVI across the CALM grid vegetation classes unlike those within the MISP transect. The RGB green indices GEI, %G, nNDVI and spectral NDVI indices seemed to capture stronger greening trends for the moist gram, seasonally flooded and wet gram vegetation classes across all years compared to classes with lower soil moisture content (e.g. dry shrub and dry/moist shrub/gram) at the Utqiaġvik CALM plots. This was also observed from the KAP and Pheno-cam images across the MISP transects in Utqiaġvik and Atqasuk. The other RGB-derived indices that correlated well with spectral NDVI were a* and TEST however, these displayed an inverse relationship to NDVI. During the 2013 growing season the true-color indices GEI and %G correlated well with spectral NDVI in capturing high productivity for all vegetation classes. The moist gram class seemed to have the highest peak greenness while the dry/moist shrub/gram class showed lower values. The wet gram and seasonally flooded classes in Utqiaġvik showed the highest peak greenness values throughout most of the 2014 growing season as displayed by the GEI, %G and NDVI indices, while the dry plant communities showed little variability in greenness between years. Both methods captured a sudden

increase in greening around week 30 for the wet gram class. All other classes showed a stable or slight decrease in the trajectory of seasonal greening for the 2014 sampling effort. In 2015 trends showed a sudden increase in greening between week 25 and 26 as seen from the GEI and %G indices. NDVI data for this year was not collected due to hardware malfunction. Peak season seems to occur around week 27 for most vegetation classes for most years of data collection. The dry/moist shrub/gram class displayed a stable decline in greening following peak season. Similar seasonal and inter-annual results were seen from the RGB and spectral greening trends in Atqasuk where the moist and moist shrub vegetation classes exhibited the highest seasonal greening values, the aquatic class showed very low values compared to the other classes, and the dry plant communities showed more variability in seasonal and inter-annual greening and in some cases higher values compared to plant similar communities in Utqiaġvik. It is important to note that these same trends were also observed from the RGB images across the MISP transect in Atqasuk for all years. During the 2012 growing season greening observed from the PLI and spectrometer showed peak greening to occur between week 30 and 31 for most vegetation classes which correlated well with findings from the MISP transects. The dry, moist, and moist shrub classes displayed similar seasonal trends as seen from GEI, %G and NDVI. Similar observations were made during the 2013 season where moist, moist shrub and wet classes had the highest variability in greenness relative to the drier communities. A drastic increase in greening occurred early in the season for most classes and continued until around week 27 where it leveled off with a slight increase until week 30 where it stabilized. The 2014 growing season was similar to the previous where moist classes greened quicker and more intensively compared to vegetation classes with a lower soil moisture.

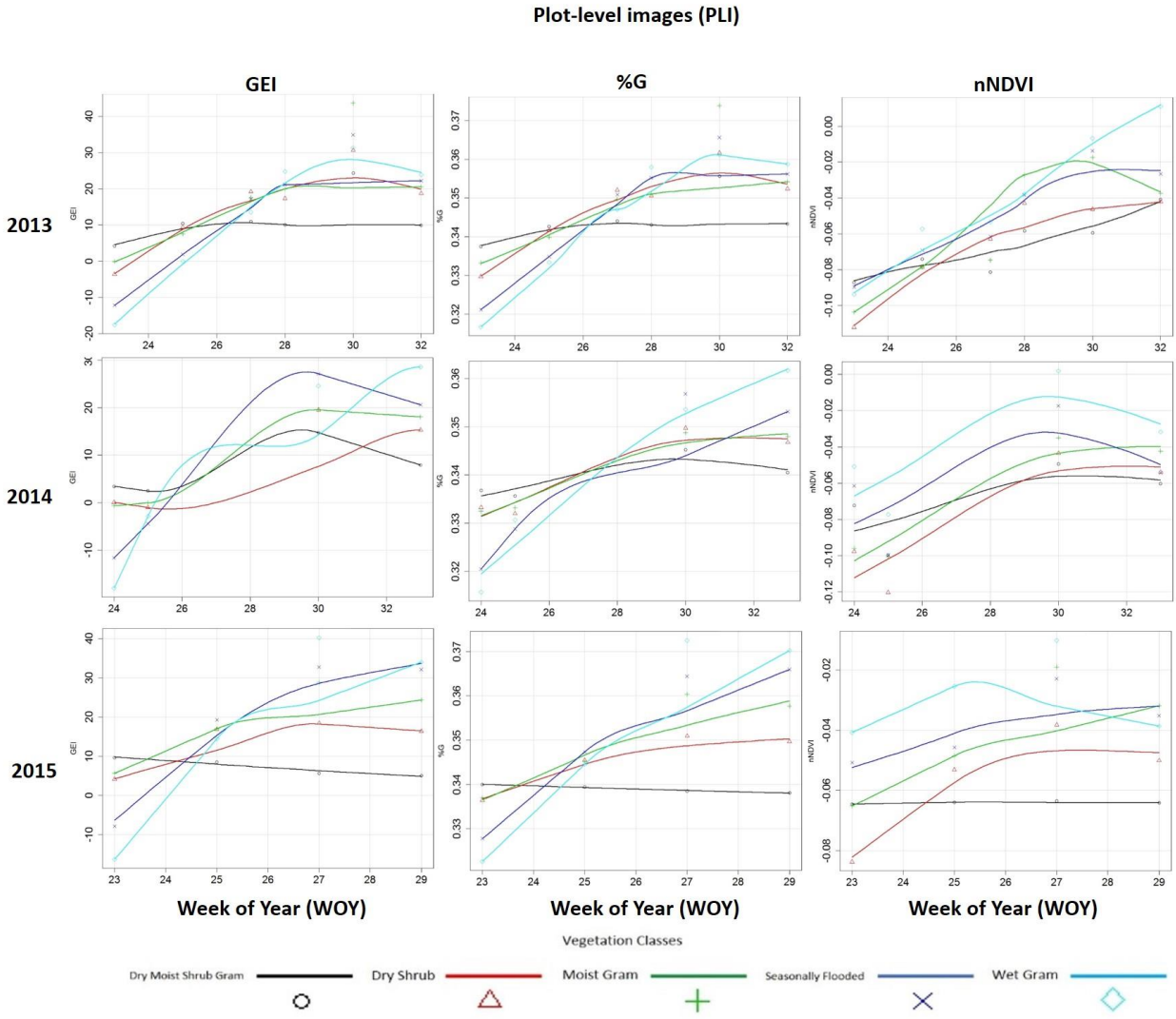

Figure 4.6a: Utqiaġvik CALM seasonal and inter-annual greening trends of all studied vegetation classes recorded from the plot-level RGB images using the GEI, %G and nNDVI indices during 2010-2015 summers. Plots were fit with a smooth loess curve and the x-axis on all plots represents WOY (23-33).

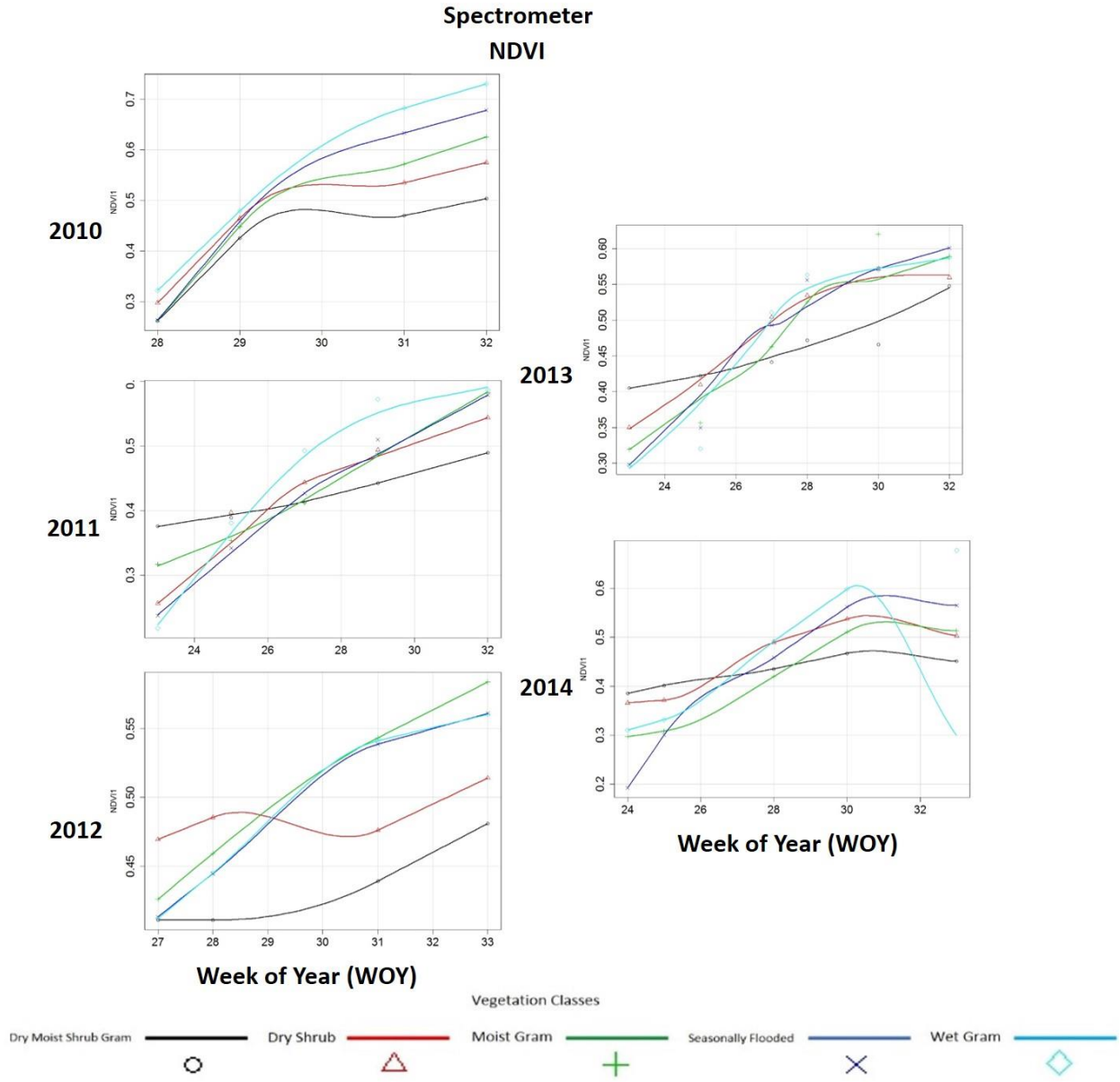

Figure 4.6b: Utqiaġvik CALM seasonal and inter-annual greening trends of all studied vegetation classes recorded from the ground-based spectrometer using the NDVI index during 2010-2015 summers. Plots were fit with a smooth loess curve and the x-axis on all plots represents WOY (23-33).

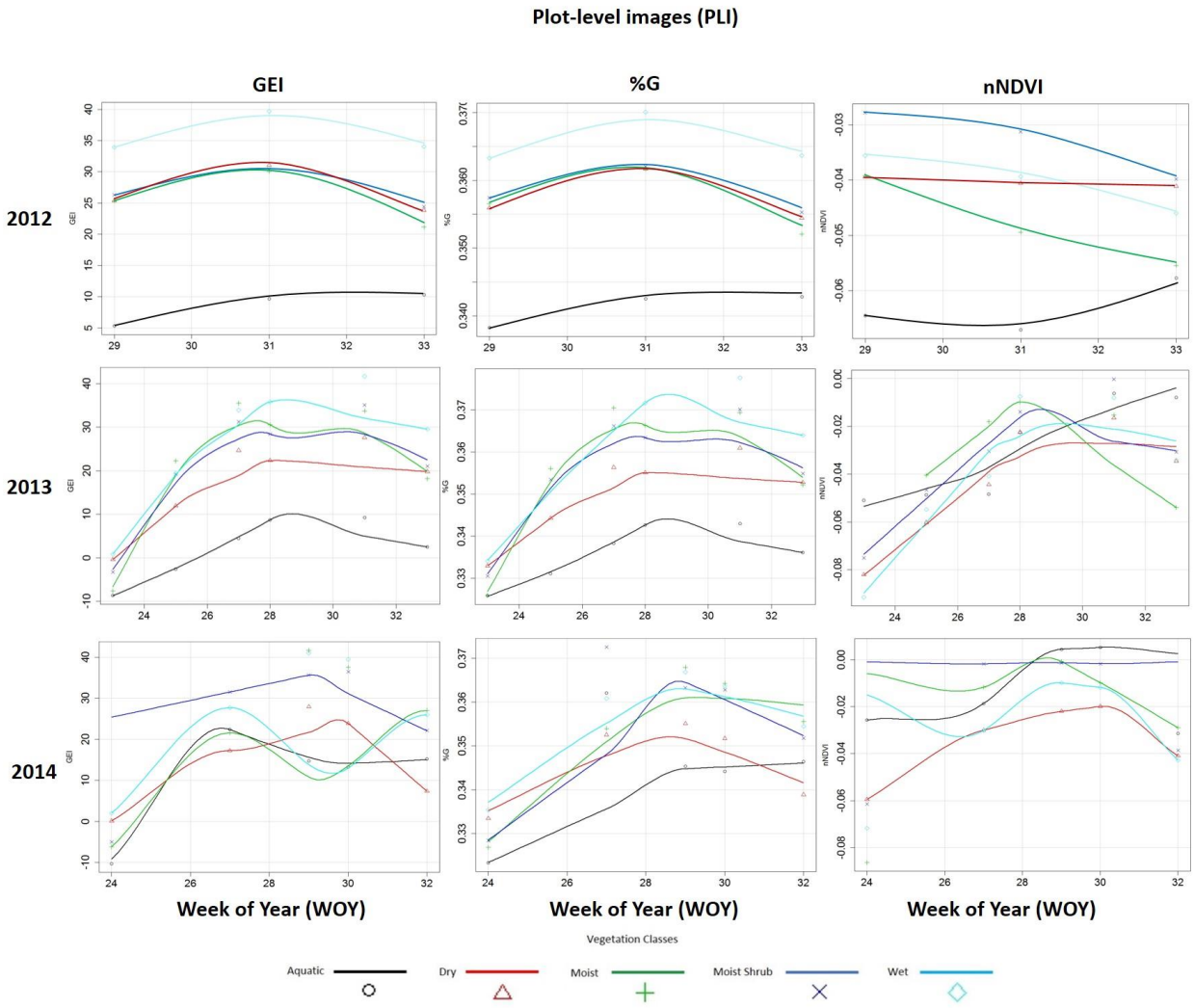

Figure 4.7a: Atqasuk CALM seasonal and inter-annual greening trends of all studied vegetation classes recorded from the plot-level RGB images using the GEI, %G and nNDVI indices during 2010-2015 summers. Plots were fit with a smooth loess curve and the x-axis on all plots represents WOY (23-33).

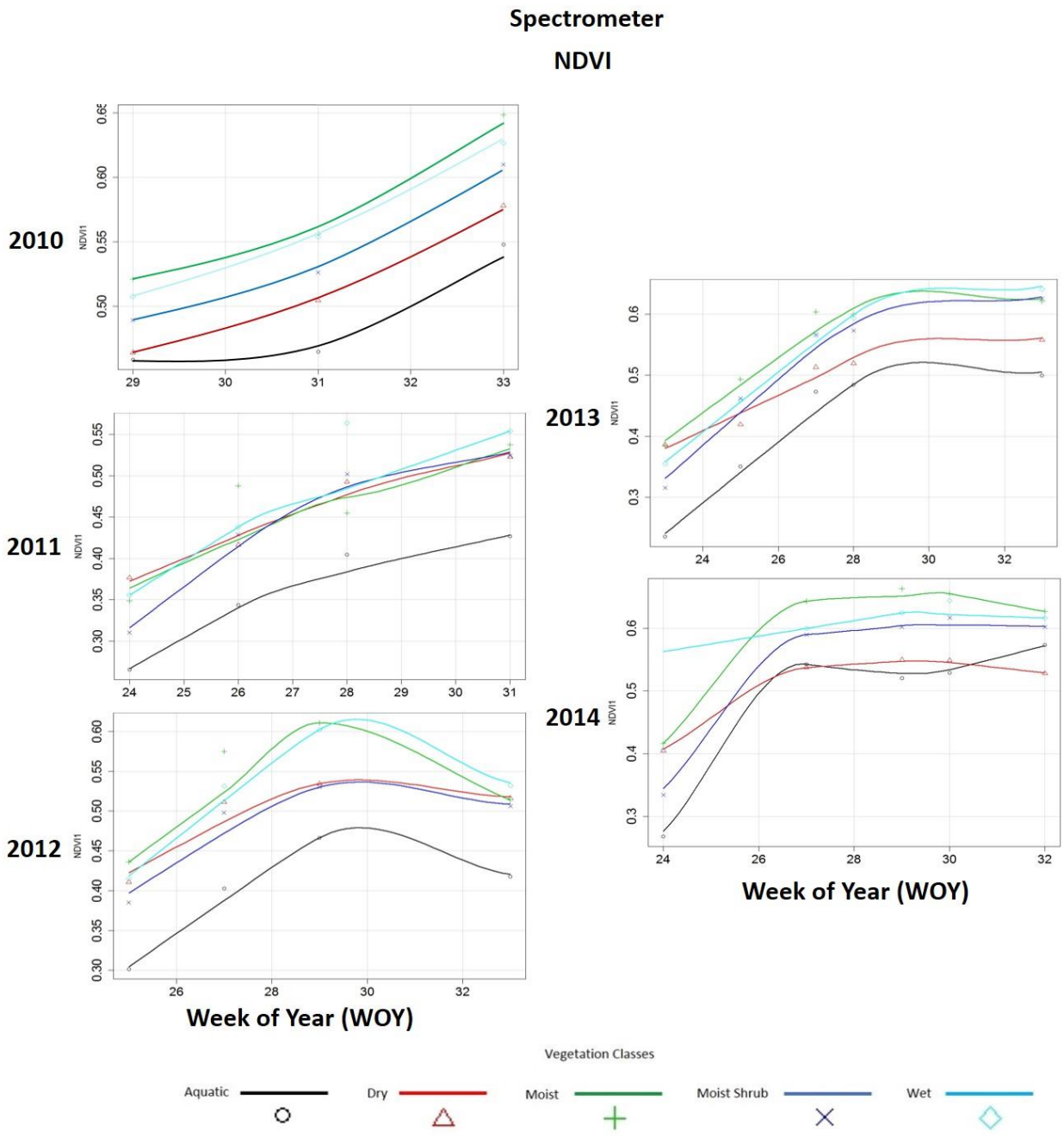

Figure 4.7b: Atqasuk CALM seasonal and inter-annual greening trends of all studied vegetation classes recorded from the ground-based spectrometer using the NDVI index during 2010-2015 summers. Plots were fit with a smooth loess curve and the x-axis on all plots represents WOY (23-33).

Five year means of each explored index were calculated using weekly values and are displayed in figures 4.7a – 4.7b for Utqiaġvik and 4.8a – 4.8b for Atqasuk. All indices seemed to capture similar seasonal mean greening trends over the course of 5 years as wetter vegetation classes (e.g. moist gram, seasonally flooded and wet gram for Utqiaġvik and moist, moist shrub and wet for Atqasuk) resulted with higher values than their drier counter-part classes (e.g. dry/moist shrub/gram and dry shrub for Utqiaġvik and the dry and aquatic classes in Atqasuk). Additionally, those more productive and wetter classes display a more distinct end of season signal as greening values drop versus the dry classes, where a very subtle signal or sometimes leveling-off occurs with little change. In order to reduce multi-collinearity from the large number of correlations being examined, mean Pearson's correlations were calculated between RGB-derived GEI, %G and nNDVI and ground-based NDVI across all vegetation classes as a whole as well as by vegetation class within the CALM plots for both Utqiaġvik and Atqasuk. In Utqiaġvik across all classes, GEI correlated significantly strong with NDVI ($r= 0.91$, $p<0.0001$) while %G also resulted with significantly strong correlations with NDVI ($r= 0.91$, $p<0.0001$). Similar but slightly weaker results were seen in Atqasuk (GEI: $r= 0.87$, $p<0.0001$; %G: $r= 0.85$, $p<0.0001$) across all vegetation classes. When averages were taken from all resulting correlations at the vegetation class level, GEI resulted with stronger correlations with NDVI in both Utqiaġvik and Atqasuk ($r= 0.94$, $p<0.0001$; and $r= 0.87$, $p<0.0001$) respectively, than %G ($r= 0.93$, $p<0.0001$; and $r= 0.85$, $p<0.0001$).

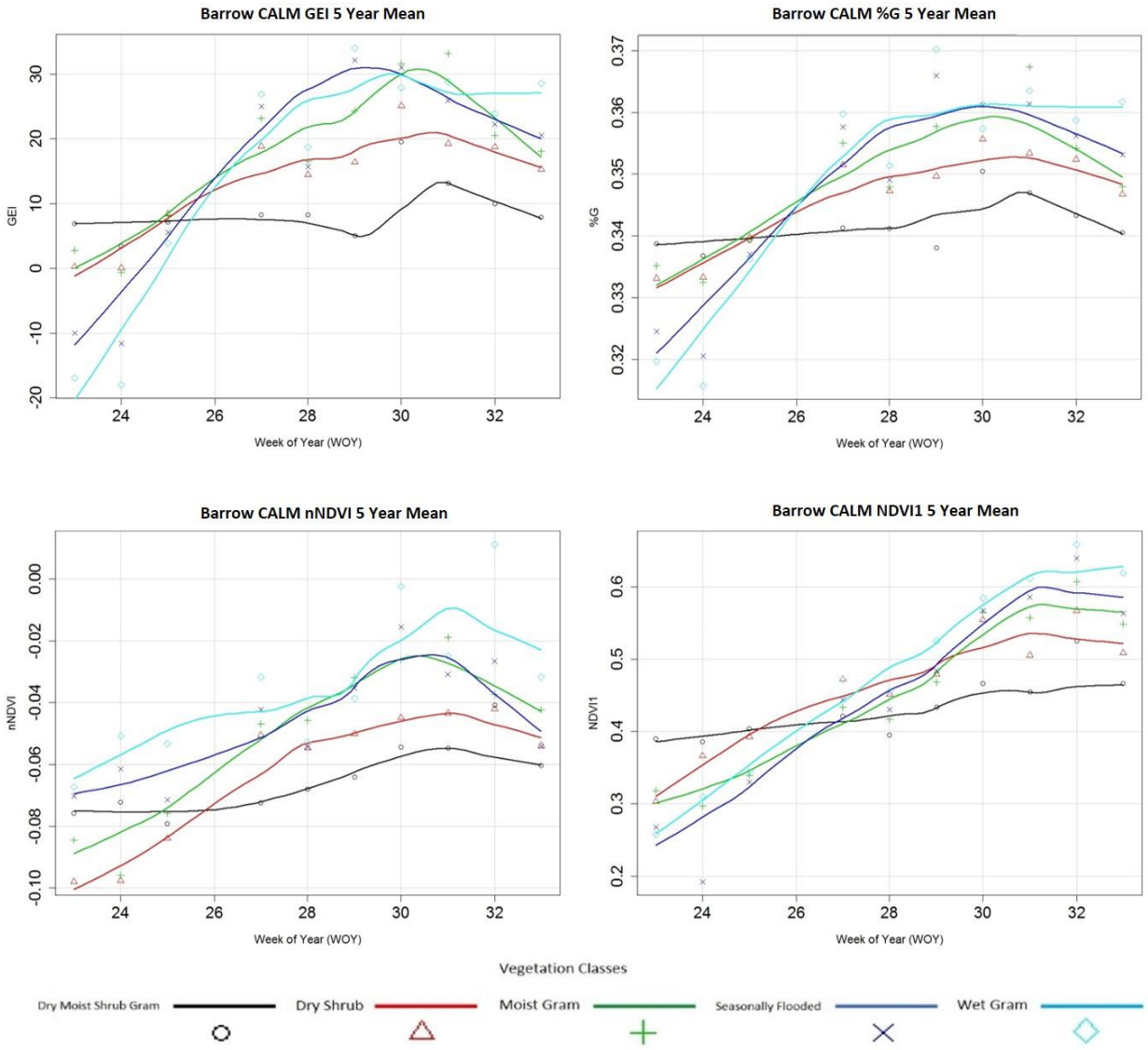

Figure 4.8a: Utqiaġvik CALM 5 year seasonal means of RGB-derived indices (GEI, %G and nNDVI) and spectrometer-derived NDVI for each vegetation class. Plots were fit with a smooth loess curve and the x-axis on all plots represents WOY (23-33).

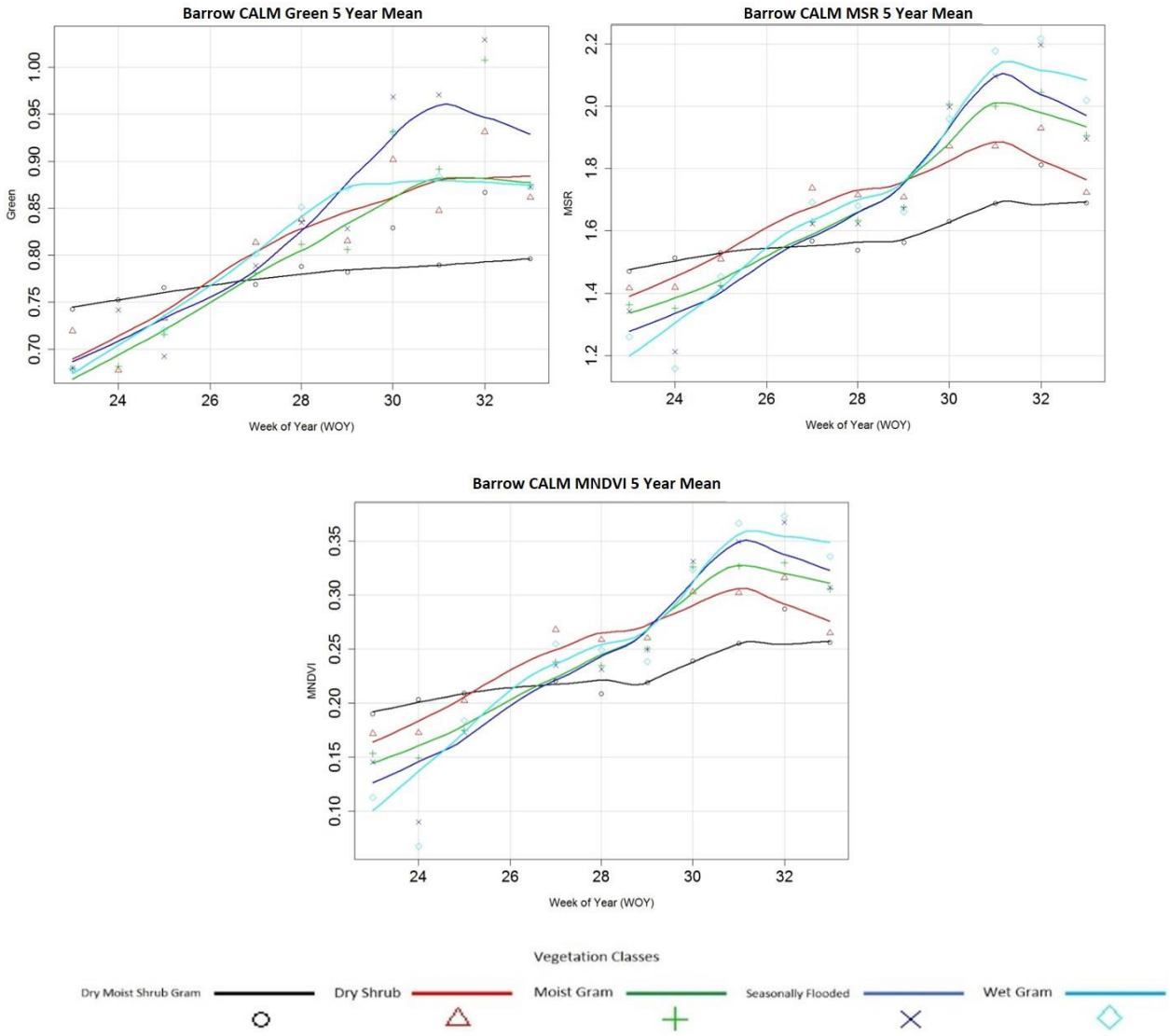

Figure 4.8b: Utqiaġvik CALM 5 year seasonal means of spectrometer-derived indices (Green, MNDVI and MSR) for each vegetation class. Plots were fit with a smooth loess curve and the x-axis on all plots represents WOY (23-33).

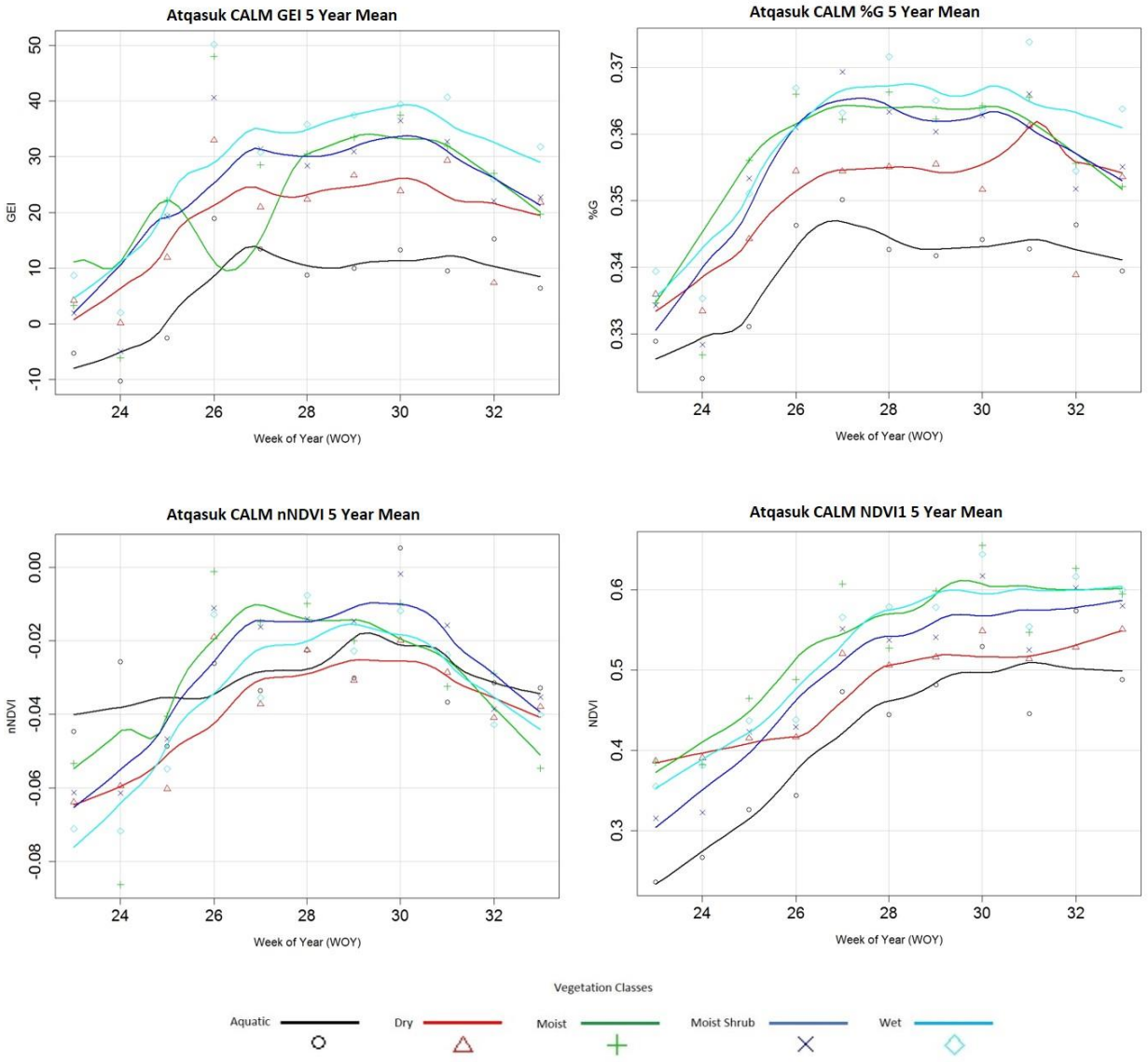

Figure 4.9a: Atqasuk CALM 5 year seasonal means of RGB-derived indices (GEI, %G and nNDVI) and spectrometer-derived NDVI for each vegetation class. Plots were fit with a smooth loess curve and the x-axis on all plots represents WOY (23-33).

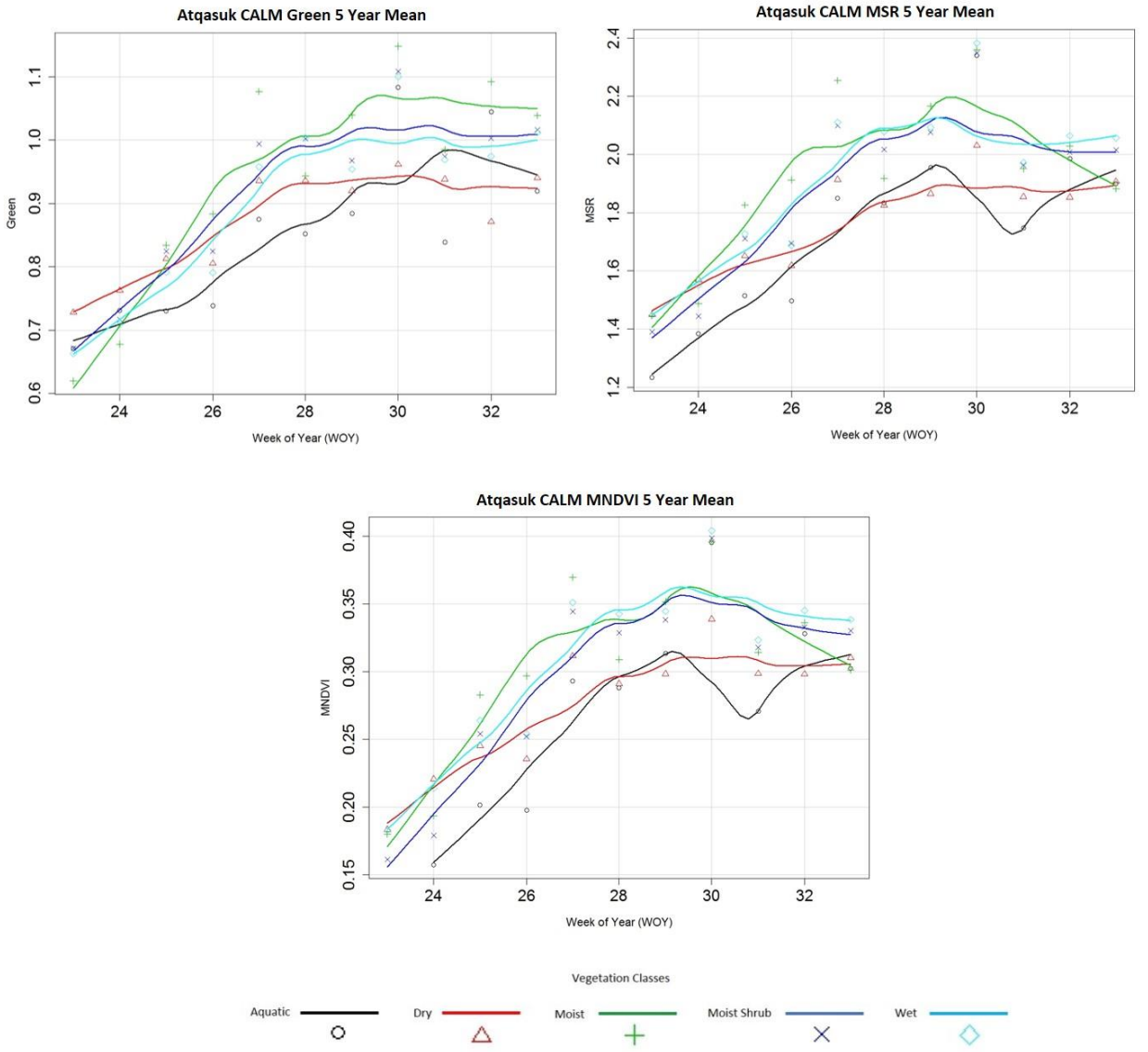

Figure 4.9b: Atqasuk CALM 5 year seasonal means of spectrometer-derived indices (Green, MNDVI and MSR) for each vegetation class. Plots were fit with a smooth loess curve and the x-axis on all plots represents WOY (23-33).

4.5.3 Associations between CALM grid RGB-derived indices and NDVI

The GEI and %G indices were able to detect subtle seasonal changes in greening throughout all years as seen from Figures 4.5 and 4.6 using the plot level camera approach. These correlated well with NDVI across all vegetation classes combined in Utqiaġvik (GEI r= 0.91, p< 0.0001; %G r= 0.91, p< 0.0001; nNDVI r= 0.79, p< 0.0001) and also for Atqasuk (GEI r= 0.87, p< 0.0001; %G r= 0.85, p< 0.0001; nNDVI r= 0.63, p< 0.0001). Furthermore, several of the

additional spectrometer-derived vegetation indices also correlated strongly with spectral NDVI across all vegetation classes, most notably the Green1 (r= 0.91, p< 0.0001), MNDVI (r= 0.96, p< 0.0001), MSR (r= 0.95, p< 0.0001), OSAVI (r=0.79, p< 0.0001) and SIPI (r=0.93, p< 0.0001) for the Utqiaġvik CALM plots. The same indices correlated well with NDVI for the Atqasuk CALM plots for all vegetation classes, especially Green1 (r=0.92, p< 0.0001), MNDVI (r= 0.92, p< 0.0001), MSR (r= 0.91, p< 0.0001), OSAVI (r= 0.82, p< 0.0001), and SIPI (r= 0.87, p< 0.0001) (Table 4.3).

Table 4.3: Pearson's correlation results (critical p-values adjusted using the Bonferroni correction) between RGB and spectrometer-derived indices and NDVI specifically, for both the Utqiaġvik and Atqasuk CALM plots across all vegetation classes and data across all years.

Location	Platform	Index	r	p
Barrow	RGB	%G	0.91	<0.0001
		GEI	0.91	<0.0001
		a*	-0.87	<0.0001
		nNDVI	0.79	<0.0001
		TEST	-0.85	<0.0001
	UNISPEC	CRI1	0.65	<0.0001
		GITELSON5	0.45	<0.0001
		GREEN1	0.91	<0.0001
		MNDVI	0.96	<0.0001
		MSR	0.95	<0.0001
		OSAVI	0.79	<0.0001
		PRI2	-0.61	<0.0001
		SIPI	0.93	<0.0001
Atqasuk	RGB	%G	0.85	<0.0001
		GEI	0.87	<0.0001
		a*	-0.81	<0.0001
		nNDVI	0.63	<0.0001
		TEST	-0.77	<0.0001
	UNISPEC	CRI1	0.70	<0.0001
		GITELSON5	0.44	<0.0001
		GREEN1	0.92	<0.0001
		MNDVI	0.92	<0.0001
		MSR	0.91	<0.0001
		OSAVI	0.82	<0.0001
		PRI2	-0.86	<0.0001
		SIPI	0.87	<0.0001

Similar to the results from the MISP transects at both locations, GEI resulted with strong correlations with NDVI for specific vegetation classes as summarized in Table 4.4 below. Strong correlations between the RGB and spectral NDVI indices in Utqiaġvik resulted from classes containing higher soil moisture such as seasonally flooded %G with r= 0.96, p< 0.0001 and GEI with 0.95, p< 0.0001 as well as for the wet gram class %G with 0.93, p< 0.0001 and GEI with 0.93, p< 0.0001. Soil moisture was also related to the strength of correlations in the Atqasuk CALM grid plots, where strong associations were observed for wetter plots (i.e. moist shrub) such as with GEI and NDVI (r=0.90, p< 0.0001), and %G (r= 0.86, p< 0.0001). GEI at the dry CALM plots resulted in an r value of 0.81 and p< 0.0001 while %G did not have a statistically significant correlation with NDVI. These results were also apparent across the Utqiaġvik and Atqasuk MISP transects where soil moisture seemed to play a key role in vegetation productivity based on greening trends observed from all sensors using the RGB-derived indices.

Also summarized in Table 4.4 are the associations between all spectral indices and NDVI for each vegetation class. At the Utqiaġvik CALM plots, the moist gram class showed the strongest correlations with CRI1 with an r= 0.88, p< 0.0001, Green1 with an r= 0.96, p< 0.0001, MNDVI with an r= 0.98, p< 0.0001, and MSR with an r= 0.98, p< 0.0001. Dry shrub tundra showed the lowest correlations of all vegetation classes but were still significant with CRI1 resulting with an r= 0.82, p< 0.0001, Green1 with an r= 0.87, p< 0.0001, MNDVI with an r= 0.94, p< 0.0001, and MSR with a r= 0.93, p< 0.0001. At the CALM plots in Atqasuk, strong correlations were also observed between most spectral indices and NDVI when analyses were broken down by vegetation class. Correlations were always stronger for classes with higher soil moisture including the moist shrub class CRI1 with r= 0.90, p< 0.0001, Green1 with r= 0.97, p< 0.0001, MNDVI with r= 0.96, p< 0.0001, and MSR with r= 0.94, p< 0.0001.

Table 4.4: Pearson's correlation results (critical p-values adjusted using the Bonferroni correction) between all indices and NDVI for both the Utqiaġvik and Atqasuk CALM plots by vegetation classes.

Location	Veg Class	Platform	Index	r	p
Barrow	DMSGRAM	UNISPEC	CRI1	0.87	<0.0001
			GITELSON5	0.81	<0.0001
			GREEN1	0.93	<0.0001
			MNDVI	0.94	<0.0001
			MSR	0.92	<0.0001
	DRY SHRUB	RGB	%G	0.93	<0.0001
			GEI	0.94	<0.0001
		UNISPEC	CRI1	0.82	<0.0001
			GITELSON5	0.78	<0.0001
			GREEN1	0.87	<0.0001
			MNDVI	0.94	<0.0001
			MSR	0.93	<0.0001
	MOIST GRAM	RGB	%G	0.90	<0.0001
			GEI	0.92	<0.0001
		UNISPEC	CRI1	0.88	<0.0001
			GITELSON5	0.92	<0.0001
			GREEN1	0.96	<0.0001
			MNDVI	0.98	<0.0001
			MSR	0.98	<0.0001
	SEASONALLY FLOODED	RGB	%G	0.96	<0.0001
			GEI	0.95	<0.0001
		UNISPEC	CRI1	0.89	<0.0001
			GREEN1	0.88	<0.0001
			MNDVI	0.98	<0.0001
			MSR	0.97	<0.0001
	WET GRAM	RGB	%G	0.93	<0.0001
			GEI	0.93	<0.0001
		UNISPEC	CRI1	0.89	<0.0001
			GREEN1	0.88	<0.0001
			MNDVI	0.94	<0.0001
			MSR	0.94	<0.0001
Location	Veg Class	Platform	Index	r	P
Atqasuk	AQUATIC	RGB	%G	0.83	<0.0001
			GEI	0.89	<0.0001
		UNISPEC	CRI1	0.79	<0.0001
			GREEN1	0.86	<0.0001
			MNDV	0.90	<0.0001
			MSR	0.88	<0.0001
	DRY	RGB	GEI	0.81	<0.0001
		UNISPEC	CRI1	0.86	<0.0001
			GITELSON5	0.74	<0.0001
			GREEN1	0.91	<0.0001
			MNDV	0.92	<0.0001
			MSR	0.91	<0.0001
	MOIST	RGB	%G	0.84	<0.0001
			GEI	0.87	<0.0001
		UNISPEC	CRI1	0.83	<0.0001
			GITELSON5	0.68	<0.0001
			GREEN1	0.97	<0.0001
			MNDV	0.93	<0.0001
			MSR	0.89	<0.0001
	MOIST SHRUB	RGB	%G	0.86	<0.0001
			GEI	0.90	<0.0001
		UNISPEC	CRI1	0.90	<0.0001
			GITELSON5	0.80	<0.0001
			GREEN1	0.97	<0.0001
			MNDV	0.96	<0.0001
			MSR	0.94	<0.0001
	WET	RGB	%G	0.87	<0.0001
			GEI	0.89	<0.0001
		UNISPEC	CRI1	0.90	<0.0001
			GITELSON5	0.88	<0.0001
			GREEN1	0.97	<0.0001
			MNDV	0.96	<0.0001
			MSR	0.94	<0.0001

4.5.4 Associations among CALM grid RGB-derived indices and spectrometer-derived indices

Based on the Pearson's correlation analyses not only did the GEI and %G indices appear to correlate well with NDVI for all vegetation classes combined (Table 4.3) as well as by vegetation class individually for all years as seen in Table 4.4 above, a cross platform comparison revealed similar associations with a number of other spectral indices as seen in Table 4.5 below. In Utqiaġvik, the GEI index correlated with a number of spectral indices but most significantly with MNDVI ($r= 0.91$, $p< 0.0001$), followed by MSR ($r= 0.89$, $p< 0.0001$), and lastly with Green1 ($r= 0.88$, $p< 0.0001$). SIPI ($r= 0.85$, $p< 0.0001$) and OSAVI ($r= 0.83$, $p< 0.0001$) also had a strong correlation with GEI. The %G index appeared to yield strong correlations with the same spectral indices all yielding r vales of 0.82 or above $p<0.0001$. It is important to note that similar relationships were seen between RGB and spectral indices at the CALM grid plots and MISP plots in Utqiaġvik. Additionally, while only GEI and %G indices correlated strongly with spectral indices at the MISP plots, several other RGB indices displayed their potential links with spectral signatures for the CALM grid plots. One is the nNDVI index, which had strong associations with Green1 ($r= 0.86$, $p< 0.0001$), MSR ($r= 0.82$, $p< 0.0001$), MNDVI ($r= 0.79$, $p< 0.0001$), and SIPI ($r=0.70$, $p< 0.0001$). The a* and TEST indices also showed strong correlations but associations with most spectral indices were negative and strong. The majority of the same signals that were observed in Utqiaġvik were also observed at the Atqasuk CALM grid plots. GEI correlated strong with spectrometer-derived indices as they all resulted with $r=0.77$, $p<0.0001$ or higher as well as the %G index which resulted with $r= 0.74$, $p<0.0001$ or higher.

Table 4.5: Cross-platform Pearson's correlation results (critical p-values adjusted using the Bonferroni correction) between RGB-derived indices and spectrometer-derived indices for both the Utqiaġvik and Atqasuk CALM plots across all vegetation classes.

Location	Index	by Index	r	p
Barrow	GEI	GREEN1	0.88	<0.0001
	GEI	MNDVI	0.91	<0.0001
	GEI	MSR	0.89	<0.0001
	GEI	OSAVI	0.83	<0.0001
	GEI	PRI2	-0.74	<0.0001
	GEI	SIPI	0.85	<0.0001
	%G	GREEN1	0.88	<0.0001
	%G	MNDVI	0.91	<0.0001
	%G	MSR	0.90	<0.0001
	%G	OSAVI	0.82	<0.0001
	%G	PRI2	-0.72	<0.0001
	%G	SIPI	0.84	<0.0001
	a*	GREEN1	-0.90	<0.0001
	a*	MNDVI	-0.88	<0.0001
	a*	MSR	-0.90	<0.0001
	a*	OSAVI	-0.68	<0.0001
	a*	PRI2	0.69	<0.0001
	a*	SIPI	-0.80	<0.0001
	nNDVI	GREEN1	0.86	<0.0001
	nNDVI	MNDVI	0.79	<0.0001
	nNDVI	MSR	0.82	<0.0001
	nNDVI	PRI2	-0.62	<0.0001
	nNDVI	SIPI	0.70	<0.0001
	TEST	GREEN1	-0.89	<0.0001
	TEST	MNDVI	-0.86	<0.0001
	TEST	MSR	-0.89	<0.0001
	TEST	OSAVI	-0.63	<0.0001
	TEST	PRI2	0.64	<0.0001
	TEST	SIPI	-0.79	<0.0001
Atqasuk	GEI	GREEN1	0.77	<0.0001
	GEI	MNDVI	0.78	<0.0001
	GEI	MSR	0.77	<0.0001
	GEI	OSAVI	0.82	<0.0001
	GEI	PRI2	-0.75	<0.0001
	GEI	SIPI	0.77	<0.0001
	%G	GREEN1	0.76	<0.0001
	%G	MNDVI	0.76	<0.0001
	%G	MSR	0.75	<0.0001
	%G	OSAVI	0.78	<0.0001
	%G	PRI2	-0.70	<0.0001
	%G	SIPI	0.74	<0.0001
	a*	GREEN1	-0.89	<0.0001
	a*	MNDVI	-0.91	<0.0001
	a*	MSR	-0.89	<0.0001
	a*	OSAVI	-0.64	<0.0001
	a*	PRI2	0.61	<0.0001
	a*	SIPI	-0.54	<0.0001
	nNDVI	GREEN1	0.82	<0.0001
	nNDVI	MNDVI	0.85	<0.0001
	nNDVI	MSR	0.83	<0.0001
	TEST	GREEN1	-0.87	<0.0001
	TEST	MNDVI	-0.88	<0.0001
	TEST	MSR	-0.86	<0.0001

To further explore the relationship between CALM RGB-derived indices and spectrometer-derived indices, correlations were performed at the vegetation class level. GEI correlated strongly with spectrometer-derived indices in both Utqiaġvik and Atqasuk for most vegetation classes. As previously observed from the MISP plots, RGB and spectral indices were able to capture greening better for plots that contained high levels of soil moisture, however this was not the case for the CALM grid plots in that regardless of soil moisture content strong

correlations resulted from the cross platform analysis for all vegetation classes. For example, the RGB-derived nNDVI and spectrometer-derived OSAVI indices were the only significant correlations for the dry moist shrub gram vegetation class in Utqiaġvik, with an r= 0.83, p< 0.0001. Overall the dry shrub class displayed the most correlations in quantity, the strongest of which were between GEI and OSAVI (r= 0.93, p< 0.0001), while also resulting with strong correlations with Green, MNDVI, MSR and SIPI (all above r=0.86, p<0.0001). %G and the same previously mentioned spectrometer-derived indices also correlated strongly, all resulting with r=0.84, p<0.0001 or higher. All other vegetation classes also displayed the same correlation trends with resulting r values of 0.82, p<0.001 or higher.

At the Atqasuk CALM plots, all vegetation classes contained high numbers of correlations between platforms, for example with the aquatic vegetation class where GEI and OSAVI (r= 0.86, p<0.001) had the strongest significant correlations. The dry class had strong associations with GEI and Green1 (r= 0.87, p<0.0001), and OSAVI (r= 0.82, p<0.001), while %G only correlated with Green1 (0.89, p<0.0001). The GEI index within the moist class correlated best with MNDVI (r= 0.86, p<0.0001), followed by OSAVI (r= 0.86, p<0.0001), Green1 (r= 0.83, p<0.0001), and MSR (r= 0.81, p<0.0001). The %G index only correlated with MNDVI (r= 0.84, p<0.0001), OSAVI (r= 0.82, p<0.0001), and Green1 (r= 0.81, p<0.0001). The moist shrub class indicated the most associations between platforms including GEI and MNDVI (r= 0.93, p<0.0001), MSR (r= 0.92, p<0.0001), Green1 (r= 0.88, p<0.0001), SIPI (r= 0.88, p<0.0001), and OSAVI (r= 0.85, p<0.0001). The %G index correlated well with MNDVI (r= 0.89, p<0.0001), MSR (r= 0.88, p<0.0001), Green1 (r= 0.86, p<0.0001), and SIPI (r= 0.83, p<0.0001). Lastly, GEI across the wet class had strong correlations with Green1 (r= 0.89, p<0.0001), MNDVI (r= 0.85, p<0.0001), MSR (r= 0.83, p<0.0001), and SIPI (r= 0.83, p<0.0001), while %G correlated with Green1 (r= 0.88, p<0.0001) and MNDVI (r= 0.82, p<0.0001) only.

4.5.5 CALM grid seasonal surface characteristics

Descriptive statistics of the yearly ground-based surface measurements collected across all CALM grid plots are summarized in Table 4.6. Similar to observations on the MISP plots soil temperature was warmest in Utqiaġvik during 2013, 2014, and 2015 with maximum temperatures reaching 7.4°C, 7.6°C, and 7.3°C, and mean summer temperatures were 3.8°C, 2.9°C, and 3.4°C respectively. Soil moisture also showed similar trends to observations from the MISP plots, where

2013 and 2014 were the wettest years where soils reached 75.5% and 72.1% respectively. Based on the mean soil moisture content, 2013 was the wettest year with 50.1% followed by 2014 with 48.1%, which also matched observations from the MISP transects. Seasonal depth of thaw was monitored at each CALM plot and 2013 had the deepest thaw depth with a maximum mean depth of 55.6 cm across all sites, followed by 2015 with 48 cm.

The Atqasuk CALM plots generally displayed warmer soil temperatures, lower soil moisture content, and deeper thaw depths than for Utqiaġvik CALM plots, which is similar to observations made for MISP transects. In Atqasuk, 2013 had the highest soil temperatures with maximum values reaching 11.3°C followed by 2014 with 9°C. Soil moisture in Atqasuk was highest during 2013 with 73.76% followed by 2014 with 67.93%. According to mean seasonal soil moisture values, 2014 and 2013 were the wettest years with 43.49% and 42.52% respectively. Atqasuk thaw depths were deepest during 2014 reaching 92 cm followed by 2012 with 85.33cm. Based on seasonal mean depths, 2013 had the deepest year reaching 43.57 cm. All data were plotted as a time series and fit with a smooth loess curve to facilitate the visualization of seasonal patterns across all years and for each vegetation class for Utqiaġvik (Figures 4.9a – 4.9c) and for Atqasuk (Figures 4.10a – 4.10c). Relationships between surface measurements for all years and all vegetation classes combined (Table 4.7) and for all years and individual vegetation classes were explored further to assess the likelihood of multicollinearity prior to utilizing the data for multiple linear regression analysis. No significant correlations resulted between the ground-based measurements, which suggests the data can be utilized for multiple linear regression analysis.

Table 4.6: Summary of the annual statistics of all ground-based surface measurements made at the Utqiaġvik and Atqasuk CALM grid plots.

Site	Enviro. Parameter	Stat	2010	2011	2012	2013	2014	2015
Barrow	Soil Temperature (°C)	Min	0.44	0.54	1.56	0.46	1	0.56
		Median	2.45	3.32	2.63	4.16	2.72	3.58
		Mean	2.66	3.35	3.01	3.84	2.94	3.40
		Max	5.52	6.12	5.14	7.39	7.6	7.32
		Std. Dev.	1.62	1.74	1.09	1.83	1.72	1.37
	Soil Moisture (%)	Min	NA	4.14	20.4	21.27	14.66	NA
		Median	NA	33.05	28.76	45.16	44.77	NA
		Mean	NA	38.96	39.24	50.12	48.18	NA
		Max	NA	71.32	61.74	75.5	72.11	NA
		Std. Dev.	NA	20.89	17.50	17.11	16.01	NA
	AL Thaw Depth (cm)	Min	12.14	3.9	9.08	9.33	1.25	5.167
		Median	26.25	25.9	28	33.03	26	36.2
		Mean	26.27	24.35	26.34	31.49	22.4	32.36
		Max	43.07	46.43	46.07	55.64	44.79	48.08
		Std. Dev.	10.02	12.95	13.30	12.19	14.13	13.89
Site	Enviro. Parameter	Stat	2010	2011	2012	2013	2014	2015
Atqasuk	Soil Temperature (°C)	Min	1.6	0.66	2.15	0.11	2.18	1.68
		Median	3.83	3.8	4	6.7	3.96	4.6
		Mean	3.70	3.61	4.18	6.60	4.60	4.38
		Max	7.08	6.12	6.45	11.27	9	7.74
		Std. Dev.	1.47	1.44	1.15	2.98	1.87	1.52
	Soil Moisture (%)	Min	NA	9.48	12.83	11.27	18.13	NA
		Median	NA	39.58	25.46	39.87	40.19	NA
		Mean	NA	38.93	30.79	42.52	43.49	NA
		Max	NA	62.68	66.63	73.76	67.93	NA
		Std. Dev.	NA	15.53	14.30	15.72	13.54	NA
	AL Thaw Depth (cm)	Min	17.79	7.41	11.58	7.5	8.78	10.32
		Median	39	33.35	29.83	43.57	35.94	39.57
		Mean	40.21	35.80	34.71	42	37.96	39.1
		Max	78	84.66	85.33	81.67	92	70.33
		Std. Dev.	16.62	19.83	19.77	19.92	21.59	18.43

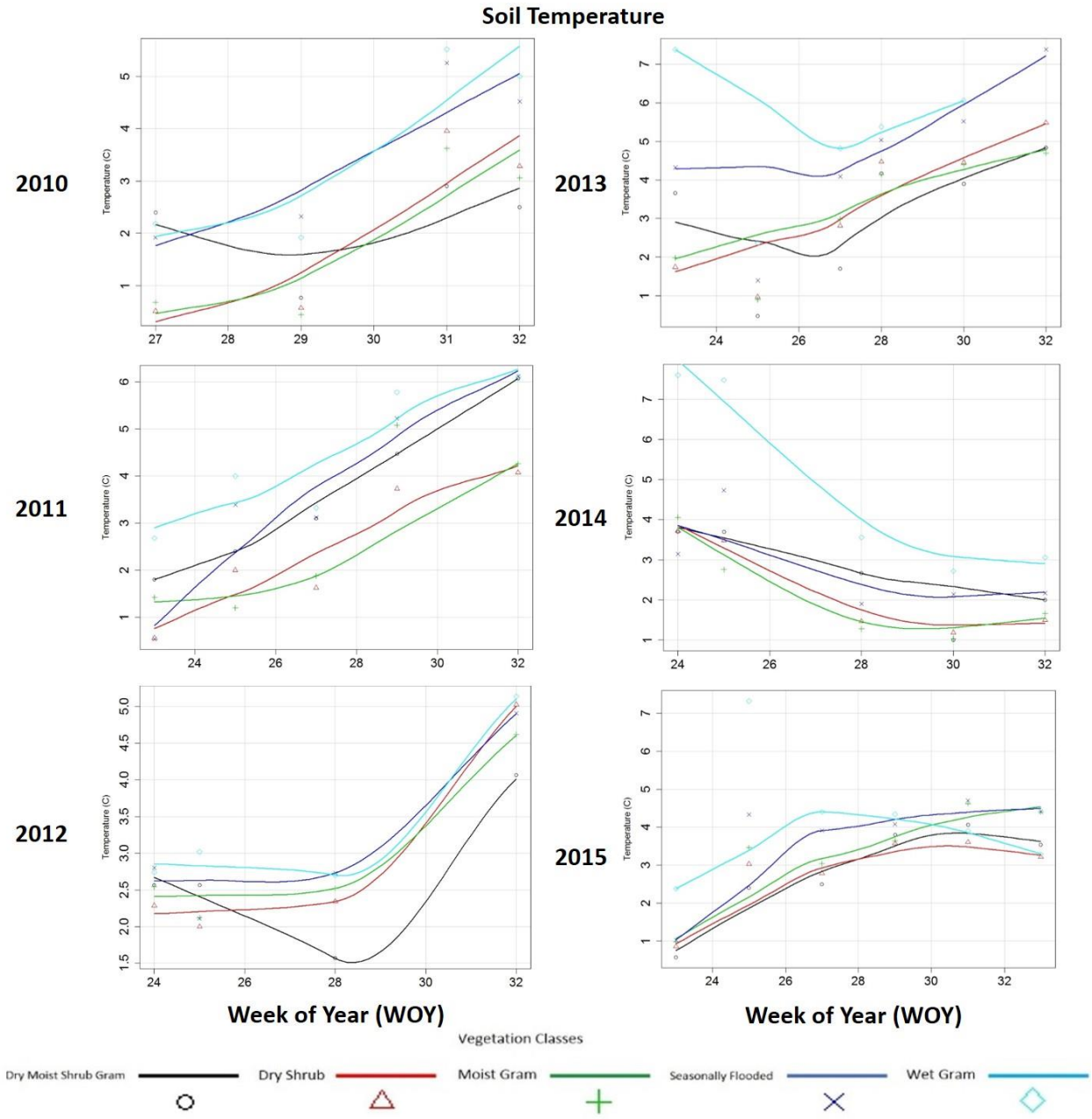

Figure 4.10a: Seasonal and inter-annual soil temperature (at ~5cm depth (°C)) averaged across each vegetation class located within the CALM plots in Utqiaġvik. Plots were fit with a smooth loess curve and the x-axis on all plots represents WOY (~23-33).

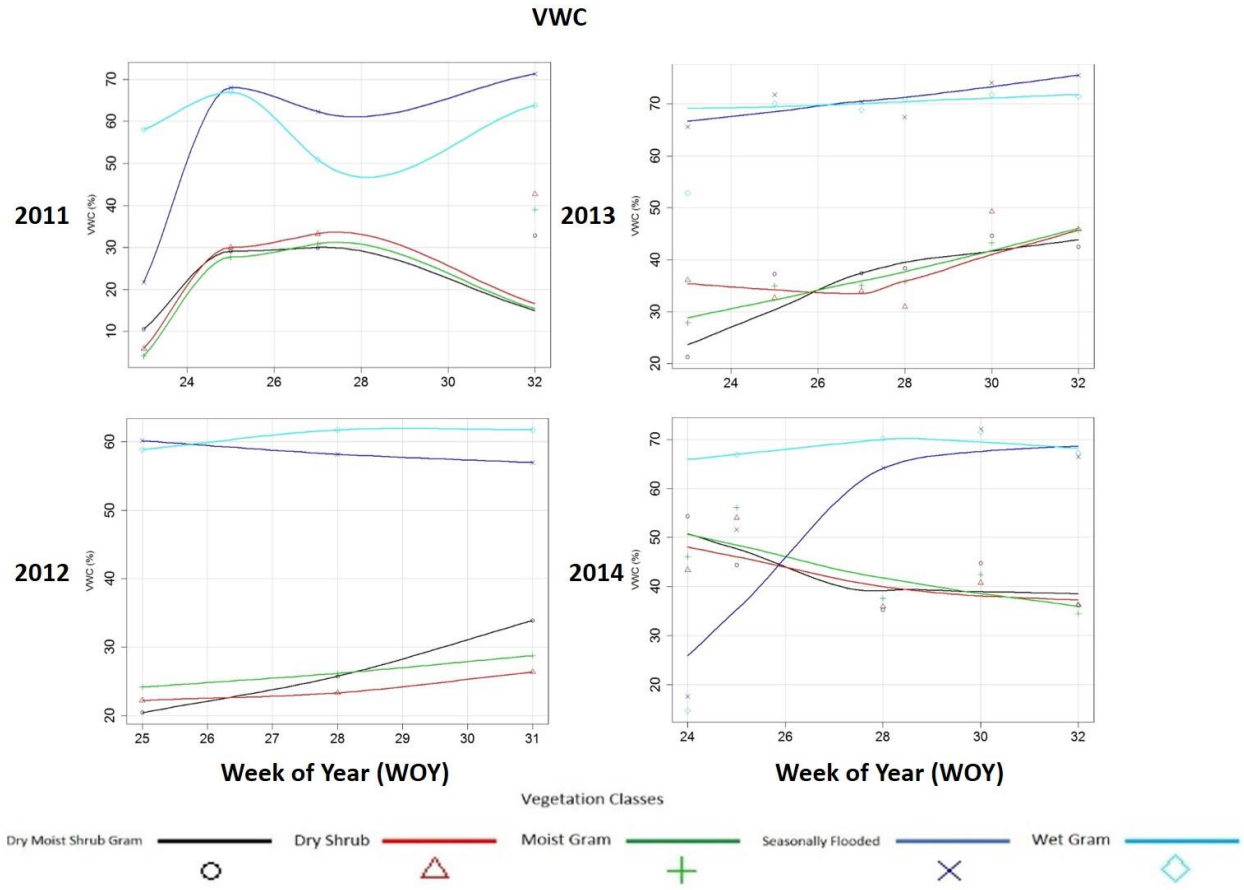

Figure 4.10b: Seasonal and inter-annual percent volumetric water content (VWC) averaged across each vegetation class located within the CALM plots in Utqiaġvik. Plots were fit with a smooth loess curve and the x-axis on all plots represents WOY (~23-33).

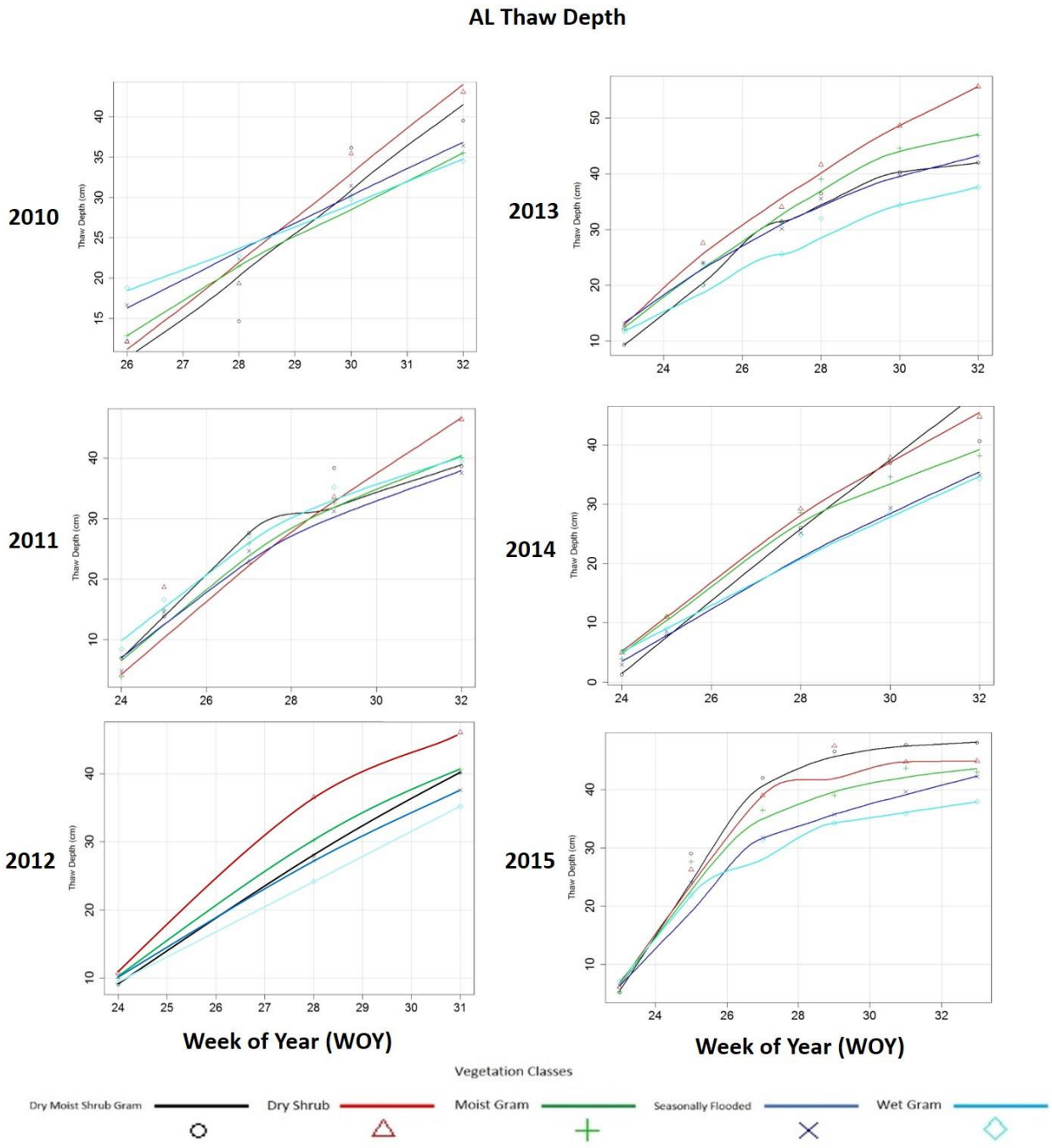

Figure 4.10c: Seasonal and inter-annual active layer thaw depth (AL (cm)) averaged across each vegetation class located within the CALM plots in Utqiaġvik. Plots were fit with a smooth loess curve and the x-axis on all plots represents WOY (~23-33).

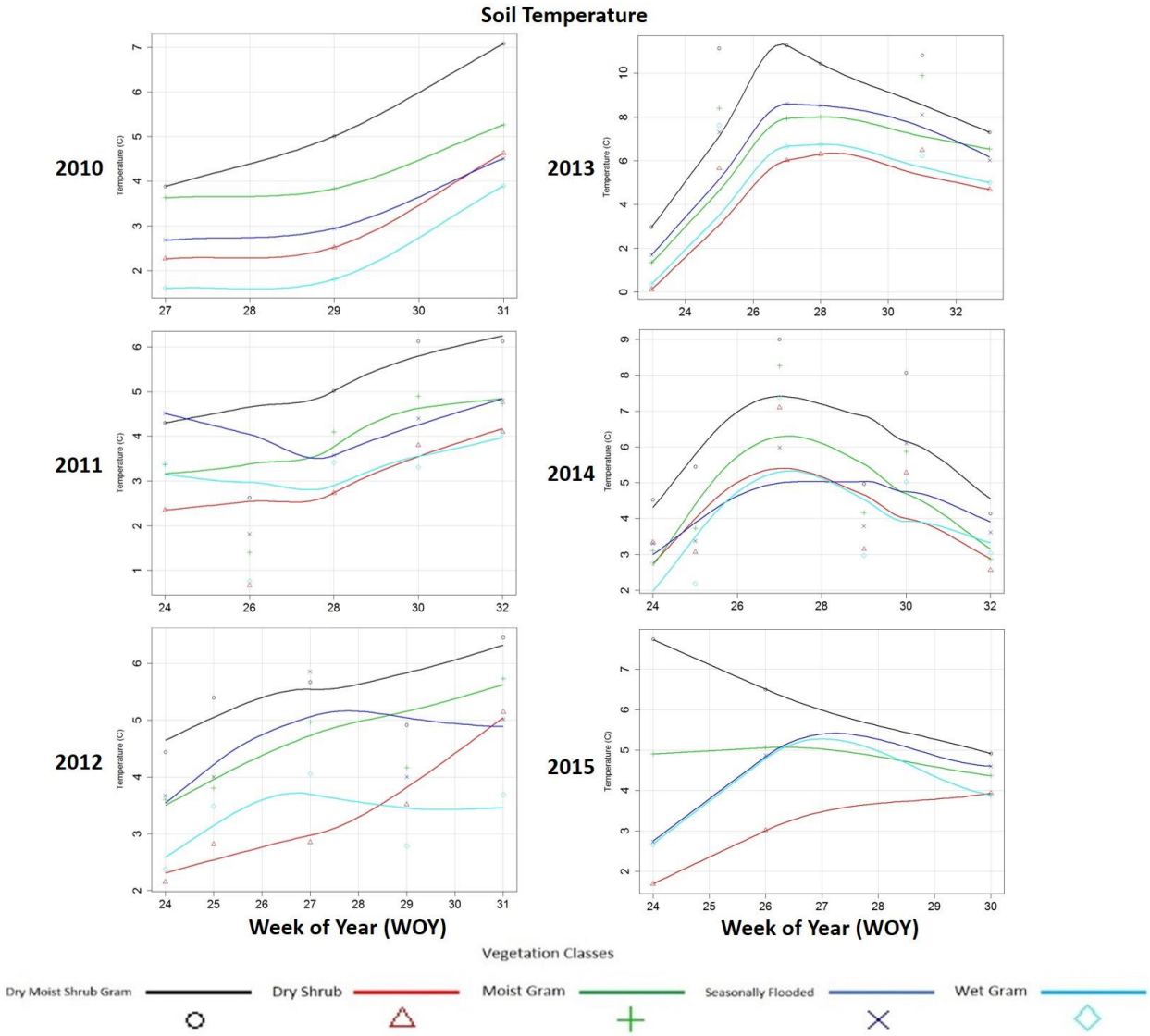

Figure 4.11a: 4.10a Seasonal and inter-annual soil temperature (at ~5cm depth (°C)) averaged across each vegetation class located within the CALM plots in Atqasuk. Plots were fit with a smooth loess curve and the x-axis on all plots represents WOY (~23-33).

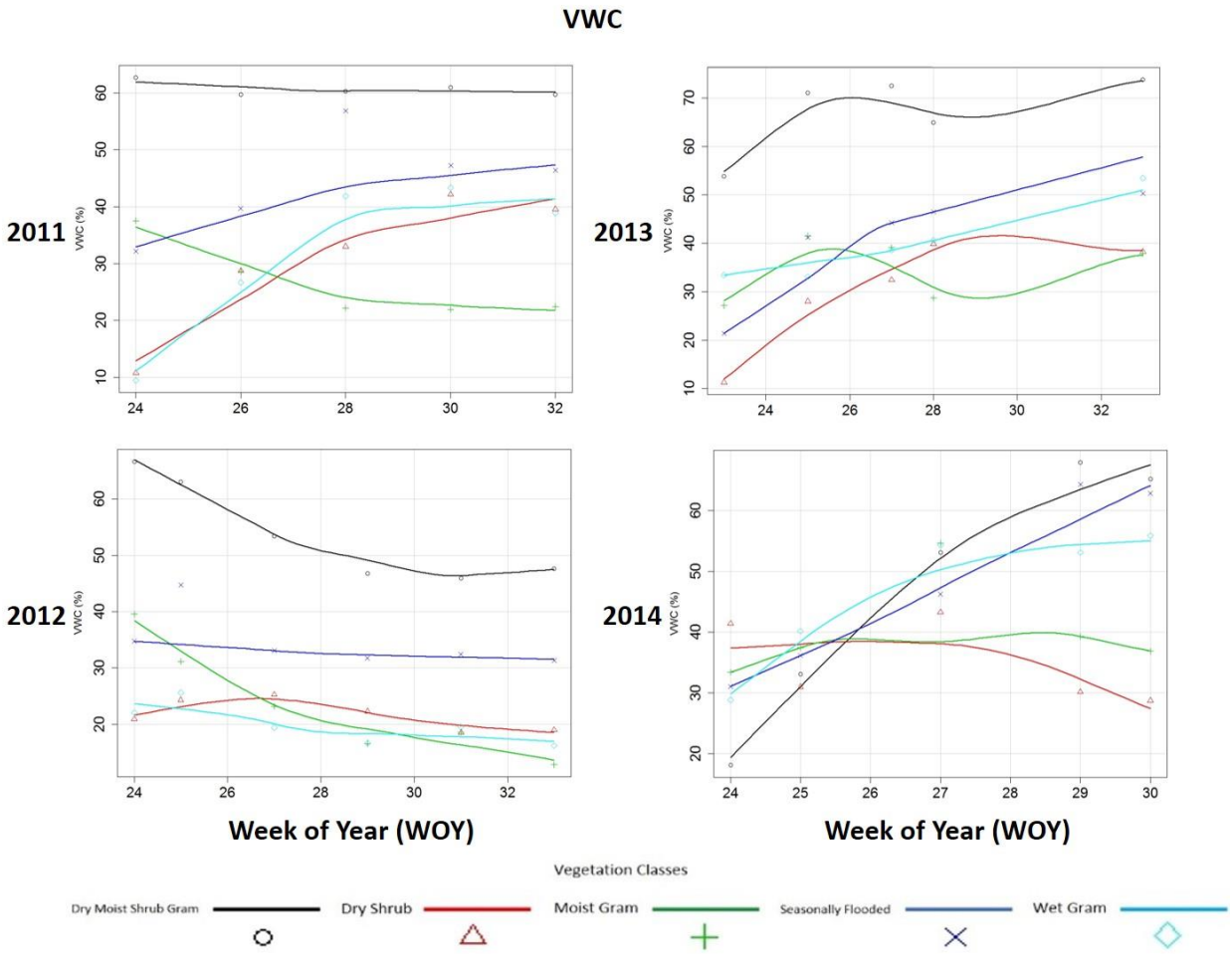

Figure 4.11b: Seasonal and inter-annual percent volumetric water content (VWC) averaged across each vegetation class located within the CALM plots in Atqasuk. Plots were fit with a smooth loess curve and the x-axis on all plots represents WOY (~23-33).

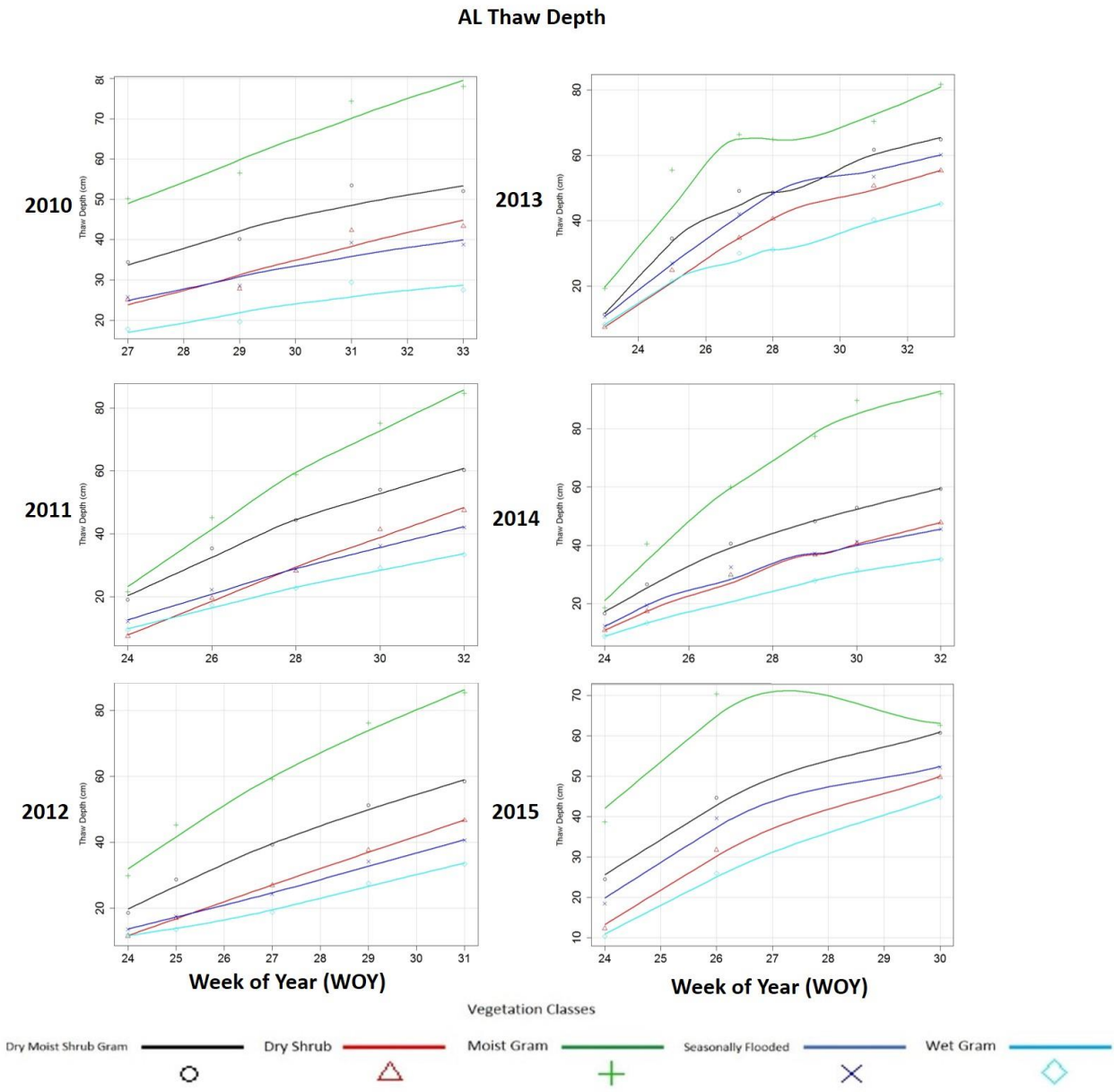

Figure 4.11c: Seasonal and inter-annual active layer thaw depth (AL (cm)) averaged across each vegetation class located within the CALM plots in Atqasuk. Plots were fit with a smooth loess curve and the x-axis on all plots represents WOY (~23-33).

Table 4.7: Statistically significant Pearson's correlation results (critical p-values adjusted using the Bonferroni correction) between all CALM grid plot ground measurements (e.g. soil temperature, VWC, and AL thaw depth) across all vegetation classes for all years of data combined and for both Utqiaġvik and Atqasuk.

Location	Index	by Index	r	p
Barrow	VWC	Soil temp	0.33	<0.001
	VWC	AL thaw depth	0.10	0.368
	Soil temp	AL thaw depth	0.22	0.0171
Atqasuk	VWC	Soil temp	0.47	<0.0001
	VWC	AL thaw depth	0.14	0.123
	Soil temp	AL thaw depth	0.47	<0.0001

4.5.6 Predicting greening from ground-based surface measurements

Based on the results acquired thus far, it can be assumed that seasonal and inter-annual phenological trends of numerous tundra vegetation types can be observed from various RGB-derived and spectrometer-derived indices. Modeling these trends has become an important task considering the tremendous impact these ecosystems can have on global systems, therefore multiple linear regression (MLR) was applied to explore how these indices are affected by tundra surface characteristics (e.g. soil, moisture, soil temperature, and active layer) and how they can be utilized to predict greening trends across multiple spatial scales. The results show that the higher the productivity of plots the better the strength of greening predictability using the ground-based measurements. For example, in Utqiaġvik regressions were strongest among ground-based measurements and spectrometer-derived indices such as seen across the majority of vegetation classes (i.e. DMSGram: Green r= 0.81, $p<0.0001$; dry shrub: Green r= 0.93, $p<0.0001$; moist gram: MSR r= 0.94, $p<0.0001$; seasonally flooded: OSAVI r= 0.87, $p<0.0001$; wet gram: OSAVI r= 0.9, $p<0.0001$), even though the RGB-derived indices also resulted with strong R^2 values. Similar regression results were observed in Atqasuk across all vegetation classes. Given these results, it can be concluded that soil temperature, VWC and AL thaw depth serve as good tools for predicting productivity of vegetation classes in both Utqiaġvik and Atqasuk, although additional ground-

based measurements such as those acquired across the MISP transects (i.e. albedo and WTD) might improve the strength of predictability.

4.5.7 Scaling: Relationships between MISP and CALM grid indices

Based on the presented results in chapter 2, it can be assumed that RGB and spectral indices have the capacity to capture phenological signals not only at the plot level but across vegetation classes spanning a wide spatial distribution. To ascertain how these data could reliably detect greening trends across the broader landscape, correlations between MISP and CALM plots were explored for all years of data and for both Utqiaġvik and Atqasuk. First we focused on correlations between sites (MISP transect and CALM grid) and among the same color spaces (e.g. RGB vs. RGB). In Utqiaġvik, correlations were strong, particularly for the moist gram class between MISP KAP %G and CALM GEI ($r= 0.87$, $p< 0.001$), and CALM %G ($r= 0.89$, $p< 0.001$). The MISP KAP a* index had strong correlations with its CALM counterpart with $r= 0.87$, $p< 0.001$. The PCAM %G index only correlated with CALM %G ($r= 0.84$, $p< 0.001$). The only other vegetation class that resulted in strong cross-site correlations in Utqiaġvik was seasonally flooded where KAP GEI and CALM GEI were strongly correlated ($r= 0.92$, $p< 0.001$) as well as with CALM %G ($r= 0.92$, $p< 0.001$). KAP a* also correlated well with CALM a* with $r= 0.95$, $p< 0.001$). The Atqasuk sites yielded a higher quantity and stronger relationships between RGB indices across all classes compared to results gained from Utqiaġvik. For example, the MISP KAP %G index had strong correlations with CALM %G ($r= 0.91$, $p< 0.001$) for the dry class, while the MISP PCAM GEI and CALM GEI ($r= 0.81$, $p< 0.001$) were close. The moist type had strong correlations among MISP KAP %G and CALM %G ($r= 0.88$, $p< 0.001$) and MISP PCAM GEI and CALM %G ($r= 0.73$, $p< 0.001$). The moist shrub had the most cross-site correlations, specifically with MISP KAP GEI and CALM GEI ($r= 0.94$, $p< 0.001$) and for MISP KAP %G and CALM %G ($r= 0.96$, $p< 0.001$). The MISP PCAM GEI came close to CALM GEI ($r= 0.93$, $p< 0.001$), and similarly so did the MISP PCAM %G and CALM %G ($r= 0.88$, $p< 0.001$). The wet vegetation class also had strong correlations between MISP KAP %G and CALM %G ($r= 0.92$, $p< 0.001$), MISP PCAM GEI and CALM GEI ($r= 0.88$, $p< 0.001$), and MISP PCAM %G and CALM %G ($r= 0.88$, $p< 0.001$).

Another strong interest of this study was to explore the associations between the same spectrometer-derived indices collected on the MISP and CALM grids for all years by vegetation class. In Utqiaġvik, all vegetation classes showed a number of strong correlations between indices

such as those with the dry/moist shrub/gram classes, where the following indices correlated well - Green1 (r=0.86, p< 0.0001), WBI (r= 0.83, p< 0.0001), MSR (r= 0.82, p< 0.0001), NDVI (r= 0.82, p< 0.0001), MNDVI (r= 0.82, p< 0.0001), and NDSWI-log (r= 0.75, p< 0.0001). The dry shrub class showed strong correlations for Green1 (r= 0.95, p< 0.0001), NDVI (r= 0.89, p< 0.0001), SIPI (r= 0.86, p< 0.0001), MNDVI, (r= 0.85, p< 0.0001), MSR (r= 0.85, p< 0.0001), NDSWI-lin (r= 0.82, p< 0.0001), CRI (r= 0.79, p< 0.0001), OSAVI (r= 0.78, p< 0.0001), and NDSWI-log (r= 0.71, p< 0.0001). All of the spectrometer-derived indices included in the analysis correlated between the moist gram MISP and CALM plots in Utqiaġvik and the strongest correlations were for NDVI (r= 0.96, p< 0.0001), MNDVI (r= 0.96, p< 0.0001), MSR (r= 0.95, p< 0.0001), OSAVI (r= 0.93, p< 0.0001), SIPI (r= 0.93, p< 0.0001), NGreen1 (r= 0.93, p< 0.0001), NDSWI-lin (r= 0.82, p< 0.0001), NDSWI-log (r= 0.81, p< 0.0001), PRI (r= 0.81, p< 0.0001), CRI (r= 0.80, p< 0.0001). The seasonally flooded vegetation class resulted in the least number of indices with strong correlations, the highest of which was for MNDVI (r= 0.97, p< 0.0001), MSR (r= 0.97, p< 0.0001), NDVI (r= 0.93, p< 0.0001), Green1 (r= 0.91, p< 0.0001), OSAVI (r= 0.85, p< 0.0001), and SIPI (r= 0.74, p< 0.0001). The wet gram class had strong correlations for OSAVI (r= 0.97, p< 0.0001), NDVI (r= 0.95, p< 0.0001), MSR (r= 0.93, p< 0.0001), MNDVI (r= 0.93, p< 0.0001), NDSWI-log (r= 0.93, p< 0.0001), Green1 (r= 0.90, p< 0.0001), SIPI (r= 0.88, p< 0.0001), NDSWI-lin (r= 0.83, p< 0.0001), and PRI (r= 0.81, p< 0.0001). In Atqasuk, all vegetation classes contained strong associations between MISP and CALM spectrometer-derived indices. The aquatic plots had the lowest number of correlations with only Green1 (r= 0.85, p< 0.0001). The dry class had strong correlations for MNDVI (r= 0.98, p< 0.0001), MSR (r= 0.97, p< 0.0001), NDVI (r= 0.96, p< 0.0001), Green1 (0.91, p< 0.0001), OSAVI (r= 0.88, p< 0.0001), SIPI (r= 0.88, p< 0.0001), Gitelson5 (r= 0.87, p< 0.0001), WBI (r= 0.86, p< 0.0001), and CRI (r= 0.82, p< 0.0001). The strongest signals for the moist class was observed for PRI (r= 0.92, p< 0.0001), NDVI (r= 0.91, p< 0.0001), Green1 (r= 0.91, p< 0.0001), OSAVI (r= 0.90, p< 0.0001), MNDVI (r= 0.89, p< 0.0001), CRI (r= 0.89, p< 0.0001), SIPI (r= 0.89, p< 0.0001), MSR (r= 0.88, p< 0.0001), WBI (r= 0.84, p< 0.0001), and Gitelson5 (r= 0.83, p< 0.0001).

It was also important in this study to decipher precisely how the ground-based measurements aligned across the different spatial scales sampled by the MISP transects and CALM grids. Therefore, correlations were applied to all data and the most significant correlations are listed in Table 4.8 for Utqiaġvik and Table 4.9 for Atqasuk. AL thaw depth correlated well between

the MISP and CALM sites in Utqiaġvik with an r= 0.97, p< 0.0001 while soil temperature also correlated well with r= 0.76, p< 0.0001 for the dry/moist shrub/gram classes. For the dry shrub vegetation class, correlations were strong for all parameters including soil moisture (r= 0.66, p< 0.001), soil temperature (r= 0.74, p< 0.0001), and thaw depth (r= 0.97, p< 0.0001). Thaw depth correlated strongly (r= 0.98, p< 0.0001) as did soil temperature (r= 0.71, p< 0.0001) for the moist gram class. All measurements correlated for the seasonally flooded class, including soil moisture (r= 0.86, p< 0.0001), soil temperature (r= 0.72, p< 0.0001), and thaw depth (r= 0.98, p< 0.0001). For the wet gram correlations were strong for soil moisture (r= 0.71, p< 0.0001), soil temperature (r= 0.59, p< 0.001), and thaw depth (r= 0.98, p< 0.0001). Surface measurements in Atqasuk were also strongly correlated, as seen from the dry class where thaw depth (r= 0.97, p< 0.0001) matched strongly, followed by soil temperature (r= 0.78, p< 0.0001), and soil moisture (r= 0.78, p< 0.0001). Only thaw depth and soil temperature correlated for the remaining vegetation classes. For the aquatic class, correlations were strong for thaw depth r= 0.91, p< 0.0001 and soil temperature r= 0.73, p< 0.0001. The moist class correlations were strong for thaw depth r= 0.93, p< 0.0001 and soil temperature r= 0.89, p< 0.0001, while the moist shrub yielded strong correlations for thaw depth r= 0.95, p< 0.0001 and soil temperature r= 0.79, p< 0.0001. Correlations were strong for thaw depth, r= 0.89, p< 0.0001 and soil temperature r= 0.75, p< 0.0001 in the wet vegetation class in Atqasuk.

Table 4.8: Utqiaġvik cross-site (MISP vs. CALM) correlations between ground-based measurements across all years.

Location	Veg Class	MISP Measure	by CALM Measure	r	p
Barrow	DMSGRAM	M_Thaw	C_Thaw	0.97	<0.001
		M_Temp	C_Temp	0.76	<0.001
	DRY SHRUB	M_VWC	C_VWC	0.66	<0.001
		M_Thaw	C_Thaw	0.97	<0.001
		M_Temp	C_Temp	0.74	<0.001
	MOIST GRAM	M_Thaw	C_Thaw	0.98	<0.001
		M_Temp	C_Temp	0.71	<0.001
	SEASONALLY FLOODED	M_VWC	C_VWC	0.86	<0.001
		M_Thaw	C_Thaw	0.98	<0.001
		M_Temp	C_Temp	0.72	<0.001
	WET GRAM	M_VWC	C_VWC	0.71	<0.001
		M_Thaw	C_Thaw	0.98	<0.001
		M_Temp	C_Temp	0.59	<0.001

Table 4.9: Atqasuk cross-site (MISP vs. CALM) correlations between ground-based measurements across all years.

Location	Veg Class	MISP Measure	by CALM Measure	r	p
Atqasuk	AQUATIC	M_Thaw	C_Thaw	0.91	<0.001
		M_Temp	C_Temp	0.73	<0.001
	DRY	M_VWC	C_VWC	0.78	<0.001
		M_Thaw	C_Thaw	0.97	<0.001
		M_Temp	C_Temp	0.78	<0.001
	MOIST	M_Thaw	C_Thaw	0.93	<0.001
		M_Temp	C_Temp	0.89	<0.001
	MOIST SHRUB	M_Thaw	C_Thaw	0.95	<0.001
		M_Temp	C_Temp	0.79	<0.001
	WET	M_Thaw	C_Thaw	0.89	<0.001
		M_Temp	C_Temp	0.75	<0.001

4.5.8 Scaling: Elevation differences between digital photogrammetry, A-LiDAR and SSI

In Chapters 2 and 3, it was established that airborne imagery can be utilized not only to document important phenological events across multiple arctic vegetation communities but also to develop high resolution elevation models of highly irregular and complex terrain such as thermokarst tundra. To further this exploration and ascertain the capacity of KAP to derive DEMs comparable in size to the base-pixel resolution of globally orbiting platforms such as MODIS, we developed DEMs across the Utqiaġvik CALM grid from data acquired by three different remote sensing platforms. These included airborne LiDAR, aerial digital photography, and satellite stereo imagery (Figure 18). Data collection, data processing and analysis were the same as that outlined for the respective platform in chapter 2. From visual inspection of the final CALM DEMs, it is obvious that all platforms have the capacity to model complex tundra landscapes but with varied degrees of precision. Overall, the LiDAR and photogrammetry approaches displayed a capacity to model elevation in a similar fashion, with each yielding DEMs having a horizontal spatial resolution of 3.5 m. The satellite derived DEM was processed to yield a 5 m spatial resolution by the PGC. When comparing the A-LiDAR DEM to a high resolution World-view 2 satellite image the elevation values seem to follow the landscape precisely, as the high centered polygons and dry regions are very clear atop the edge of the dry thaw lake basin (DTLB), while the lower wet areas within the DTLB are not as clearly depicted and are instead displayed as a single shade of color or elevation value. The A-LiDAR DEM was also able to discern the large drainage system that passes from the higher elevations to the DTLB clearly seen in the satellite image (figure 18). The aerial images acquired from the helicopter were also able to develop an accurate DEM via digital photogrammetry. However, the helicopter-derived DEM had more “noise” along the margins of the CALM grid, which resulted in some areas of high-centered polygonal tundra not being clearly defined compared to the DEM derived from the A-LiDAR. Conversely, the helicopter-derived DEM was able to model the topographic variability of low-lying wetter regions well. An important outcome was that the resulting DEMs of the Utqiaġvik MISP grid acquired from the airborne photography system (i.e. KAP) also showed a capacity to capture lower wetter regions or troughs between polygons more effectively than LiDAR systems. The stereo imagery on the other hand was not as successful at modeling the elevation of heterogeneous terrain, yielding a coarse and lower resolution DEM than the other two platforms.

Cross-validation analysis results revealed SESMs that highlighted areas of high uncertainty from each model by visually plotting residuals between measured and predicted values. The A-Photography DEM resulted in a large number of error values clustered randomly but with highest values around the margins of the CALM grid while the A-LiDAR DEM displayed a low number of erroneous values that were evenly distributed throughout the study area and along the margins of sampling swaths. When comparing the final DEM elevation values against each other, correlations indicated that the A-LiDAR and SSI elevations values were closest ($r= 0.98$, $p< 2.2e-16$) followed by A-LiDAR and A-Photography ($r= 0.90$, $p< 2.2e-16$), and lastly between A-Photography and SSI ($r= 0.88$, $p< 2.2e-16$). However, the SSI platform seems to be estimating elevation low compared to the other two datasets. A-Photography and A-LiDAR had a closer association and values seem to very close to the 1 to 1 line (Figure 4.13), but the photography approach seems to be estimating slightly lower values than the LiDAR system also.

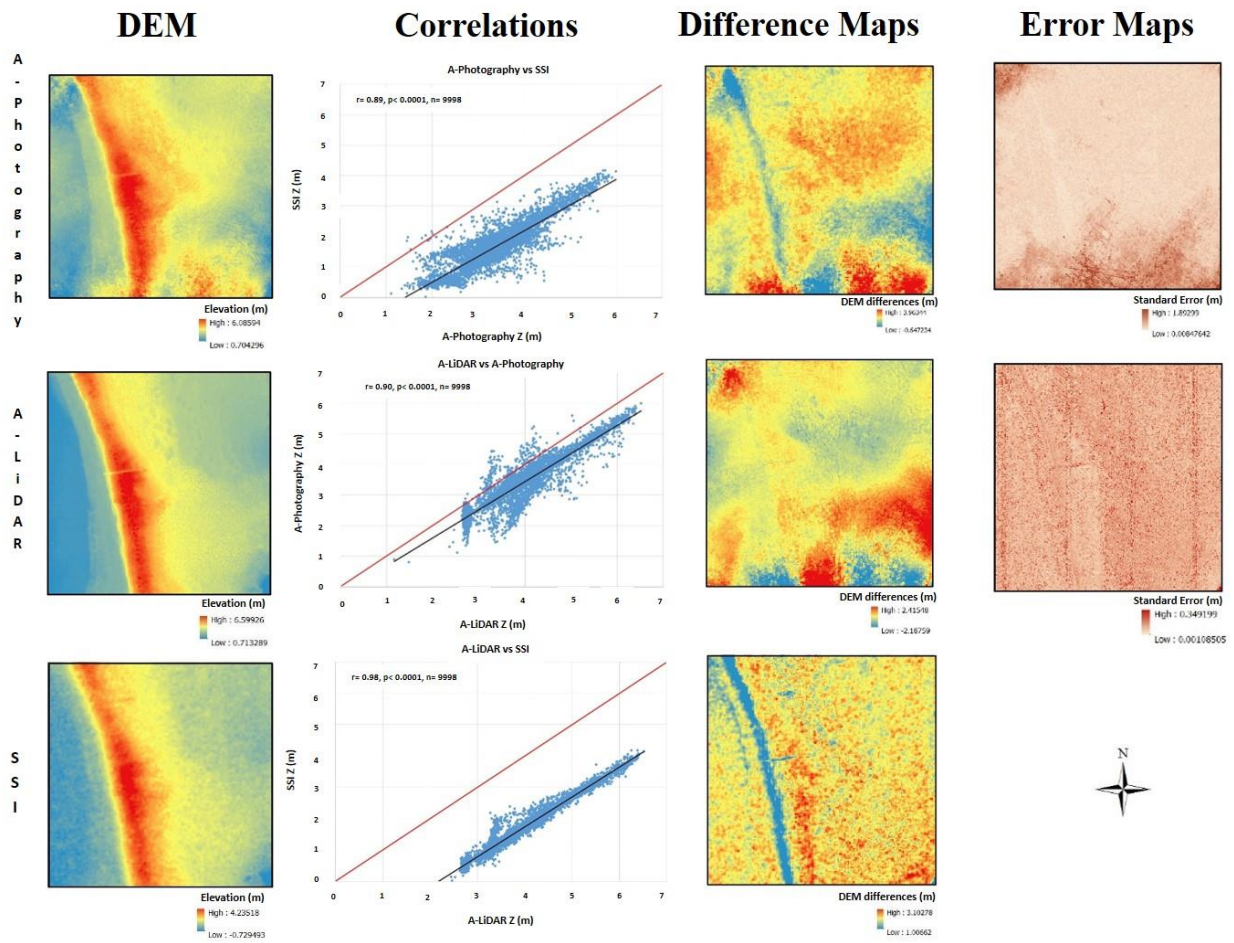

Figure 4.12: Shown from left to right: final EBK interpolated DEMs, inter-platform Pearson's elevation correlations (red line depicts 1:1; elevation (Z) values are in meters), differences between final DEMs (all DEM surfaces were subtracted from the A-LiDAR DEM which was used as the reference surface and A-Photography was used as reference when comparing with SSI) and standard error maps highlighting areas of uncertainty for each approach except from the SSI since no point clouds were available.

The EBK interpolation method was able to model elevation well from both A-Photography and A-LiDAR PCs as seen from the resulting simple linear regressions between the GCP elevations and PC elevations below (Figure 4.12). The A-LiDAR PC seemed to capture elevation values slightly higher (approximately 0.5 meters) than the measured GCP elevations while the A-Photography PC showed more variation in values.

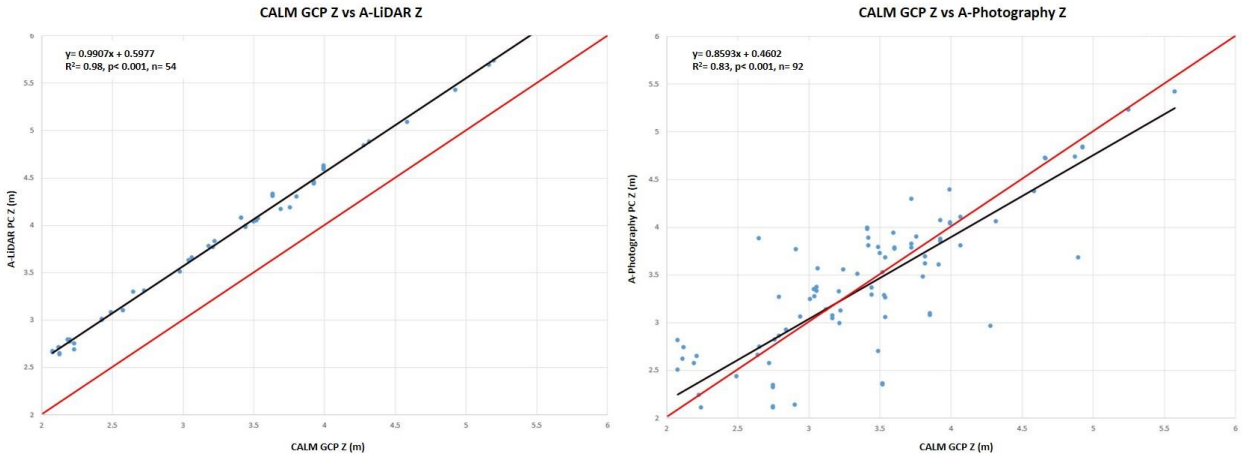

Figure 4.13: Simple linear regressions between GCP elevation and each PC dataset elevation (meters) acquired from A-LiDAR and A-Photography system for the 20 cm buffers. The red line depicts 1:1 relationship between the variables. Additionally, the 10 cm buffer data displayed similar results (not displayed).

Surface hydrology of the Utqiaġvik CALM grid was modeled by calculating drainage lines, flow accumulation, and catchment drainage points for surface water flow. As seen in figure 20, all models depicted these characteristics differently. The A-LiDAR and SSI DEMs were able to yield more coarse drainage lines and flow along the edge of the DTLB. The A-photography DEM produced a more dense hydrology model compared to the other platforms making it more difficult to denote the obvious regions of flow and water accumulation.

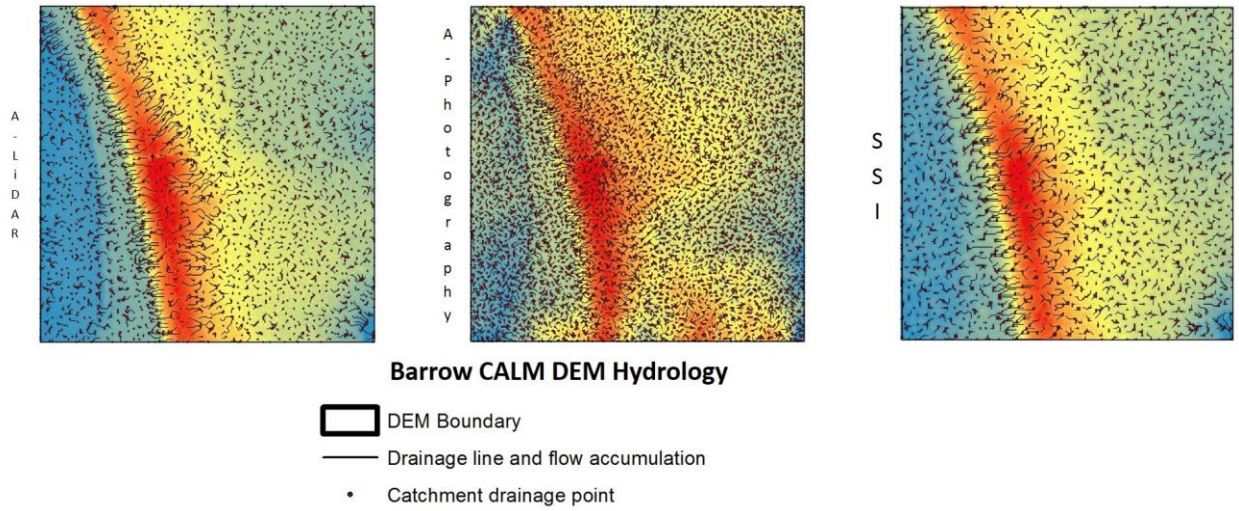

Figure 4.14: Surface hydrology depicting catchment drainage points, drainage lines, and flow accumulation points for the Utqiaġvik CALM as depicted by each DEM.

Basic point cloud statistics highlight that for smaller tundra landscapes (< 1ha) analysis of digital photography with the SFM approach can produce dense PCs (i.e. millions of points) that are comparable to that of the T-LiDAR systems. Of the three systems, the A-Photography system was able to capture lower elevations (i.e. min= 1.81 meters). Similar results were observed across the Utqiaġvik CALM grid as the A-Photography system captured the lowest elevation values of the two approaches (i.e. min= 0.713 meters). The results from the DEM statistics shows similar results where the A-Photography system yielded very similar results to the LiDAR system. Tables 4.10 - 4.13 summarize basic PC and DEM statistics corresponding to each platform used across both MISP and CALM grids.

Table 4.10: BE DEM site basic point cloud statistics acquired from each platform.

	BE DEM Site								
Platform	Total points (0.25 ha)	Point Density (m^2)	Max	Min	Mean	Median	Skewness	St Dev	Kurtosis
T-LiDAR	2,646,804	1059	3.01	1.895	2.47	2.4	-0.11	0.16	2.73
A-Photography	2,122,596	850	2.8	1.81	2.33	2.33	-0.1411	0.164	2.23
A-LiDAR	36,284	15	2.67	1.89	2.3	2.3	-0.31	0.154	2.4

Table 4.11: Utqiaġvik CALM basic point cloud statistics acquired from each platform.

			CALM Grid						
Platform	Total Points (100 ha)	Point Density (m^2)	Max	Min	Mean	Median	Skewness	St Dev	Kurtosis
A-Photography	6,616,671	6.61	6.58	0.713	3.386	3.3163	0.37197	0.8962	2.7712
A-LiDAR	14,571,378	14.57	6.63	0.721	3.912	3.76	0.70559	0.8614	3.1372

Table 4.12: BE DEM site basic DEM statistics acquired from each platform. All values are approximate.

				BE DEM Site						
Platform	Avg. Equipment Cost (US $)	Acquisition Cost (US $)	Spatial Resolution (cm)	Altitude Range (m)	Acquisition Altitude (m)	DEM computing time (days)	Raw file size (GB)	DEM Z		
								Range (m)	Max (m)	Min (m)
T-LiDAR	120K	1K	0.2	1-5	2	~3	~10	1.1	3.01	1.89
A-Photography	1K	0	0.4	1-500	17.5	~1	~2	1	2.8	1.81
A-LiDAR	300K	10K	100	500-1500	700	~2	~5	0.78	2.67	1.89
SSI	300M	$50 (per scene)	500	800K - 900K	800K	~10	~5	0.5	3.1	2.6

Table 4.13: Utqiaġvik CALM basic DEM statistics acquired from each platform. All values are approximate.

				CALM Grid						
Platform	Avg. Equipment Cost (US $)	Acquisition Cost (US $)	Spatial Resolution (m)	Altitude Range (m)	Acquisition Altitude (m)	DEM computing time (days)	Raw file size (GB)	DEM Z		
								Range (m)	Max (m)	Min (m)
A-Photography	1K	0	3.5	1-500	380	~2	~4	5.86615	6.57949	0.713335
A-LiDAR	300K	10K	3.5	500-1500	700	~2	~5	5.885971	6.59926	0.713289
SSI	300M	$50 (per scene)	5	800K - 900K	800K	~10	~5	4.96467	4.23518	-0.729493

4.6 DISCUSSION

The goal of this chapter was to utilize and extend the same approaches applied previously in chapters 2 and 3 to a larger landscape area (CALM grids) to assess the capacities of RGB digital imaging on different sensing platforms for capturing tundra phenological dynamics from different vegetation classes. For the most part, results from this chapter aligned well with those obtained from chapters 2 and 3. In particular, wetter classes at both locations and across both CALM grids showed more seasonal and inter-annual phenological variability than classes of lower soil moisture regimes. The results observed from the approaches used in chapters 3 and 4 suggest that vegetation communities that are more seasonally productive are those that are driving the greening signals and not necessarily the amount or percentage of water although productivity and water available

go hand in hand and can help explain these results. The majority of optical sampling sensors used were able to predict strong for wet classes better than drier vegetation communities and a large number of RGB-derived indices and spectrometer-derived indices had strong correlations with NDVI, arguably the most widely used spectral index in ecosystem science studies. This index has been found to correlate well with above ground biomass in tundra ecosystems and is related to a number of physical properties of vegetation such as the leaf area index (LAI) (*Boelman et al.*, 2003; *Goswami et al.*, 2011). Future research should aim to further explore the relationships between RGB-derived indices from low-cost sensors with these types of vegetation properties in order to gauge a better understanding of the potential of using these indices for monitoring tundra ecosystem structure and function across multiple spatial and temporal scales.

Airborne digital photography and photogrammetric analyses were shown to have capacities for effectively modeling seasonal changes in the phenology of tundra landscapes plot to landscape scales (meters to kilometers). These systems appeared to be particularly adept at differentiating seasonal trends and inter-annual differences in the phenological trends of discrete plant communities. Additionally, these relatively low-cost systems have shown the suitability, and adaptability for multi-temporal and multi-scale ecological sampling of low and high arctic landscapes and a capacity to deliver new knowledge pertaining to likely ecological mechanisms underpinning trends observed at circum-arctic scales. Moreover, these particular airborne approaches (i.e. KAP) have shown to be limited in their capacity to model at large special scales but have shown to be a surrogate for using unmanned aerial vehicles (UAVs) or drones for filling these gaps. Findings from this study support the use of drones and provide an outlet for further exploring signals from these systems such as spectral unmixing and spectro-directional analysis of reflectance spectra.

These results provide an insight into the sensitivity of all indices to document seasonal trends and inter-annual differences in vegetation phenology and suggests further analysis utilizing these data could ascertain likely biophysical controls of such variability in ecosystem properties and processes. Also, further exploration into the capacity of RGB-derived and spectrometer-derived indices to document biophysical characteristics (i.e. LAI and biomass) of arctic tundra vegetation communities and their related accuracy and uncertainty of each is needed. Additionally, few studies have focused on exploring the use of different indices for documenting and quantifying biophysical characteristics of tundra vegetation considering the similarity between the bands and

wavelengths used for calculation across multiple remote sensing approaches. Lastly, there is also a need to assess the utility of RGB sensors to be used for the validation of satellite derived products suitable for defining seasonal and inter-annual phenological trends over large spatial scales. The latter is explored in Chapter 5.

4.7 CONCLUSION

Building on chapters 2 and 3 from this dissertation, chapter 4 explored 1) the use of airborne digital photogrammetry for capturing microtopographic variability in a tundra landscape spanning an spatially distributed layout and 2) the capacity of digital cameras for monitoring plot-level plant phenology where plots were spatially distributed throughout a landscape typical of polygonised tundra in high and low arctic landscapes. Initially, the digital photogrammetry approach taken was able to develop an accurate DEM of the CALM grid in Utqiaġvik, however, it resulted in highlighting the limiting and high-dependence on ground control points for accurately aligning aerial images to large areas. The final DEMs produced by the A-LiDAR system resulted in the highest accuracy (i.e. least amount of error throughout the model), however based on the linear regression models performed, this system seems to be overestimating elevation values when compared to the GCP elevation values. The SSI-derived DEM performed poorly, resulting in a coarse DEM and underestimation of elevation values by about 2 meters. Generally, the majority of sensors were sensitive to vegetation classes containing higher soil moisture content, which correlates with those classes being more productive in both localities (Utqiaġvik and Atqasuk). This suggests these sensors have the capacity to capture seasonal and inter-annual changes in vegetation structure and productivity for high-arctic tundra ecosystems. Similar results were observed to those reported in chapter 3, in that a number of RGB-derived indices correlated strongly with a number of spectrometer-derived indices in monitoring vegetation productivity or greenness. This highlights the need to investigate the collinearity of vegetation indices as most are

calculated using spectral bands that are the same or proximal to one another within the electromagnetic spectrum. Additionally, further investigations are needed to assess the capacity of RGB-derived indices for modeling other vegetation indices such as LAI and above ground biomass.

4.8 REFERENCES

Aber, J. S., R. J. Sobieski, D. a Distler, and M. C. Nowak (1999), Kite Aerial Photography for Environmental Site Investigations, , *102*(1), 57–67, doi:10.2307/3628217.

Aber, J. S., S. W. Aber, and F. Pavri (2002), Unmanned Small-Format Aerial Photography From Kites for Acquiring Large-Scale , High-Resolution , Multiview-Angle Imagery, *Int. Arch. Photogramm. Remote Sens. Spat. Inf. Sci.*, *34*(1), 1–6.

Aber, J. S., D. Eberts, and S. W. Aber (2005), Applications of kite aerial photography: Biocontrol of salt cedar (Tamarix) in the western United States, *Trans. Kansas Acad. Sci.*, *108*(1 & 2), 63–66, doi:10.1660/0022-8443(2005)108[0063:AOKAPB]2.0.CO;2.

ACIA (2004a), Impacts of a Warming Arctic: Arctic Climate Impact Assessment, *Cambridge Univ. Press*, 1046, doi:10.2277/0521617782.

ACIA (2004b), Impacts of a Warming Arctic: Arctic Climate Impact Assessment, *Cambridge Univ. Press*, 1046, doi:10.2277/0521617782.

Andresen, C. G. (2014), Monitoring and understanding decadal scale changes in hydrology, productivity and carbon balance in Arctic tundra ponds, , 108.

Andresen, C. G., and V. L. Lougheed (2015), Disappearing Arctic tundra ponds: Fine-scale analysis of surface hydrology in drained thaw lake basins over a 65 year period (1948–2013), , 1–14, doi:10.1002/2014JG002778.Received.

Andresen, C. G., S. A. Vargas, V. L. Lougheed, and C. E. Tweedie (2014), Kite-based Aerial Photography (KAP): A Low Cost, Effective Tool for Wetland Research, *Wetl. Sci. Pract.*, *Dec*(December), 28–31.

Arft, a. M. et al. (1999), Responses of Tundra plants to experimental warming: Meta-analysis of the International Tundra Experiment, *Ecol. Monogr.*, *69*(4), 491–511, doi:10.1890/0012-9615(1999)069[0491:ROTPTE]2.0.CO;2.

Bangen, S. G., J. M. Wheaton, N. Bouwes, B. Bouwes, and C. Jordan (2014), A methodological intercomparison of topographic survey techniques for characterizing wadeable streams and rivers, *Geomorphology*, *206*, 343–361, doi:10.1016/j.geomorph.2013.10.010.

Battersby, S. E., D. “daan” Strebe, and M. P. Finn (2016), Shapes on a plane: evaluating the impact of projection distortion on spatial binning, *Cartogr. Geogr. Inf. Sci.*, *406*(May), 1–12, doi:10.1080/15230406.2016.1180263.

Beamish, A. L., W. Nijland, M. Edwards, N. C. Coops, and G. H. R. Henry (2016), Phenology and vegetation change measurements from true colour digital photography in high Arctic tundra, *NRC Res. Press*, *49*(May), 33–49.

Bhardwaj, A., L. Sam, A. Bhardwaj, and F. J. Martín-Torres (2016), LiDAR remote sensing of the cryosphere: Present applications and future prospects, *Remote Sens. Environ.*, *177*, 125–143, doi:10.1016/j.rse.2016.02.031.

Bhatt, U. S. et al. (2010), Circumpolar Arctic tundra vegetation change is linked to sea ice decline, *Earth Interact.*, *14*(8), doi:10.1175/2010EI315.1.

Bhatt, U. S., D. a. Walker, M. K. Raynolds, P. a. Bieniek, H. E. Epstein, J. C. Comiso, J. E. Pinzon, C. J. Tucker, and I. V. Polyakov (2013), Recent declines in warming and vegetation greening trends over pan-arctic tundra, *Remote Sens.*, *5*(9), 4229–4254, doi:10.3390/rs5094229.

Biasi, C., W. Wanek, O. Rusalimova, C. Kaiser, C. Biasi, W. Wanek, C. Kaiser, H. Meyer, and A. Richter (2017), Microtopography and Plant-Cover Controls on Nitrogen Dynamics in Hummock Tundra Ecosystems in Siberia Meyer , Pavel Barsukov and Andreas Richter Published by : INSTAAR , University of Colorado Stable URL : http://www.jstor.org/stable/4095862 REFERENCES Li, , *37*(4), 435–443.

Boelman, N. T., M. Stieglitz, H. M. Rueth, M. Sommerkorn, K. L. Griffin, G. R. Shaver, and J. a Gamon (2003), Response of NDVI, biomass, and ecosystem gas exchange to long-term warming and fertilization in wet sedge tundra., *Oecologia*, *135*(3), 414–421, doi:10.1007/s00442-003-1198-3.

Boelman, N. T., L. Gough, J. R. McLaren, and H. Greaves (2011a), Does NDVI reflect variation in the structural attributes associated with increasing shrub dominance in arctic tundra?, *Environ. Res. Lett.*, *6*(3), 35501, doi:10.1088/1748-9326/6/3/035501.

Boelman, N. T., L. Gough, J. R. McLaren, and H. Greaves (2011b), Does NDVI reflect variation in the structural attributes associated with increasing shrub dominance in arctic tundra?, *Environ. Res. Lett.*, *6*, 35501, doi:10.1088/1748-9326/6/3/035501.

Bradley, N. L., C. A. Leopold, J. Ross, and W. Huffaker (1999), Phenological changes reflect climate change in Wisconsin., *Proc. Natl. Acad. Sci. U. S. A.*, *96*(August), 9701–9704, doi:10.1073/pnas.96.17.9701.

Brown, J., P. C. Miller, L. L. Tieszen, and F. L. Bunnell (1980), *An Arctic Ecosystem: The Coastal Tundra at Barrow, Alaska*.

Brown, J., F. E. Nelson, and K. M. Hinkel (2000), The circumpolar active layer monitorign (CALM) program research designs and initial results, *Polar Geogr.*, *3*(May 2012), 162–165.

Cabin, R. J., R. J. Mitchell, E. Siemann, D. Wedin, and K. S. N. Bio (2000), To Bonferroni or Not to Bonferroni : When and How Are the Questions Published by : Wiley on behalf of the Ecological Society of America Stable URL : http://www.jstor.org/stable/20168454 How Are the Questions To Bonferroni or Not to Bonferroni : When and, , *81*(3), 246–248.

Carlisle, B. H. (2005), Modelling the spatial distribution of DEM error, *Trans. GIS*, *9*(4), 521–540, doi:10.1111/j.1467-9671.2005.00233.x.

Carter, J., Schmid, K., Waters, K., Betzhold, L., Hadley, B., Mataosky, R., Halleran, J. (2012), Lidar 101 : An Introduction to Lidar Technology , Data , and Applications, *NOAA Coast. Serv. Cent.*, (November), 76.

Chapin, F. S. et al. (2005), Role of Land-Surface Changes in Arctic Summer Warming, *Science (80-.).*, *657*(2005), 9–13, doi:10.1126/science.1117368.

Chaplot, V., F. Darboux, H. Bourennane, S. Leguédois, N. Silvera, and K. Phachomphon (2006), Accuracy of interpolation techniques for the derivation of digital elevation models in relation to landform types and data density, *Geomorphology*, *77*(1–2), 126–141, doi:10.1016/j.geomorph.2005.12.010.

Chen, C., and T. Yue (2010), A method of DEM construction and related error analysis, *Comput. Geosci.*, *36*(6), 717–725, doi:10.1016/j.cageo.2009.12.001.

Claudio, H. C., Y. Cheng, D. a. Fuentes, J. a. Gamon, H. Luo, W. Oechel, H. L. Qiu, A. F. Rahman, and D. a. Sims (2006), Monitoring drought effects on vegetation water content and fluxes in chaparral with the 970??nm water band index, *Remote Sens. Environ.*, *103*(3), 304–311, doi:10.1016/j.rse.2005.07.015.

Cleland, E. E., I. Chuine, A. Menzel, H. a. Mooney, and M. D. Schwartz (2007), Shifting plant phenology in response to global change, *Trends Ecol. Evol.*, *22*(7), 357–365, doi:10.1016/j.tree.2007.04.003.

Dandois, J. P., and E. C. Ellis (2010), Remote sensing of vegetation structure using computer vision, *Remote Sens.*, *2*(4), 1157–1176, doi:10.3390/rs2041157.

Dandois, J. P., and E. C. Ellis (2013), High spatial resolution three-dimensional mapping of vegetation spectral dynamics using computer vision, *Remote Sens. Environ.*, *136*, 259–276, doi:10.1016/j.rse.2013.04.005.

Darnell, A. R., N. J. Tate, and C. Brunsdon (2008), Improving user assessment of error implications in digital elevation models, *Comput. Environ. Urban Syst.*, *32*(4), 268–277, doi:10.1016/j.compenvurbsys.2008.02.003.

Delbart, N., T. Le Toan, L. Kergoat, and V. Fedotova (2006), Remote sensing of spring phenology in boreal regions: A free of snow-effect method using NOAA-AVHRR and SPOT-VGT data (1982-2004), *Remote Sens. Environ.*, *101*(1), 52–62, doi:10.1016/j.rse.2005.11.012.

Desmet, P. J. J. (1997), Effects Of Iinterpolation Errors On The Aanalysis Of DEMs, *Earth Surf. Process. Landforms*, *22*(June 1996), 563–580.

Dowling, T., A. Read, and J. Gallant (2009), Very high resolution DEM acquisition at low cost using a digital camera and free software, *18th World IMACS/MODSIM09 Congr.*, (July), 2479–2485.

Elmendorf, S. C. et al. (2012a), Global assessment of experimental climate warming on tundra vegetation: Heterogeneity over space and time, *Ecol. Lett.*, *15*(2), 164–175, doi:10.1111/j.1461-0248.2011.01716.x.

Elmendorf, S. C. et al. (2012b), Plot-scale evidence of tundra vegetation change and links to recent summer warming, *Nat. Clim. Chang.*, *2*(6), 453–457, doi:10.1038/nclimate1465.

Epstein, H. E., M. K. Raynolds, D. a Walker, U. S. Bhatt, C. J. Tucker, and J. E. Pinzon (2012), Dynamics of aboveground phytomass of the circumpolar Arctic tundra during the past three decades, *Environ. Res. Lett.*, *7*(1), 15506, doi:10.1088/1748-9326/7/1/015506.

Erdoğan, S. (2010), Modelling the spatial distribution of DEM error with geographically weighted regression: An experimental study, *Comput. Geosci.*, *36*(1), 34–43, doi:10.1016/j.cageo.2009.06.005.

Esri (2001), ArcGIS Geostatistical Analyst: Statistical Tools for Data Exploration, Modeling, and Advanced Surface Generation, , (August), 19.

ESRI (2013), Overview of Arc Hydro Terrain Preprocessing Workflows, , (February), 13.

Von Fischer, J. C., R. C. Rhew, G. M. Ames, B. K. Fosdick, and P. E. Von Fischer (2010), Vegetation height and other controls of spatial variability in methane emissions from the Arctic coastal tundra at Barrow, Alaska, *J. Geophys. Res. Biogeosciences*, *115*(3), 1–11, doi:10.1029/2009JG001283.

Fisher, P. (1998), Improved modeling of elevation error with Geostatistics, *Geoinformatica*, *2*(3), 215–233, doi:10.1023/A:1009717704255.

Fonstad, M. a., J. T. Dietrich, B. C. Courville, J. L. Jensen, and P. E. Carbonneau (2013), Topographic structure from motion: A new development in photogrammetric measurement, *Earth Surf. Process. Landforms*, *38*(4), 421–430, doi:10.1002/esp.3366.

Fraser, R. H., I. Olthof, T. C. Lantz, and C. Schmitt (2016), UAV Photogrammetry for Mapping Vegetation in the Low-Arctic, *Arct. Sci.*, *102*(June), 1–51, doi:10.1139/as-2016-0008.

Gamon, J. a, G. P. Kershaw, S. Williamson, and D. S. Hik (2012a), Microtopographic patterns in an arctic baydjarakh field: do fine-grain patterns enforce landscape stability?, *Environ. Res. Lett.*, *7*(1), 15502, doi:10.1088/1748-9326/7/1/015502.

Gamon, J. a., Y. Cheng, H. Claudio, L. MacKinney, and D. a. Sims (2006), A mobile tram system for systematic sampling of ecosystem optical properties, *Remote Sens. Environ.*, *103*(3), 246–254, doi:10.1016/j.rse.2006.04.006.

Gamon, J. a., K. F. Huemmrich, R. S. Stone, and C. E. Tweedie (2013), Spatial and temporal variation in primary productivity (NDVI) of coastal Alaskan tundra: Decreased vegetation growth following earlier snowmelt, *Remote Sens. Environ.*, *129*, 144–153, doi:10.1016/j.rse.2012.10.030.

Gamon, J. A., G. P. Kershaw, S. Williamson, and D. S. Hik (2012b), Microtopographic patterns in an arctic baydjarakh field: do fine-grain patterns enforce landscape stability?, *Environ. Res. Lett.*, *7*(1), 15502, doi:10.1088/1748-9326/7/1/015502.

Gao, J. (1997), Resolution and accuracy of terrain representation by grid DEMs at a micro-scale, *Int. J. Geogr. Inf. Sci.*, *11*(2), 199–212, doi:10.1080/136588197242464.

Gao, X., and a. R. Huete (2000), Validation of MODIS land surface reflectance and vegetation indices with multi-scale high spatial resolution data, *IGARSS 2000. IEEE 2000 Int. Geosci. Remote Sens. Symp. Tak. Pulse Planet Role Remote Sens. Manag. Environ. Proc. (Cat. No.00CH37120)*, 533–535, doi:10.1109/IGARSS.2000.861620.

Gitelson, A. a, Y. Zur, O. B. Chivkunova, and M. N. Merzlyak (2002), Assessing carotenoid content in plant leaves with reflectance spectroscopy., *Photochem. Photobiol.*, *75*(3), 272–281, doi:10.1562/0031-8655(2002)0750272ACCIPL2.0.CO2.

Gitelson, A. A., F. Verlag, Y. Gritz, and M. N. Merzlyak (2003), Relationships between leaf chlorophyll content and spectral reflectance and algorithms for non-destructive chlorophyll assessment in higher plant leaves, , *282*.

Goetz, S. J., A. G. Bunn, G. J. Fiske, and R. a Houghton (2005), Satellite-observed photosynthetic trends across boreal North America associated with climate and fire disturbance., *Proc. Natl. Acad. Sci. U. S. A.*, *102*(38), 13521–5, doi:10.1073/pnas.0506179102.

Gong, J., L. Zhllin, Q. Zhu, H. Sui, and Y. Zhou (2000), Effects of Various Factors on the Accuracy of DEMs : An Intensive Experimental Investigation, *Photogramm. Eng. Remote Sens.*, *66*(9), 1113–1117.

Goswami, S., J. a. Gamon, and C. E. Tweedie (2011), Surface hydrology of an arctic ecosystem: Multiscale analysis of a flooding and draining experiment using spectral reflectance, *J. Geophys. Res. Biogeosciences*, *116*(1), 1–14, doi:10.1029/2010JG001346.

Harwin, S., and A. Lucieer (2012), Assessing the accuracy of georeferenced point clouds produced via multi-view stereopsis from Unmanned Aerial Vehicle (UAV) imagery, *Remote Sens.*, *4*(6), 1573–1599, doi:10.3390/rs4061573.

Haugen, R.K., and Brown, J. (1980), Coastal-Inland Distributions of Summer Air Temperature and Precipitation in Northern Alaska, *Arct. Alp. Res.*, *12*(4), 403–412.

Healey, N. C., Oberbauer, S.F., Ahrends, H.E., Dierick, D., Welker, J.M., Leffler, A.J., Hollister, R.D., Vargas, S.A., Tweedie, C. E. (2014), A Mobile Instrumented Sensor Platform for Long-Term Terrestrial Ecosystem Analysis: An Example Application in an Arctic Tundra Ecosystem, *J. Environ. Informatics*, *24*(1), 1–10, doi:10.3808/jei.201400278.

Heimsath, A. M., and H. Farid (2002), Hillslope topography from unconstrained photographs, *Math. Geol.*, *34*(8), 929–952, doi:10.1023/A:1021364623017.

Helbig, M., J. Boike, M. Langer, P. Schreiber, B. R. K. Runkle, and L. Kutzbach (2013), Spatial and seasonal variability of polygonal tundra water balance: Lena River Delta, northern Siberia (Russia), *Hydrogeol. J.*, *21*(1), 133–147, doi:10.1007/s10040-012-0933-4.

Henry, G. H R and Molau, U. (1997), Tundra plants and climate change : the International Tundra Experiment (ITEX), , *3*, 1–9.

Henry, G., R. Hollister, I. S. Jónsdóttir, K. Klanderlud, U. Molau, S. F. Oberbauer, P. Webber, and P. Wookey (2013), The International Tundra Experiment: An Arctic Monitoring Network,

Hinzman, L. D., C. J. Deal, a. D. Mcguire, S. H. Mernild, I. V. Polyakov, and J. E. Walsh (2013), Trajectory of the Arctic as an integrated system, *Ecol. Appl.*, *23*(8), 1837–1868, doi:10.1890/11-1498.1.

Hollister, R. D. (2003), Response of Tundra Vegetation to Temperature: Implications for Forcasting Vegetation Change,

Hollister, R. D., and K. J. Flaherty (2010), Above- and below-ground plant biomass response to experimental warming in northern Alaska, *Appl. Veg. Sci.*, *13*(3), 378–387, doi:10.1111/j.1654-109X.2010.01079.x.

Hollister, R. D., P. J. Webber, and C. E. Tweedie (2005), The response of Alaskan arctic tundra to experimental warming: Differences between short- and long-term responses, *Glob. Chang. Biol.*, *11*(4), 525–536, doi:10.1111/j.1365-2486.2005.00926.x.

Hollister, R. D., P. J. Webber, and C. Bay (2014), Plant Response to Temperature in Northern Alaska : Implications for Predicting Vegetation Change PLANT RESPONSE TO TEMPERATURE IN NORTHERN ALASKA :, , *86*(6), 1562–1570.

Huemmrich, K. F. et al. (2010), Remote sensing of tundra gross ecosystem productivity and light use efficiency under varying temperature and moisture conditions, *Remote Sens. Environ.*, *114*(3), 481–489, doi:10.1016/j.rse.2009.10.003.

Huemmrich, K. F., J. Gamon, C. E. Tweedie, P. P. K. Campbell, D. Landis, and E. Middleton (2013), Arctic Tundra Vegetation Functional Types Based on Photosynthetic Physiology and Optical Properties, , 1–37.

Humphreys, E. R., and P. M. Lafleur (2011), sequestration in two low Arctic tundra ecosystems?, *Geophys. Res. Lett.*, *38*(9), 3–7, doi:10.1029/2011GL047339.

Hunter, G. j., and M. F. Goodchild (1997), Modeling the Uncertainty of Slope and Aspect Estimates Derived from Spatial Databases,

Hutchinson, M. F., T. Xu, and J. a Stein (2011), Recent Progress in the ANUDEM Elevation Gridding Procedure, *Geomorphometry*, 19–22.

Ide, R., and H. Oguma (2013), A cost-effective monitoring method using digital time-lapse cameras for detecting temporal and spatial variations of snowmelt and vegetation phenology in alpine ecosystems, *Ecol. Inform.*, *16*, 25–34, doi:10.1016/j.ecoinf.2013.04.003.

IPCC (2014), Climate Change 2014: Synthesis Report. Contribution of Working Groups I, II and III to the Fifth Assessment Report of the Intergovernmental Panel on Climate Change.

Jarihani, A. a., J. N. Callow, T. R. McVicar, T. G. Van Niel, and J. R. Larsen (2015), Satellite-derived Digital Elevation Model (DEM) selection, preparation and correction for hydrodynamic modelling

in large, low-gradient and data-sparse catchments, *J. Hydrol.*, *524*, 489–506, doi:10.1016/j.jhydrol.2015.02.049.

Javernick, L., J. Brasington, and B. Caruso (2014), Modeling the topography of shallow braided rivers using Structure-from-Motion photogrammetry, *Geomorphology*, *213*, 166–182, doi:10.1016/j.geomorph.2014.01.006.

Jia, G. J. (2003), Greening of arctic Alaska, 1981–2001, *Geophys. Res. Lett.*, *30*(20), 3–6, doi:10.1029/2003GL018268.

Jorgenson, M. T., M. Kanevskiy, Y. Shur, N. Moskalenko, D. R. N. Brown, K. Wickland, R. Striegl, and J. Koch (2015), Journal of Geophysical Research : Earth Surface, , 1–18, doi:10.1002/2015JF003602.Received.

Kasischke, E.S., et al. (2014), A Concise Experiment Plan for the Arctic-Boreal Vulnerability Experiment, *http://above.nasa.gov/acep/acep_final_pdf.pdf. Accessed 1/25/2015.*

Keenan, T. F. et al. (2014), Tracking forest phenology and seasonal physiology using digital repeat photography : a critical assessment, , *24*(6), 1478–1489.

Komarkova, V., and Webber, P. J. (1980), Two Low Arctic Vegetation Maps near Atkasook , Alaska, , *12*(4), 447–472.

Krivoruchko, K. (2004), Introduction to Modeling Spatial Processes Using Geostatistcal Analyst, *Esri*, 1–27.

Kurc, S. a., and L. M. Benton (2010), Digital image-derived greenness links deep soil moisture to carbon uptake in a creosotebush-dominated shrubland, *J. Arid Environ.*, *74*(5), 585–594, doi:10.1016/j.jaridenv.2009.10.003.

Laidler, G. J., P. M. Treitz, and D. M. Atkinson (2008), Remote Sensing of Arctic Vegetation : Relations between the NDVI , Spatial Resolution and Vegetation Cover on Boothia Peninsula , Nunavut Author (s): Gita J . Laidler , Paul M . Treitz and David M . Atkinson Published by : Arctic Institute of North Amer, , *61*(1), 1–13.

Lara, M. J., a. D. McGuire, E. S. Euskirchen, C. E. Tweedie, K. M. Hinkel, A. N. Skurikhin, V. E. Romanovsky, G. Grosse, W. R. Bolton, and H. Genet (2014), Polygonal tundra geomorphological change in response to warming alters future CO 2 and CH 4 flux on the Barrow Peninsula, *Glob. Chang. Biol.*, (August), n/a-n/a, doi:10.1111/gcb.12757.

Lassueur, T., S. Joost, and C. F. Randin (2006), Very high resolution digital elevation models: Do they improve models of plant species distribution?, *Ecol. Modell.*, *198*(1–2), 139–153, doi:10.1016/j.ecolmodel.2006.04.004.

Leberl, F., a Irschara, T. Pock, P. Meixner, M. Gruber, S. Scholz, and a Wiechert (2010), Point Clouds: Lidar versus 3D Vision, *Photogramm. Eng. Remote Sens.*, *76*(10), 1123–1134, doi:0099-1112/10/7610–1123.

Lefsky, M. a, W. B. Cohen, G. G. Parker, and J. David (2014), Lidar Remote Sensing for Ecosystem Studies, , *52*(1), 19–30.

Li, Z. (2014), Watershed modeling using arc hydro based on DEMs: a case study in Jackpine watershed, *Environ. Syst. Res.*, *3*(1), 11, doi:10.1186/2193-2697-3-11.

Liljedahl, A.K., Hinzman, L.D., Schulla, J. (2012), Ice-Wedge Polygon Type Controls Low-Gradient Watershed-Scale Hydrology,

Liljedahl, A. K. et al. (2016), Pan-Arctic ice-wedge degradation in warming permafrost and influence on tundra hydrology, *Nat. Geosci.*, *9*(April), 312–318, doi:10.1038/ngeo2674.

Lin, D. H., D. R. Johnson, C. Andresen, and C. E. Tweedie (2012), High spatial resolution decade-time scale land cover change at multiple locations in the Beringian Arctic (1948–2000s), *Environ. Res. Lett.*, *7*(2), 25502, doi:10.1088/1748-9326/7/2/025502.

Liu, H. Q., and A. Huete (1995), Feedback based modification of the NDVI to minimize canopy background and atmospheric noise, *IEEE Trans. Geosci. Remote Sens.*, *33*(2), 457–465, doi:10.1109/36.377946.

Liu, Z. L. Z., S. C. S. Cui, and Q. Y. Q. Yan (2008), Building extraction from high resolution satellite imagery based on multi-scale image segmentation and model matching, *2008 Int. Work. Earth Obs. Remote Sens. Appl.*, doi:10.1109/EORSA.2008.4620321.

Lucht, W. (2002), Climatic Control of the High-Latitude Vegetation Greening Trend and Pinatubo Effect, *Science (80-.).*, *296*(5573), 1687–1689, doi:10.1126/science.1071828.

Marzolff, I., J. B. Ries, and K. D. Albert (2002), Kite aerial photography for gully monitoring in sahelian landscapes, , 18–20.

McCune, B., and Grace, J. . (2002), Analysis of Ecological Communities, *MjM Softw. Des. Gleneden Beach, McKinney M.L*, *127*(January 2002), 247–260, doi:10.1016/S0022-0981(03)00091-1.

Menzel, a, and P. Fabian (1999), Growing season extended in Europe, *Nature*, *397*(6721), 659, doi:10.1038/17709.

Migliavacca, M. et al. (2011), Using digital repeat photography and eddy covariance data to model grassland phenology and photosynthetic CO2 uptake, *Agric. For. Meteorol.*, *151*(10), 1325–1337, doi:10.1016/j.agrformet.2011.05.012.

Myneni, R. B., C. D. Keeling, C. J. Tucker, G. Asrar, and R. R. Nemani (1997), Increased plant growth in the northern high latitudes from 1981 to 1991, *Nature*, *386*(6626), 698–702, doi:10.1038/386698a0.

Nelson, F. E., S. I. Outcalt, J. Brown, N. I. Shiklomanov, and K. M. Hinkel (1998), Spatial and Temporal Attributes of the Active-Layer Thickness Record, Barrow, Alaska, U.S.A., , (55), 797–802.

Nelson, S. and (2015), Circumpolar Active Layer Monitoring (CALM) Program, *Natl. Snow Ice Data Cent.*, 1–3.

Noh, M.-J., and I. M. Howat (2015a), Automated stereo-photogrammetric DEM generation at high latitudes: Surface Extraction with TIN-based Search-space Minimization (SETSM) validation and demonstration over glaciated regions, *GIScience Remote Sens.*, *1603*(June 2015), 1–20, doi:10.1080/15481603.2015.1008621.

Noh, M.-J., and I. M. Howat (2015b), Automated stereo-photogrammetric DEM generation at high latitudes: Surface Extraction with TIN-based Search-space Minimization (SETSM) validation and demonstration over glaciated regions, *GIScience Remote Sens.*, *1603*(June 2015), 1–20, doi:10.1080/15481603.2015.1008621.

Oberbauer, S. F. et al. (2007), Tundra CO2 fluxes in response to experimental warming across lattitudinal and moisture gradients, *Ecol. Monogr.*, *77*(2), 221–238, doi:10.1890/06-0649.

Oberbauer, S. F. et al. (2013a), Phenological response of tundra plants to background climate variation tested using the International Tundra Experiment,

Oberbauer, S. F. et al. (2013b), Phenological response of tundra plants to background climate variation tested using the International Tundra Experiment., *Philos. Trans. R. Soc. Lond. B. Biol. Sci.*, *368*(1624), 20120481, doi:10.1098/rstb.2012.0481.

Oberbauer, S. F. et al. (2013c), Phenological response of tundra plants to background climate variation tested using the International Tundra Experiment., *Philos. Trans. R. Soc. Lond. B. Biol. Sci.*, *368*(1624), 20120481, doi:10.1098/rstb.2012.0481.

Olivas, P. C., S. F. Oberbauer, C. E. Tweedie, W. C. Oechel, and A. Kuchy (2010), Responses of CO2 flux components of Alaskan Coastal Plain tundra to shifts in water table, *J. Geophys. Res. Biogeosciences*, *115*(4), 1–13, doi:10.1029/2009JG001254.

Osterkamp, T. E., M. . Jorgenson, E. A. G. Schuur, Y. L. Shur, M. . Kanevskiy, J. G. Vogel, and V. E. Tumskoy (2009), Physical and Ecological Changes Associated with Warming Permafrost and Thermokarst in Interior Alaska, *Permafr. Periglac. Process.*, *136*(January), 107–136, doi:10.1002/ppp.

Painter, S. L., J. D. Moulton, and C. J. Wilson (2012), Modeling challenges for predicting hydrologic response to degrading permafrost, *Hydrogeol. J.*, *21*(Hydrogeology of Cold Regions), 221–224, doi:10.1007/s10040-012-0917-4.

Park, H., Y. Kim, and J. S. Kimball (2016), Widespread permafrost vulnerability and soil active layer increases over the high northern latitudes inferred from satellite remote sensing and process model assessments, *Remote Sens. Environ.*, *175*, 349–358, doi:10.1016/j.rse.2015.12.046.

Peichl, M., O. Sonnentag, and M. B. Nilsson (2014), Bringing Color into the Picture: Using Digital Repeat Photography to Investigate Phenology Controls of the Carbon Dioxide Exchange in a Boreal Mire, *Ecosystems*, *18*(1), 115–131, doi:10.1007/s10021-014-9815-z.

Penuelas, J., I. Filella, J. A. Gamon, B. Y. J. Penuelas, I. Filella, and A. Gamon (1995), Assessment of photosynthetic radiation-use efficiency with spectral reflectance, , *131*(3), 291–296.

Post, E. et al. (2009), Ecological dynamics across the Arctic associated with recent climate change., *Science*, *325*(5946), 1355–1358, doi:10.1126/science.1173113.

Raaflaub, L. D., and M. J. Collins (2006), The effect of error in gridded digital elevation models on the estimation of topographic parameters, *Environ. Model. Softw.*, *21*(5), 710–732, doi:10.1016/j.envsoft.2005.02.003.

Rango, A., A. Laliberte, and C. Winters (2008), Role of aerial photos in compiling a long-term remote sensing data set, *J. Appl. Remote Sens.*, *2*(1), 23541, doi:10.1117/1.3009225.

Raynolds, M. K., J. C. Comiso, D. A. Walker, and D. Verbyla (2008), Relationship between satellite-derived land surface temperatures, arctic vegetation types, and NDVI, *Remote Sens. Environ.*, *112*(4), 1884–1894, doi:10.1016/j.rse.2007.09.008.

Richardson, A. D., J. P. Jenkins, B. H. Braswell, D. Y. Hollinger, S. V. Ollinger, and M. L. Smith (2007), Use of digital webcam images to track spring green-up in a deciduous broadleaf forest, *Oecologia*, *152*(2), 323–334, doi:10.1007/s00442-006-0657-z.

Richardson, A. D., B. H. Braswell, D. Y. Hollinger, J. P. Jenkins, and S. V. Ollinger (2009), Near-surface remote sensing of spatial and temporal variation in canopy phenology, *Ecol. Appl.*, *19*(6), 1417–1428, doi:10.1890/08-2022.1.

Richardson, A. D., T. F. Keenan, M. Migliavacca, Y. Ryu, O. Sonnentag, and M. Toomey (2013), Climate change, phenology, and phenological control of vegetation feedbacks to the climate system, *Agric. For. Meteorol.*, *169*, 156–173, doi:10.1016/j.agrformet.2012.09.012.

Rondeaux, G., M. Steven, and F. Baret (1996), Optimization of Soil-Adjusted Vegetation Indices, , *107*(August 1994), 95–107.

Rosnell, T., and E. Honkavaara (2012), Point cloud generation from aerial image data acquired by a quadrocopter type micro unmanned aerial vehicle and a digital still camera, *Sensors*, *12*(1), 453–480, doi:10.3390/s120100453.

Saitoh, T. M., S. Nagai, N. Saigusa, H. Kobayashi, R. Suzuki, K. N. Nasahara, and H. Muraoka (2012), Assessing the use of camera-based indices for characterizing canopy phenology in relation to gross primary production in a deciduous broad-leaved and an evergreen coniferous forest in Japan, *Ecol. Inform.*, *11*, 45–54, doi:10.1016/j.ecoinf.2012.05.001.

Schuur, E. et al. (2008), Vulnerability of Permafrost Carbon to Climate Change : Implications for the Global Carbon Cycle, *Bioscience*, *58*(8), 701–714.

Schwartz, M. D. (1998), Green-wave phenology, *Nature*, *394*, 839–840, doi:10.1038/29670.

Screen, J. a, and I. Simmonds (2010), The central role of diminishing sea ice in recent Arctic temperature amplification., *Nature*, *464*(7293), 1334–1337, doi:10.1038/nature09051.

Shaver, G. R., L. E. Street, E. B. Rastetter, M. T. Van Wijk, and M. Williams (2007), Functional convergence in regulation of net CO_2 flux in heterogeneous tundra landscapes in Alaska and Sweden, *J. Ecol.*, *95*(4), 802–817, doi:10.1111/j.1365-2745.2007.01259.x.

Sims, D. A., and J. A. Gamon (2002), Relationships between leaf pigment content and spectral reflectance across a wide range of species , leaf structures and developmental stages, , *81*, 337–354.

Smith, L. C., Y. Sheng, G. M. Macdonald, and L. D. Hinzman (2005), Disappearing Arctic lakes, , *XXX*(June), 2005.

Snavely, N., S. M. Seitz, and R. Szeliski (2008), Modeling the world from Internet photo collections, *Int. J. Comput. Vis.*, *80*(2), 189–210, doi:10.1007/s11263-007-0107-3.

Solano, R., K. Didan, A. Jacobson, and A. Huete (2010), MODIS Vegetation Index User ' s Guide (MOD13 Series), , *2010*(May).

Sommerkorn, M. (2008), Micro-topographic patterns unravel controls of soil water and temperature on soil respiration in three Siberian tundra systems, *Soil Biol. Biochem.*, *40*(7), 1792–1802, doi:10.1016/j.soilbio.2008.03.002.

Steinwand, D. A., J. A. Hutchinson, and J. P. Snyder (1995), Map Projections for Global and Continental Data Sets and an Analysis of Pixel Distortion Caused by Reprojection, *Photogrammatic Eng. Remote Sens.*, *61*(12), 1487–1497.

Stewart, K. J., P. Grogan, D. S. Coxson, and S. D. Siciliano (2014), Topography as a key factor driving atmospheric nitrogen exchanges in arctic terrestrial ecosystems, *Soil Biol. Biochem.*, *70*(3), 96–112, doi:10.1016/j.soilbio.2013.12.005.

Stow, D. a. et al. (2004), Remote sensing of vegetation and land-cover change in Arctic Tundra Ecosystems, *Remote Sens. Environ.*, *89*(3), 281–308, doi:10.1016/j.rse.2003.10.018.

Streletskiy, D. A., N. I. Shiklomanov, F. E. Nelson, and A. E. Klene (2007), 13 Years of Observations at Alaskan CALM Sites: Long-term Active Layer and Ground Surface Temperature Trends, *Proc. 9th Int. Conf. Permafr.*, 1–6.

Sullivan, P. F., S. J. T. Arens, R. A. Chimner, and J. M. Welker (2008), Temperature and microtopography interact to control carbon cycling in a high arctic fen, *Ecosystems*, *11*(1), 61–76, doi:10.1007/s10021-007-9107-y.

Sumerling, G. (2011), Lidar Analysis in ArcGIS ® 10 for Forestry Applications, *ESRI White Pap.*, (January), 53.

Tape, K., M. Sturm, and C. Racine (2006), The evidence for shrub expansion in Northern Alaska and the Pan-Arctic, *Glob. Chang. Biol.*, *12*(4), 686–702, doi:10.1111/j.1365-2486.2006.01128.x.

Throckmorton, H. M. et al. (2016), Active layer hydrology in an arctic tundra ecosystem: Quantifying water sources and cycling using water stable isotopes, *Hydrol. Process.*, *4986*(August), 4972–4986, doi:10.1002/hyp.10883.

Torre Jorgenson, M. et al. (2013), Reorganization of vegetation, hydrology and soil carbon after permafrost degradation across heterogeneous boreal landscapes, *Environ. Res. Lett.*, *8*(3), 35017, doi:10.1088/1748-9326/8/3/035017.

Triggs, B., P. F. McLauchlan, R. I. Hartley, and A. W. Fitzgibbon (2000), Bundle Adjustment — A Modern Synthesis, *Vis. Algorithms Theory Pract.*, *1883*, 298–372, doi:10.1007/3-540-44480-7_21.

Tucker, C. J. (1978), Red and Photographic Infrared Linear Combinations for Monitoring Vegetation,

Tucker, C. J. (1999), Higher Northern Latitude NDVI and Growing Season Trends from 1982 to 1999,

Tucker, C. J., and P. J. Sellers (2007), Satellite remote sensing of primary production, *Int. J. Remote Sens.*, *7*(11), 1395–1416, doi:10.1080/01431168608948944.

Usery, E. L., M. P. Finn, J. D. Cox, S. Ruhl, M. Bearden, E. L. Usery, M. P. Finn, J. D. Cox, and T. Beard (2003), Projecting global datasets to achieve equal areas, , *30*(1), 69–79.

Ustin, S. L., and J. A. Gamon (2010), Tansley review Remote sensing of plant functional types, , 795–816.

Vaze, J., J. Teng, and G. Spencer (2010), Impact of DEM accuracy and resolution on topographic indices, *Environ. Model. Softw.*, *25*(10), 1086–1098, doi:10.1016/j.envsoft.2010.03.014.

Villarreal, S., R. D. Hollister, D. R. Johnson, M. J. Lara, P. J. Webber, and C. E. Tweedie (2012), Tundra vegetation change near Barrow, Alaska (1972–2010), *Environ. Res. Lett.*, *7*(1), 15508, doi:10.1088/1748-9326/7/1/015508.

Vorosmarty, C. J., a. D. McGuire, and J. E. Hobbie (2010), Scaling Studies in Arctic System Science and Policy Support: A Call to Research, *U.S. Arct. Res. Comm.*, 76 pages.

Vörösmarty, C. J., L. D. Hinzman, B. J. Peterson, D. H. Bromwich, L. C. Hamilton, J. Morison, V. E. Romanovsky, M. Sturm, R. S. Webb, and D. L. Kane (2001), The Hydrologic Cycle and its Role in Arctic and Global Environmental Change: A Rationale and Strategy for Synthesis Study The Hydrologic Cycle and its Role in Arctic and Global Environmental Change, *NSF-ARCSS Hydrol. Work. Steer. Comm.*, *84*(September).

Walker, D. a et al. (2012), Environment, vegetation and greenness (NDVI) along the North America and Eurasia Arctic transects, *Environ. Res. Lett.*, *7*(1), 15504, doi:10.1088/1748-9326/7/1/015504.

Walker, M., and C. Wahren (2006), Plant community responses to experimental warming across the tundra biome, *Proc. …*, *103*(5), 1342–6, doi:10.1073/pnas.0503198103.

Ward, R. D., N. G. Burnside, C. B. Joyce, and K. Sepp (2013), The use of medium point density LiDAR elevation data to determine plant community types in Baltic coastal wetlands, *Ecol. Indic.*, *33*, 96–104, doi:10.1016/j.ecolind.2012.08.016.

Webber, P. J., and M. D. Walker (1991), The International Tundra Experiment (ITEX): Resolution, , 1990.

Wehr, A., and U. Lohr (1999), Airborne laser scanning—an introduction and overview, *ISPRS J. Photogramm. Remote Sens.*, *54*(2–3), 68–82, doi:10.1016/S0924-2716(99)00011-8.

Westergaard-Nielsen, A., M. Lund, B. U. Hansen, and M. P. Tamstorf (2013), Camera derived vegetation greenness index as proxy for gross primary production in a low Arctic wetland area, *ISPRS J. Photogramm. Remote Sens.*, *86*, 89–99, doi:10.1016/j.isprsjprs.2013.09.006.

Westoby, M. J., J. Brasington, N. F. Glasser, M. J. Hambrey, and J. M. Reynolds (2012), "Structure-from-Motion" photogrammetry: A low-cost, effective tool for geoscience applications, *Geomorphology*, *179*, 300–314, doi:10.1016/j.geomorph.2012.08.021.

Wilson, J. P. (2012), Digital terrain modeling, *Geomorphology*, *137*(1), 107–121, doi:10.1016/j.geomorph.2011.03.012.

Wu, S., J. Li, and G. H. Huang (2008), A study on DEM-derived primary topographic attributes for hydrologic applications: Sensitivity to elevation data resolution, *Appl. Geogr.*, *28*(3), 210–223, doi:10.1016/j.apgeog.2008.02.006.

Zeng, H., G. Jia, and H. Epstein (2011), Recent changes in phenology over the northern high latitudes detected from multi-satellite data, *Environ. Res. Lett.*, *6*(4), 45508, doi:10.1088/1748-9326/6/4/045508.

Zhang, Z., D. L. Kane, and L. D. Hinzman (2000), Development and application of a spatially-distributed arctic hydrological and thermal process model (ARHYTHM), *Hydrol. Process.*, *14*(6), 1017–1044, doi:10.1002/(SICI)1099-1085(20000430)14:6<1017::AID-HYP982>3.0.CO;2-G.

Zona, D., D. A. Lipson, R. C. Zulueta, S. F. Oberbauer, and W. C. Oechel (2011), Microtopographic controls on ecosystem functioning in the Arctic Coastal Plain, *J. Geophys. Res. Biogeosciences*, *116*(3), 1–12, doi:10.1029/2009JG001241.

Chapter 5: Multi-temporal Comparison of Primary Productivity (NDVI) Across High Arctic Tundra Landscapes as Observed From Multi-scale Optical Sensing Platforms

5.1 INTRODUCTION

High arctic tundra ecosystems are undergoing dramatic impacts from climate warming. Impacts are altering ecosystem properties and processes that includes permafrost degradation (*Torre Jorgenson et al.,* 2013) and a deepening of thaw depth (*Schuur et al.,* 2008), surface hydrological change (*Smith et al.,* 2005; *Andresen and Lougheed*, 2015), increases in surface temperature and precipitation (*ACIA*, 2004a) and evapotranspiration (*IPCC*, 2014), shifts in plant community composition (*Villarreal et al.,* 2012) and distribution (*Tape et al.,* 2006; Lin et al. 2011), and ecosystem function (*Oberbauer et al.*, 2007; *Gamon et al.*, 2012; Lara et al., 2012). The Arctic plays an important role in Earth System processes where feedbacks from climate change impacts in the arctic have been shown to positively enhance global warming (*Screen and Simmonds*, 2010) , and shift regional hydrological cycles (*Vörösmarty et al.*, 2001; *Andresen and Lougheed*, 2015). Results from long-term monitoring (*Henry, G. H R and Molau*, 1997; *Oberbauer et al.*, 2013), experimental studies (*Hollister and Flaherty*, 2010; *Goswami et al.*, 2011; *Lin et al.*, 2012; *Lara et al.*, 2014; *Andresen and Lougheed*, 2015), and modeling (*Oberbauer et al.*, 2007; *Olivas et al.*, 2010) suggest such change can catalyze further shifts in tundra ecosystem structure and function that has the potential to positively enhance greenhouse warming and alter regional biodiversity. Additionally, arctic plant communities and their responses to warming trends are poorly understood and often differ across multiple spatial scales (*Boelman et al.*, 2003; *Stow et al.*, 2004; *Vorosmarty et al.*, 2010). Aberrances appear to be related to landscape heterogeneity (*Gamon et al.*, 2012b), microtopography (*Vargas et al. in prep. Biasi et al.*, 2017) and to ecological factors like plant species interactions.

Over the past couple of decades, plant phenology has become increasingly acknowledged as modeling studies began to demonstrate how phenology can not only be sensitive to year-to-year variability but also could serve as an indicator of long-term responses of terrestrial ecosystems to climate change (*Schwartz*, 1998; *Menzel and Fabian*, 1999; *Bradley et al.*, 1999). Phenology varies greatly over vast geographic extents depending on climate zones and land cover types as well as at smaller spatial scales, such as between vegetation communities and by species (*Cleland et al.*,

2007; *Richardson et al.*, 2013). The phenological trends of arctic tundra has been observed at multiple spatial scales including the species level (*Hollister*, 2003; *Oberbauer et al.*, 2013a), plot level (*Huemmrich et al*. 2013), landscape (*Boelman et al.*, 2011), and regional to circum-arctic scales using satellite remote sensing approaches that span multiple spatial scales (*Lucht*, 2002; *Stow et al.*, 2004; *Laidler et al.*, 2008; *Raynolds et al.*, 2008; *Bhatt et al.*, 2010), however all approaches have limitations. Plot-level efforts have focused on tracking seasonal and inter-annual shifts in species and plant communities but are generally limited in their capacity to quantify these changes at larger spatial scales. Small-scale plot level efforts are also labor intensive (*Hollister et al.*, 2005; *Richardson et al.*, 2007) and can lack spectral and other metrics that are otherwise important for linking to studies using remote sensing methods that examine larger spatial scales (*Goetz et al.*, 2005; *Post et al.*, 2009; *Boelman et al.*, 2011; *Epstein et al.*, 2012; *Gamon et al.*, 2013). Additionally, these approaches typically represent responses at small scales and few studies have examined how such small scale processes scale to larger spatial scales (sensu Goswami et al. 2011). Time-series satellite imagery and spectral analyses has been used to demonstrate the capacity of early season shifts in phenology or increases in vegetation biomass at large regional scales across the Arctic (*Myneni et al.*, 1997; *Tucker*, 1999; *Delbart et al.*, 2006) but have generally not been linked to ground-based observations of changes in plant community composition or structure and/or the timing of plant species pheno-phase development (*sensu* Bhatt et al. 2010), and can be compromised by the persistent cloud cover and weather characteristics of the Arctic (*Stow et al.*, 2004). Satellite approaches can fill the limiting spatial scale gap of plot-level studies by capturing responses at regional to global scales but the thematic content is lost and resolution is generally compromised.

Several studies have shown the ability of satellite and airborne data to extract biophysical parameters of Arctic tundra using vegetation indices derived from spectroscopy such as the popular normalized difference vegetation index (NDVI) (*Vierling et al.*, 1997; *Stow et al.*, 2004; *Huemmrich et al.*, 2010; *Epstein et al.*, 2012). These indices are mathematical compressions of reflectance spectra in the regions of sensed wavelengths which are represented by one value. NDVI is an important input for regional and global climate models, vegetation productivity models, and land/atmosphere energy flux models. Spaceborne observations (i.e. Moderate Resolution Imaging Spectroradiometer (MODIS) and Advanced Very High Resolution Radiometer (AVHRR)) of tundra ecosystem NDVI has indicated that circum-arctic vegetation productivity or "greenness"

has increased during the long-term satellite record (*Jia*, 2003; *Bhatt et al.*, 2013). The majority of spaceborne platforms utilize pointed or wide imaging swaths to collect land surface data and thus, are directly influenced by the bidirectional reflectance distribution function (BRDF) which can result in significant changes to surface reflectance spectra that can in some cases lead to miscalculation of land surface productivity, structure and function. Implementing the spectro-directional domain of reflectance data has been shown to improve upon the accuracy of shrub canopy mapping (*Selkowitz*, 2010) as well as improve upon biomass estimation (*Buchhorn et al.*, 2016), which could assist in monitoring arctic ecosystems and ultimately improve upon modeling of landscape and global processes.

Large knowledge gaps remain for how arctic vegetated surfaces significantly reflect and absorb incoming solar radiation, however, because the majority of existing studies have focused on ground-based measurements and few have explored the spectro-directional reflectance characteristics of remote sensing approaches. These types of parameters vary across spatial scales, across vegetation types, and over time and can easily be misinterpreted. There is also an emerging need for cross-validation of multi-scale sampling approaches that are focused on understanding phenological patterns and change trends in the Arctic using mid-altitude airborne-spectroscopy that link similar plot to landscape scale approaches. This study focuses on exploring the capacity of different remote sensing approaches that span multiple spatial, temporal and spectral resolutions in an effort to assess their relative strengths, weaknesses and optimal use.

5.2 OBJECTIVES

The primary objective of this study is to evaluate the relative effectiveness of multiple optical sensors and ground to satellite sampling platforms for capturing seasonal trends in the vegetation phenology of high-arctic tundra plant communities. For this study, spectrometer-derived vegetation indices along with indices derived from the red, green and blue (RGB) color spaces acquired from digital cameras were used as proxies of vegetation biomass and productivity, which previous studies have shown to be strongly correlated in a range of ecosystems including desert shrub lands (*Kurc and Benton*, 2010), alpine grassland (*Migliavacca et al.*, 2011), forests (*Richardson et al.*, 2009; *Keenan et al.*, 2014), and low-arctic tundra (*Westergaard-Nielsen et al.*, 2013; *Beamish et al.*, 2016). Specifically RGB indices were acquired from time-lapse digital

cameras or Pheno-cams and by kite aerial photography (KAP), as well as from plot-level spectrometers (UNISPEC) across multiple spatial and temporal scales.

5.3 MATERIALS AND METHODS

5.3.1 Study area

All optical measurements were conducted as part of the Arctic Observing Network's International Tundra Experiment (AON-ITEX) initiative and took place along the Mobile Instrumented Sensor Platform (MISP) sites and Circumpolar Active Layer Monitoring (CALM) subset grids located near the towns of Utqiagvik (71°18'N, 156°40'W) and Atqasuk (70°29'N, 157°25'W) in northern Alaska (Figure 5.1 and 5.2). Table 5.1 shows a summary the vegetation types, classes, landform types and dominant species present at each plot with the CALM grids and MISP transects in both Utqiaġvik and Atqasuk.

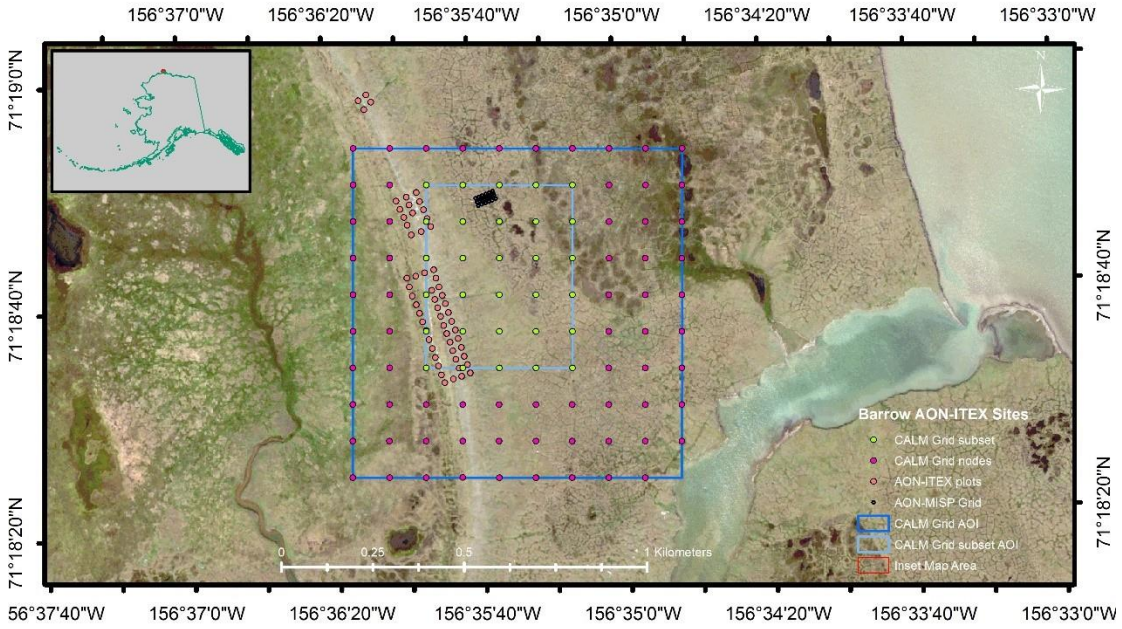

Figure 5.1: True color World View 2 image captured during the summer of 2013 displaying location of the Utqiaġvik AON-ITEX sites including ITEX warming plots, MISP grid, CALM grid and study subset, with corresponding nodes and areas of interest. All maps are projected to the NAD83 UTM zone 4 datum.

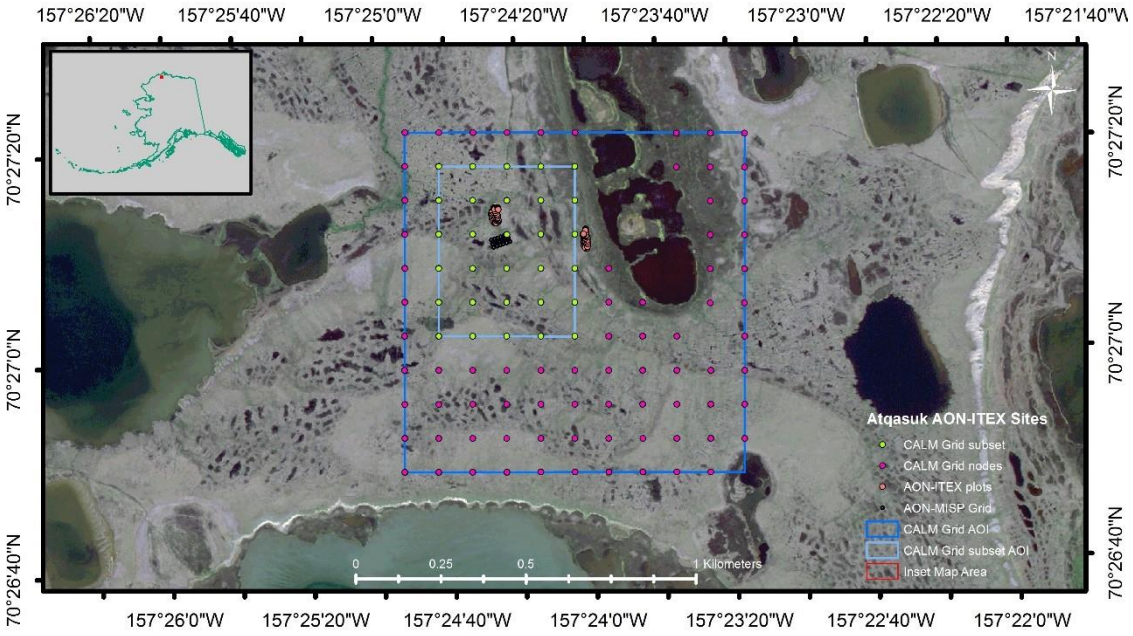

Figure 5.2: True color World View 2 image captured during the summer of 2013 displaying location of the Atqasuk AON-ITEX sites including ITEX warming plots, MISP grid, CALM grid and study subset, with corresponding nodes and areas of interest. All maps are projected to the NAD83 UTM zone 4 datum.

Table 5.1: Summary of the MISP transects and CALM plots present at Utqiaġvik and Atqasuk. The vegetation types and classes, wetland names, dominant species and landform types selected were based on Lin et al. (2011), Webber, (1980), Healey et al., (2014), and Andresen et al. in prep.

Parameters	Barrow					Atqasuk				
Vegetation Type	Dry Heath/ Mesic Heath		Moist Meadow	Wet Meadow		Dry Heath/ Mesic Heath	Moist Meadow		Wet Meadow	
Wetland Name	Dry dwarf shrub graminoid tundra	Dry-moist dwarf shrub graminoid tundra	Moist graminoid tundra	Seasonally flooded gramonoid tundra	Wet graminoid tundra	Dry shrub graminoid tundra	Moist graminoid tundra	Moist shrub graminoid tundra	Wet graminoid tundra	Aquatic graminoid tundra
Vegetation Class	Dry shrub	Dry-moist shrub-gram	Moist gram	Seasonally flooded	Wet gram	Dry	Moist	Moist shrub	Wet	Aquatic
Dominant Species	*Salix pulchra, Lazula arctica*	*Eriophorum spp.*	*Carex aquatilis/stans*	*pleaurocarpous mosses/ Arctophila fulva*	*Arctophila fulva*	*Cassiope tetragona*	*Vaccinium Vitis-idaea*	*Salix pulchra*	*Carex aquatilis*	*Arctophila fulva*
Landform Type	High center polygon/ Stabilized sand dune	High center polygon	Low center polygon/ low land	Marsh	Pond/lake	Stabilized sand dune/ snow patch	High center polygon	Low center polygon/low land	Marsh	Pond/lake
Mean Peak Season VWC (%)	42	35.4	55.8	70.5	63.5	30.6	31.03	40.1	59.3	49.8
Elevation (MASL)	3					30				
Mean Annual Temperature (°C)	-12.6					-11.9				
Mean July Temperature (°C)	3					7.2				
Average Maximum Thaw Depth (cm)	35-39					36-75+				

5.3.2 Data collection

5.3.2.1 Spectral reflectance and RGB images

All field sampling was executed by Systems Ecology Laboratory (SEL) researchers from the University of Texas at El Paso (UTEP) at all sampling locations during the snow-free growing periods between 2010 and 2015. Ground-based spectral reflectance measurements were acquired over all plots within the MISP (weekly) and CALM grids (every other week) using a dual-channel mobile field spectrometer (UniSpec DC, PP Systems, Amesbury MA, USA). This system allows for simultaneous radiance and irradiance measurements following dark current and white panel measurements, which permit calibrated reflectance measurements of targets. Reflectance spectra were used to quantify a gamut of spectral vegetation indices that included the Normalized Difference Vegetation Index (NDVI) (*Tucker*, 1978), Mean Simple Ratio (MSR) (*Sims and Gamon*, 2002), Modified Normalized Difference Vegetation Index (MNDVI) (*Liu and Huete*, 1995) and Structure Independent Pigment Index (SIPI) (*Penuelas et al.*, 1995). Please refer to chapters 2 and 3 for a detailed description of the spectrometer used in this study. Additionally, reflectance data was collected across each MISP transect using a mobile suite of sensors suspended from cables and processed to yield seasonal NDVI values by researchers from Florida International University (FIU). Please refer to *Healey et al.*, 2014 for more information on MISP data collection and processing methodologies acquired from the robotic sensor system.

The RGB digital imagery of the MISP transect were acquired from two platforms, namely a Kite aerial photography (KAP) system and Pheno-cams. KAP images were acquired roughly every week at ~ 60 meters above the MISP transects. The Pheno-cams were programmed to capture scenes every hour, however weather and logistical limitations impacted the frequency distribution of image capture in some cases. A full description of the KAP system and Pheno-cams is provided in Section 1 and 2. A slightly different approach was used for monitoring the CALM grid subset plots. For these, plot-level images (PLIs) were acquired at 1-2 meters off the ground with a NADIR view every two weeks using the same *Panasonic Lumix DMC-TS3* digital camera used for KAP image acquisitions.

NASA's MODIS sensor on board the Terra satellite provided all satellite-derived land surface products used in this study. MODIS has become amongst the most common and well-used satellite platforms for the assessment of ecosystem properties at regional to global scales and

represents the penultimate challenge for linking ground-based observations with satellite platforms (*Gao and Huete*, 2000; *Bhatt et al.*, 2010; *Gamon et al.*, 2013). MODIS NDVI time-series data was selected based on the location of dominant vegetation classes across landscapes in Utqiaġvik and Atqasuk using the *Global Subsets Tool: MODIS Collection 6 Land Products* (https://modis.ornl.gov/cgi-bin/MODIS/global/subset.pl). This tool was made available by the Oakridge National Laboratory and serves the purpose of extracting time-series of MODIS land surface products. These products yield a 16-day composite of NDVI at a 250 meter spatial resolution. Time series imagery was chosen for dates between early June and late August yielding averages for six exact dates (DOY: 161, 177, 193, 209, 225, and 241) for summers 2010-2015. This approach facilitated the comparison with comparable time-series data derived from RGB and spectrometer-derived plot level data as previously described above. Table 5.2 depicts the calculated spectral and RGB indices calculated for this study.

Table 5.2: List of indices used in this study with corresponding equations and references. Digital camera formulas refer to the camera color channel information (digital numbers; DNs) while the spectrometer-derived formulas pertain to the reflectance wavelength (nm).

Platform	Index Name	Index	Formula	Reference
Digital Camera	Green Excess	GEI	$2 * G_{DN} - (R_{DN}+B_{DN})$	Richardson et al., 2007
Digital Camera	Red digital number	Red DN	R_{DN}	Richardson et al., 2007
Digital Camera	Green digital number	Green DN	G_{DN}	Richardson et al., 2007
Digital Camera	Blue digital number	Blue DN	B_{DN}	Richardson et al., 2007
Digital Camera	Total digital number	Total RGB	$(R_{DN} + G_{DN} + B_{DN})/3$	Richardson et al., 2007
Digital Camera	Percent red	%R	$(R_{DN})/(R_{DN}+G_{DN}+B_{DN})$	Richardson et al., 2007
Digital Camera	Percent green	%G	$(G_{DN})/(R_{DN}+G_{DN}+B_{DN})$	Richardson et al., 2007
Digital Camera	Percent blue	%B	$(B_{DN})/(R_{DN}+G_{DN}+B_{DN})$	Richardson et al., 2007
Digital Camera	Lightness	L*	**See Reference	Paschos, 2001
Digital Camera	A-red-green	A*	**See Reference	Paschos, 2001
Digital Camera	B-blue-yellow	B*	**See Reference	Paschos, 2001
Digital Camera	AnyColor	AnyColor	**See Reference	Paschos, 2001
Digital Camera	Hue	Hue	**See Reference	Paschos, 2001
Digital Camera	Saturation	Saturation	**See Reference	Paschos, 2001
Digital Camera	Value	Value	**See Reference	Paschos, 2001
Digital Camera	nNDVI	nNDVI	$(R_{DN}-G_{DN})/(R_{DN}+G_{DN})$	Ramirez et al., in prep
Digital Camera	Test	TEST(L*A*)	A*(1+(L*)/(255))	Ramirez et al., in prep
Spectrometer	Carotenoid 1	CRI1	(1/R510)-(1/R550)	Gitelson et al., 2002
Spectrometer	Carotenoid 2	CRI2	(1/R510)-(1/R700)	Gitelson et al., 2002
Spectrometer	Gitelson 4	Gitelson4	(1/R550)-(1/R750)	Gitelson et al., 2003
Spectrometer	Gitelson 5	Gitelson5	(1/R700)-(1/R800)	Gitelson et al., 2003
Spectrometer	Greenness 1	Green1	(R554/R675)	Huemmrich K.H., personal communication
Spectrometer	Modified Normalized Difference Vegetation Index	MNDVI	(R750-R705)/(R750+R705-(2*R445))	Liu and Huete, 1995
Spectrometer	Modified Simple Ratio	MSR	(R750-R445)/(R705-R445)	Sims and Gamon, 2002
Spectrometer	Normalized Difference Soil Water Index- linear	NDSWI-lin	(R460-R1000)/(R460+R1000)	Goswami et al., 2011
Spectrometer	Normalized Difference Soil Water Index- log	NDSWI-log	(log(R1000) - log(R460))/(log(R1000) + log(R460))	Goswami et al., 2011
Spectrometer	Normalized Difference Vegetation Index	NDVI	(R800-R680)/(R800+R680)	Tucker, 1978
Spectrometer	Optimized Soil Adjusted Vegetation Index	OSAVI	1.16*(R800-R670)/(R800+R670+0.16)	Rondeaux et al., 1996
Spectrometer	Photochemical Reflectance Index 2	PRI 2	(R530-R550)/(R530+R550)	Sims and Gamon, 2002
Spectrometer	Structure Independent Pigment Index	SIPI	(R800-R450)/(R800-R650)	Peñuelas et al., 1995
Spectrometer	Water Band Index	WBI	(R900/R970)	Claudio et al., 2006

5.3.2.2 Satellite imagery and land cover classification maps

High-resolution *Quickbird* imagery was acquired from *Manley et al.* (2006) and *DigitalGlobe* through the Polar Geospatial Center (PGC) and the University of Minnesota (U of M), and was used for this study to develop land cover classification maps of the study areas. Multiple cloud-free scenes from summer 2002 and 2008 were used to classify the Utqiaġvik area in order to cover the entire peninsula while only one localized scene from summer 2005 was used for the local Atqasuk area, which created a large difference in areas being analyzed for each site.

To maximize inter-comparison with ground-based spectral and RGB measurements, all satellite images utilized for this study were restricted to seasonal acquisitions between mid-June and mid-August around peak growing season. All scenes were orthorectified and corrected for radiometric, sensor, and geometric distortion by the provider.

The Utqiaġvik images were composed of four multispectral (2.4m) bands and one panchromatic (0.6m) band. All bands were fused using a principal components sharpening method in order to maintain spatial and spectral quality (*Vijayaraj et al*., 2006). Plot level species cover data from studies conducted in 1999 and 2010 as a contribution to the IBP-TBP efforts focused around the Utqiaġvik area along with a minimum distance algorithm and image stack described above, were used to train a supervised classification in ENVI (version 4.4). Post classification, a majority filter with a kernel size 3 by 3 meters was applied to the map in order to improve spatial alignment among the classes. The Atqasuk land cover classification employed a similar approach to that of *Lin et al.*(2012). Both land cover classification maps were created a number of years ago for the use on other studies (*Villarreal and Andresen,* 2012).

The Utqiaġvik map produced a total of ten vegetation classes, five of which were represented in the study areas. Four of the five land cover classes were represented for the study area in Atqasuk. To include the missing land cover class in Atqasuk (moist shrub tundra), a historical land classification map developed by *Komarkova and Webber*, (1980) was used to locate a suitable expanse of this land cover class within the study area for which MODIS NDVI data could be extracted. Table 5.3 shows the relation and fusion between the Atqasuk vegetation classes used in this study and those selected from the 1980 study as well as their dominant vascular plant taxa and landform types typically associated with each class.

Moreover, each seasonal MODIS NDVI time-series dataset was downloaded using the *USGS EarthExplorer* tool (https://earthexplorer.usgs.gov/) for both the Utqiaġvik and Atqasuk sampling areas across all years of this study, in order to further explore the delineation and location of each final MODIS pixel. A single MODIS peak season NDVI for 2015 (DOY 241) scene for both Utqiaġvik and Atqasuk were used to calculate area and percent cover of each vegetation class within each MODIS pixel sampled.

Table 5.3: Relationship between vegetation classes selected for the Atqasuk study area and those of the vegetation map created by Komarkova and Webber (1980) including dominant vascular plant taxa and landform typical of each class.

Veg Class	Vargas 2017 Vascular Taxa	Komarkova and Webber 1980 Vascular Taxa	Komarkova and Webber 1980 Landform
AQUATIC	*Arctophila Fulva*	*Arctophila Fulva*	Lake, pond
WET	*Carex Aquatilis*	*Carex Aquatilis*	Marsh
MOIST SHRUB	*Salix Pulchra*	*Salix Pulchra, Eriophorum Vaginatum, Carex Aquatilis*	Low-center polygon, low land
MOIST	*Vaccinium Vitis-idaea*	*Eriophorum Vaginatum, Carex Aquatilis*	High-center polygon
DRY	*Cassiope Tetragona*	*Cassiope Tetragona, Dryas Integrifolia*	Stabilized sand dune, snow patch

5.3.3 Data processing

5.3.3.1 Plot level vegetation classification

As part of this collaborative effort, researchers from Grand Valley State University (GVSU) collected plot level plant species cover data along both MISP transects during the 2011 summer field season, while similar plant community composition and structure data was collected across all CALM subset plots during the 2010 and 2012-2015 sampling periods. For more detailed field sampling methods please refer to chapters 2 and 3 of this dissertation. These data were employed to classify all plots into discrete vegetation classes by applying a Hierarchical Cluster Analysis using PC-ORD 6 statistical software (MjM Software Design Gleneden Beach, OR, USA). Sorensen's similarity coefficient was used with a flexible beta linkage method ($\beta = -0.25$) to minimize chaining (*McCune and Grace 2002*). A cutoff of less than 50% similarity for the Utqiaġvik communities and 55% for the Atqasuk plant communities was used to cluster these plots into suitable land cover classes that corresponded to land cover maps (see section 3.2.2).

5.3.3.2 Spectral and RGB vegetation indices

All raw spectral reflectance data collected in the field using the hand-held spectrometer was analyzed and processed using a custom software developed by the SEL called *rHyperSpec* (https://sel-jornada.shinyapps.io/rHyperSpec/). This software allows for quick visualization of raw radiance, irradiance and reference data acquired specifically from a *PP Systems Unispec DC* spectrometer and data QA/QC prior to the processing of reflectance indices. Additionally, this tool

provides an alternative to traditional processing approaches with faster processing times, added user functions and immediate calculation of a gamut of spectral indices suitable for the extraction of vegetation and water properties (*Laney,* 2012), (see Table 5.2, *spec*). Calculated indices were exported as a text file and averaged to yield one value per plot per field sampling date. Reflectance data acquired from the MISP robotic tram system were processed by FIU researchers to yield plot-level NDVI for both the Utqiaġvik and Atqasuk MISP transects. Final values were averaged to yield one value per MISP plot per field sampling day.

All plot-level and airborne digital images were visually checked for quality by removing those that were considered sub-par (i.e. blurry, distorted brightness values, cloud cover, condensation etc.). Gaps in the image time-series across all platforms were observed due to either poor weather conditions (i.e. high winds and water condensation) causing equipment malfunction of image distortion (i.e. Pheno-cams) or from sampling frequencies of the KAP and PLI approaches, which were acquired weekly to every-other week. Due to the different collection approaches used for each platform, all image datasets were processed slightly differently. For KAP, the two best kite images from each flight acquisition were chosen, while the number of images used for the Pheno-cams varied between four and six per day, aimed within 3 hours of solar noon. All images of the CALM subset plots were also acquired within 3 hours of solar noon and only one final image per acquisition date was selected for analysis. All digital imagery were analyzed and processed using the *Phenology Analyzer* software, developed within the Systems Ecology Laboratory (SEL) at the University of Texas at El Paso (UTEP) (*Ramirez, et al.* patent pending). Regions of interest (ROI) were created for each final image selected (from KAP, Pheno-cam, and PLI), across each individual plot and for all MISP transects and CALM subset plots. Since the Pheno-cams were stationary and relatively stable, all final images were batch processed by year allowing for quick processing times. A total of 46 ROIs were created for the Utqiaġvik MISP Pheno-cam dataset, while only 42 resulted for the Atqasuk grid due to the limitation of the low-horizontal angle of view of each time-lapse camera. KAP imagery was manually processed for each final image selected and a total of 50 ROIs for both MISP transects were delineated from

the airborne platform, attributed to the NADIR view angle of the system. Similarly, all PLIs for the CALM subset plots were also manually processed individually to maximize the integrity of image to image registration and ensure the same ROI was being analyzed for each. One ROI was developed for each CALM plot at both sites. The resulting index values calculated from the two kite aerial images were averaged to yield mean daily values for each KAP flight – plot combination. Because of the hourly spacing between Pheno-cam images and to account for variability in relative brightness values (i.e. cloud cover) from this approach, daily mean values across all images were calculated for each plot.

5.4 DATA ANALYSIS

All spectral indices from each plot and platform combination were averaged by WOY and matched to corresponding vegetation classes calculated from the plot level classification mentioned in sections 3.4.1 and 4.3.1.1. This was done in order to standardize analysis and for facilitation of inter-comparison between datasets, due to the varied temporal resolutions and collection frequencies of the data throughout the study. Both land cover classification maps and one peak-season MODIS NDVI (DOY 214, year 2015) scene from each site were utilized to determine precise geographical locations containing the highest cover of each vegetation class at both sampling locations (Figures 5.4 and 5.5). Initially both MODIS NDVI scenes were clipped to the areas of interest, projected to the NAD83 UTM zone 4 datum, then each MODIS pixel was delineated and the total area and percent cover of each land cover class from each map was calculated for each MODIS pixel using *ArcGIS* 10.2. Table 5.4 summarizes the total area and percent cover of each vegetation class across the entire Utqiaġvik peninsula, while Table 5.5 represents the same for the Atqasuk area. All pixels were classified into a particular vegetation class based on the dominant class within that pixel and coordinates for those pixels that had the highest values were acquired. These coordinates provided the locations where exact time-series of MODIS NDVI values would be extracted using the ORNL subset tool. Tables 5.6 and 5.7 summarize the total area and percent vegetation class coverage of each MODIS pixel for both Utqiaġvik and Atqasuk respectively that were selected for further analysis. Furthermore, we explored the delineation and locations of all MODIS NDVI time-series pixels to test whether or not each scene and corresponding cells aligned across all scenes and years. This approach would

provide an insight into how precise the sampling locations of MODIS NDVI products are and ensured each vegetation class is getting represented equally within each 250m^2 pixel (Figure 5.3). Prior to any analysis, all datasets were re-projected to the same horizontal and vertical datum (NAD83 UTM zone 4) for facilitating proper alignment of all datasets.

Pearson's correlations between indices were calculated across all vegetation classes, years, and platforms as well as for each vegetation class separately for both locations using *SAS JMP version 4.0.4* and *RStudio version 1.0.136* (*cor.test()* function) (Tables 5.8 and 5.9). Seasonal trends are plotted as scatter plots fit with a loess curve by year and vegetation class and are summarized in Figures 5.6 – 5.7. Linear regression (LR) was applied using the *lm()* function in *RStudio,* between indices that correlated highly with MODIS NDVI, such as the ground-based NDVI (TRAM and UNISPEC). Since the MODIS NDVI products are widely used for landscape to global scales, we explored the predictability of this index using the spectrometer-derived indices acquired across the MISP and CALM plots. Regression models were plotted against each other and are summarized in Figures 5.8 for Utqiaġvik and 5.9 for Atqasuk.

5.5 RESULTS

5.5.1 MODIS NDVI pixel delineation

All NDVI time-series datasets acquired from the MODIS platform were delineated, placed on-top of one another and locations of pixels were examined to test for alignment across both landscapes. Overall the delineated pixels do align spatially across the x and y plane. However, some scenes resulted with different sized or grouped pixels (e.g. larger than 250 m^2 (6.25 ha)), potentially from the spectral reflectance algorithm that calculated an average value per pixel based on multiple observations and ultimately compromised the accuracy of sampling each vegetation classes equally by pixel. Large numbers of "NoData" values (in this case NDVI) were observed for areas within and around bodies of water (i.e. lakes and deep ponds) and along the edges of the Utqiaġvik peninsula footprint, which was also where the largest volumes of mis-matching occurred. Figure 5.3 shows the outline of each pixel across the Utqiaġvik peninsula study area and a close up of an area of mis-match between pixels (different sized pixels) for different scenes of the same 2013 summer as well as a close up of the same area but depicting the water bodies from the land cover classification map as reference. Another important artifact that was observed from the MODIS delineated pixels was that most were slightly smaller than 250 m^2 pixel (231.65 m^2).

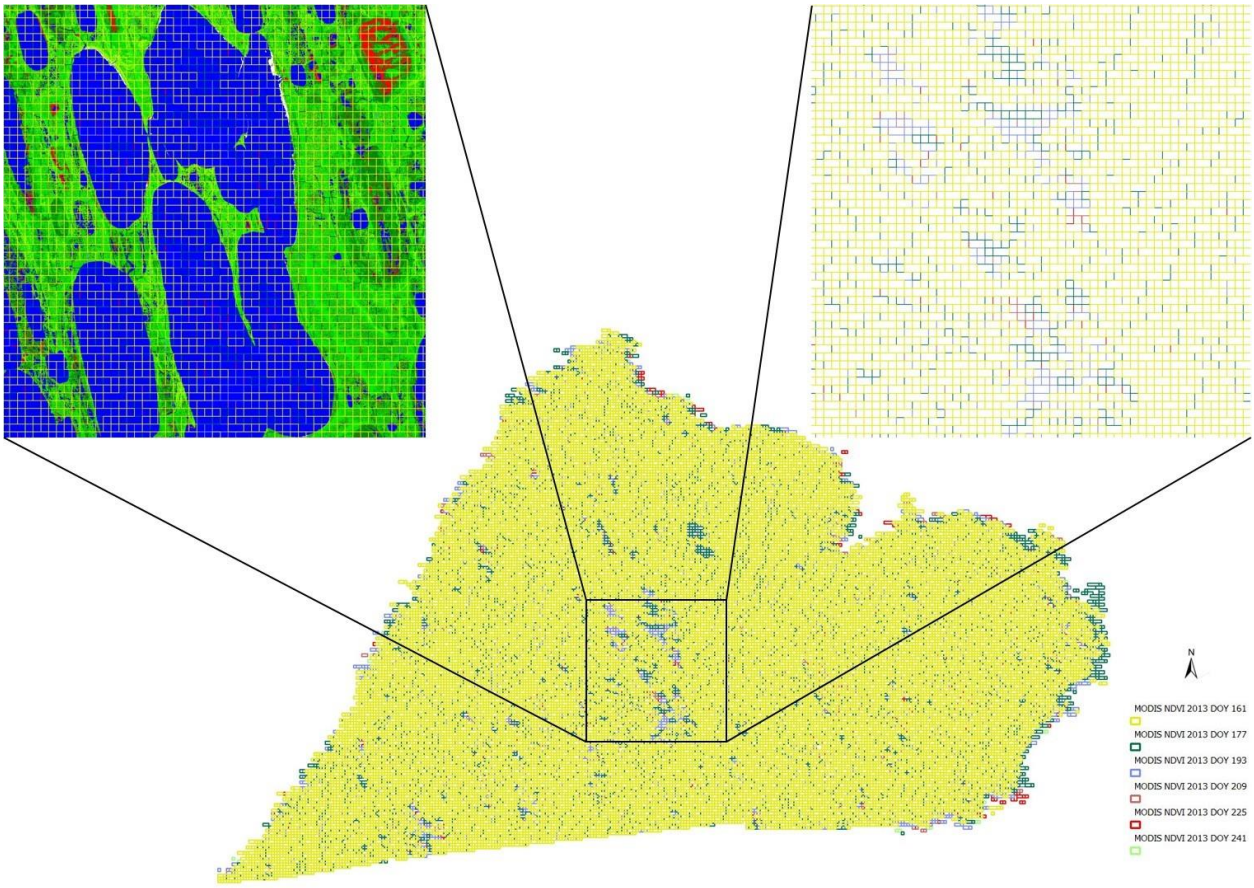

Figure 5.3: Map of the Utqiaġvik peninsula depicting the delineation of the 2013 MODIS NDVI time-series dataset. Highlighted in the top-right image is a closer look at the outline of each pixel for each DOY sampled for the 2013 summer, and the top-left image displays the outline of the same area but draped over the land cover classification map.

5.5.2 Vegetation class distribution across landscapes

From the land cover classification maps for both Utqiaġvik and Atqasuk generated from high spatial resolution WorldView2 satellite imagery, total cover of each land cover class was calculated across each landscape. Moist graminoid tundra was the predominant cover for the coastal landscape across of the Utqiaġvik peninsula with a total of 47,236.37 hectares or about 28.59% coverage of the mapped landscape. Wet graminoid tundra followed with a total cover of 25,573.316 hectares or roughly 15.48% of the total landscape. Seasonally flooded tundra covered

24,742.884 hectares or about 14.97% of the mapped area and 9.73% of the landscape or roughly 16,077.84 hectares was covered by dry-moist shrub-graminoid tundra. Dry shrub tundra covered approximately 0.34% of the total landscape or only about 561.913 hectares. The remaining 30.89% of the landscape was comprised of a combination of unused classes from the land cover maps, such as open water, aquatic, dry graminoid tundra, and bare/urban classes which were not included in this study.

The Atqasuk landscape displayed similar results as the Utqiaġvik area, resulting with moist graminoid tundra predominating with a total cover of 1026.3 hectares or roughly 40.87% of the mapped area. Wet graminoid tundra followed with a cover of 309.639 hectares or 12.33%. Dry graminoid tundra covered 272.54 hectares or 10.85% of the mapped landscape. The aquatic tundra class in Atqasuk had a sparse cover at 99.61 hectares of about 3.97% of the mapped area. As mentioned previously, total area and percent cover for moist shrub tundra near Atqasuk were not quantified due to the low-cover of this land cover type in the mapped area. The remaining 31.98% of the landscape is composed of a combination of unclassified, water, and bare ground that were not included in this study.

Total area and percent cover of each vegetation class were quantified within the delineated MODIS NDVI pixels from the DOY 241 from summer 2015 and are summarized in Table 5.6 for Utqiaġvik and Table 5.7 for Atqasuk. In Utqiaġvik, the resulting pixel classified as the Wet graminoid pixel resulted with a total cover of approximately 4.85 hectares of the total 6.25 hectares that made up that pixel, which amounted to about 90% of the pixel. Seasonally flooded tundra classified pixel covered an area of about 7.57 hectares and dominated about 70% of the pixel. Moist graminoid tundra and dry-moist shrub-graminoid tundra classified pixels consisted of 9.54 and 5.29 hectares respectively, with a cover of 88% and 98% of each corresponding pixel. Dry shrub tundra pixels covered an area of about 0.6 hectares and totaled 11% of the pixel, while moist graminoid tundra displayed the highest cover at 2.52 hectares or roughly 46.97% of the pixel. Dry shrub tundra had a negligible cover within the landscape classified in MODIS pixels. Even though pixel number 28,603 was dominated by the moist graminoid class, it had the highest concentration of dry shrub tundra within the mapped area and was classified as the dry shrub tundra. The same metrics were computed for the Atqasuk landscape where aquatic tundra classified MODIS pixel covered an area of 3.65 hectares and predominated 23% of the sampled pixels. The wet and moist graminoid tundra classified pixels had an area of 3.83 and 11.44 hectares, which totaled 36% and

53% of each pixel respectively. Dry graminoid tundra classified pixels covered a significantly larger area than in Utqiaġvik with a cover of 3.78 hectares or 35% coverage of the mapped area. Similar to the dry shrub class from the Utqiaġvik classification, the dry class in Atqasuk was also classified as dry even though the moist class was predominant for this particular area because this particular location had the highest concentration of dry vegetation land cover types.

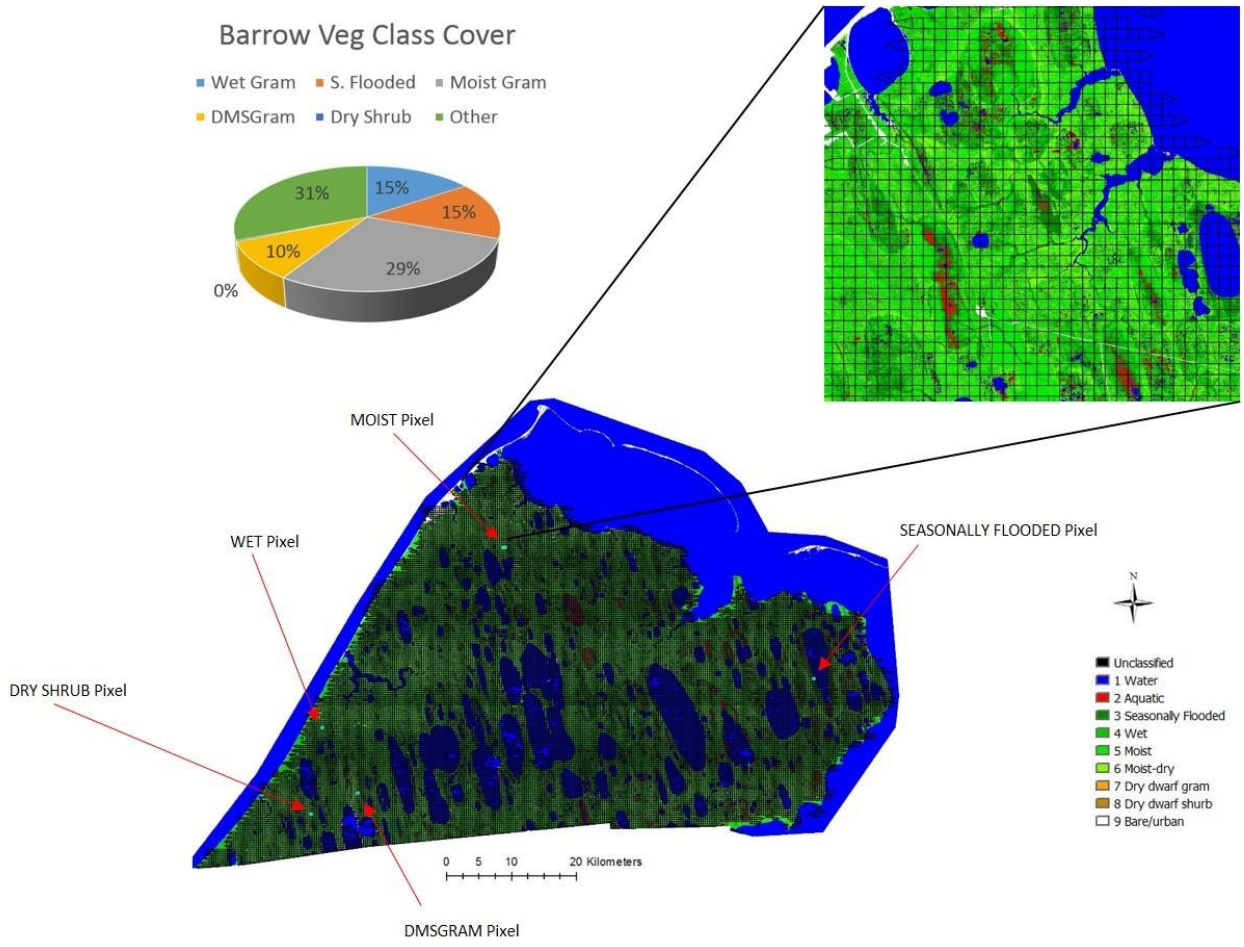

Figure 5.4: The land cover classification map of the Utqiaġvik peninsula showing location of pixels containing dominant vegetation classes (red arrows) across the landscape. The image at the top right corner displays a high resolution view and delineation of each MODIS NDVI pixel acquired from DOY 241 from the 2015 summer. The top left pie chart summarizes resulting predominant vegetation class across the land cover classification map.

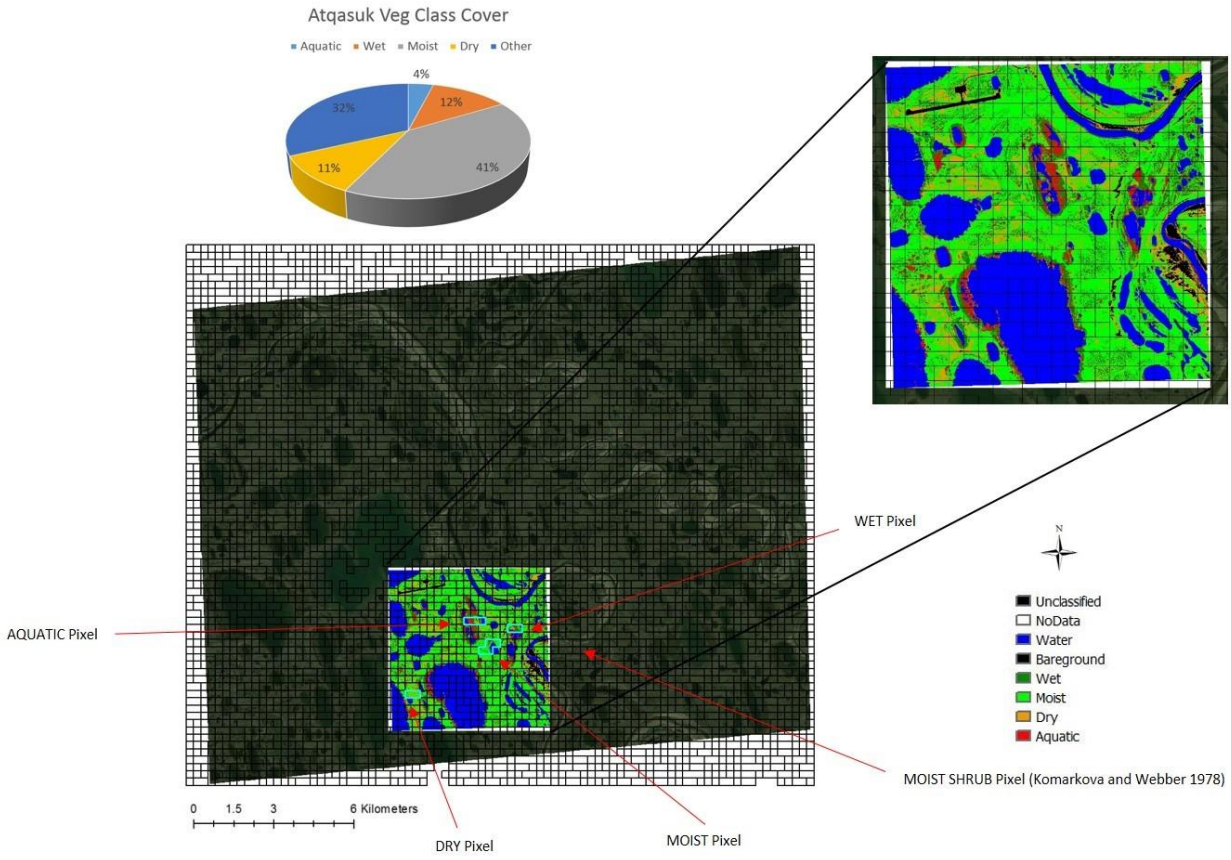

Figure 5.5: The land cover classification map of the local Atqasuk area showing location of pixels containing dominant vegetation classes (red arrows) across the landscape. The image at the top right corner displays a closer look at the cover classes and delineation of each MODIS NDVI pixel acquired from DOY 241 from the 2015 summer). The top left pie chart depicts resulting predominant vegetation class across the land cover classification map.

Table 5.4: Total vegetation area and percent cover across the Utqiaġvik peninsula pertaining to the MODIS NDVI dataset from DOY 241, year 2015. The landscape within the footprint of the land cover map is dominated by moist graminoid tundra vegetation classes.

Total Class Coverage Across Barrow QB Vegetation Map						
Site	Veg Map	Dominant Veg Class	Veg Class	Total area coverage per scene (m^2)	Total area coverage per scene (ha)	Total percent coverage per scene (%)
Barrow	Quickbird 2012	MOIST GRAM	WET GRAM	255,733,163	25573	15.48
			SEASONALLY FLOODED	247,428,846	24742	14.97
			MOIST GRAM	472,363,701	47236	28.59
			DMSGRAM	160,778,402	16077	9.73
			DRY SHRUB	5,619,134	561	0.34

Table 5.5: Total vegetation area and percent cover across the local Atqasuk area pertaining to the MODIS NDVI dataset from DOY 241, year 2015. The landscape within the footprint of the land cover map is dominated by moist tundra vegetation classes.

Total Class Coverage Across Atqasuk QB Vegetation Map						
Site	Veg Map	Dominant Veg Class	Veg Class	Total area coverage per scene (m^2)	Total area coverage per scene (ha)	Total percent coverage per scene (%)
Atqasuk	Quickbird 2012	MOIST	AQUATIC	996100	99	3.97
			WET	3096393	309	12.33
			MOIST SHRUB	NA	NA	NA
			MOIST	10263068	1026	40.87
			DRY	2725440	272	10.85

Table 5.6: Total vegetation area and percent cover for each Utqiaġvik MODIS NDVI pixel from DOY 241, year 2015 used for analysis. Note that the predominant class given the total percent cover per MODIS pixel, for the classified "dry shrub" class was actually "moist gram" (46.97%) but the analysis showed that this particular pixel had the highest concentration of dry shrub across the entire Utqiaġvik area, therefore this pixel location was used to represent the dry shrub classes in Utqiaġvik.

Site	MODIS Pixel	Dominant Veg Class	Veg Class	Total area coverage per pixel (m^2)	Total area coverage per pixel (ha)	Total percent coverage per pixel (%)
Barrow	18887	WET GRAM	WET GRAM	48524	4.85	90.36
			SEASONALLY FLOODED	1737	0.17	3.24
			MOIST GRAM	2591	0.25	4.83
			DMSGRAM	846	0.08	1.58
			DRY SHRUB	0	0	0.00
	13556	SEASONALLY FLOODED	WET GRAM	3636	0.36	3.39
			SEASONALLY FLOODED	75730	7.57	70.53
			MOIST GRAM	22994	2.29	21.41
			DMSGRAM	4583	0.45	4.27
			DRY SHRUB	0.482	0.0004	0.00
	2077	MOIST GRAM	WET GRAM	1758	0.17	1.64
			SEASONALLY FLOODED	119	0.01	0.11
			MOIST GRAM	95394	9.53	88.83
			DMSGRAM	9578	0.95	8.92
			DRY SHRUB	306	0.03	0.29
	26204	DMSGRAM	WET GRAM	614	0.06	1.14
			SEASONALLY FLOODED	0	0	0.00
			MOIST GRAM	130	0.01	0.24
			DMSGRAM	52940	5.29	98.58
			DRY SHRUB	16.66	0.001	0.03
	28603	DRY SHRUB	WET GRAM	7325	0.73	13.64
			SEASONALLY FLOODED	2730	0.27	5.08
			MOIST GRAM	25224	2.52	46.97
			DMSGRAM	8483	0.84	15.80
			DRY SHRUB	5929	0.59	11.04

Table 5.7: Total vegetation area and percent cover for each Atqasuk MODIS NDVI pixel from DOY 241, year 2015 used for analysis. Note that the predominant class given the total percent cover per MODIS pixel, for the classified "dry" class was actually "moist" (55.39%) but the analysis showed that this particular pixel had the highest concentration of dry across the Atqasuk area, therefore this pixel location was used to represent the dry classes in Atqasuk.

Site	MODIS Pixel	Dominant Veg Class	Veg Class	Total area coverage per pixel (m^2)	Total area coverage per pixel (ha)	Total percent coverage per pixel (%)
Atqasuk	131	AQUATIC	AQUATIC	36535.68	3.65	22.70
			WET	26280	2.62	16.33
			MOIST SHRUB	NA	NA	NA
			MOIST	21969	2.19	13.65
			DRY	22212.36	2.22	13.80
	152	WET	AQUATIC	26566.92	2.65	24.76
			WET	38296.44	3.82	35.70
			MOIST SHRUB	NA	NA	NA
			MOIST	24547.68	2.45	22.88
			DRY	8444.52	0.84	7.87
	198	MOIST	AQUATIC	4516.56	0.45	2.10
			WET	36867.96	3.68	17.14
			MOIST SHRUB	NA	NA	NA
			MOIST	114423.48	11.44	53.19
			DRY	16404.84	1.64	7.63
	292	DRY	AQUATIC	326.52	0.03	0.30
			WET	8467.56	0.84	7.88
			MOIST SHRUB	NA	NA	NA
			MOIST	59492.52	5.94	55.39
			DRY	37763.28	3.77	35.16

5.5.3 Seasonal and inter-annual greening trends

Seasonal and inter-annual trends in greening were observed at different spatial scales, from the various sensing platforms for the Utqiaġvik and Atqasuk landscapes. Please refer to chapters 2 and 3 from this dissertation for methods and resulting correlations between these sensors. This chapter has focused on including MODIS NDVI for analyzing its spectral associations to previously calculated greening indices for specific vegetation classes. Figures 5.6 and 5.7 show the seasonal greening trends over the course of the study as observed at the CALM and MISP grids by the spectrometer indices and MODIS sensor.

The vegetation classes sampled in Utqiaġvik that had a higher soil moisture content (e.g. moist gram, seasonally flooded, and wet gram) displayed higher greenness values at peak season and more variability between years than vegetation typified by a drier soil moisture status.

Vegetation classes with a lower soil moisture (e.g. dry moist shrub gram and dry shrub) displayed lower peak season greening values and less variability both within and between growing seasons. Very similar signals were observed by NDVI as sensed by the spectrometer and MODIS platforms across the Utqiaġvik plots in which wetter classes experienced more greening variability and intensity when compared to the drier classes. For most vegetation classes and across most plots (MISP and CALM), NDVI trends steadily increased throughout the snow-free growing season and began to decline around week 31 on average. In some years, a late season greening was observed for the Utqiaġvik MISP and CALM plots for 2011 and 2015 as well as during 2010 and 2011 respectively. Similarly, the MISP robotic tram NDVI and MODIS NDVI showed a strong decline in greening beginning around week 30 during 2012 and 2013, as well as for 2010 and 2012 respectively for wetter vegetation classes. A dramatic increase in greening occurred during the 2015 growing season around week 27 as observed by the KAP GEI and %G indices and Unispec over the MISP plots as well as by the GEI and %G indices for the CALM plots. The MODIS NDVI on the other hand displayed a decline in greening during this time.

Similar to Utqiaġvik and for both RGB and spectral sensor output, vegetation classes in Atqasuk with a higher soil moisture content (moist and moist shrub tundra) showed more variability in greening between years than drier classes (e.g. dry). All indices observed peak greenness and subsequent senescence during week 30 in 2012, and week 29 for 2013 and 2014 (except from the MISP tram). Contrary to Utqiaġvik, trends captured by all sensors in Atqasuk

seem to show high variability (more variation in greening values across the growing season) between vegetation classes overall.

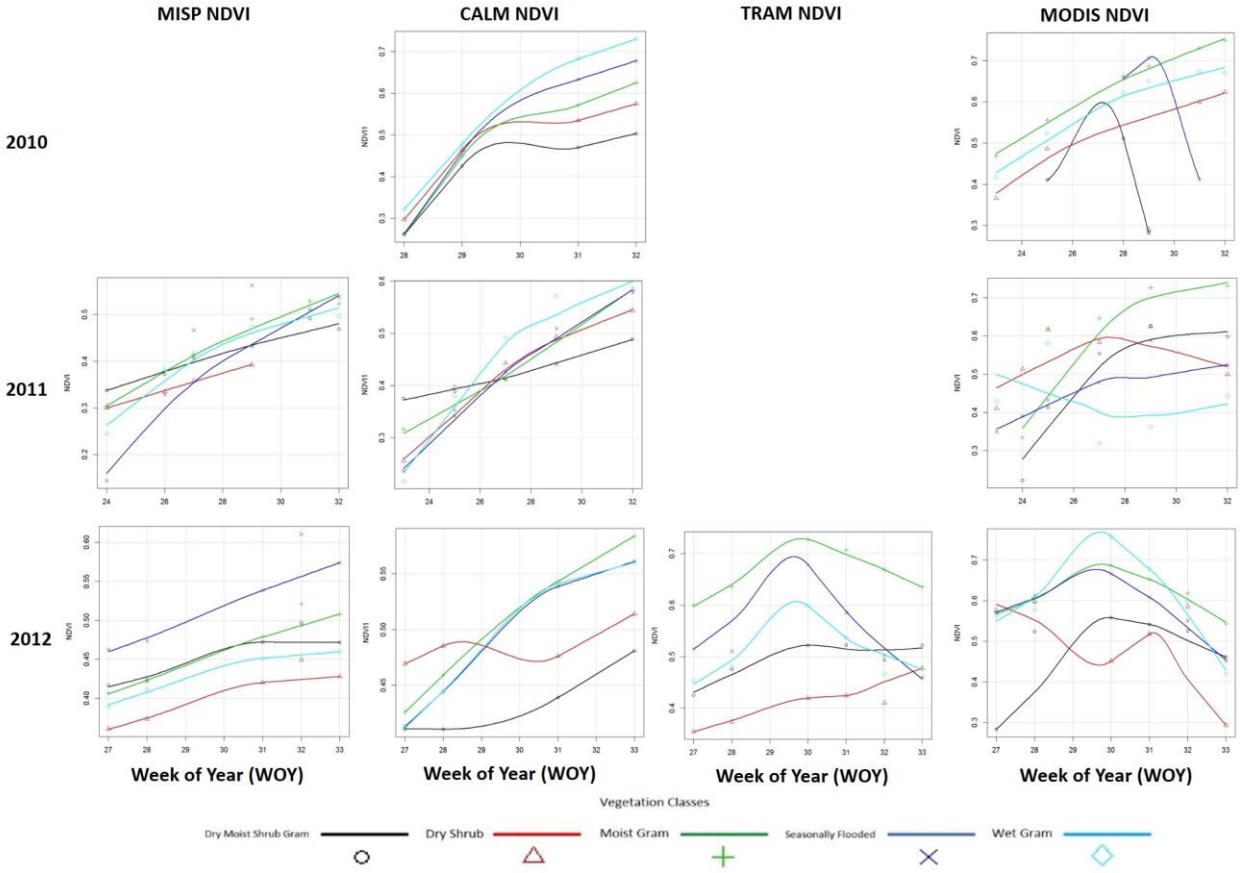

Figure 5.6a: Seasonal and inter-annual NDVI greening trends (2010-2012) for the Utqiaġvik MISP and CALM vegetation classes as observed by the ground-based spectrometer, MISP tram and MODIS sensors.

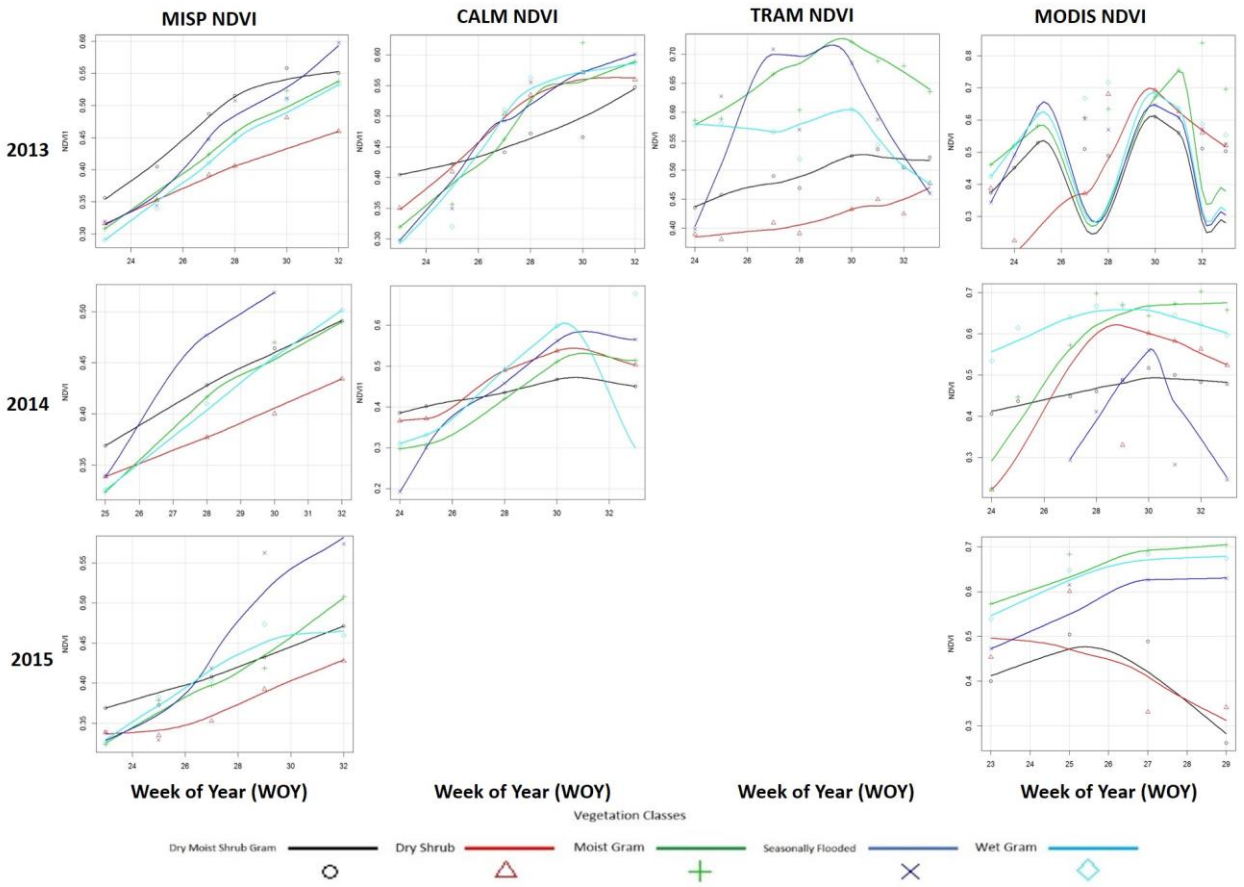

Figure 5.6b: Seasonal and inter-annual NDVI greening trends (2013-2015) for the Utqiaġvik MISP and CALM vegetation classes as observed by the ground-based spectrometer, MISP tram and MODIS sensors.

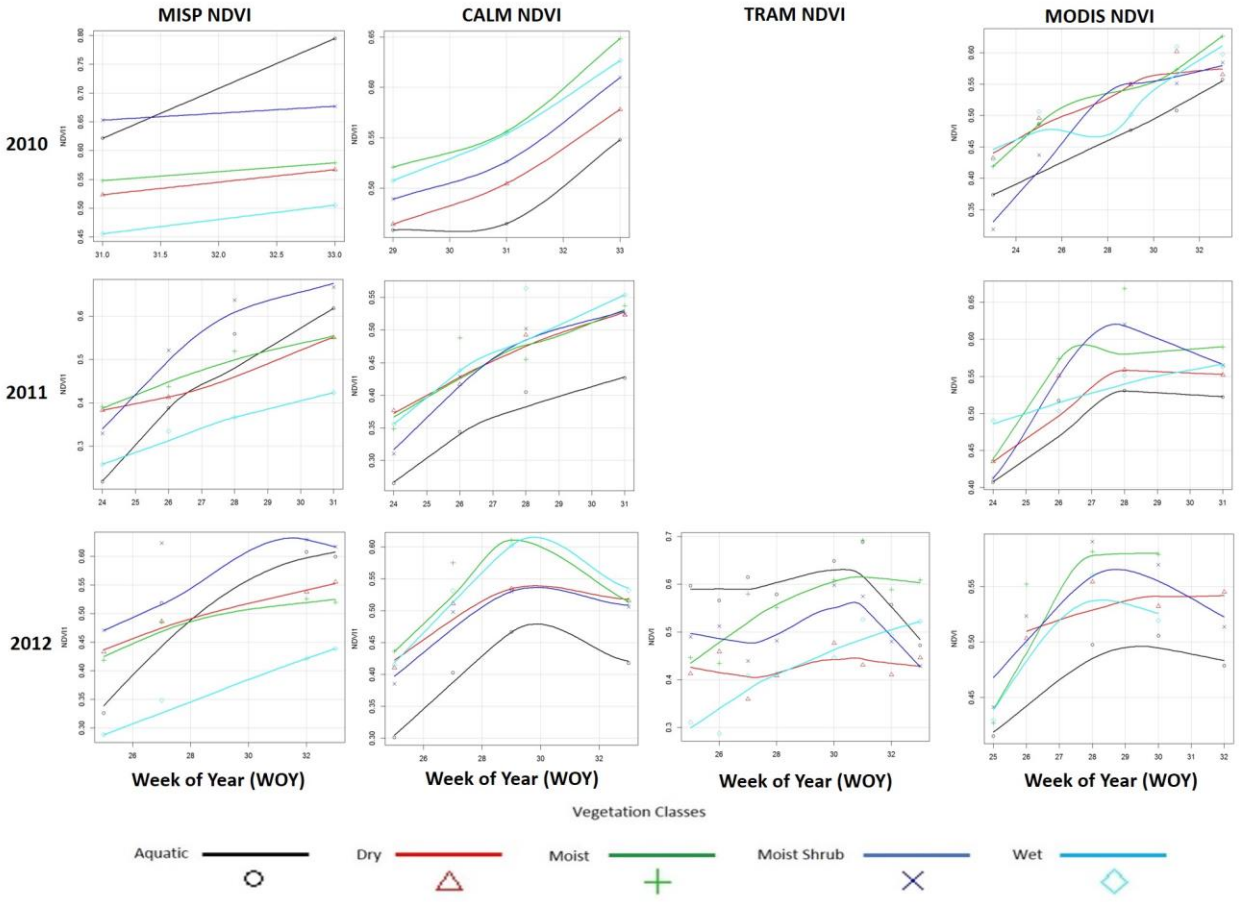

Figure 5.7a: Seasonal and inter-annual NDVI greening trends (2010-2012) for the Atqasuk MISP and CALM vegetation classes as observed by the ground-based spectrometer, MISP tram and MODIS sensors.

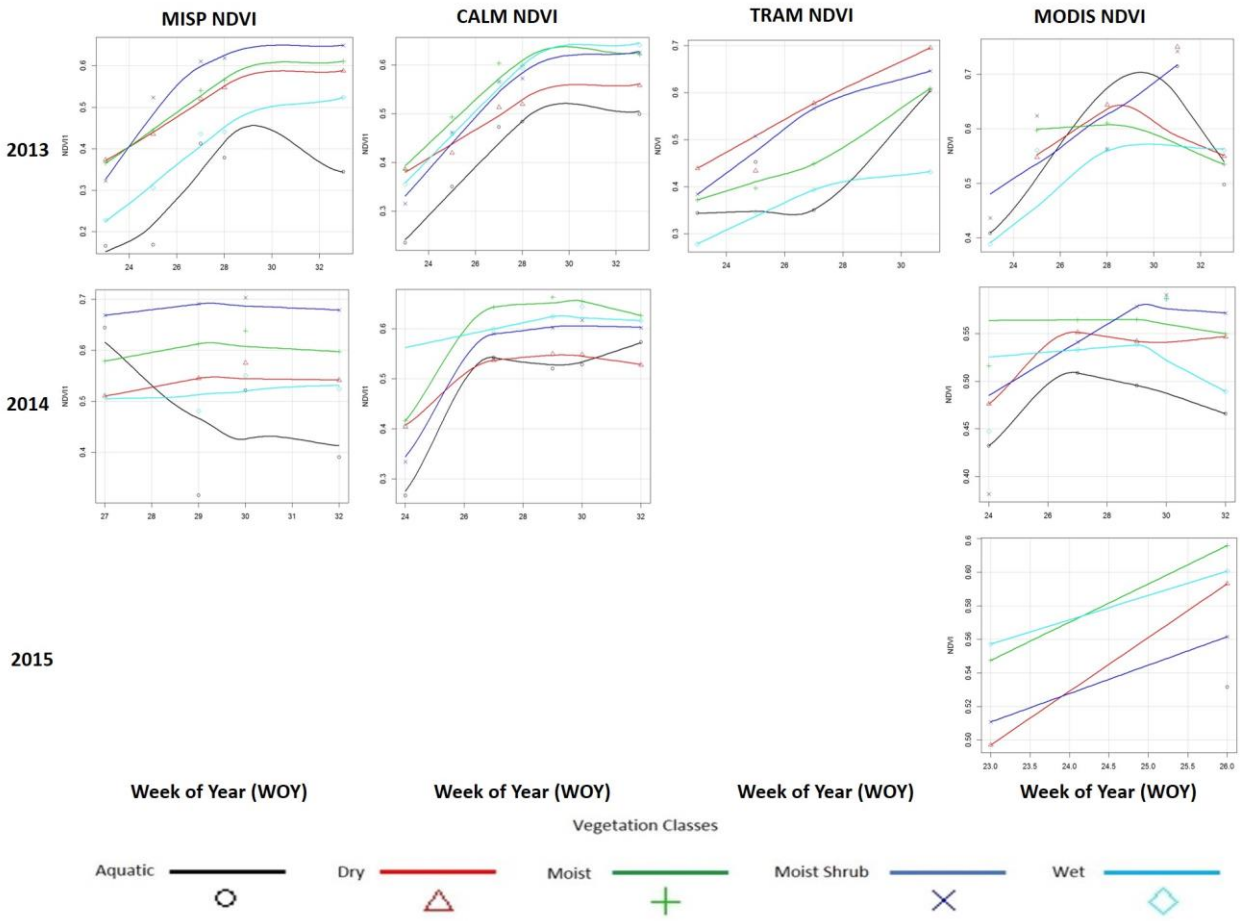

Figure 5.7b: Seasonal and inter-annual NDVI greening trends (2013-2015) for the Atqasuk MISP and CALM vegetation classes as observed by the ground-based spectrometer, MISP tram and MODIS sensors.

5.5.4 Inter-comparison of greening indices and sampling platforms

Correlations were calculated between both RGB and spectral green indices and MODIS NDVI across all years and for each vegetation class at both Utqiaġvik and Atqasuk. Focusing on the Utqiaġvik CALM grid data across all years and vegetation classes, NDVI from the Unispec DC sensor resulted with low correlations with MODIS NDVI ($r= 0.34$, $p<0.0001$, $n=109$) while the RGB indices had slightly stronger associations (GEI: $r= 0.54$, $p<0.0001$, $n= 76$ and %G: $r= 0.54$, $p<0.0001$, $n= 76$). Similarly for the Utqiaġvik MISP plots, spectral NDVI from the Unispec DC and MODIS sensor also resulted with low correlations ($r= 0.29$, $p<0.0001$, $n=120$), while both PCAM (GEI $r= 0.32$, $p<0.0001$, $n= 107$; %G $r= 0.23$, $p<0.0001$, $n=107$) and KAP (GEI $r= 0.26$,

p<0.0001, n= 107; %G r= 0.33, p<0.0001, n= 103) RGB indices also correlated poorly with MODIS NDVI. The NDVI acquired from the MISP tram sensor had the closest associations with MODIS NDVI (r= 0.55, p<0.0001, n= 69). The strongest correlations resulted between the CALM indices and MODIS NDVI.

When looking at correlations between each vegetation class for the Utqiaġvik CALM grid, the NDVI from the Unispec DC correlated poorly with MODIS NDVI for the wet gram class (r= 0.27, p= 0.206, n= 24), while the plot level green RGB indices resulted with strong associations with MODIS (GEI r= 0.79, p<0.0001, n= 16 and %G r= 0.77, p<0.0001, n= 16). Similar trends were seen for the seasonally flooded classes in Utqiaġvik, (NDVI: r= 0.08, p= 0.7211, n= 21; GEI: r= 0.45, p= 0.108, n= 14; and %G: r= 0.44, p= 0.114, n= 14). The moist gram had the strongest associations of all vegetation classes between NDVI and the satellite sensor with r= 0.63, p=0.001, n= 23, and RGB indices as well GEI r= 0.70, p<0.001, n= 16 and %G r= 0.68, p<0.001, n=16. Unispec NDVI for the dry moist shrub gram classes also resulted with low correlations with MODIS NDVI (r=0.24, p= 0.276, n=21), while again the RGB indices seemed to associate well with the satellite sensor yielding GEI r= 0.69, p=0.003, n=16 and %G r= 0.70 p<0.001, n=16. Correlations corresponding to the dry shrub classes were strong amongst all RGB and spectral sensors (NDVI: r=0.48, p=0.03, n=20; GEI: r= 0.57, p=0.03, n=14 and %G: r= 0.51, p=0.06, n=14).

Results varied between vegetation classes for the Utqiaġvik MISP grid, such as NDVI from the Unispec DC sensor also correlated poorly with MODIS NDVI for the wet gram class (r= 0.24, p= 0.235, n= 26), RGB indices from the KAP sensor were slightly stronger (GEI r=0.3, p= 0.158, n=23 and %G r= 0.36, p= 0.094, n= 23), and those from the PCAM were even stronger yet (GEI r= 0.47, p<0.01, n= 28 and %G r= 0.42, p<0.02, n=28). The MISP tram NDVI correlated the strongest with MODIS of all indices with r= 0.56, p<0.04, n= 14. The lowest associations were seen between the Unispec DC NDVI and MODIS for the seasonally flooded classes (r= 0.08, p=0.71, n= 22), while those from the RGB sensors were slightly stronger (KAP GEI: r=0.02, p= 0.926, n= 21; KAP %G: r= 0.26, p= 0.304, n= 17; PCAM GEI: r= 0.39, p<0.05, n= 27; PCAM %G: r= 0.28, p= 0.155, n= 27). Once again the MISP tram NDVI resulted with strong associations with the satellite sensor for the seasonally flooded classes (r= 0.83, p= 0.0001, n= 14). Similar to the signal seen for the CALM classes the moist gram seemed to show the strongest associations of all vegetation classes between Unispec NDVI and MODIS (r= 0.73, p<0.001, n= 26), as well as

the RGB indices from both sensors (KAP GEI: r=0.64, p<0.001, n=23; KAP %G: r= 0.67, p<0.001, n=23; PCAM GEI: r= 0.69, p<0.001, n= 27; and PCAM %G: r= 0.70, p<0.001, n= 27). Again, the MISP tram NDVI resulted with strong correlations with MODIS r= 0.60, p<0.001, n= 14). The dry moist shrub gram classes displayed strong correlation values between Unispec DC NDVI and MODIS NDVI (r= 0.52, p<0.001, n= 24), while the RGB indices had slightly lower associations (KAP GEI: r=0.26, p<0.001, n= 20 and KAP %G: r= 0.35, p<0.001, n= 20). No correlations resulted between the PCAM indices and MODIS due to missing data and the MISP tram NDVI once again resulted with strong associations with MODIS (r= 0.70, p<0.05, n= 14). The dry shrub classes seemed to have strong correlations between KAP RGB indices and MODIS (KAP GEI: r=0.37, p= 0.112, n= 20 and KAP %G: r= 0.41, p=0.075, n=20) than those acquired from the PCAM sensor (GEI: r= 0.28, p= 0.176, n=25 and %G: r= 0.24, p= 0.25, n=25). The Unispec DC correlated poorly with MODIS for the dry shrub classes (r= 0.27, p=0.217, n= 22), while the MISP tram NDVI resulted with poor negatively correlated values (r= -0.15, p= 0.61, n= 13). Other RGB and spectral indices were also correlated with MODIS NDVI as also seen from the chapter 4 study.

Overall and across all vegetation classes, correlations for Atqasuk were stronger than those seen in Utqiaġvik between all RGB and spectral indices and MODIS NDVI. The NDVI from the Unispec DC sensor correlated strong with the satellite sensor (r= 0.7, p<0.0001, n= 75) across all vegetation classes and years for the Atqasuk CALM grid. The plot level RGB indices also resulted with strong correlations (with GEI r= 0.61, p<0.0001, n=50; %G r= 0.64, p<0.0001, n=50). In addition to the commonly correlated indices previously mentioned and reported on, other RGB (nNDVI r= 0.55, p<0.0001, n= 50; a* r= -0.63, p<0.0001, n= 50; TEST r= -0.60, p<0.0001, n= 50) and spectral indices (GREEN r= 0.66, p<0.0001, n= 75; MNDVI r= 0.62, p<0.0001, n= 74; OSAVI r= 0.67, p<0.0001, n= 75) were also strongly correlated with MODIS NDVI which are all summarized in Table 5.11. Associations for the Atqasuk MISP grid also resulted to be very strong between all indices and MODIS NDVI, as seen with the Unispec DC NDVI (r= 0.56 p<0.0001, n= 77) as well as from the RGB sensors from both the airborne system (KAP GEI r= 0.71, p<0.0001, n=60; KAP %G r= 0.68, p<0.0001, n= 58) and time-lapse system (PCAM GEI r= 0.63, p<0.0001, n= 81; PCAM %G r= 0.56, p<0.0001, n=78). The strongest correlations between indices were seen across the CALM grid than the MISP grid similar to what was observed in Utqiaġvik.

Focusing on the correlations between each vegetation class across the Atqasuk CALM grid, plot-based spectral NDVI resulted with close associations with MODIS NDVI (r= 0.7, p<0.05,

n=14) for the aquatic classes, while the plot RGB indices correlated poorly (GEI r= 0.4, p= 0.322, n=8 and %G r= 0.39, p= 0.341, n=8). The wet classes which consist of slightly drier soil moisture when compared to aquatic classes, also resulted with strong associations for both spectral and RGB (NDVI r= 0.74, p<0.05, n= 17; GEI r= 0.82, p<0.05, n=11 and %G r= 0.78, p<0.05, n=11). As seen in Utqiaġvik, the moist shrub classes in Atqasuk also displayed the strongest correlations out of all the studied classes as seen from all sensors (NDVI r= 0.82, p<0.05, n= 15; GEI r= 0.75, p<0.05, n=11 and %G r= 0.78, p<0.05, n=11). Moderate correlations were observed by the spectral sensor for the moist classes (NDVI r=0.47, p= 0.079, n= 15), while strong associations resulted from the RGB sensors (GEI r= 0.75, p<0.05, n= 10 and %G r= 0.78, p<0.05, n=10). Overall, the dry classes yielded strong correlations with MODIS NDVI (NDVI r=0.59, p<0.05, n=14; GEI r= 0.65, p<0.05, n=10 and %G r= 0.77, p<0.05, n=10).

Associations between RGB and spectral indices and MODIS NDVI were strong amongst all the vegetation classes in the Atqasuk MISP grid as seen with the aquatic classes (NDVI r= 0.71, p<0.05, n=14; KAP GEI r=0.63, p<0.05, n=12; KAP %G r= 0.73, p<0.05, n=10; PCAM GEI r= 0.67, p<0.05, n=15; PCAM %G r= 0.63, p<0.05, n=14) however, The MISP tram NDVI correlated poorly with MODIS NDVI (r= 0.31, p= 0.38, n=10). The wet classes also showed strong correlations between MODIS NDVI and spectral indices (NDVI r= 0.65, p<0.05, n=17) as well as with RGB indices (KAP GEI r=0.80, p<0.05, n=13; KAP %G r= 0.82, p<0.05, n=13; PCAM GEI r= 0.78, p<0.05, n=17 and PCAM %G r= 0.75, p<0.05, n=17). The tram NDVI associated well with MODIS NDVI (r= 0.58, p= 0.06, n=11). Once again the moist shrub class displayed the strongest correlations out of all classes observed between indices and MODIS NDVI (NDVI r= 0.76, p<0.05, n= 16; KAP GEI r=0.84, p<0.05, n=13; KAP %G r= 0.83, p<0.05, n=13; PCAM GEI r= 0.74, p<0.05, n=17; PCAM %G r= 0.59, p<0.05, n=15; Tram NDVI r= 0.57, p<0.05, 13). Poor correlations resulted for the moist classes as seen from the spectrometer (NDVI r= 0.33, p=0.21, n=16) but slightly better associations from the RGB sensors (KAP GEI r=0.58, p= 0.06, n=11; KAP %G r= 0.57, p=0.07, n=11; PCAM GEI r= 0.56, p<0.05, n=16; PCAM %G r= 0.54, p<0.05, n=16) and the tram NDVI (r= 0.57, p<0.05, n=10). Similarly, associations were strong for the dry classes across the Atqasuk MISP grid as observed by all sensors (NDVI r= 0.59, p<0.05, n=14; KAP GEI r=0.81, p<0.05, n=11; KAP %G r= 0.84, p<0.05, n=11; PCAM GEI r= 0.63, p<0.05, n=16; PCAM %G r= 0.65, p<0.05, n=16; tram NDVI r= 0.8, p<0.05, n=10). A suite of other RGB and spectral indices also correlated strongly with MODIS NDVI across all vegetation

classes. The strongest of which were observed over the moist shrub classes as seen within the CALM grid (GREEN r= 0.82, p<0.05, n=15; MNDVI r= 0.78, p<0.05, n=15; OSAVI r=0.82, p<0.05, n=15; nNDVI r=0.68, p<0.05, n=11).

Table 5.8: Pearson's correlation results (critical p-values adjusted using the Bonferroni correction) between both the RGB and spectrometer-derived indices and MODIS NDVI values by site, across all years and data for the Utqiaġvik vegetation classes.

Site	Platform	Index	r	P	n
CALM	SPEC	GREEN	0.37	<0.0001	98
		NDVI1	0.34	<0.0001	109
	PLOT RGB	GEI	0.54	<0.0001	76
		PctG	0.54	<0.0001	76
		nNDVI	0.60	<0.0001	76
		a*	-0.59	<0.0001	76
		TEST	-0.53	<0.0001	76
MISP	TRAM	NDVI	0.55	<0.0001	69
	KAP RGB	GEI	0.26	<0.0001	107
		PctG	0.33	<0.0001	103
	PCAM RGB	GEI	0.32	<0.0001	107
		PctG	0.23	<0.01	107
	SPEC	NDVI1	0.29	<0.001	120

Table 5.9: Pearson's correlation results (critical p-values adjusted using the Bonferroni correction) between both the RGB and spectrometer-derived indices and MODIS NDVI values by site, across all years and data for the Atqasuk vegetation classes.

ATQ CORRELATIONS- Indices vs MODIS NDVI (2010-2015) ALL VEG CLASS					
Site	Platform	Index	r	p	n
CALM	SPEC	GREEN	0.66	<0.0001	75
		MNDVI	0.62	<0.0001	74
		MSR	0.59	<0.0001	75
		NDVI1	0.70	<0.0001	75
		OSAVI	0.67	<0.0001	75
		SIPI	0.55	<0.0001	73
	PLOT RGB	GEI	0.61	<0.0001	50
		PctG	0.64	<0.0001	50
		nNDVI	0.55	<0.0001	50
		a*	-0.63	<0.0001	50
		TEST	-0.61	<0.0001	50
MISP	TRAM	NDVI	0.54	<0.0001	54
	KAP RGB	GEI	0.71	<0.0001	60
		PctG	0.68	<0.0001	58
	PCAM RGB	GEI	0.63	<0.0001	81
		PctG	0.56	<0.0001	78
	SPEC	NDVI1	0.56	<0.0001	77

Overall, lower predictability of MODIS NDVI was observed from the plot-level NDVI acquired from both the TRAM and UNISPEC system at both Utqiaġvik and Atqasuk. UNISPEC NDVI had the lowest ability to predict MODIS NDVI with R^2= 0.09, p< 0.001, followed by the CALM NDVI R^2= 0.113, p< 0.001 and lastly by the TRAM system R^2= 0.3073, p< 0.001 across the Utqiaġvik study. Overall in Atqasuk, predictability was stronger although still low and results were inverse of those in Utqiaġvik as seen lowest from the TRAM system R^2= 0.2864, p< 0.001, then followed by the UNISPEC NDVI R^2= 0.3104, p< 0.001 and lastly across the CALM plots R^2= 0.4873, p< 0.001. All regression models are displayed in Figure 5.8 for Utqiaġvik and Figure 5.9 for Atqasuk below. Moreover, based on these regressions it seems like MODIS is overestimating NDVI across all vegetation classes when compared to the ground-based NDVI values acquired over the 6 year period of this study. These findings are supported by other studies and provide an insight into the uncertainty of such widely used methods.

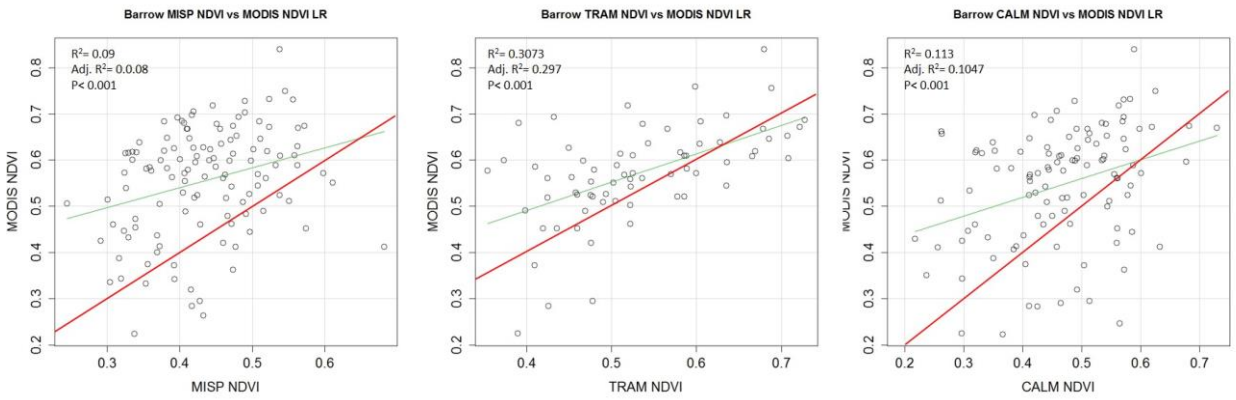

Figure 5.8: Simple linear regression models between NDVI (acquired from the ground-based spectrometer and MISP TRAM system) and MODIS NDVI for the Utqiaġvik MISP and CALM plots. The red line in the plots represents the 1:1 line between NDVI values.

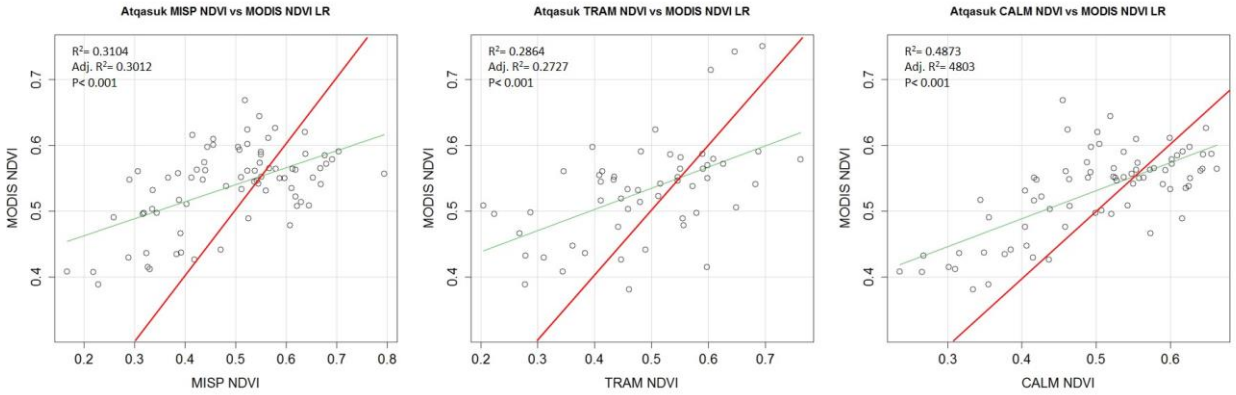

Figure 5.9: Simple linear regression models between NDVI (acquired from the ground-based spectrometer and MISP TRAM system) and MODIS NDVI for the Atqasuk MISP and CALM plots. The red line in the plots represents the 1:1 line between NDVI values.

5.6 DISCUSSION

NDVI has become well-used as a proxy for primary productivity in various ecosystems but few studies have focused on the inter-comparison of NDVI and seasonal greening trends between sampling platforms, sensors, indices, vegetation types, and spatial scale of the sampling. This study differs from others in that these relationships were explored across multiple spatial (meters to

kilometers) and temporal (seasonal and inter-annual) scales, for multiple plant communities spanning a soil moisture gradient (wet to dry in two northern arctic landscapes that exhibit different climatic patterns, landscape characteristics and plant community composition.

Overall, associations between RGB, spectrometer-derived indices and MODIS NDVI were strong for Atqasuk compared to Utqiaġvik, which are similar to the results acquired for chapters 2 and 3. This suggests that most sensors are more sensitive to signals from vegetation classes present across the Atqasuk landscape, which might be due to the higher plant productivity seen from higher volumes of biomass in Atqasuk (*Hollister*, 2003; *Oberbauer et al.*, 2013). Studies such as *Buchhorn et al.*, 2013 support this assumption as they concluded that arctic sites that overall contained greater vegetation biomass and taller shrubs resulted with higher reflectance in the NIR range along the North American Arctic Transect (NAAT). Correlations were stronger between indices and MODIS NDVI for vegetation classes sampled within the CALM grid plots than those within the MISP grids in Utqiaġvik, while results were more variable in Atqasuk. Another observation from this study was that poor correlations between all indices and MODIS NDVI prevailed in vegetation classes that represented the most extreme soil moisture regimes at each sampling location (dry and aquatic), while those classes that fell in between (moist to wet classes) resulted in the strongest correlations. Regression models showed that MODIS NDVI had low predictability using the RGB indices across all sites and locations. When modeling the predictability of plot-level NDVI acquired from both the TRAM system and the UNISPEC, using MODIS NDVI results also showed low R^2 values. Additionally, the MODIS platform seems to be over estimating NDVI as seen across both Utqiaġvik and Atqasuk (Figure 5.10 and 5.11) which has also been reported in other studies (*Gamon et al.*, 2013).

The land cover classification maps utilized for this study facilitated the delineation of vegetation classes spanning both landscapes and supports the former observations (chapters 2 and 3) of sensor sensitivity to those classes containing higher soil moisture. Results showed that moist graminoid tundra covers 28.59% and 40.87% of the landscape in Utqiaġvik and Atqasuk respectively, accounting for a large portion of the land cover across these northern arctic regions. Additionally, dry classes seem to be less abundant across the Utqiaġvik peninsula (0.34%) than in the Atqasuk area (10.85%), however consideration needs to be given to the total area being examined from each land cover class map. Perhaps a better approach would be to quantify vegetation cover based on equal areas of land cover maps to better gage the representative cover

of each class at the landscape level for these two regions. Nonetheless, this approach served to offer insight into the phenological trends in predominant vegetation classes present across both landscapes.

The major finding from this chapter highlights how MODIS NDVI generally does not capture the phenological variability noted by ground and mid-altitude platforms. One likely explanation for this is the major misalignment (pixel size calculations) between MODIS NDVI time-series datasets as seen in Figure 5.5. Workflows that derive the MODIS land cover products such as the 16-day NDVI composite used in this study, typically sense pixels compromised by cloud, smoke, BRDF issues, and other factors and replace pixel values with those of neighboring pixels that have not been compromised after which algorithms that generate NDVI and other products are computed (*Solano et al.*, 2010). Another possible anomaly that could have impacted this study was that the 250 x 250 m MODIS pixels used in this study tended to be smaller (231.65 x 231.65 meters), following projection using a sinusoidal projection. Other studies have shown that cylindrical shapes displayed in a two dimensional plane can create artifacts such as a reduction in pixel sizes of resulting raster datasets (*Steinwand et al.*, 1995; *Usery et al.*, 2003; *Battersby et al.*, 2016).

Based on results from this study and previous chapters, we conclude that each sensor varies in its capacity to adequately capture vegetation greening dynamics for different tundra plant communities at different spatial scales. Each approach does have the capacity to provide improved sensing capacities for specific purposes, which suggests new approaches could be developed to better target specific ecosystem properties and processes. For example, plot level Pheno-cams could be tested for their capacity to capture pheno-phase development at the plot-level, while KAP and other airborne systems (i.e. drones and fixed wing unmanned aerial vehicles) can offer improved coverage of mid-scale efforts during conditions that prevent adequate satellite observations (e.g. cloud cover etc.). Airborne sensors onboard manned aircraft systems such as those planned by the NASA Arctic-Boreal Vulnerability Experiment (ABoVE) as well as by the National Ecological Observatory Network (NEON) will offer a unique opportunity to further assess the relative efficacy of the MODIS platform and derived products and potential solutions.

There is an urgent need for improved fusion and coupling between remote sensing platforms focused on improving understanding of the dynamic and changing arctic at multiple spatial scales.

5.7 CONCLUSION

Given the limitations of remote sensing in the Arctic and the results from the previous three chapters, the goals of this chapter were to explore the capacity of these low-cost alternatives in monitoring tundra landscape structure and function spanning an area typical of that sampled by globally orbiting satellite platforms such as MODIS (1 km^2). Specifically, we explored the phenological spatiotemporal variability across the MISP transects and CALM grids for both Utqiaġvik and Atqasuk, including predominant vegetation classes present throughout each landscapes and spatial scales ranging from plot level to the pixel scale of the MODIS NDVI land cover products. Using land cover classification maps of the Utqiaġvik and Atqasuk areas we calculated the percentage of each vegetation class across the entire landscape and within each MODIS pixel and results suggest that the predominant vegetation class at both locations is moist and wet classes. This raises the possibility of satellite signals being driven by these particularly productive land cover types versus those that contain drier soil moisture contents. Moreover, when comparing phenology across the various spatiotemporal scales, little accordance was seen between all ground-based indices and those observed from the spaceborne MODIS platform in Utqiaġvik, however correlations were stronger in Atqasuk. Alignment of MODIS time-series datasets was also explored for this study and findings highlight the need to further quantify the accuracy of MODIS algorithms for calculating surface reflectance as well as the potential effect the bidirectional reflectance distribution functions (BRDF) have on these spaceborne platforms and their methods for acquiring data.

5.8 REFERENCES

Aber, J. S., R. J. Sobieski, D. a Distler, and M. C. Nowak (1999), Kite Aerial Photography for Environmental Site Investigations, , *102*(1), 57–67, doi:10.2307/3628217.

Aber, J. S., S. W. Aber, and F. Pavri (2002), Unmanned Small-Format Aerial Photography From Kites for Acquiring Large-Scale , High-Resolution , Multiview-Angle Imagery, *Int. Arch. Photogramm. Remote Sens. Spat. Inf. Sci.*, *34*(1), 1–6.

Aber, J. S., D. Eberts, and S. W. Aber (2005), Applications of kite aerial photography: Biocontrol of salt cedar (Tamarix) in the western United States, *Trans. Kansas Acad. Sci.*, *108*(1 & 2), 63–66, doi:10.1660/0022-8443(2005)108[0063:AOKAPB]2.0.CO;2.

ACIA (2004a), Impacts of a Warming Arctic: Arctic Climate Impact Assessment, *Cambridge Univ. Press*, 1046, doi:10.2277/0521617782.

ACIA (2004b), Impacts of a Warming Arctic: Arctic Climate Impact Assessment, *Cambridge Univ. Press*, 1046, doi:10.2277/0521617782.

Andresen, C. G. (2014), Monitoring and understanding decadal scale changes in hydrology, productivity and carbon balance in Arctic tundra ponds, , 108.

Andresen, C. G., and V. L. Lougheed (2015), Disappearing Arctic tundra ponds: Fine-scale analysis of surface hydrology in drained thaw lake basins over a 65 year period (1948–2013), , 1–14, doi:10.1002/2014JG002778.Received.

Andresen, C. G., S. A. Vargas, V. L. Lougheed, and C. E. Tweedie (2014), Kite-based Aerial Photography (KAP): A Low Cost, Effective Tool for Wetland Research, *Wetl. Sci. Pract.*, *Dec*(December), 28–31.

Arft, a. M. et al. (1999), Responses of Tundra plants to experimental warming: Meta-analysis of the International Tundra Experiment, *Ecol. Monogr.*, *69*(4), 491–511, doi:10.1890/0012-9615(1999)069[0491:ROTPTE]2.0.CO;2.

Bangen, S. G., J. M. Wheaton, N. Bouwes, B. Bouwes, and C. Jordan (2014), A methodological intercomparison of topographic survey techniques for characterizing wadeable streams and rivers, *Geomorphology*, *206*, 343–361, doi:10.1016/j.geomorph.2013.10.010.

Battersby, S. E., D. “daan” Strebe, and M. P. Finn (2016), Shapes on a plane: evaluating the impact of projection distortion on spatial binning, *Cartogr. Geogr. Inf. Sci.*, *406*(May), 1–12, doi:10.1080/15230406.2016.1180263.

Beamish, A. L., W. Nijland, M. Edwards, N. C. Coops, and G. H. R. Henry (2016), Phenology and vegetation change measurements from true colour digital photography in high Arctic tundra, *NRC Res. Press*, *49*(May), 33–49.

Bhardwaj, A., L. Sam, A. Bhardwaj, and F. J. Martín-Torres (2016), LiDAR remote sensing of the cryosphere: Present applications and future prospects, *Remote Sens. Environ.*, *177*, 125–143, doi:10.1016/j.rse.2016.02.031.

Bhatt, U. S. et al. (2010), Circumpolar Arctic tundra vegetation change is linked to sea ice decline, *Earth Interact.*, *14*(8), doi:10.1175/2010EI315.1.

Bhatt, U. S., D. a. Walker, M. K. Raynolds, P. a. Bieniek, H. E. Epstein, J. C. Comiso, J. E. Pinzon, C. J. Tucker, and I. V. Polyakov (2013), Recent declines in warming and vegetation greening trends over pan-arctic tundra, *Remote Sens.*, *5*(9), 4229–4254, doi:10.3390/rs5094229.

Biasi, C., W. Wanek, O. Rusalimova, C. Kaiser, C. Biasi, W. Wanek, C. Kaiser, H. Meyer, and A. Richter (2017), Microtopography and Plant-Cover Controls on Nitrogen Dynamics in Hummock Tundra Ecosystems in Siberia Meyer , Pavel Barsukov and Andreas Richter Published by : INSTAAR , University of Colorado Stable URL : http://www.jstor.org/stable/4095862 REFERENCES Li, , *37*(4), 435–443.

Boelman, N. T., M. Stieglitz, H. M. Rueth, M. Sommerkorn, K. L. Griffin, G. R. Shaver, and J. a Gamon (2003), Response of NDVI, biomass, and ecosystem gas exchange to long-term warming and fertilization in wet sedge tundra., *Oecologia*, *135*(3), 414–421, doi:10.1007/s00442-003-1198-3.

Boelman, N. T., L. Gough, J. R. McLaren, and H. Greaves (2011a), Does NDVI reflect variation in the structural attributes associated with increasing shrub dominance in arctic tundra?, *Environ. Res. Lett.*, *6*(3), 35501, doi:10.1088/1748-9326/6/3/035501.

Boelman, N. T., L. Gough, J. R. McLaren, and H. Greaves (2011b), Does NDVI reflect variation in the structural attributes associated with increasing shrub dominance in arctic tundra?, *Environ. Res. Lett.*, *6*, 35501, doi:10.1088/1748-9326/6/3/035501.

Bradley, N. L., C. A. Leopold, J. Ross, and W. Huffaker (1999), Phenological changes reflect climate change in Wisconsin., *Proc. Natl. Acad. Sci. U. S. A.*, *96*(August), 9701–9704, doi:10.1073/pnas.96.17.9701.

Brown, J., P. C. Miller, L. L. Tieszen, and F. L. Bunnell (1980), *An Arctic Ecosystem: The Coastal Tundra at Barrow, Alaska*.

Brown, J., F. E. Nelson, and K. M. Hinkel (2000), The circumpolar active layer monitorign (CALM) program research designs and initial results, *Polar Geogr.*, *3*(May 2012), 162–165.

Cabin, R. J., R. J. Mitchell, E. Siemann, D. Wedin, and K. S. N. Bio (2000), To Bonferroni or Not to Bonferroni : When and How Are the Questions Published by : Wiley on behalf of the Ecological Society of America Stable URL : http://www.jstor.org/stable/20168454 How Are the Questions To Bonferroni or Not to Bonferroni : When and, , *81*(3), 246–248.

Carlisle, B. H. (2005), Modelling the spatial distribution of DEM error, *Trans. GIS*, *9*(4), 521–540, doi:10.1111/j.1467-9671.2005.00233.x.

Carter, J., Schmid, K., Waters, K., Betzhold, L., Hadley, B., Mataosky, R., Halleran, J. (2012), Lidar 101 : An Introduction to Lidar Technology , Data , and Applications, *NOAA Coast. Serv. Cent.*, (November), 76.

Chapin, F. S. et al. (2005), Role of Land-Surface Changes in Arctic Summer Warming, *Science (80-.).*, *657*(2005), 9–13, doi:10.1126/science.1117368.

Chaplot, V., F. Darboux, H. Bourennane, S. Leguédois, N. Silvera, and K. Phachomphon (2006), Accuracy of interpolation techniques for the derivation of digital elevation models in relation to landform types and data density, *Geomorphology*, *77*(1–2), 126–141, doi:10.1016/j.geomorph.2005.12.010.

Chen, C., and T. Yue (2010), A method of DEM construction and related error analysis, *Comput. Geosci.*, *36*(6), 717–725, doi:10.1016/j.cageo.2009.12.001.

Claudio, H. C., Y. Cheng, D. a. Fuentes, J. a. Gamon, H. Luo, W. Oechel, H. L. Qiu, A. F. Rahman, and D. a. Sims (2006), Monitoring drought effects on vegetation water content and fluxes in chaparral with the 970??nm water band index, *Remote Sens. Environ.*, *103*(3), 304–311, doi:10.1016/j.rse.2005.07.015.

Cleland, E. E., I. Chuine, A. Menzel, H. a. Mooney, and M. D. Schwartz (2007), Shifting plant phenology in response to global change, *Trends Ecol. Evol.*, *22*(7), 357–365, doi:10.1016/j.tree.2007.04.003.

Dandois, J. P., and E. C. Ellis (2010), Remote sensing of vegetation structure using computer vision, *Remote Sens.*, *2*(4), 1157–1176, doi:10.3390/rs2041157.

Dandois, J. P., and E. C. Ellis (2013), High spatial resolution three-dimensional mapping of vegetation spectral dynamics using computer vision, *Remote Sens. Environ.*, *136*, 259–276, doi:10.1016/j.rse.2013.04.005.

Darnell, A. R., N. J. Tate, and C. Brunsdon (2008), Improving user assessment of error implications in digital elevation models, *Comput. Environ. Urban Syst.*, *32*(4), 268–277, doi:10.1016/j.compenvurbsys.2008.02.003.

Delbart, N., T. Le Toan, L. Kergoat, and V. Fedotova (2006), Remote sensing of spring phenology in boreal regions: A free of snow-effect method using NOAA-AVHRR and SPOT-VGT data (1982-2004), *Remote Sens. Environ.*, *101*(1), 52–62, doi:10.1016/j.rse.2005.11.012.

Desmet, P. J. J. (1997), Effects Of Iinterpolation Errors On The Aanalysis Of DEMs, *Earth Surf. Process. Landforms*, *22*(June 1996), 563–580.

Dowling, T., A. Read, and J. Gallant (2009), Very high resolution DEM acquisition at low cost using a digital camera and free software, *18th World IMACS/MODSIM09 Congr.*, (July), 2479–2485.

Elmendorf, S. C. et al. (2012a), Global assessment of experimental climate warming on tundra vegetation: Heterogeneity over space and time, *Ecol. Lett.*, *15*(2), 164–175, doi:10.1111/j.1461-0248.2011.01716.x.

Elmendorf, S. C. et al. (2012b), Plot-scale evidence of tundra vegetation change and links to recent summer warming, *Nat. Clim. Chang.*, *2*(6), 453–457, doi:10.1038/nclimate1465.

Epstein, H. E., M. K. Raynolds, D. a Walker, U. S. Bhatt, C. J. Tucker, and J. E. Pinzon (2012), Dynamics of aboveground phytomass of the circumpolar Arctic tundra during the past three decades, *Environ. Res. Lett.*, *7*(1), 15506, doi:10.1088/1748-9326/7/1/015506.

Erdoğan, S. (2010), Modelling the spatial distribution of DEM error with geographically weighted regression: An experimental study, *Comput. Geosci.*, *36*(1), 34–43, doi:10.1016/j.cageo.2009.06.005.

Esri (2001), ArcGIS Geostatistical Analyst: Statistical Tools for Data Exploration, Modeling, and Advanced Surface Generation, , (August), 19.

ESRI (2013), Overview of Arc Hydro Terrain Preprocessing Workflows, , (February), 13.

Von Fischer, J. C., R. C. Rhew, G. M. Ames, B. K. Fosdick, and P. E. Von Fischer (2010), Vegetation height and other controls of spatial variability in methane emissions from the Arctic coastal tundra at Barrow, Alaska, *J. Geophys. Res. Biogeosciences*, *115*(3), 1–11, doi:10.1029/2009JG001283.

Fisher, P. (1998), Improved modeling of elevation error with Geostatistics, *Geoinformatica*, *2*(3), 215–233, doi:10.1023/A:1009717704255.

Fonstad, M. a., J. T. Dietrich, B. C. Courville, J. L. Jensen, and P. E. Carbonneau (2013), Topographic structure from motion: A new development in photogrammetric measurement, *Earth Surf. Process. Landforms*, *38*(4), 421–430, doi:10.1002/esp.3366.

Fraser, R. H., I. Olthof, T. C. Lantz, and C. Schmitt (2016), UAV Photogrammetry for Mapping Vegetation in the Low-Arctic, *Arct. Sci.*, *102*(June), 1–51, doi:10.1139/as-2016-0008.

Gamon, J. a, G. P. Kershaw, S. Williamson, and D. S. Hik (2012a), Microtopographic patterns in an arctic baydjarakh field: do fine-grain patterns enforce landscape stability?, *Environ. Res. Lett.*, *7*(1), 15502, doi:10.1088/1748-9326/7/1/015502.

Gamon, J. a., Y. Cheng, H. Claudio, L. MacKinney, and D. a. Sims (2006), A mobile tram system for systematic sampling of ecosystem optical properties, *Remote Sens. Environ.*, *103*(3), 246–254, doi:10.1016/j.rse.2006.04.006.

Gamon, J. a., K. F. Huemmrich, R. S. Stone, and C. E. Tweedie (2013), Spatial and temporal variation in primary productivity (NDVI) of coastal Alaskan tundra: Decreased vegetation growth following earlier snowmelt, *Remote Sens. Environ.*, *129*, 144–153, doi:10.1016/j.rse.2012.10.030.

Gamon, J. A., G. P. Kershaw, S. Williamson, and D. S. Hik (2012b), Microtopographic patterns in an arctic baydjarakh field: do fine-grain patterns enforce landscape stability?, *Environ. Res. Lett.*, *7*(1), 15502, doi:10.1088/1748-9326/7/1/015502.

Gao, J. (1997), Resolution and accuracy of terrain representation by grid DEMs at a micro-scale, *Int. J. Geogr. Inf. Sci.*, *11*(2), 199–212, doi:10.1080/136588197242464.

Gao, X., and a. R. Huete (2000), Validation of MODIS land surface reflectance and vegetation indices with multi-scale high spatial resolution data, *IGARSS 2000. IEEE 2000 Int. Geosci. Remote Sens. Symp. Tak. Pulse Planet Role Remote Sens. Manag. Environ. Proc. (Cat. No.00CH37120)*, 533–535, doi:10.1109/IGARSS.2000.861620.

Gitelson, A. a, Y. Zur, O. B. Chivkunova, and M. N. Merzlyak (2002), Assessing carotenoid content in plant leaves with reflectance spectroscopy., *Photochem. Photobiol.*, *75*(3), 272–281, doi:10.1562/0031-8655(2002)0750272ACCIPL2.0.CO2.

Gitelson, A. A., F. Verlag, Y. Gritz, and M. N. Merzlyak (2003), Relationships between leaf chlorophyll content and spectral reflectance and algorithms for non-destructive chlorophyll assessment in higher plant leaves, , *282*.

Goetz, S. J., A. G. Bunn, G. J. Fiske, and R. a Houghton (2005), Satellite-observed photosynthetic trends across boreal North America associated with climate and fire disturbance., *Proc. Natl. Acad. Sci. U. S. A.*, *102*(38), 13521–5, doi:10.1073/pnas.0506179102.

Gong, J., L. Zhllin, Q. Zhu, H. Sui, and Y. Zhou (2000), Effects of Various Factors on the Accuracy of DEMs : An Intensive Experimental Investigation, *Photogramm. Eng. Remote Sens.*, *66*(9), 1113–1117.

Goswami, S., J. a. Gamon, and C. E. Tweedie (2011), Surface hydrology of an arctic ecosystem: Multiscale analysis of a flooding and draining experiment using spectral reflectance, *J. Geophys. Res. Biogeosciences*, *116*(1), 1–14, doi:10.1029/2010JG001346.

Harwin, S., and A. Lucieer (2012), Assessing the accuracy of georeferenced point clouds produced via multi-view stereopsis from Unmanned Aerial Vehicle (UAV) imagery, *Remote Sens.*, *4*(6), 1573–1599, doi:10.3390/rs4061573.

Haugen, R.K., and Brown, J. (1980), Coastal-Inland Distributions of Summer Air Temperature and Precipitation in Northern Alaska, *Arct. Alp. Res.*, *12*(4), 403–412.

Healey, N. C., Oberbauer, S.F., Ahrends, H.E., Dierick, D., Welker, J.M., Leffler, A.J., Hollister, R.D., Vargas, S.A., Tweedie, C. E. (2014), A Mobile Instrumented Sensor Platform for Long-Term Terrestrial Ecosystem Analysis: An Example Application in an Arctic Tundra Ecosystem, *J. Environ. Informatics*, *24*(1), 1–10, doi:10.3808/jei.201400278.

Heimsath, A. M., and H. Farid (2002), Hillslope topography from unconstrained photographs, *Math. Geol.*, *34*(8), 929–952, doi:10.1023/A:1021364623017.

Helbig, M., J. Boike, M. Langer, P. Schreiber, B. R. K. Runkle, and L. Kutzbach (2013), Spatial and seasonal variability of polygonal tundra water balance: Lena River Delta, northern Siberia (Russia), *Hydrogeol. J.*, *21*(1), 133–147, doi:10.1007/s10040-012-0933-4.

Henry, G. H R and Molau, U. (1997), Tundra plants and climate change : the International Tundra Experiment (ITEX), , *3*, 1–9.

Henry, G., R. Hollister, I. S. Jónsdóttir, K. Klanderlud, U. Molau, S. F. Oberbauer, P. Webber, and P. Wookey (2013), The International Tundra Experiment: An Arctic Monitoring Network,

Hinzman, L. D., C. J. Deal, a. D. Mcguire, S. H. Mernild, I. V. Polyakov, and J. E. Walsh (2013), Trajectory of the Arctic as an integrated system, *Ecol. Appl.*, *23*(8), 1837–1868, doi:10.1890/11-1498.1.

Hollister, R. D. (2003), Response of Tundra Vegetation to Temperature: Implications for Forcasting Vegetation Change,

Hollister, R. D., and K. J. Flaherty (2010), Above- and below-ground plant biomass response to experimental warming in northern Alaska, *Appl. Veg. Sci.*, *13*(3), 378–387, doi:10.1111/j.1654-109X.2010.01079.x.

Hollister, R. D., P. J. Webber, and C. E. Tweedie (2005), The response of Alaskan arctic tundra to experimental warming: Differences between short- and long-term responses, *Glob. Chang. Biol.*, *11*(4), 525–536, doi:10.1111/j.1365-2486.2005.00926.x.

Hollister, R. D., P. J. Webber, and C. Bay (2014), Plant Response to Temperature in Northern Alaska : Implications for Predicting Vegetation Change PLANT RESPONSE TO TEMPERATURE IN NORTHERN ALASKA :, , *86*(6), 1562–1570.

Huemmrich, K. F. et al. (2010), Remote sensing of tundra gross ecosystem productivity and light use efficiency under varying temperature and moisture conditions, *Remote Sens. Environ.*, *114*(3), 481–489, doi:10.1016/j.rse.2009.10.003.

Huemmrich, K. F., J. Gamon, C. E. Tweedie, P. P. K. Campbell, D. Landis, and E. Middleton (2013), Arctic Tundra Vegetation Functional Types Based on Photosynthetic Physiology and Optical Properties, , 1–37.

Humphreys, E. R., and P. M. Lafleur (2011), sequestration in two low Arctic tundra ecosystems?, *Geophys. Res. Lett.*, *38*(9), 3–7, doi:10.1029/2011GL047339.

Hunter, G. j., and M. F. Goodchild (1997), Modeling the Uncertainty of Slope and Aspect Estimates Derived from Spatial Databases,

Hutchinson, M. F., T. Xu, and J. a Stein (2011), Recent Progress in the ANUDEM Elevation Gridding Procedure, *Geomorphometry*, 19–22.

Ide, R., and H. Oguma (2013), A cost-effective monitoring method using digital time-lapse cameras for detecting temporal and spatial variations of snowmelt and vegetation phenology in alpine ecosystems, *Ecol. Inform.*, *16*, 25–34, doi:10.1016/j.ecoinf.2013.04.003.

IPCC (2014), Climate Change 2014: Synthesis Report. Contribution of Working Groups I, II and III to the Fifth Assessment Report of the Intergovernmental Panel on Climate Change.

Jarihani, A. a., J. N. Callow, T. R. McVicar, T. G. Van Niel, and J. R. Larsen (2015), Satellite-derived Digital Elevation Model (DEM) selection, preparation and correction for hydrodynamic modelling

in large, low-gradient and data-sparse catchments, *J. Hydrol.*, *524*, 489–506, doi:10.1016/j.jhydrol.2015.02.049.

Javernick, L., J. Brasington, and B. Caruso (2014), Modeling the topography of shallow braided rivers using Structure-from-Motion photogrammetry, *Geomorphology*, *213*, 166–182, doi:10.1016/j.geomorph.2014.01.006.

Jia, G. J. (2003), Greening of arctic Alaska, 1981–2001, *Geophys. Res. Lett.*, *30*(20), 3–6, doi:10.1029/2003GL018268.

Jorgenson, M. T., M. Kanevskiy, Y. Shur, N. Moskalenko, D. R. N. Brown, K. Wickland, R. Striegl, and J. Koch (2015), Journal of Geophysical Research : Earth Surface, , 1–18, doi:10.1002/2015JF003602.Received.

Kasischke, E.S., et al. (2014), A Concise Experiment Plan for the Arctic-Boreal Vulnerability Experiment, *http://above.nasa.gov/acep/acep_final_pdf.pdf. Accessed 1/25/2015.*

Keenan, T. F. et al. (2014), Tracking forest phenology and seasonal physiology using digital repeat photography : a critical assessment, , *24*(6), 1478–1489.

Komarkova, V., and Webber, P. J. (1980), Two Low Arctic Vegetation Maps near Atkasook , Alaska, , *12*(4), 447–472.

Krivoruchko, K. (2004), Introduction to Modeling Spatial Processes Using Geostatistcal Analyst, *Esri*, 1–27.

Kurc, S. a., and L. M. Benton (2010), Digital image-derived greenness links deep soil moisture to carbon uptake in a creosotebush-dominated shrubland, *J. Arid Environ.*, *74*(5), 585–594, doi:10.1016/j.jaridenv.2009.10.003.

Laidler, G. J., P. M. Treitz, and D. M. Atkinson (2008), Remote Sensing of Arctic Vegetation : Relations between the NDVI , Spatial Resolution and Vegetation Cover on Boothia Peninsula , Nunavut Author (s): Gita J . Laidler , Paul M . Treitz and David M . Atkinson Published by : Arctic Institute of North Amer, , *61*(1), 1–13.

Lara, M. J., a. D. McGuire, E. S. Euskirchen, C. E. Tweedie, K. M. Hinkel, A. N. Skurikhin, V. E. Romanovsky, G. Grosse, W. R. Bolton, and H. Genet (2014), Polygonal tundra geomorphological change in response to warming alters future CO 2 and CH 4 flux on the Barrow Peninsula, *Glob. Chang. Biol.*, (August), n/a-n/a, doi:10.1111/gcb.12757.

Lassueur, T., S. Joost, and C. F. Randin (2006), Very high resolution digital elevation models: Do they improve models of plant species distribution?, *Ecol. Modell.*, *198*(1–2), 139–153, doi:10.1016/j.ecolmodel.2006.04.004.

Leberl, F., a Irschara, T. Pock, P. Meixner, M. Gruber, S. Scholz, and a Wiechert (2010), Point Clouds: Lidar versus 3D Vision, *Photogramm. Eng. Remote Sens.*, *76*(10), 1123–1134, doi:0099-1112/10/7610–1123.

Lefsky, M. a, W. B. Cohen, G. G. Parker, and J. David (2014), Lidar Remote Sensing for Ecosystem Studies, , *52*(1), 19–30.

Li, Z. (2014), Watershed modeling using arc hydro based on DEMs: a case study in Jackpine watershed, *Environ. Syst. Res.*, *3*(1), 11, doi:10.1186/2193-2697-3-11.

Liljedahl, A.K., Hinzman, L.D., Schulla, J. (2012), Ice-Wedge Polygon Type Controls Low-Gradient Watershed-Scale Hydrology,

Liljedahl, A. K. et al. (2016), Pan-Arctic ice-wedge degradation in warming permafrost and influence on tundra hydrology, *Nat. Geosci.*, *9*(April), 312–318, doi:10.1038/ngeo2674.

Lin, D. H., D. R. Johnson, C. Andresen, and C. E. Tweedie (2012), High spatial resolution decade-time scale land cover change at multiple locations in the Beringian Arctic (1948–2000s), *Environ. Res. Lett.*, *7*(2), 25502, doi:10.1088/1748-9326/7/2/025502.

Liu, H. Q., and A. Huete (1995), Feedback based modification of the NDVI to minimize canopy background and atmospheric noise, *IEEE Trans. Geosci. Remote Sens.*, *33*(2), 457–465, doi:10.1109/36.377946.

Liu, Z. L. Z., S. C. S. Cui, and Q. Y. Q. Yan (2008), Building extraction from high resolution satellite imagery based on multi-scale image segmentation and model matching, *2008 Int. Work. Earth Obs. Remote Sens. Appl.*, doi:10.1109/EORSA.2008.4620321.

Lucht, W. (2002), Climatic Control of the High-Latitude Vegetation Greening Trend and Pinatubo Effect, *Science (80-.).*, *296*(5573), 1687–1689, doi:10.1126/science.1071828.

Marzolff, I., J. B. Ries, and K. D. Albert (2002), Kite aerial photography for gully monitoring in sahelian landscapes, , 18–20.

McCune, B., and Grace, J. . (2002), Analysis of Ecological Communities, *MjM Softw. Des. Gleneden Beach, McKinney M.L*, *127*(January 2002), 247–260, doi:10.1016/S0022-0981(03)00091-1.

Menzel, a, and P. Fabian (1999), Growing season extended in Europe, *Nature*, *397*(6721), 659, doi:10.1038/17709.

Migliavacca, M. et al. (2011), Using digital repeat photography and eddy covariance data to model grassland phenology and photosynthetic CO2 uptake, *Agric. For. Meteorol.*, *151*(10), 1325–1337, doi:10.1016/j.agrformet.2011.05.012.

Myneni, R. B., C. D. Keeling, C. J. Tucker, G. Asrar, and R. R. Nemani (1997), Increased plant growth in the northern high latitudes from 1981 to 1991, *Nature*, *386*(6626), 698–702, doi:10.1038/386698a0.

Nelson, F. E., S. I. Outcalt, J. Brown, N. I. Shiklomanov, and K. M. Hinkel (1998), Spatial and Temporal Attributes of the Active-Layer Thickness Record, Barrow, Alaska, U.S.A., , (55), 797–802.

Nelson, S. and (2015), Circumpolar Active Layer Monitoring (CALM) Program, *Natl. Snow Ice Data Cent.*, 1–3.

Noh, M.-J., and I. M. Howat (2015a), Automated stereo-photogrammetric DEM generation at high latitudes: Surface Extraction with TIN-based Search-space Minimization (SETSM) validation and demonstration over glaciated regions, *GIScience Remote Sens.*, *1603*(June 2015), 1–20, doi:10.1080/15481603.2015.1008621.

Noh, M.-J., and I. M. Howat (2015b), Automated stereo-photogrammetric DEM generation at high latitudes: Surface Extraction with TIN-based Search-space Minimization (SETSM) validation and demonstration over glaciated regions, *GIScience Remote Sens.*, *1603*(June 2015), 1–20, doi:10.1080/15481603.2015.1008621.

Oberbauer, S. F. et al. (2007), Tundra CO2 fluxes in response to experimental warming across lattitudinal and moisture gradients, *Ecol. Monogr.*, *77*(2), 221–238, doi:10.1890/06-0649.

Oberbauer, S. F. et al. (2013a), Phenological response of tundra plants to background climate variation tested using the International Tundra Experiment,

Oberbauer, S. F. et al. (2013b), Phenological response of tundra plants to background climate variation tested using the International Tundra Experiment., *Philos. Trans. R. Soc. Lond. B. Biol. Sci.*, *368*(1624), 20120481, doi:10.1098/rstb.2012.0481.

Oberbauer, S. F. et al. (2013c), Phenological response of tundra plants to background climate variation tested using the International Tundra Experiment., *Philos. Trans. R. Soc. Lond. B. Biol. Sci.*, *368*(1624), 20120481, doi:10.1098/rstb.2012.0481.

Olivas, P. C., S. F. Oberbauer, C. E. Tweedie, W. C. Oechel, and A. Kuchy (2010), Responses of CO2 flux components of Alaskan Coastal Plain tundra to shifts in water table, *J. Geophys. Res. Biogeosciences*, *115*(4), 1–13, doi:10.1029/2009JG001254.

Osterkamp, T. E., M. . Jorgenson, E. A. G. Schuur, Y. L. Shur, M. . Kanevskiy, J. G. Vogel, and V. E. Tumskoy (2009), Physical and Ecological Changes Associated with Warming Permafrost and Thermokarst in Interior Alaska, *Permafr. Periglac. Process.*, *136*(January), 107–136, doi:10.1002/ppp.

Painter, S. L., J. D. Moulton, and C. J. Wilson (2012), Modeling challenges for predicting hydrologic response to degrading permafrost, *Hydrogeol. J.*, *21*(Hydrogeology of Cold Regions), 221–224, doi:10.1007/s10040-012-0917-4.

Park, H., Y. Kim, and J. S. Kimball (2016), Widespread permafrost vulnerability and soil active layer increases over the high northern latitudes inferred from satellite remote sensing and process model assessments, *Remote Sens. Environ.*, *175*, 349–358, doi:10.1016/j.rse.2015.12.046.

Peichl, M., O. Sonnentag, and M. B. Nilsson (2014), Bringing Color into the Picture: Using Digital Repeat Photography to Investigate Phenology Controls of the Carbon Dioxide Exchange in a Boreal Mire, *Ecosystems*, *18*(1), 115–131, doi:10.1007/s10021-014-9815-z.

Penuelas, J., I. Filella, J. A. Gamon, B. Y. J. Penuelas, I. Filella, and A. Gamon (1995), Assessment of photosynthetic radiation-use efficiency with spectral reflectance, , *131*(3), 291–296.

Post, E. et al. (2009), Ecological dynamics across the Arctic associated with recent climate change., *Science*, *325*(5946), 1355–1358, doi:10.1126/science.1173113.

Raaflaub, L. D., and M. J. Collins (2006), The effect of error in gridded digital elevation models on the estimation of topographic parameters, *Environ. Model. Softw.*, *21*(5), 710–732, doi:10.1016/j.envsoft.2005.02.003.

Rango, A., A. Laliberte, and C. Winters (2008), Role of aerial photos in compiling a long-term remote sensing data set, *J. Appl. Remote Sens.*, *2*(1), 23541, doi:10.1117/1.3009225.

Raynolds, M. K., J. C. Comiso, D. A. Walker, and D. Verbyla (2008), Relationship between satellite-derived land surface temperatures, arctic vegetation types, and NDVI, *Remote Sens. Environ.*, *112*(4), 1884–1894, doi:10.1016/j.rse.2007.09.008.

Richardson, A. D., J. P. Jenkins, B. H. Braswell, D. Y. Hollinger, S. V. Ollinger, and M. L. Smith (2007), Use of digital webcam images to track spring green-up in a deciduous broadleaf forest, *Oecologia*, *152*(2), 323–334, doi:10.1007/s00442-006-0657-z.

Richardson, A. D., B. H. Braswell, D. Y. Hollinger, J. P. Jenkins, and S. V. Ollinger (2009), Near-surface remote sensing of spatial and temporal variation in canopy phenology, *Ecol. Appl.*, *19*(6), 1417–1428, doi:10.1890/08-2022.1.

Richardson, A. D., T. F. Keenan, M. Migliavacca, Y. Ryu, O. Sonnentag, and M. Toomey (2013), Climate change, phenology, and phenological control of vegetation feedbacks to the climate system, *Agric. For. Meteorol.*, *169*, 156–173, doi:10.1016/j.agrformet.2012.09.012.

Rondeaux, G., M. Steven, and F. Baret (1996), Optimization of Soil-Adjusted Vegetation Indices, , *107*(August 1994), 95–107.

Rosnell, T., and E. Honkavaara (2012), Point cloud generation from aerial image data acquired by a quadrocopter type micro unmanned aerial vehicle and a digital still camera, *Sensors*, *12*(1), 453–480, doi:10.3390/s120100453.

Saitoh, T. M., S. Nagai, N. Saigusa, H. Kobayashi, R. Suzuki, K. N. Nasahara, and H. Muraoka (2012), Assessing the use of camera-based indices for characterizing canopy phenology in relation to gross primary production in a deciduous broad-leaved and an evergreen coniferous forest in Japan, *Ecol. Inform.*, *11*, 45–54, doi:10.1016/j.ecoinf.2012.05.001.

Schuur, E. et al. (2008), Vulnerability of Permafrost Carbon to Climate Change : Implications for the Global Carbon Cycle, *Bioscience*, *58*(8), 701–714.

Schwartz, M. D. (1998), Green-wave phenology, *Nature*, *394*, 839–840, doi:10.1038/29670.

Screen, J. a, and I. Simmonds (2010), The central role of diminishing sea ice in recent Arctic temperature amplification., *Nature*, *464*(7293), 1334–1337, doi:10.1038/nature09051.

Shaver, G. R., L. E. Street, E. B. Rastetter, M. T. Van Wijk, and M. Williams (2007), Functional convergence in regulation of net CO_2 flux in heterogeneous tundra landscapes in Alaska and Sweden, *J. Ecol.*, *95*(4), 802–817, doi:10.1111/j.1365-2745.2007.01259.x.

Sims, D. A., and J. A. Gamon (2002), Relationships between leaf pigment content and spectral reflectance across a wide range of species , leaf structures and developmental stages, , *81*, 337–354.

Smith, L. C., Y. Sheng, G. M. Macdonald, and L. D. Hinzman (2005), Disappearing Arctic lakes, , *XXX*(June), 2005.

Snavely, N., S. M. Seitz, and R. Szeliski (2008), Modeling the world from Internet photo collections, *Int. J. Comput. Vis.*, *80*(2), 189–210, doi:10.1007/s11263-007-0107-3.

Solano, R., K. Didan, A. Jacobson, and A. Huete (2010), MODIS Vegetation Index User ' s Guide (MOD13 Series), , *2010*(May).

Sommerkorn, M. (2008), Micro-topographic patterns unravel controls of soil water and temperature on soil respiration in three Siberian tundra systems, *Soil Biol. Biochem.*, *40*(7), 1792–1802, doi:10.1016/j.soilbio.2008.03.002.

Steinwand, D. A., J. A. Hutchinson, and J. P. Snyder (1995), Map Projections for Global and Continental Data Sets and an Analysis of Pixel Distortion Caused by Reprojection, *Photogrammatic Eng. Remote Sens.*, *61*(12), 1487–1497.

Stewart, K. J., P. Grogan, D. S. Coxson, and S. D. Siciliano (2014), Topography as a key factor driving atmospheric nitrogen exchanges in arctic terrestrial ecosystems, *Soil Biol. Biochem.*, *70*(3), 96–112, doi:10.1016/j.soilbio.2013.12.005.

Stow, D. a. et al. (2004), Remote sensing of vegetation and land-cover change in Arctic Tundra Ecosystems, *Remote Sens. Environ.*, *89*(3), 281–308, doi:10.1016/j.rse.2003.10.018.

Streletskiy, D. A., N. I. Shiklomanov, F. E. Nelson, and A. E. Klene (2007), 13 Years of Observations at Alaskan CALM Sites: Long-term Active Layer and Ground Surface Temperature Trends, *Proc. 9th Int. Conf. Permafr.*, 1–6.

Sullivan, P. F., S. J. T. Arens, R. A. Chimner, and J. M. Welker (2008), Temperature and microtopography interact to control carbon cycling in a high arctic fen, *Ecosystems*, *11*(1), 61–76, doi:10.1007/s10021-007-9107-y.

Sumerling, G. (2011), Lidar Analysis in ArcGIS ® 10 for Forestry Applications, *ESRI White Pap.*, (January), 53.

Tape, K., M. Sturm, and C. Racine (2006), The evidence for shrub expansion in Northern Alaska and the Pan-Arctic, *Glob. Chang. Biol.*, *12*(4), 686–702, doi:10.1111/j.1365-2486.2006.01128.x.

Throckmorton, H. M. et al. (2016), Active layer hydrology in an arctic tundra ecosystem: Quantifying water sources and cycling using water stable isotopes, *Hydrol. Process.*, *4986*(August), 4972–4986, doi:10.1002/hyp.10883.

Torre Jorgenson, M. et al. (2013), Reorganization of vegetation, hydrology and soil carbon after permafrost degradation across heterogeneous boreal landscapes, *Environ. Res. Lett.*, *8*(3), 35017, doi:10.1088/1748-9326/8/3/035017.

Triggs, B., P. F. McLauchlan, R. I. Hartley, and A. W. Fitzgibbon (2000), Bundle Adjustment — A Modern Synthesis, *Vis. Algorithms Theory Pract.*, *1883*, 298–372, doi:10.1007/3-540-44480-7_21.

Tucker, C. J. (1978), Red and Photographic Infrared Linear Combinations for Monitoring Vegetation,

Tucker, C. J. (1999), Higher Northern Latitude NDVI and Growing Season Trends from 1982 to 1999,

Tucker, C. J., and P. J. Sellers (2007), Satellite remote sensing of primary production, *Int. J. Remote Sens.*, *7*(11), 1395–1416, doi:10.1080/01431168608948944.

Usery, E. L., M. P. Finn, J. D. Cox, S. Ruhl, M. Bearden, E. L. Usery, M. P. Finn, J. D. Cox, and T. Beard (2003), Projecting global datasets to achieve equal areas, , *30*(1), 69–79.

Ustin, S. L., and J. A. Gamon (2010), Tansley review Remote sensing of plant functional types, , 795–816.

Vaze, J., J. Teng, and G. Spencer (2010), Impact of DEM accuracy and resolution on topographic indices, *Environ. Model. Softw.*, *25*(10), 1086–1098, doi:10.1016/j.envsoft.2010.03.014.

Villarreal, S., R. D. Hollister, D. R. Johnson, M. J. Lara, P. J. Webber, and C. E. Tweedie (2012), Tundra vegetation change near Barrow, Alaska (1972–2010), *Environ. Res. Lett.*, *7*(1), 15508, doi:10.1088/1748-9326/7/1/015508.

Vorosmarty, C. J., a. D. McGuire, and J. E. Hobbie (2010), Scaling Studies in Arctic System Science and Policy Support: A Call to Research, *U.S. Arct. Res. Comm.*, 76 pages.

Vörösmarty, C. J., L. D. Hinzman, B. J. Peterson, D. H. Bromwich, L. C. Hamilton, J. Morison, V. E. Romanovsky, M. Sturm, R. S. Webb, and D. L. Kane (2001), The Hydrologic Cycle and its Role in Arctic and Global Environmental Change: A Rationale and Strategy for Synthesis Study The Hydrologic Cycle and its Role in Arctic and Global Environmental Change, *NSF-ARCSS Hydrol. Work. Steer. Comm.*, *84*(September).

Walker, D. a et al. (2012), Environment, vegetation and greenness (NDVI) along the North America and Eurasia Arctic transects, *Environ. Res. Lett.*, *7*(1), 15504, doi:10.1088/1748-9326/7/1/015504.

Walker, M., and C. Wahren (2006), Plant community responses to experimental warming across the tundra biome, *Proc. …*, *103*(5), 1342–6, doi:10.1073/pnas.0503198103.

Ward, R. D., N. G. Burnside, C. B. Joyce, and K. Sepp (2013), The use of medium point density LiDAR elevation data to determine plant community types in Baltic coastal wetlands, *Ecol. Indic.*, *33*, 96–104, doi:10.1016/j.ecolind.2012.08.016.

Webber, P. J., and M. D. Walker (1991), The International Tundra Experiment (ITEX): Resolution, , 1990.

Wehr, A., and U. Lohr (1999), Airborne laser scanning—an introduction and overview, *ISPRS J. Photogramm. Remote Sens.*, *54*(2–3), 68–82, doi:10.1016/S0924-2716(99)00011-8.

Westergaard-Nielsen, A., M. Lund, B. U. Hansen, and M. P. Tamstorf (2013), Camera derived vegetation greenness index as proxy for gross primary production in a low Arctic wetland area, *ISPRS J. Photogramm. Remote Sens.*, *86*, 89–99, doi:10.1016/j.isprsjprs.2013.09.006.

Westoby, M. J., J. Brasington, N. F. Glasser, M. J. Hambrey, and J. M. Reynolds (2012), "Structure-from-Motion" photogrammetry: A low-cost, effective tool for geoscience applications, *Geomorphology*, *179*, 300–314, doi:10.1016/j.geomorph.2012.08.021.

Wilson, J. P. (2012), Digital terrain modeling, *Geomorphology*, *137*(1), 107–121, doi:10.1016/j.geomorph.2011.03.012.

Wu, S., J. Li, and G. H. Huang (2008), A study on DEM-derived primary topographic attributes for hydrologic applications: Sensitivity to elevation data resolution, *Appl. Geogr.*, *28*(3), 210–223, doi:10.1016/j.apgeog.2008.02.006.

Zeng, H., G. Jia, and H. Epstein (2011), Recent changes in phenology over the northern high latitudes detected from multi-satellite data, *Environ. Res. Lett.*, *6*(4), 45508, doi:10.1088/1748-9326/6/4/045508.

Zhang, Z., D. L. Kane, and L. D. Hinzman (2000), Development and application of a spatially-distributed arctic hydrological and thermal process model (ARHYTHM), *Hydrol. Process.*, *14*(6), 1017–1044, doi:10.1002/(SICI)1099-1085(20000430)14:6<1017::AID-HYP982>3.0.CO;2-G.

Zona, D., D. A. Lipson, R. C. Zulueta, S. F. Oberbauer, and W. C. Oechel (2011), Microtopographic controls on ecosystem functioning in the Arctic Coastal Plain, *J. Geophys. Res. Biogeosciences*, *116*(3), 1–12, doi:10.1029/2009JG001241.

Chapter 6: General Discussion

6.1 Overview of dissertation goals and objectives

The research presented in this dissertation has been driven by the urgent need to better understand the impacts climate change is having on arctic terrestrial ecosystem structure and function across multiple spatiotemporal scales. The effects of climate change on arctic terrestrial ecosystems are spatially and temporally complex, consisting of responses ranging from the plot to landscape and global scales (*Vorosmarty et al.*, 2010; *IPCC*, 2014). Specifically, this dissertation research focused on addressing several key challenges associated with scaling observations across multiple remote sensing platforms and sensors and spatiotemporal scales. Improving linkages between research findings made at plot to regional scales remains a challenge due to the lack of adequate low/mid altitude sampling platforms and scaling methodologies.

The prime motivation of this study was to advance observational capacities suitable for documenting multi-scale environmental change in arctic terrestrial landscapes through the development and testing of novel ground-based and low-altitude remote sensing approaches. Specifically, we employed digital repeat photography (Pheno-cams) and digital cameras attached to inexpensive kites to monitor the phenological dynamics of various vegetation communities that included study sites with contiguous plots arranged along a transect spanning multiple land cover types in polygonal tundra, to plots situated across several hectares at two locations in northern Alaska. Additionally, the kite aerial photography (KAP) system was utilized along with advanced computer vision techniques including Structure from Motion (SfM) to test the capacity of this system for modeling complex tundra surface elevation across a thermokarst landscape. Listed below are the key findings of this study and suggestions for future research that could be catalyzed by this study.

6.2 Summary and significance of research findings

This dissertation is composed of six chapters that includes a general introduction and discussion (this chapter) and four research intensive chapters that have been formatted for publication. The author of this dissertation is the primary author (writing and data analysis) on all chapters presented and oversaw field data collection conducted by multiple mostly undergraduate research assistants. The study was designed in a manner where each chapter builds upon the

knowledgebase gained in previous chapters and included the use and re-use of data collected from sites and sampling platforms associated with the International Tundra Experiment that is supported in the US through the NSF-funded Arctic Observing Network. Sections 6.2.1 to 6.2.4 below present research highlights and summarize the significance of research findings associated with each of the research intensive chapters presented in chapters two through five above.

6.2.1 How well can low-cost kite aerial photography and advanced computer vision techniques model the microtopographic heterogeneity of changing tundra surfaces? (Chapter 2)

A fine-scale digital elevation model of a thermokarst study area was produced from a gamut of overlapping digital aerial images acquired from an inexpensive mid-altitude KAP platform. Images were processed using an advanced computer vision technique (SfM) and resulting models were compared to those derived from traditional ground and airborne LiDAR remote sensing platforms (i.e. T-LiDAR and A-LiDAR) and satellite-derived DEMs. Analyses compared the accuracy, resulting errors, and efficacy of the methodologies used. The KAP system proved to be useful in modeling the spatial heterogeneity of the tundra elevational surface including all landscape landforms and features (i.e. high/low-centered polygons, ridges and troughs) and produced a high resolution and accurate DEM that contained relatively low error values (<0.04m) throughout the study area. The resulting DEM also correlated well with reference GCP elevation values and the T-LiDAR DEM. Additionally, the DEM produced from this approach was utilized to model surface hydrological dynamics including drainage and flow lines and catchment boundaries, which are typically used by ecosystem scientists to examine the ecohydrology, energy balance, controls of vegetation distribution and other ecosystem properties and processes in arctic landscapes. This system provided an easy-to-execute, low-cost alternative to traditional sampling platforms without the need for users to have acquired an advanced knowledge of remote sensing and photogrammetry. Additionally, this approach provided an advantage over the T-LiDAR method in that data acquisition occurred from a NADIR view angle that allowed for better feature extraction and point-feature matching of the landscape that appeared to successfully map the topobathy of small water bodies unlike the LiDAR platforms employed.

Results from the error analysis of this study highlighted that the KAP system produced error values localized to one section of the study area. However they seemed to be randomly

distributed within this problematic area and were not predictable, which might introduce problems when attempting to apply the approach to larger study areas. These errors might have manifested from either a) user error related to GCP placement across landform types; b) the inherent nature of the complex surface heterogeneity being sampled; c) the photogrammetric image processing algorithms applied; and/or d) the DEM interpolation algorithm used. Future studies would be well versed to develop a research approach that is cognizant of such sources of error and plan accordingly. The need for consistent winds in order to fly the kite and the need for a large number and equal distribution of GCPs across the study area appeared to be the major limitations of this system, which might affect studies across other ecosystems that experience little to no wind and those aiming cover large landscape areas. Overall, the KAP system proved to be suitable for capturing the microtopographic heterogeneity of tundra surfaces at small-spatial scales and findings match those of other similar studies focused on assessing similar metrics at other arctic sites (*Fraser et al.*, 2016) and ecosystems (*Fonstad et al.*, 2013; *Dandois and Ellis*, 2013).

6.2.2 How does imagery from kite aerial photography and fixed time-lapse digital cameras (Pheno-cams) compare in their capacity to monitor plot-level phenological dynamics of arctic vegetation communities? (Chapter 3)

This chapter explored the use of inexpensive digital imaging systems (RGB indices) for monitoring plot-level phenology across vegetation classes that were spatially contiguous (along a sampling transect) at two locations typical of high and low arctic polygonal tundra on the Coastal Plain of northern Alaska. Results were compared to traditional and generally more expensive optical remote sensing approaches (spectral indices) used to make similar measurements. We observed strong correlations between plot-level RGB-derived indices and spectrometer-derived indices for tundra vegetation classes typical of high soil moisture levels. RGB indices derived from KAP proved to be a better predictor of greening across wet vegetation classes than RGB indices derived from Pheno-cams in both locations. This is likely associated with the NADIR view angle of the KAP system versus the oblique-view of the Pheno-cams, which can be a direct cause of spectro-directional signals from the various view-angles. Pheno-cams, which sample at higher rates than the KAP used in this study might also be more sensitive to fluctuations in atmospheric light conditions that prevail over small-temporal scales and can saturate or alter image acquisitions. Thus, these results suggest that each approach might be suitable for studies focused on answering

different research questions. Pheno-cams are seemingly most appropriate for relatively small-scale plot-level or species-specific studies whereas the KAP system appears to be most suited to plot-landscape level studies.

Both RGB systems were relatively inexpensive and required users to have only minimal training compared to arguably traditionally hyperspectral radiometric approaches utilized for ground-based remote sensing of vegetation phenology (*Gamon et al.*, 2006; *Goswami et al.*, 2011). Although several other studies have utilized similar digital repeat imaging systems in arctic ecosystem studies (*Westergaard-Nielsen et al.*, 2013; *Andresen*, 2014), none have explored the relative applicability and capacity of aerial digital sampling from platforms such as the KAP system, which is an analogue of unmanned vehicle platforms that have until recently been difficult to fly legally in US air space. Our findings have provided insight to the potential of using these approaches for monitoring arctic tundra phenological dynamics of multiple vegetation classes as well as their corresponding landform types. Moreover, these particular airborne approaches (i.e. KAP) have provided support for the use of drones or unmanned aerial vehicles (UAVs) for filling the spatial and temporal remote sensing gaps that have faced arctic ecologists for decades. Such platforms have the potential to facilitate the monitoring of these rapidly changing ecosystems.

6.2.3 Can the use of multi-scale digital imaging systems be scaled to improve measurements of ecosystem properties and processes at the landscape level? (Chapter 4)

Building on chapters 2 and 3 from this dissertation, chapter 4 explored 1) the use of airborne digital photogrammetry for capturing microtopographic variability in a tundra landscape spanning an area typical of that sampled by globally orbiting satellite platforms such as MODIS (1 km^2); and 2) the capacity of digital cameras for monitoring plot-level plant phenology where plots were spatially distributed throughout a landscape typical of polygonised tundra in high and low arctic landscapes. Analysis of the large-scale DEMs across the CALM grids produced from KAP yielded comparable results to those models derived from A-LiDAR and stereo satellite imagery. The overall spatial resolution of the LiDAR and photogrammetry approaches yielded DEMs with a spatial resolution of 3.5 m, while the satellite derived DEM resulted in a slightly courser DEM (5m). The digital images captured from a helicopter were able to develop an accurate DEM, however it resulted in errors along the margins of the study site that caused some high-centered polygon areas to be poorly characterized compared to the A-LiDAR-derived DEM.

Conversely, the helicopter-derived DEM was able to model the wetter and generally low-lying water bodies and troughs well, which is consistent with the results of from chapter 2 for this land cover type. Additionally, the surface hydrology of the Utqiaġvik CALM grid was modeled by calculating drainage and flow lines and catchment boundaries for all DEMs, which showed that the helicopter RGB-derived DEM resulted in a dense flow model that was difficult to interpret - most likely as a result of the random errors present in the resulting DEM.

The analysis of multi-year observations from plot-level RGB-derived indices were compared to plot-level spectrometer reflectance measurements across the CALM grid subsets and similar results observed at the transect level (MISP) were prevailed over the spatially-distributed plots spanning the CALM grids. Generally, the majority of sensors were sensitive to vegetation classes containing higher soil moisture content in both localities (Utqiaġvik and Atqasuk). The spectrometer-derived indices were less predictable from the RGB platform within the dry vegetation classes. This suggests that signals being observed in reports of 'greening of the arctic' studies on the arctic Coastal Plain are being driven by changes within wet land cover classes although more studies are needed to explore this further. Based on these results and those from other studies (*Gamon et al.,* 2013), uncertainty remains as to what vegetation classes are driving the phenological changes in landscapes level studies that utilize globally orbiting satellite platforms such as MODIS for their base data.

6.2.4 How do results from ground-based and low-altitude digital remote sensing of the spatiotemporal variability in ecosystem processes compare with those from satellite remote sensing platforms? (Chapter 5)

Similar to the previous chapter, this study builds upon results and observations highlighted in previous studies (chapters 2-4). Specifically, we explored the phenological spatiotemporal variability across the MISP transects and CALM grids for both Utqiaġvik and Atqasuk, including vegetation classes within these landscapes and spatial scales ranging from plot level studies to the pixel scale of the MODIS NDVI land cover product. Overall, results match those recorded in chapters 2 and 3 and highlight that correlations between RGB-derived and spectrometer-derived indices and MODIS NDVI were strong for Atqasuk and weaker for Utqiaġvik. Additionally, correlations between RGB and spectral indices and MODIS NDVI were stronger for CALM subset grid plots than those from the MISP transects in Utqiaġvik, while results were more variable in

Atqasuk. One key finding from this study suggests that NDVI being calculated from the MODIS platform is overestimating seasonal and peak greening relative to ground based measurements.

Analysis of MODIS time-series datasets suggest that several factors, including the misalignment between delineated MODIS pixels in the NDVI land cover product could be related to both the overestimation of greening and the generally poor correlation with ground based platforms. Land cover classification maps were utilized to quantify the predominant vegetation classes present across both landscapes and results show that moist classes cover about 28.59% of the landscape in Utqiaġvik and roughly 40.87% of the landscape in Atqasuk. Dry classes were less abundant for both Utqiaġvik (0.34%) and Atqasuk (10.85%) across each mapped area. The major finding of this study highlights how MODIS NDVI is limited in its capacity to capture seasonal and inter-annual phenological dynamics relative to ground-based and mid-altitude platforms. Future studies are needed to address these discrepancies in order to facilitate the innovation of improved analytical methods from which an improved understanding of the changing arctic can be developed.

6.3 SIGNIFICANCE OF THE STUDY

This study addressed issues recognized by the scientific community as urgent for furthering our understanding of change in ecosystem structure and function in the Arctic (*Vorosmarty et al.*, 2010; *Kasischke, E.S. et al.*, 2014; *Nelson*, 2015). For example, there is a need for time and cost-efficient low/mid-altitude sensor platforms capable of detecting changes in arctic terrestrial regional and landscape composition, vegetation phenology, terrain structure and overall productivity across seasonal, inter-annual, and long-term temporal frames (*Healey, N.C.*, 2014). Another major issue facing arctic landscape ecologists is the development of remote sensing systems that can sample below cloud-cover as this is a persistent constraint to satellite remote sensing approaches, especially in coastal regions. Furthermore, research into the validation of satellite derived products has recently increased in prominence along with the need to inter-compare plot to landscape-level ecosystem properties and processes in order to better understand the causes and consequences of the changing arctic and its potential effects on global processes.

This study is among the first to utilize spectral data collected from the long-term environmental observing program associated with the International Tundra Experiment (ITEX), which was designed to examine the variability in arctic and alpine species and plant community

response to climate variability and change across a broad range of climatic and geographical scales (*Arft et al.*, 1999). Additionally, this is one of a few studies that has developed and tested the efficacy of cost-effective alternative digital imaging approaches suitable for examining and quantifying not only tundra surface structure but also vegetation phenology. The integration of digital sensing platforms with novel advanced computer vision techniques (SfM) shows promise for advancing understanding of arctic ecological systems and their linkages to global processes. This study is also relatively unique in that it's one of a few to test these remote sensing approaches at multiple spatial and temporal scales. Moreover, this study used readily available land surface products acquired from orbiting satellites (MODIS) to help decipher mechanisms that could be driving these satellite-detected changes and compared them to ground-based and low/mid altitude sampling datasets collected across 6 arctic growing seasons (*Goetz et al.*, 2005; *Bhatt et al.*, 2010; *Boelman et al.*, 2011; *Epstein et al.*, 2012; *Gamon et al.*, 2013; *Huemmrich et al.*, 2013). Overall, this study has advanced understanding of arctic ecosystem processes and how arctic ecosystem science can be benefitted from engineering and analytical approaches associated with multi-scale and multi-platform remote sensing approaches.

6.4 SUGGESTIONS FOR FUTURE RESEARCH

The mid-scale digital imaging sensors and associated image analysis employed throughout this dissertation have demonstrated the propensity of these technologies for monitoring seasonal to inter-annual variability in the phenological dynamics of high and low arctic tundra landscapes and the plant communities represented within each. Based on research findings, several notable priorities for future research have emerged. These include:

1. Assessing why products derived from globally orbiting satellite platform such as MODIS do not align well with output from ground-based and low-altitude remote sensing methods.

2. Further explore the effect that the view-angle and sun geometries (e.g. BRDF) have on spaceborne and airborne remote sensing platforms and their resulting ability to capture biophysical characteristics of vegetated surfaces.

3. Test spectral unmixing and its capacity to decompose the fine-scale details of land surface products at the sub-pixel level.

4. Testing the efficacy of using Pheno-cams for deriving pheno-phase trends at the plot-level, which has the potential to facilitate high-spatiotemporal resolution monitoring of fine-scale species and plant community-level phenological dynamics.

5. Taking advantage of recent technological advances in GPS systems and computer learning as well as recent changes in Federal Aviation Authority regulations of Unmanned Aerial Vehicle operations to quantitatively explore how these technologies along with SfM and other novel analytical tools could enhance terrain modeling and the fusion of such geomorphic trends with phenological change studies in the Arctic and elsewhere.

Curriculum Vita

Sergio A. Vargas Zesati

Environmental Science and Engineering, Ph.D.

Sergio earned his Bachelor of Science in Environmental Science with a concentration in Biology degree from the University of Texas at El Paso in 2009 and beginning in 2010 he joined the doctor program in Environmental Science and Engineering at UTEP under the direction of Dr. Craig E. Tweedie.

Dr. Vargas has contributed his scientific findings to a series of national and international peer reviewed journals including the Journal of Environmental Informatics and the Journal of Wetland Science and Practice. Additionally, he has presented his work at conferences such as The Polar International Polar Year and at The American Geophysical Union conferences in an effort to contribute to better regional understanding of Arctic ecosystems' structure and function. Dr. Vargas has been a recipient of numerous honors and awards including the Dr. Diana Natalicio Doctoral Fellowship Award, which is a recognition by the university president Dr. Natalicio to the most outstanding doctoral candidate at UTEP. While pursuing his degree, Dr. Vargas worked as a Graduate Research Assistant for The Systems Ecology Laboratory within the Biological Sciences Department and spent over 300 days in the northern regions of Alaska, collecting field data across various arctic landscapes.

Dr. Vargas's Dissertation entitled, "Advancing Spatial and Spectral Resolution Remote Sensing for Observing Plant Community Response to Environmental Variability and Change in the Alaskan Arctic," was supervised by Dr. Craig E. Tweedie and is an interdisciplinary study that focused on developing and testing low-cost sensors for monitoring landscape scale change in the

Arctic as a response to climate variability and change. Dr. Vargas research interests focus on testing existing remote sensing methods for observing arctic plant community response to warming as well as assessing long-term changes at different spatial and temporal scales. Lastly, he has accepted to stay on with the Systems Ecology Laboratory as a Post-Doctoral Research Fellow and work on various projects including recently funded work by NASA-ABoVE which will expand on his research interests by focusing on exploring multi-temporal and spatial scale remote sensing approaches for monitoring landscape scale changes to arctic plant communities.

Permanent address: 221 Fremont Ln.

El Paso, Texas 79912. vargas.sergio1209@gmail.com

This dissertation was typed by Sergio A. Vargas Zesati